An Investigation into the Manufacturing of Complex, Three-Dimensional Components using Continuous Fibre Reinforced Thermoplastic Composites

Shivasi Mashau

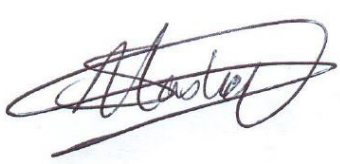
A dissertation submitted to the Faculty of Engineering and the Built Environment, University of the Witwatersrand, Johannesburg, in fulfilment of the requirements for the degree of Master of Science in Engineering.

Johannesburg, October 2017

Declaration

I declare that this dissertation is my own, unaided work, except where otherwise acknowledged. It is being submitted for the degree of Master of Science in Engineering in the University of the Witwatersrand, Johannesburg. It has not been submitted before for any degree or examination at any other university.

Signed this 20th day of October 2017



Shivasi Mashau

Acknowledgements

I would like to express my sincere gratitude to the engineering teams at Aerosud Aviation for the continuous support during the course of this research. I would also like to thank Prof R. Reid for his guidance and supervision in the preparation of this dissertation.

Abstract

This research looks into the manufacturing process of complex geometries using continuous fibre reinforced thermoplastics (CFRTP). The purpose of this work was to develop methods that will enable the production of defect free complex components.

This was achieved by investigating the key process parameters in the CFRTP manufacturing process, and optimizing them in order to improve the quality of components. The investigations were performed with the aid of software making use of the finite element method, and this was found to be instrumental in predicting the formability of geometries. The research showed that the formability of complex geometry is largely determined by the ability of the laminate to be draped into the required geometry. The forming mechanisms that take place during the draping process can be linked to the formation of defects where draping is unsuccessful.

The study also showed that the quality of the drape can be influenced by blank and tool design factors. It was also shown that the blank can be manipulated using a restraint mechanism to improve the formability of geometries. The effect of processing parameters such as forming speed, forming pressure and tool temperature were also investigated. The research resulted in the formulation of guidelines to follow when manufacturing CFRTP components. The developments that were made were successfully implemented to improve the formability of a complex component that had previously been difficult to form without defects.

Contents

Declaration **i**

Acknowledgements **ii**

Abstract **iii**

Contents **iv**

List of Figures **xi**

List of Tables **xvii**

1 Introduction **1**

1.1 Purpose of Research 1

1.2 Research Background 1

1.3 Research Motivation 2

2 Literature Survey **4**

2.1 Manufacturing of Composites 4

2.1.1 Material Configurations and Manufacturing Techniques 4

2.1.2 Thermosets, Thermoplastics and Stamp Forming 6

2.2 Rubber-Die Forming 8
2.2.1 Prepreg Sheet and Blank 8
2.2.2 Forming Process 9
2.3 Forming Simulation 11
2.4 Forming Parameters 13
2.5 Formation Mechanisms 14
2.6 Behaviour of Thermoplastic Resin During Forming 19
2.7 Inspection of CFRTP Components 22

3 Objectives **24**

3.1 Assess the use of AniForm as a predictive tool 24
3.2 Define the key process parameters for the forming process 24
3.3 Identify the significance of forming mechanisms to the forming process 24

4 Apparatus **25**

4.1 Aerosud CFRTP Facility 25
4.2 Forming Tools 30
4.3 Aniform 32

5 Methodology **34**

6 Validation of AniForm **36**

7 Development of CFRTP Forming Principles **40**

7.1 Introduction 40
7.2 Investigation 1: Tool Design Considerations 43

7.2.1 Tool Configuration 43
7.2.2 Tool Design 47
7.2.2.1 Problem Background 47
7.2.2.2 Identification of cause of problems and proposed solution . . 48
7.2.2.3 Methodology 48
7.2.2.4 Results 50
7.2.2.5 Discussion 53
7.2.2.6 Conclusions 54
7.3 Investigation 2: Lower Connection Unit study 55
7.3.1 Problem Background 55
7.3.2 Identification of cause of problems 58
7.3.3 Proposed solution 60
7.3.3.1 Blank Boundary Control 60
7.3.3.2 Blank Geometry Optimization 62
7.3.3.3 Blank Pre-Draping 64
7.3.4 Results 66
7.3.5 Discussion 70
7.3.6 Conclusions 71
7.4 Investigation 3: The effect of blank design 72
7.4.1 Problem Background 72
7.4.2 Objective 72
7.4.3 Proposed solution 72

7.4.3.1 C-Section . . . 72
7.4.3.2 Z-Section . . . 75
7.4.4 Results . . . 76
7.4.4.1 C-section: Simulated Results . . . 77
7.4.4.2 C-section: Experimental Results . . . 82
7.4.4.3 Z-Section: Simulated Results . . . 87
7.4.4.4 Z-Section: Experimental Results . . . 93
7.4.5 Discussion . . . 95
7.4.5.1 C-section . . . 95
7.4.5.2 Z-section . . . 98
7.4.6 Conclusions . . . 99
7.5 Investigation 4: The effect of spring stiffness . . . 100
7.5.1 Problem Background and Identification of Cause . . . 100
7.5.2 Proposed solution . . . 100
7.5.3 Results . . . 103
7.5.3.1 C-Section: Simulated results . . . 104
7.5.3.2 C-section: Experimental results . . . 108
7.5.3.3 Z-section: Simulated results . . . 110
7.5.3.4 Z-section: Experimental results . . . 113
7.5.4 Discussion . . . 115
7.5.4.1 C-section . . . 115
7.5.4.2 Z-section . . . 117

7.5.5 Conclusions 120

7.6 Investigation 5: The effect of material orientation 121

7.6.1 Background and Objective 121

7.6.2 Methodology 121

7.6.3 Results 122

7.6.4 Discussion 123

7.6.5 Conclusions 124

7.7 Investigation 6: The effect of tool temperature 125

7.7.1 Problem Background 125

7.7.2 Objective and proposed solution 127

7.7.3 Results 127

7.7.4 Discussion 130

7.7.5 Conclusions 130

7.8 Investigation 7: The effect of blank heating 131

7.8.1 Problem Background 131

7.8.2 Identification of cause of problems and proposed solution 133

7.8.3 Results 134

7.8.4 Discussion 135

7.8.5 Conclusions 135

7.9 Investigation 8: Simulated study of the effect of tool inclination 136

7.9.1 Background 136

7.9.2 Objective and Methodology 136

7.9.3 Results . . . 136
7.9.4 Discussion . . . 141
7.9.5 Conclusions . . . 142
7.10 Investigation 9: Simulated study of the effect of forming speed . . . 143
7.10.1 Background . . . 143
7.10.2 Objective and Methodology . . . 143
7.10.3 Results . . . 144
7.10.4 Discussion . . . 144
7.10.5 Conclusions . . . 145
7.11 Investigation 10: The effect of forming pressure . . . 146
7.11.1 Background . . . 146
7.11.2 Objective and Methodology . . . 146
7.11.3 Results . . . 146
7.11.4 Discussion . . . 148
7.11.5 Conclusions . . . 148

8 Final Discussion **149**

9 Final Conclusions **153**

10 Recommendations **155**

11 References **156**

A Material Data Sheets **164**

B Tool Heating System Design **173**

B.0.0.1 Determination of Power Requirements 173

C Spring Data **178**

D Simulation Results **180**

D.1 LCU Results 181

D.2 C-Section Results 183

D.3 Z-Section Results 217

D.4 Rib Results 245

E Theoretical Investigation Results **252**

E.1 Tool Inclination 253

E.2 Tool Direction 260

E.3 Forming Speed 267

F Non Destructive Inspection Report **273**

G Drawings **276**

List of Figures

2.1 Performance of thermoplastic composite manufacturing processes [13]. 5

2.2 The rubber-die forming process [29] 9

2.3 Typical pressure and temperature trend during forming [24]. 10

2.4 Forming mechanisms for woven fabrics [7]. 15

2.5 Forming mechanisms for woven fabrics [7]. 16

2.6 Forming with a cylindrical punch. (a) geometry of the tools, (b) tensile stiffness only, (c) small bending stiffness, (d) higher bending stiffness [9]. 18

2.7 Capillary rheometer[34]. 19

2.8 The dependence of melt viscosity on shear rate (top) (320°C, L/D = 40/1), and temperature (bottom) (L/D = 40/1) [34]. 20

2.9 Sample with defect (left) and A-scan illustration (right) [26] 23

4.1 Aerosud CFRTP 600 tons hydraulic press 25

4.2 Aerosud CFRTP 80 tons hydraulic press. 26

4.3 Aerosud CFRTP 80 ton hydraulic press, press-bed side. 27

4.4 80 ton hydraulic press IR-oven. 28

4.5 80 ton hydraulic press control panel. 29

4.6 Forming tools. 31

4.7 AniForm results interpretation guide [4]. 33

6.1 A comparison of the shear angle prediction by Aniform to experimental results. 38

6.2 A comparison of the fibre stress prediction by Aniform to experimental results. 39

7.1 LCU geometry and material direction. 40

7.2 Rudder assembly. 41

7.3 Z-section and C-section geometry. 42

7.4 Z-section and C-section drawings. 43

7.5 (A)Shear angle distribution, (B) Thickness distribution. 45

7.6 Metal-rubber tool. 46

7.7 Leading edge results. 47

7.8 (A) Surfaces used for blank development, (B) Final tool design. 49

7.9 Z-section tool design and Z-section blank design relation. 50

7.10 Shear angle results for ply 1, forming surfaces only (top) and completed tool (bottom). 51

7.11 Shear angle results for ply 2, forming surfaces only (top) and completed tool (bottom). 52

7.12 Defects on the LCU 56

7.13 Fibre stretching and laminate bridging. 57

7.14 (Top) Trimmed component and (Bottom) Oversized blank. 58

7.15 LCU geometery. 59

7.16 Laminate bridging. 59

7.17 (A) Clamp & springs, (B) Frame & blank 61

7.18 Optimized LCU blank. 62

7.19 Proposed LCU forming set-up. 63

7.20 Blank sag during heating. 64

7.21 Pre-draped LCU blank. 65

7.22 Forming simulation of the LCU during tool closure, also showing the simulation set-up. 66

7.23 Simulated progression of LCU deformation 67

7.24 Simulation results for the LCU formability study. 68

7.25 Experimental results for the LCU manufactured with the BRM and optimized blank. 69

7.26 Blank designs for the C-section geometry. 73

7.27 Blank sag for different blank designs. 74

7.28 Blank designs for the Z-section geometry. 75

7.29 Deformation of blanks 1,2 and 3 before full tool closure. 77

7.30 C-section blank 1 results, ply 1 above and ply 2 below. 78

7.31 C-section blank 2 results, ply 1 above and ply 2 below. 79

7.32 C-section blank 3 results, ply 1 above and ply 2 below. 80

7.33 C-section blank 4 results, ply 1 above and ply 2 below. 81

7.34 Pre-drape shape for (A) blank 1, (B) blank 2 and (C) blank 3. The yellow markers denote the curvature of the blank sag and the red lines denote the lines of first contact with the tool. 82

7.35 Pre-drape shape for blank 4 83

7.36 Results for C-section manufactured from blank 1. Spring stiffness - 0.09 N/mm. 84

7.37 Results for C-section manufactured from blank 2. Spring stiffness - 0.09 N/mm. 85

7.38 Results for C-section manufactured from blank 3. Spring stiffness - 0.09 N/mm. 86

7.39 Z-section blank 1 results. Deformation before tool closure (top) and the resulting shear angle distribution at full tool closure for ply 1 (middle) and ply 2 (bottom). Spring stiffness - 0.09 N/mm. 88

7.40 Z-section blank 2 results. Deformation before tool closure (top) and the resulting shear angle distribution at full tool closure for ply 1 (middle) and ply 2 (bottom). Spring stiffness - 0.09 N/mm. 89

7.41 Z-section blank 3 results. Shear angle distribution at full tool closure for ply 1, above and ply 2, below. Spring stiffness - 0.09 N/mm. 90

7.42 Z-section blank 2 fibre stress 1 results. Ply 1 above and ply 2 below. Spring stiffness - 0.09 N/mm. 91

7.43 Z-section blank 3 fibre stress 1 results. Ply 1 above and ply 2 below. Spring stiffness - 0.09 N/mm. 92

7.44 Results for Z-section manufactured from blank 2 formed with a spring stiffness of 0.09 N/mm. 93

7.45 Results for Z-section manufactured from blank 3 formed with a spring stiffness of 0.09 N/mm. 94

7.46 The evolution of a buckled region [4]. 95

7.47 Set-up for blank 3. 96

7.48 Tag showing the melt zones 97

7.49 C-section blank 3 spring stiffness - 0.09 N/mm 101

7.50 Results for Z-section manufactured from blank 2 with a spring stiffness of 0.09 N/mm. 102

7.51 C-section blank 3 shear angle simulation results with a 0.23 N/mm spring stiffness. Ply 1 above and ply 2 below. 104

7.52 C-section blank 3 fibre stress 1 simulation results with a 0.23 N/mm spring stiffness. Ply 1 above and ply 2 below. 105

7.53 C-section blank 3 fibre stress 2 simulation results with a 0.23 N/mm spring stiffness. Ply 1 above and ply 2 below. 106

7.54 Fibre stress response guide. 107

7.55 C-section spring stiffness - 0.23 N/mm 109

7.56 Shear angle Z-section results, spring stiffness - 0.23 N/mm. Ply 1 above and ply 2 below. 110

7.57 Fibre stress 1 Z-section results, spring stiffness - 0.23 N/mm. Ply 1 above and ply 2 below. 111

7.58 Fibre stress 2 Z-section results, spring stiffness - 0.23 N/mm. Ply 1 above and ply 2 below. 112

7.59 Z-section results, spring stiffness - 0.23 N/mm. 114

7.60 Material orientation for specimens 1 and 2. 121

7.61 Fibre buckling in regions marked A and B. 122

7.62 Weaving of the fabric showing the warp tows in tension and the weft tows un-tensioned [33]. 123

7.63 (A)Thermoplastic residue on the tool, (B) & (C) resin burn on tool side and (D) rubber side for reference. 126

7.64 Z-section component manufactured with a tool setting of 230°C (above) and on the right to 210°C (below). 127

7.65 Effect of tool temp on forming. 128

7.66 Heat distribution of the Z-section tool. 129

7.67 Insufficient blank heating. 132

7.68 Effect of blank heating on forming. 134

7.69 Blank deformation sequence for two tool orientations. 137

7.70 Ply 1 shear angle results for the tool inclined through 0° and 30°. 138

7.71 Ply 1 fibre stress results in direction 1 for the tool inclined through 0° and 30°. 139

7.72 Ply 1 fibre stress results in direction 2 for the tool inclined through 0° and 30°. 140

7.73 Geometry definition for the 25 bar sample (top) and the 30 bar sample (bottom) for the Z-section. 147

B.1 A - Shear Angle, B - Fibre stress 1 173

B.2 Tool temperature distribution (A) Z-section, (B) C-section. 176

List of Tables

2.1 Forming mechanisms and their associated defects. 15

4.1 600 ton Hydraulic Press Specifications. 30

4.2 Interpretation of AniForm results [4]. 32

7.1 C-Section results for increasing BRM stiffness from 0.09 N/mm to 0.23 N/mm. 108

7.2 Z-Section results for increasing BRM stiffness from 0.09 N/mm to 0.23 N/mm. 113

7.3 The effect of rotating the tool by 30° on the formability of the plies. 141

7.4 The effect of increasing forming speed on the formability. 144

B.1 Properties of the metal tool. 174

B.2 Heating Cartridge Properties 177

1 Introduction

1.1 Purpose of Research

This purpose of this research was to develop methods that will be utilised to accurately predict the formability of complex components manufactured from continuous fibre reinforced thermoplastic (CFRTP) composite materials. The forming of CFRTP laminates into complex parts requires an in-depth knowledge of the behaviour of the constituents of the laminate during the forming process [20]. The development of finite element software that simulates the forming process presents an opportunity to monitor the behaviour of the laminate during forming. Having insight into the behaviour of the blank will allow for the development of manufacturing approaches that minimise and possibly eliminate the occurrence of manufacturing defects in CFRTP components.

1.2 Research Background

A composite material is defined as a material which on the macro-scale consists of two or more distinct material types acting in unison. This definition encompasses a wide range of material, from reinforced concrete to the combination of different wood species, but the term is used as a generic for fibre reinforced plastics (FRP) [28]. This composite consists of reinforcing fibres that are embedded in a plastic matrix to give a material that displays properties superior to that of the fibre or the plastic acting individually. There are multitudes of reinforcing fibres and plastic matrix systems to choose from when designing a composite material.

FRPs have many advantages when they are compared to traditional engineering materials. Besides the high strength and low weight properties, they offer high specific stiffness, low thermal expansion and good corrosion resistance. They have an anisotropic structure which allows them to be adapted to the mechanical loading of the component. FRPs also have the capacity to conform to complicated contours which greatly simplifies the manufacturing of

complex shapes [37]. These properties all make FRPs well suited for use in the manufacturing of aircraft structures. The substitution of metals by better performing lightweight materials in aircraft structures not only improves the efficiency of the aircraft but is also in line with the global trends towards the reduction of the carbon footprint of the aviation industry [3].

The technology behind composites has to date progressed to a stage where carbon FRPs are used in primary components, including the wings and fuselage. The current generation A350 XWB has a composite composition greater than 50%, marking a significant milestone for aircraft production[2]. This aircraft represents the first Airbus aircraft that utilises a greater percentage of composite technologies than metallic applications. Its fuselage panels, frames, window frames, clips, and doors are made from CFRTP. The application of composites to this aircraft has stretched its service intervals from 6 to 12 years since there is no need for fatigue and corrosion checks, which in turn reduces maintenance costs [2].

This shows that there is a clear drive for the use of CFRTPs in aircraft components and that their use can be successfully implemented. This essentially leaves the CFRTP manufacturing industry with a mandate to improve their manufacturing skills by ensuring the production of defect free components and broadening the nature (shape and size) of components that they can manufacture. This research focuses on the manufacturing process used to manufacture thermoplastic based composites. Thermoplastics form a small portion of the composite industry when compared to thermoset based composites but there is an interest in the development of thermoplastic manufacturing processes. Processes that take advantage of some of the properties that are unique to thermoplastics are being developed. These include the ease of automation due to the fact that they can be reheated and reformed which is not possible with thermosets.

1.3 Research Motivation

The growing use of CFRTP requires the industry to place itself in a position where it can produce high quality (defect free) parts in the most economical manner (minimal scrap). This research makes an attempt at improving the understanding of the production process of CFRTP components. It is hoped that this research will enable the prediction of the formability of the components thereby adding valuable insight into the manufacturing process whilst also removing the trial and error element from the development of the CFRTP manufacturing process. This research is in line with the improvement of the CFRTP manufacturing process as it aims to develop tools that can be used to form components through a process with predictable quality and accuracy.

This research deals with the manufacture of CFRTP components from fully consolidated pre-impregnated laminates through a stamp forming process. This forming process makes the components susceptible to the occurrence of defects such as folds and wrinkles. It is necessary to develop procedures that allow for CFRTP components to be formed without these manufacturing defects. It is further necessary to understand the forming mechanisms that take place during the stamp forming process. The occurrence of these mechanisms is related to the nature of formability that can be achieved. The processing conditions under which defect-free components are formed need to be understood so that they can be utilised to repeatedly reproduce defect-free components [23].

CFRTPs are compatible with novel manufacturing technologies. The thermoplastic matrix gives the composite the ability to be fusion welded through resistance or induction welding techniques. These welding techniques are a viable way to reduce cost and weight through fastener elimination. Gulfstream and Fokker Aerostructures developed the tail assembly of the G650 business jet utilising induction welding. The structure achieved a 10% weight saving and a 20% cost reduction over a thermoset composite structure [16].

This research will also involve the use of a newly developed virtual laminate forming simulation tool. The use of a numerical tool to simulate the forming process removes the trial and error approach when developing new CFRTP components. This is expected to have a positive impact on the cost effectiveness of the development process. Numerical methods are used to predict the micro and macro mechanical behaviour of the laminate, the result of which is software that is capable of predicting fibre stresses, fibre paths, ply thickness, wrinkling and other phenomena involved in forming [20].

2 Literature Survey

2.1 Manufacturing of Composites

Composites that are used in structural components consist of fibres that are bundled into tows which are usually woven into sheets to increase the load bearing capability of the component [37]. Traditionally, these sheets are laid out into a mould with a layer of plastic matrix in between so that the matrix impregnates the fibres when this fibre-plastic stack is cured at a high temperature and pressure to create the composite product. The lay-up was traditionally done manually (by hand) but automatic fibre lay-up technologies have been developed. The layered composite is referred to as a laminate and each woven layer as a lamina (or ply). The composite material is also available in pre-impregnated (prepreg) form. These are woven sheets that have been pre-impregnated to speed up the manufacturing process, they are then simply cut into the desired shape then laid into the mould and cured.

2.1.1 Material Configurations and Manufacturing Techniques

Thermoplastic composites are available in different configurations. They can be procured in the form of uni-directional tapes and unwoven sheets. In this form, they can be used to manufacture simple components with very high strength. They are available in the form of laminated woven sheets. They are also available in short and long fibre configurations, which provide the lowest mechanical performance but the highest degree of geometric complexity. Thermoplastics also have applications where they are used without fibre reinforcement, in which case they are not considered to be composite materials.

Thermoplastics can be processed using the processes that are typical in the manufacture of plastics such as thermoforming, compression moulding and injection moulding. To select the appropriate manufacturing process, one must consider; the nature of the product (size and shape), the material type and configuration (prepreg or non-prepreg, continuous or short fibres). Figure 2.1 identifies the compatibility of the manufacturing techniques with the material configurations. It also presents a comparison of the expected mechanical performance of products produced from the manufacturing techniques as well as the geometric complexity achievable from the material configurations.

This research investigates the production of components manufactured using the compression moulding technique. There is an interest in increasing the complexity of products manufactured using the compression moulding technique. This would allow complex components to be formed without sacrificing the mechanical performance offered by woven laminates.

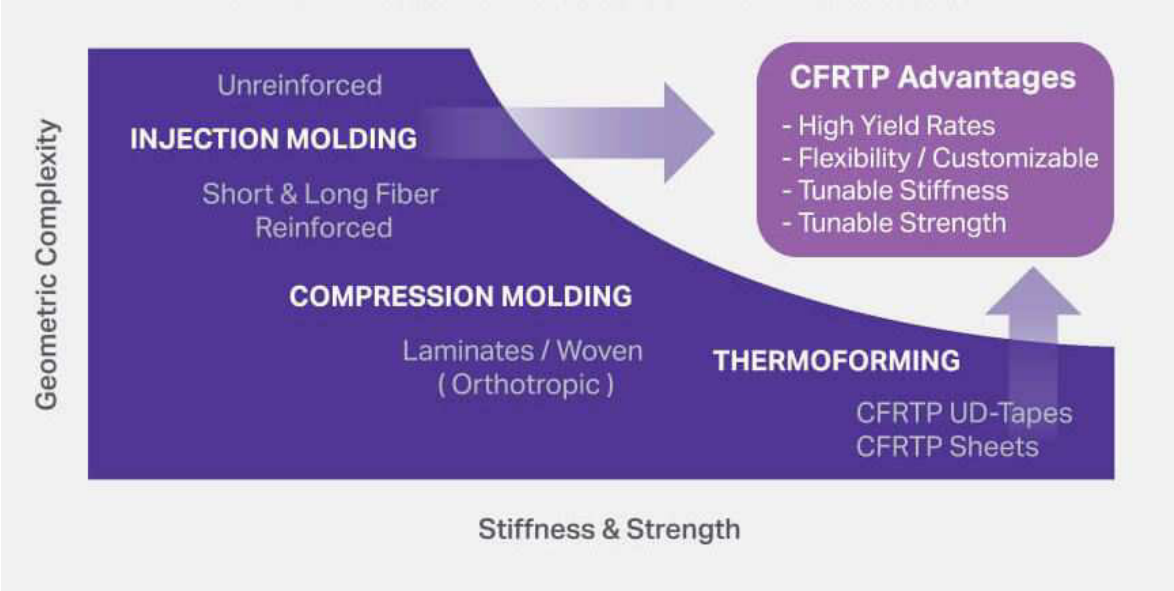


Figure 2.1: Performance of thermoplastic composite manufacturing processes [13].

2.1.2 Thermosets, Thermoplastics and Stamp Forming

The composites that have been produced throughout the years have been made with either a thermoset or a thermoplastic matrix system. Each of these plastics offers advantages and disadvantages and the choice is made through careful consideration of the environment in which the material will be utilised. Thermoset based FRPs are used extensively in comparison to thermoplastics, mainly because they are low viscosity liquids which makes them easier to work with. The low viscosity also makes them well suited for fibre impregnation [8].

There has recently been a great deal of interest in thermoplastic composite material due to developments in the rapid processing of this material to meet high production and volume requirements [10]. This has been made possible by exploiting the fact that thermoplastic composites can be reheated and formed to create a product. In contrast, during the curing process of a thermoset plastic, the plastic undergoes an irreversible chemical reaction making the cured geometry permanent. To take advantage of the fact that thermoplastics can be heated and formed, a stamp forming process similar to that of sheet-metal forming has been developed. Furthermore, thermoset pregreg sheets need to be stored at -18°C to prevent them from curing before they are formed and intentionally cured. Whereas thermoplastic prepreg sheets can be stored at room temperature eliminating the need for refrigeration of the prepreg.

Thermoplastics are a material solution that eliminates the need for investing in autoclaves at the final leg of composite part fabrication. The CFRTP laminates are obtained from a supplier in the form of a fully consolidated sheet. The manufacturing process now consists of cutting the material needed from the prepreg sheet and then forming it to produce the required geometry. The curing time associated with thermosets is eliminated from the process allowing for very short cycle times [20].

The following presents the advantages and disadvantages of thermoplastic composites in comparison to thermoset composites:

Advantages:

- Good toughness and damage resistance.
- Ability to use short cycle-time thermoforming methods.
- Room temperature storage.
- Low moisture uptake.
- Good fire retardancy properties.
- Ability to reform components.
- Very low void content.
- Alternatives to manufacturing without using autoclaves.

Disadvantages

- Higher processing temperatures (200-400°C) and pressures (10-50 bar) - due to high viscosity.
- High initial raw material cost over thermosets
- Typically higher tooling cost.

2.2 Rubber-Die Forming

The manufacturing processes that are discussed in this section detail the processes that apply specifically to this research. The manufacturing technology which is dealt with here is the manufacture of CFRTP components using the rubber-die forming process. Rubber-die forming falls within the compression moulding range in the plot depicted in Figure 2.1. The sections that follow highlight the major segments of this manufacturing process.

The manufacturing process follows the following procedure;

1. production of the pre-consolidated prepreg sheet,
2. cutting of an approximate component shape from the prepreg,
3. heating of the cut-out in an oven,
4. transfer of the cut-out to the moulding tools where it is formed into the shape of the final component by pressing it between a rubber and a metal tool,
5. post forming the component to finish and detail it.

2.2.1 Prepreg Sheet and Blank

The first stage in this CFRTP thermoforming process is the production of the pre-consolidated laminate sheet. The reinforced thermoplastic prepreg sheets are available in configurations of 1 to 24 plies with fibre orientations specified by the customer [32]. The prepreg sheet is cut using a water-jet cutter to obtain a near net shape of the final product with allowance reserved for handling and edge trimming. This cut-out is referred to as a blank.

2.2.2 Forming Process

Rubber forming is a manufacturing technique based on sheet-metal forming technologies The CFRTP blank replaces the sheet-metal blank and everything else remains practically similar (see Figure 2.2). The blank is heated in an oven, after which it is transferred to the forming tool where it is pressed between a rubber punch and a pre-heated shaped metal die. The metal die is pre-heated to maintain forming temperature. The temperature of the metal die affects the cooling rate experienced by the blank.

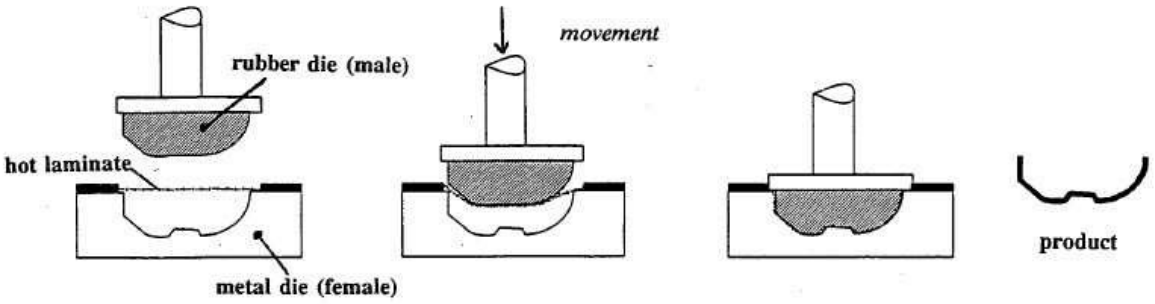


Figure 2.2: The rubber-die forming process [29]

The forming stroke is executed in 3 seconds or less, this together with the fact that autoclave operations are eliminated from the forming process reduces the cycle time for a part to the order of a few minutes. This makes the rubber-die forming process suitable for achieving the necessary rapid production rates [29].

As the laminate is formed, it cools very rapidly due to the contact with the relatively cooler tool since the blank is heated to about 400°C depending on the material and the tool to about 200°C. Once the temperature of the laminate has reduced to below the thermoplastic resin recrystallization level, the pressure can be removed since the part will then be in a stable geometric state [24]. Figure 2.3 shows the variation of the temperature and pressure on the blank from the point where it leaves the oven until it is formed. It could be argued that the rapid cooling is not ideal for forming. This is because it increases the viscosity of the thermoplastic which inhibits the forming mechanisms that are necessary for producing properly shaped components. However, it is partly the reason why the components can be removed from the forming tools quickly which makes the short cycle times possible.

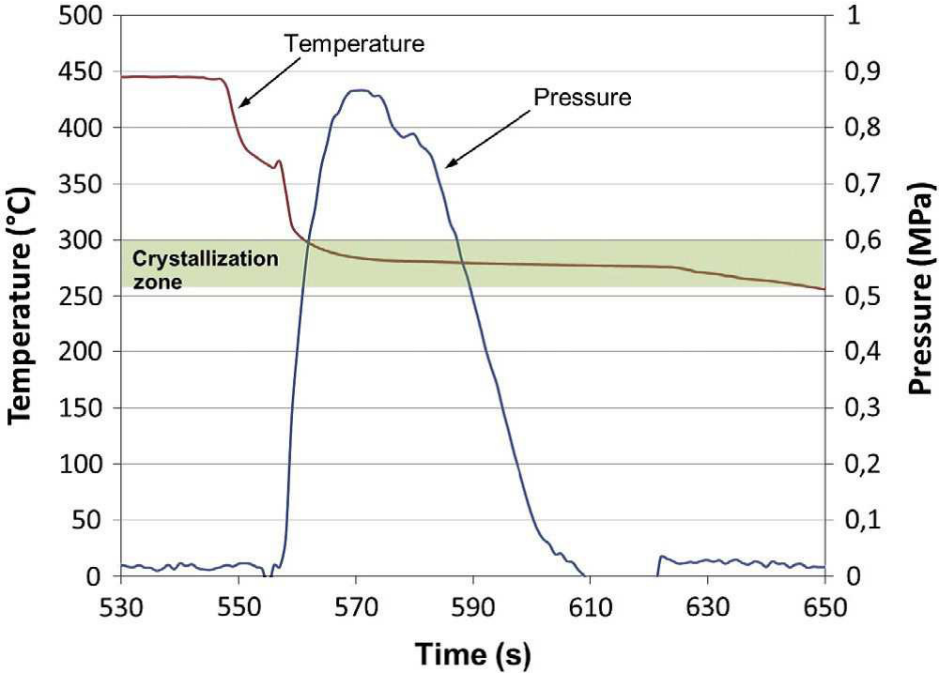


Figure 2.3: Typical pressure and temperature trend during forming [24].

2.3 Forming Simulation

In the production of CFRTP components, manufacturing and performance are addressed in parallel and not by a conventional serial approach. This approach implies that the formability of the product is factored in during the design phase. This approach together with the use of a forming simulation tool can be used to predict, identify and eliminate practices that impact negatively on the forming. Predicting the behaviour of fibre reinforced laminates through computerized simulations helps avoid costly trial-and-error runs by aiding in the creation of manufacturing practices that help produce defect free components [17].

A forming simulation tool is used to gain a better understanding of the forming mechanisms that deform the flat laminate into the end geometry. This provides knowledge that can be used to reduce or avoid forming defects in CFRTP products. Regions that are prone to the formation of defects such as corners and surfaces with double curvature can be addressed by modifying the product geometry, material, lay-up, and process parameter settings. This may eventually lead to the production of a product without any defects [18]. Geometries that cannot be successfully produced using the stamp form process can also be identified by using the simulation software.

PAM-COMPOSITES is a simulation software that can be used to predict defects early in the development cycle of composite products. PAM-COMPOSITES allows for the analysis and optimization of individual manufacturing operations. These operations can be linked by transferring material history from one operation to the next (change in fibre orientations, curing degree, temperature distribution). A composite simulation module (PAM-FORM) within PAM-COMPOSITES, is used to simulate the thermoforming process of fibre reinforced composite materials made from thermoplastics. PAM-FORM allows the modelling of stamping using two rigid tools, rubber pad forming and many more. The module can be used to predict fibre orientation, thickness distribution, optimum initial flat pattern, stresses, strains, bridging and wrinkling [15].

AniForm Suite is a simulation package tailored for the forming process of fibre reinforced sheet material, such as laminates comprising woven fabrics and uni-directionally reinforced pre-pregs. An improved understanding of the laminate forming process is obtained by fast and intuitive visualisation of the simulation results. The software predicts; fibre paths, changing ply thickness, adverse fibre stresses, wrinkling, and other phenomena that appear upon forming. The anticipation of these phenomena in the early design phases allows for efficient product and process optimisation. This lead to a reduction of product development costs and lead times [5].

The aforementioned is an indication of the capabilities of simulation software that is available in the market. AniForm was chosen to be used as the simulation software for this research. The reason for this choice was due to the relation AniForm has with the supplier of the CFRTP material that was used. AniForm has performed material characterization tests on the material for use on the package. The material properties could be acquired from AniForm together with the simulation package. AniForm uses knowledge of the material's mechanical behaviour at manufacturing temperature as well as tool-ply and ply-ply interface friction to predict the response of the laminate as the moulding tools compress it to the final geometry [21].

2.4 Forming Parameters

The parameters that affect the manufacturing of CFRTP components can be grouped into three categories; (1) parameters of the laminate design process, (2) parameters associated with the geometry of the product and (3) parameters of the forming process [22]. Parameters from any group can be changed to improve the formability and quality of components.

Laminate Design Parameters

- Fibre orientation and layup sequence
- Number of plies
- Thickness of each ply
- Influence of lay-up sequence on wrinkling/formability
- Fabric parameters (weave pattern, tow size and spacing)

Geometric Parameters

- Types of curvature, flat, single or double (i.e. the complexity of the component shape)
- Draw depth relative to width and breadth
- Bend radii

Forming Parameters

- Temperature
- Pressure
- Laminate boundary conditions
- Forming speed

2.5 Formation Mechanisms

The formability of CFRTPs is mainly limited by the drapability of the textile. Drapability refers to the manner in which a fabric maps a surface that it is laid on. A successful drape is one that has the entire fabric in contact with the forming tool without any folds, wrinkles or tearing. The drapability of the fabric depends on the properties of the weave (weave type, tow size), the laminate (fibre orientation, stacking sequence, number of plies), the mechanical properties of the laminate as well as the geometry being draped [29].

The fabric is able to deform and drape onto the tool surface due to a number of forming mechanisms. As a fabric drapes into a geometry there is an initial straightening and de-crimping of the fibres. After this, there is only limited forming potential provided by fibre strain due to their high stiffness. Forming geometries with single curvature require the fabric to bend out-of-plane, the out-of plane bending stiffness is significantly lower and decoupled from the in-plane stiffness. As the laminate bends out of plane the plies will assume different radii so that they slide relative to each other, this mechanism is referred to as inter-ply shear [25].

When forming geometries with double curvature, the fabric takes up a mechanism called intra-ply shear. Intra-ply shear requires the angle between warp and weft tows to change so that the fabric can accommodate the geometry. The angle through which the tows shear is referred to as the shear angle. Fibre slippage occurs when axial tensile forces on a tow exceed the frictional forces from the neighbouring tows. In the final stage of press forming the fabric is compressed, and the plies are compacted to consolidate the laminate [25]. Figure 2.4 presents diagrams showing some of the mechanisms.

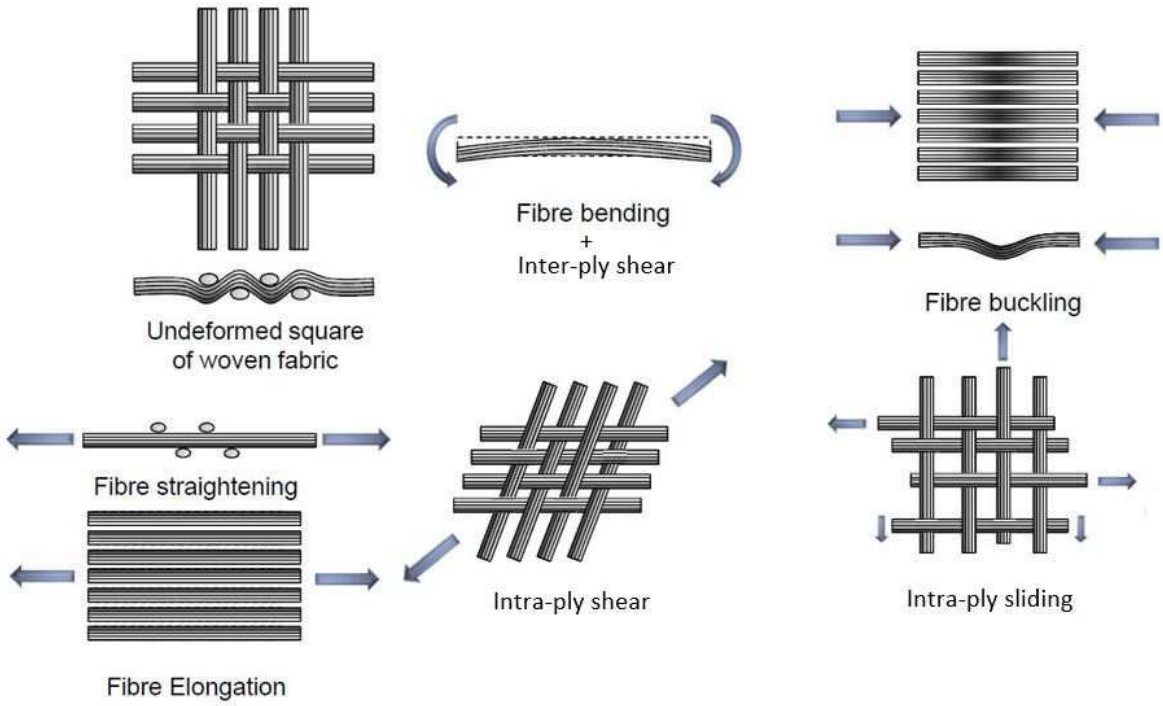


Figure 2.4: Forming mechanisms for woven fabrics [7].

The forming mechanisms are also the source of defects. Defects related to draping can be linked to a forming mechanism that has failed to manifest in an acceptable manner. For instance, inadequate compaction results in voids in the laminate. While excessive compaction leads to high fibre volume fractions which degrades the strength properties of the laminate. Table 2.1 presents a list of the mechanisms and their related defects.

Table 2.1: Forming mechanisms and their associated defects.

Forming Mechanism	**Defect**
Tensile Strain	Fibre breakage, Resin squeeze out
Compressive Strain	Fibre and Ply buckling
Inter-ply Shear	Fibre and Ply buckling
Intra-ply Shear	Ply wrinkling
Compaction	Porosity, Voids and Non-consolidation

The most prevalent defect when forming complex geometry is ply wrinkling. The ply wrinkling phenomenon is related to the intra-ply forming mechanism. Figure 2.5 shows what happens to the fibres during intra-ply shear. The fibres tows have freedom to shear until they are in contact with neighbouring tows. At this point any additional shearing that takes place will result in the fabric wrinkling. The largest shear angle that the ply can attain before wrinkling takes place is called the shear locking angle. The locking angle places a limit on the formability of a fabric [7].

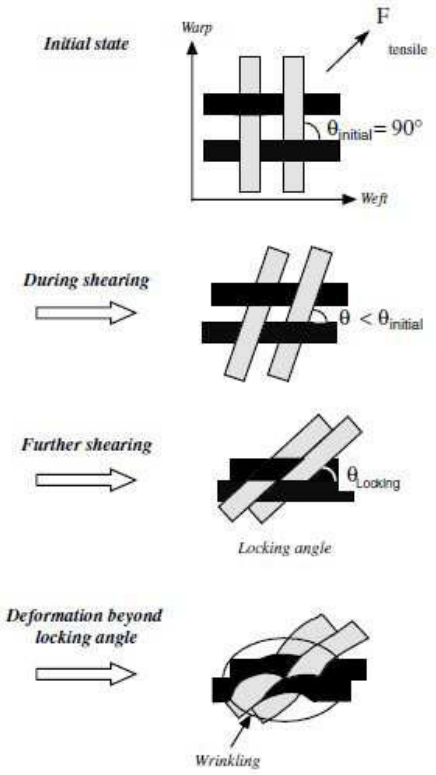


Figure 2.5: Forming mechanisms for woven fabrics [7].

There is little in the form of published work from manufacturers who may have had similar problems. This is mostly attributed to the fact that solutions that are created to combat these manufacturing problems become valuable intellectual property for the manufacturers concerned. Manufacturers often compete for contracts and the development of processes that allow the manufacturer to produce superior products.

The current focus of researchers in this field is the characterization of the properties that are critical in the description of the forming mechanisms [25]. These characterizations are used to develop and refine simulation software such as AniForm. The quality of the simulations depends on the mechanical properties that are taken into account. There are some assumptions that are made in the present work such as the independence of the in-plane shear and bending rigidities [9].

It has been noted that wrinkles can be prevented in industrial settings by the addition of forming constraints such as blank holders [35]. These constraints apply a tension to the fibres which works to reduce the formation of wrinkles. However, it is generally accepted that wrinkling is a global phenomenon and there is no simple relation between the shear angle and the wrinkles [9]. Figure 2.6 (a) shows the set up of a cylinder that was being used to press a laminate. The laminate was constrained by the red, yellow and green blocks. The results shown in insert (b) indicate a simulation where the fibres are defined with only tensile stiffness and no bending stiffness. In insert (c) a small amount of bending stiffness is introduced and then higher amount for insert (d). These results allow the coupling effect of tensile and bending rigidities on the shear distribution and wrinkling on the fabric to be identified. Wrinkles are formed due to all the strains and rigidities of the fabric (tension, in-plane shear and bending) and also due to boundary conditions [35].

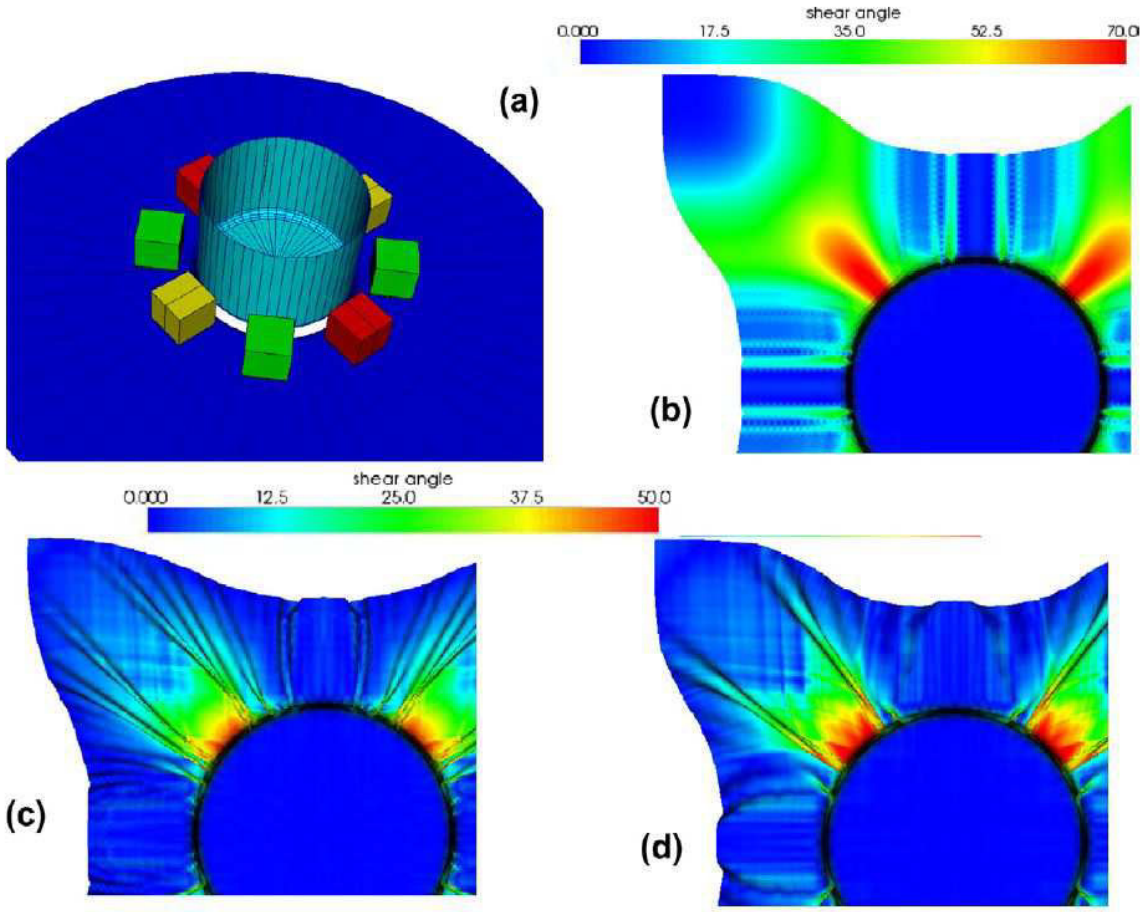


Figure 2.6: Forming with a cylindrical punch. (a) geometry of the tools, (b) tensile stiffness only, (c) small bending stiffness, (d) higher bending stiffness [9].

2.6 Behaviour of Thermoplastic Resin During Forming

Thermoplastic resins melt and exhibit a degree of fluidity when they are heated above their melting temperature. The resulting semi-fluid flows with a degree of stickiness, this property is referred to as the viscosity of the fluid. It is a measure of the internal friction within a fluid. The viscosity of a thermoplastic resin (fluidity) is usually represented as a melt mass-flow rate (MFR) index. The MFR is obtained by extruding molten resin through an orifice by the action of a constant weight. The mass of resin discharged is measured against time to determine the mass flow rate. PPS is a non-Newtonian fluid and therefore its melt viscosity will vary with the apparent shear rate [34].

A slightly modified method of measurement has been developed to circumvent the varying shear rate. The set-up for this method is shown in Figure 2.7, the device in this set-up is referred to as a capillary rheometer. The device detects the load require to extrude the molten resin at a constant rate. The melt velocity can then be determined by relating the volumetric flow rate, shear rate, shear stress and melt viscosity equations. This method allows the melt viscosity to be determine in the standard unit of $Pa{\cdot}s$ [34].

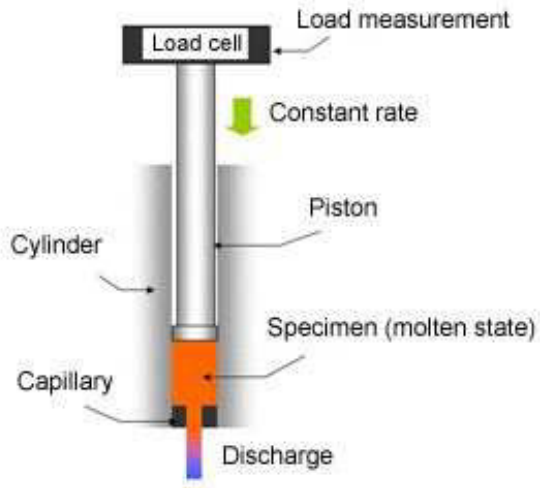


Figure 2.7: Capillary rheometer[34].

The chart at the top of Figure 2.8 shows the variation of melt viscosity with shear rate. The charts show the properties of a range of polyphenylene sulfide (PPS) resins called 'Torelina'. The resins are produced by Toray Plastics for use in injection moulding. PPS is classified as pseudo-plastic due to the fact that its melt viscosity decreases with increasing shear rate. The melt viscosity is also dependent on temperature, it decreases as the temperature rises [34]. These charts illustrate the response of the internal friction of PPS resin for changes in the temperature and shear rate properties.

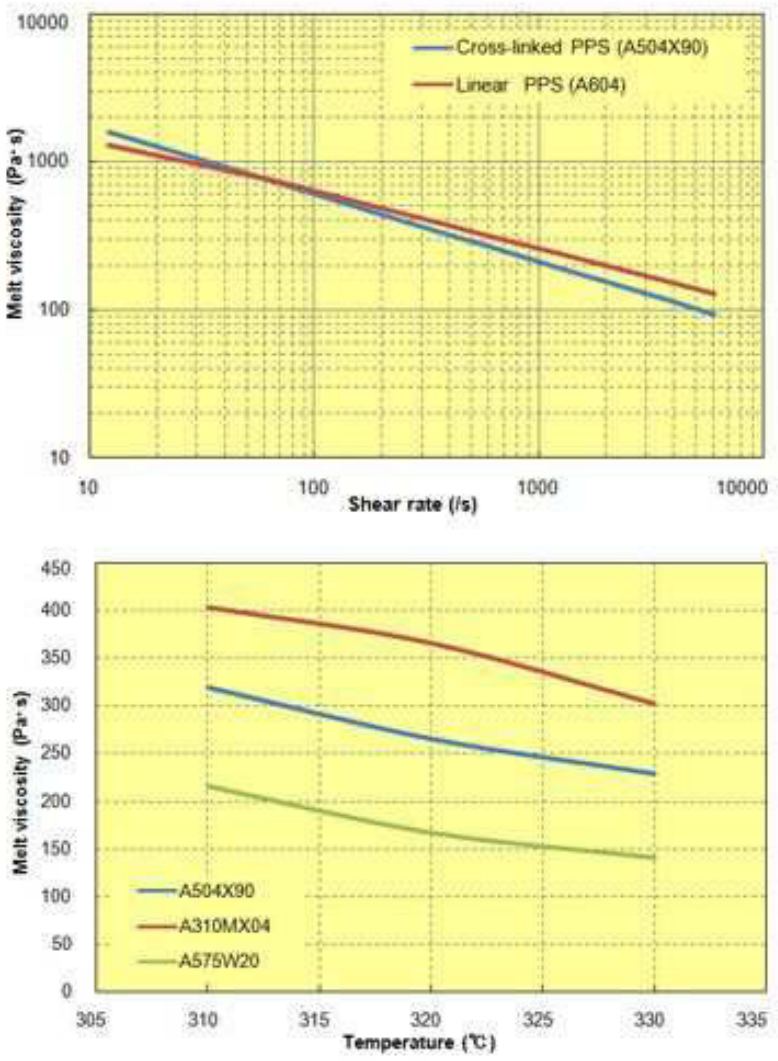


Figure 2.8: The dependence of melt viscosity on shear rate (top) (320°C, L/D = 40/1), and temperature (bottom) (L/D = 40/1) [34].

Two thermoplastics were used in this research, namely PPS and polyetherimide (PEI).

PPS is a semi-crystalline engineering plastic that is widely used in the production of precision injection moulded parts. PPS offers a wide range of advantages such as; excellent strength, high heat resistance, chemical resistance, good electrical properties and good dimensional stability[31]. PPS does have a few disadvantages such as brittleness and tendency to warp [31]. The filling of PPS with fibres and fillers aids in overcoming its inherent brittleness[30]. PPS has a low viscosity which allows is to be moulded with a high loading of fillers and reinforcements [30]. The flame retardant properties make it an ideal choice for electrical applications involving high temperatures [31]. PPS is an ideal material choice for automotive parts exposed to high temperatures, automotive fluids, or mechanical stress [27]. The ability to mould complex parts to tight tolerances also makes the material suitable for application on high level components [27].

PEI has properties that are similar to those of PPS but with lower strength. PPS is selected over PEI where significant loads are present. PEI is a valuable material in the medical, electronics and other fields that demand moderate strength and rigidity in high-heat applications [27].

2.7 Inspection of CFRTP Components

There is a requirement for composite components to be inspected to determine their eligibility for their purpose without destroying the specimen. Non-destructive inspection (NDI) entails the checking for the existence of defects associated with the forming mechanisms presented in Table 2.1. The inspection of composite material poses a particular challenge because of its non-homogeneous and anisotropic nature [19]. Ultra-sonic inspection methods are widely used for the inspection of composite components. The method relies on the laws of physics that govern the propagation of sound waves. This allows for the revelation of defects within the laminate that are not visible to the eye. Ultra-sonic devices are integrated with positional encoders, controllers and software to create an imaging system [26]. The images that are produced are essentially a map of the flaws which allows accurate description of the size and position of the defects.

The three most common methods for collecting ultra-sonic data are known in the NDI world as A-scan, B-scan and C-scan presentations. Each presentation mode provides a different way of looking at and evaluating the region of material being inspected. Modern computerized ultrasonic scanning systems can display data in all three presentation forms simultaneously [12].

An ultra-sonic instrument typically records two fundamental parameters of an echo: how large it is (amplitude), and where it occurs in time with respect to a zero point (pulse transit time). The transit time is usually correlated to the reflector (defect) depth or distance, based on the sound velocity of the test material and the simple relationship $distance = velocity \cdot time$ The most basic presentation of ultrasonic waveform data is in the form of a waveform display commonly referred to as an A-scan. The output of this scan is presented on a simple grid with the vertical axis representing amplitude and the horizontal axis representing time [26].

Consider the specimen in Figure 2.9 with discontinuities labelled B and C. The A-scan illustration of the specimen is also shown in Figure 2.9. An initial pulse (labelled IP) is generated at time 0 seconds. As the transducer probe is moved from left to right along the scanning surface, discontinuities will appear on the display. At time zero when the probe is on the left side, only signal IP and signal A (the ultra-sonic energy reflected by surface A) will show. As the probe moves to the right, signal A will disappear and signal BW (denoting Back Wall) will appear showing the step in the thickness of the specimen. Signal BW will appear at a time slightly after where signal A was situated. As the probe moves further to the right and passes over flaw B, the signal B will appear at a position slightly halfway between signals IP and BW. This indicates that the flaw is located halfway between the scanning surface and the back wall. When the probe moves over the flaw labelled C, signal C will appear. Signal

C will appear earlier than where B did since the sound wave travels a shorter distance to reach flaw C. The position of the defect (depth) can be found by noting the time delay of the flaw signal and factoring in the velocity of the ultra-sonic wave. The size of the defect is found by analyzing the height of the amplitude signal.

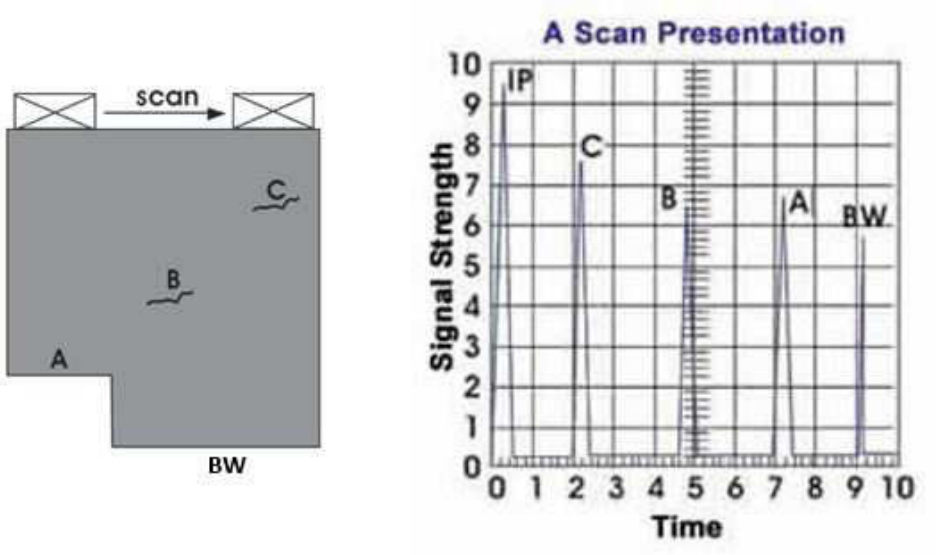


Figure 2.9: Sample with defect (left) and A-scan illustration (right) [26]

3 Objectives

3.1 Assess the use of AniForm as a predictive tool

Assess the applicability of AniForm in the prediction of press-formed CFRTP laminates by performing a study to investigate the relationship between the simulation results and experimental data. This will be achieved by documenting correlations between the numerical and experimental results.

3.2 Define the key process parameters for the forming process

Assess the parameters that affect the manufacturing of CFRTP components and identify the parameters that have the most significant influence on the formability of components. Investigate the optimal setting for these key process parameters to achieve good formability.

3.3 Identify the significance of forming mechanisms to the forming process

Identify the forming mechanisms that have a significant influence on the formability of components. The forming mechanisms need to be tracked and assessed because the occurrence of defects is closely related to the mechanisms and the manner in which they manifest. Establish which mechanisms are desirable and which are undesirable as well as their limitations. Analyse the production process with the intention of identifying practices that aid or impede the forming (i.e. forming mechanisms) of components.

4 Apparatus

4.1 Aerosud CFRTP Facility

The research was undertaken at the Aerosud Aviation CFRTP manufacturing facility. The facility is equipped with 2 hydraulic machine presses. The presses are equipped with infra-red ovens and a shuttle system that transports the material between the work stations. The large press is rated to 600 tons and the smaller press to 80 tons, the 600 tons press is presented in Figure 4.1. The rating of the press and the size of the press beds determine the size of parts that can be manufactured. All other equipment and services that were required to support the forming process were made available by Aerosud Aviation and any services that could not provided for in-house were subcontracted.



Figure 4.1: Aerosud CFRTP 600 tons hydraulic press

Figures 4.2 A and B show the main sections and systems that make up the hydraulic press.

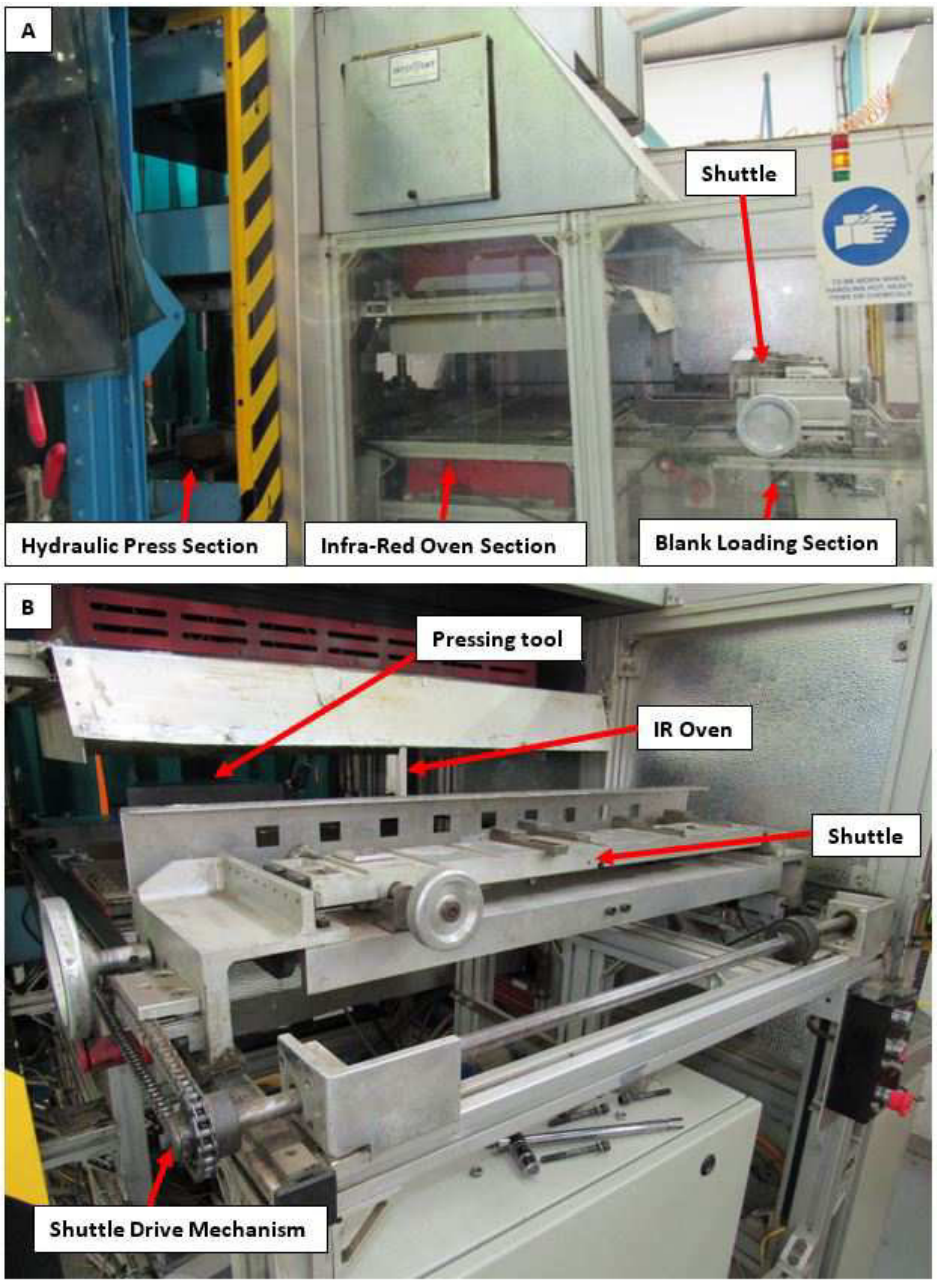


Figure 4.2: Aerosud CFRTP 80 tons hydraulic press.

Figure 4.3 shows the components that are involved in the forming stroke. The top tool was mounted onto the press-ram and the bottom tool onto the press bed. The top tool was equipped with cartridge heaters, the connection to the power supply can be seen. The press-ram moved down to action the forming stroke which effectively closed the tool-set. The motion was guided by guide cylinders that ensured that the tool set remained aligned.

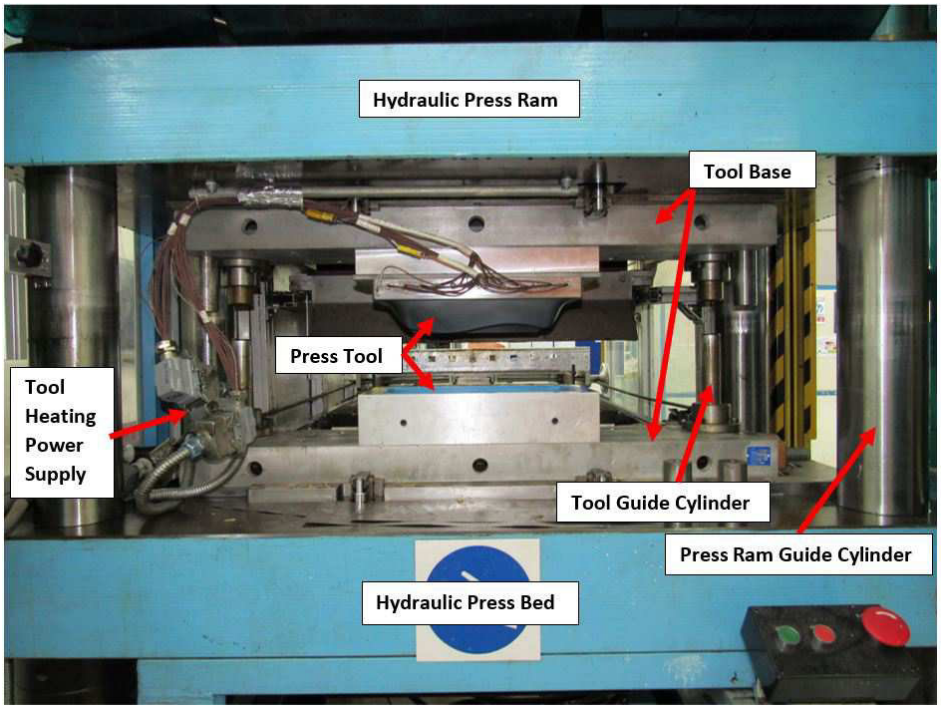


Figure 4.3: Aerosud CFRTP 80 ton hydraulic press, press-bed side.

The top insert in Figure 4.4 shows the IR oven that is used to heat the laminates. The oven has heating lamps position above and below the blank to provide an optimum heat distribution. The oven is equipped with heat shields that aid in shielding the oven from the environment. The bottom insert in Figure 4.4 shows the oven in operation. The laminate is shown suspended from a frame that was specifically designed to fit the different blanks.

The 80 ton hydraulic press is equipped with the control panel shown in Figure 4.5 A. This interface is used to operate all the systems that make up the hydraulic press. The control panel also allows for critical press parameters to be monitored during the pressing cycle (Figure 4.5 B). The apparatus that is being presented is of the 80 ton hydraulic press, the 600 ton hydraulic press is a scaled up version of the 80 ton hydraulic press. It is identical in layout and operation.

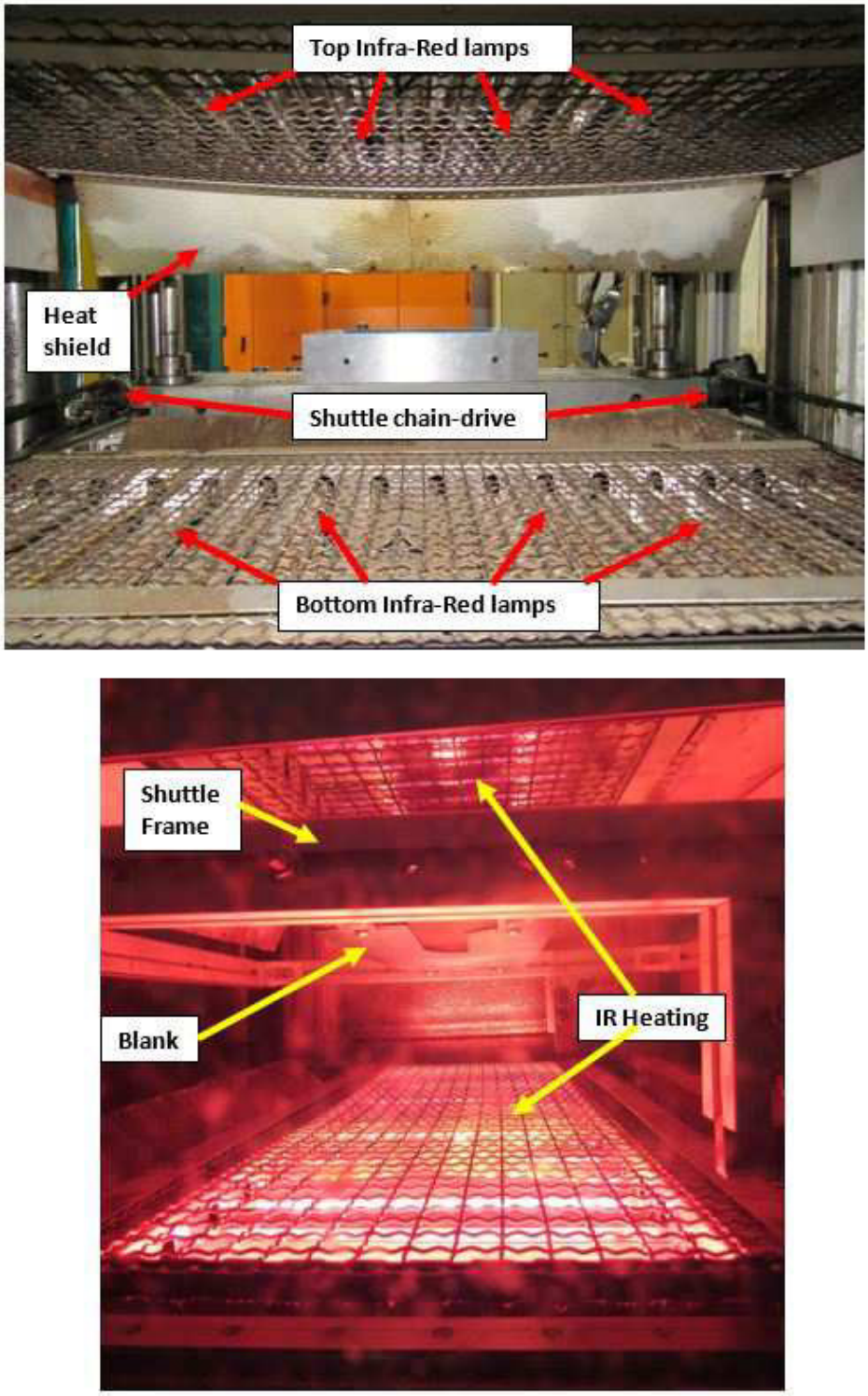


Figure 4.4: 80 ton hydraulic press IR-oven.

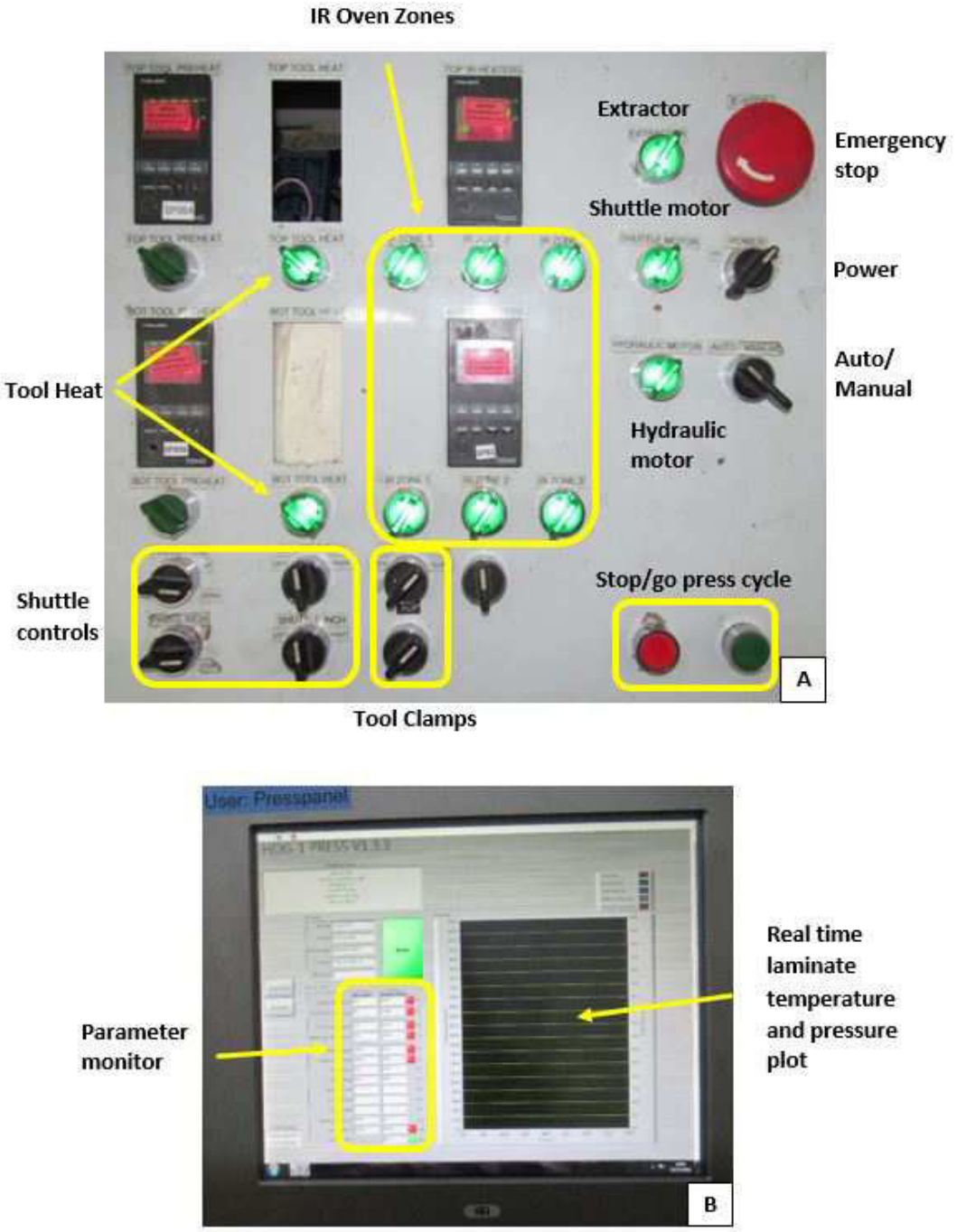


Figure 4.5: 80 ton hydraulic press control panel.

Table 4.1: 600 ton Hydraulic Press Specifications.

Hydraulic Press	Maximum force: 600 ton (4 pillar press)
	Tool Heating: ±200°C within 2 hours*
	Integrated SQL (Structured Query Language) database for receipt handling and reporting
IR Oven	226 lamps with total output of 312kW
	Heating bed divided into 4 individually controlled heating zones
	Emissivity temperature measurement for heat supply control
Shuttle	Maximum operating speed: 1,5m/s
	Drive encoder position feedback

*Depends on tool size.

The two hydraulic presses are identical in operation. The small press is equipped with 1 pillar and can achieve a maximum force of 80 tons. The small press is also equipped with a smaller heating oven.

4.2 Forming Tools

Figure 4.6 presents some of the tools that were used during the investigations. Insert A shows a tool set mounted onto the press and insert B shows the male punch attached to the ram of the press and the rubber die to the bed. Insert C and D shows another tool pair. The machining of the steel tools was contracted to a service provider who had the resources required to produce the complex geometry. The complete tool-sets were assembled by the tool-shop facility at Aerosud. The rubber tools were also cast at the Aerosud facility.

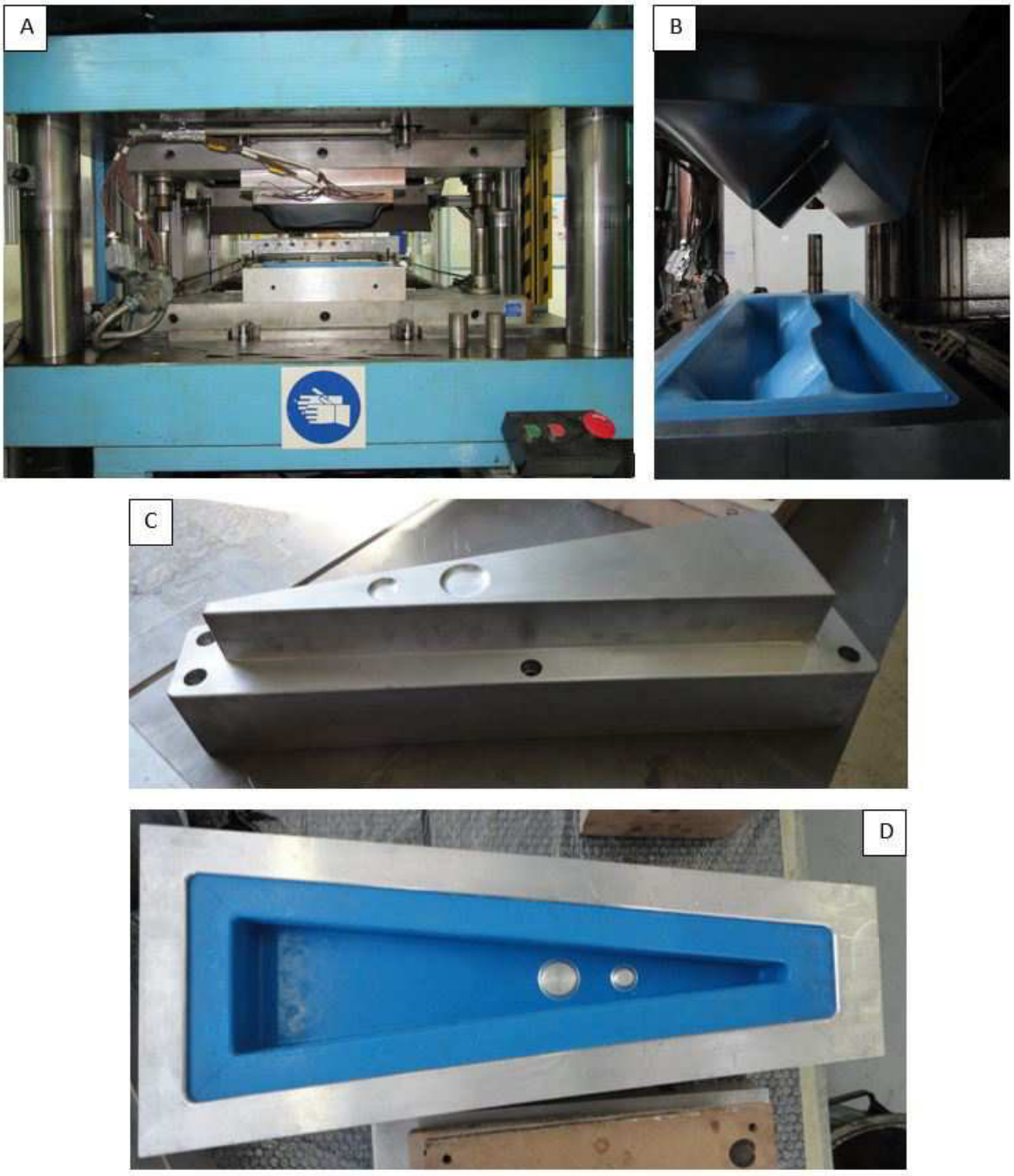


Figure 4.6: Forming tools.

4.3 Aniform

AniForm was used as the tool to conduct the theoretical investigations. This section serves to justify the use of AniForm and also familiarise the reader with the interpretation of the results obtained from AniForm. The results from Aniform can be categorised into qualitative and quantitative results. The qualitative results were obtained by examining the deformation of the laminate as it forms the part. Folds and wrinkles can be identified if the mesh resolution is sufficiently fine to represent them. The quantitative results describe what happens to the laminate as it is deformed. The state of the quantitative results in the laminate's final geometry can be used to make assertions on the formability of the geometry. The qualitative results are all a function of the quantitative results, they are effectively a physical/geometric interpretation of the quantitative data.

Table 4.2 presents the quantitative results and the forming defects that they can be used to identify, as well as the criteria for defect identification according to AniForm. Figure 4.7 details how the results are interpreted to identify the existence of defects. Figures 4.7 A and B show plots of fibre stress with the presence of fibre stress concentrations. This type of stress distribution can be linked to the defects listed in Table 4.2 that relate to fibre stress. Figure 4.7 C presents a shear angle plot with shear localization, this predicts the occurrence of wrinkles. Whereas, the shear plot presented in Figure 4.7 D presents a smooth shear distribution which predicts good formability.

Table 4.2: Interpretation of AniForm results [4].

Result	**Defect**	**Criteria**
Shear angle	Ply wrinkling	Shear localisation
Fibre stress	Resin squeeze-out	$>$ 15 MPa and stress concentration
	Fibre & ply buckling	$<$ 0 MPa

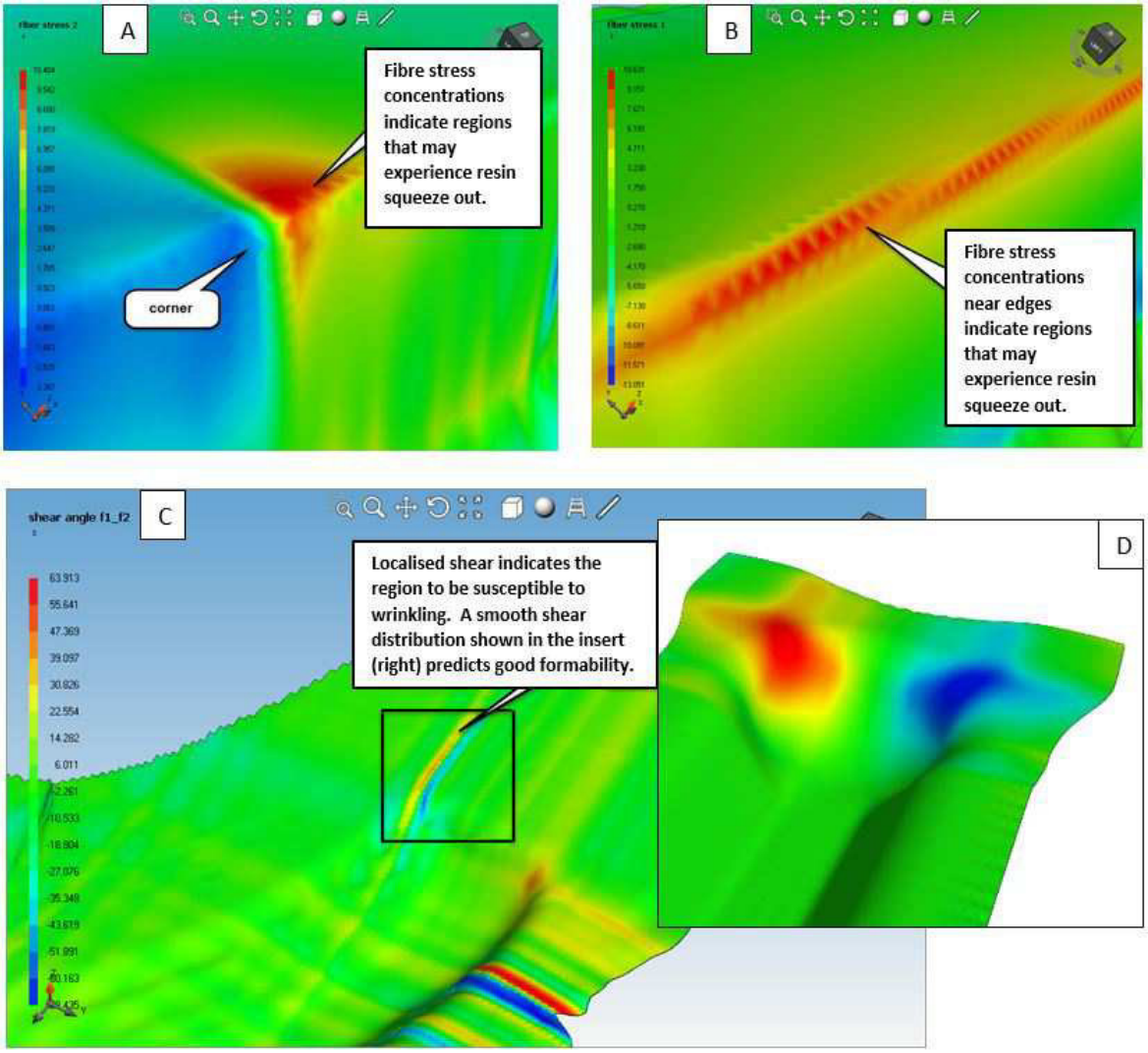


Figure 4.7: AniForm results interpretation guide [4].

5 Methodology

1. **Confirm the validity of the AniForm simulation solutions.**

   The validity of AniForm was assessed by comparing the simulation results to that of identical components produced via experiments. This was done by replicating components that presented good formability and those that showed bad formability or had defects. The results of this comparative study have been presented in Section 6. The comparative study also served as an instrument for the creation of links between the forming mechanisms observed in AniForm and their manifestation in the manufactured product.

   An overview of the results of this study is discussed in Section 6. Specific details of the validation study have been omitted as they mirror the details that are presented in the body of the document.

2. **Investigate the suitability of different geometries to the manufacturing process and formulate suitable manufacturing processes for producing the geometries.**

   After establishing confidence in the applicability of AniForm, it was used to predict the formability of complex geometries. AniForm was used to investigate the effects of the parameters of the forming process. The analysis of the effects of these parameters on the formability allowed for the key process parameters to be identified. The identification of key process parameters and establishing their influence enabled the development of guidelines to follow when developing the manufacturing process for CFRTP components.

   (a) The investigations began with an assessment of existing forming tools that were being used to manufacture CFRTP components. These tools were produced before there was access to simulation software. Shortcomings in the design of tools were noted and efforts were made to address these findings using the simulation software. This work has been documented in Section 7.2.

(b) The investigations were then redirected to the analysis of a component that Aerosud had flagged as a 'problem' part. The part was prone to significant manufacturing defects originating from the pressing process. Techniques were formulated using AniForm to improve the manufacturability of the component. The solutions that were formulated using the software were replicated in practice. The results of this investigation are presented in Section 7.3.

(c) As the investigations in paragraph (b) above were carried out, theories were postulated about the effects of the various process parameters on the manufacturability of the component. Test pieces and investigations were formulated to investigate the effect of the process parameters on the product. These investigations have been documented in Sections 7.4 through to 7.11. The investigations analyze the effect of; blank design, laminate boundary control, material orientation, tool temperature, blank temperature, forming speed and pressure on the forming process.

6 Validation of AniForm

The AniForm software is intended for use in modelling the forming of CFRTP composites. The model used by AniForm employs simplifying assumptions that help speed up the convergence of solutions. For instance, the fibre model makes use of a fibre stiffness value that is less than the real stiffness of the material. The lower stiffness can be used because the fibre strain mechanism is limited and requires more energy compared to intra-ply shear and fibre bending, which as a result, dominate the forming. Consequently, the fibre stress results are expected to be different to the stress experienced by the fibres in the practice. The predictions in AniForm are performed with tools that are represented by rigid bodies where as the forming tools that were utilised in this research were rigid-nonrigid sets. According to AniForm, using a non-rigid body for the rubber tool would increase the complexity of the problem without necessarily giving an appreciably better solution [4]. The analysis in AniForm also assumes an isothermal laminate, in practice the forming process involves a significant amount of heat transfer. The aforementioned are all statements of the assumptions that AniForm uses in its model.

A study was conducted to validate the solutions obtained from AniForm. The validity of Aniform was assessed by comparing the simulation results to that of identical components produced via experiments. This also gave insight into the interpretation of the results.

Figures 6.1 and 6.2 present a comparison of these results for complex geometries with predictions of resin squeeze-out and wrinkling. The simulation result presented in Figure 6.1 shows the predicted shear angle distribution in the first ply of the laminate after the geometry has been draped. The notation represents orthogonal tows as 0° and this figure increases or decreases as the ply experiences intra-ply shear. The predictions of the geometry in Figure 6.1 show shear localization in the 3 marked regions. The presence of shear localization indicates that the region has a susceptibility to develop wrinkles and indeed, one of the regions developed a wrinkle in the practical experiment.

The simulation results presented in Figure 6.2 shows the predicted fibre stress in the first and second plies (above and below respectively). These are marked 'Fibre Stress 1' meaning that these are fibre aligned with 'Direction 1' and 'Direction 2' would be orthogonal to this direction and marked 'Fibre Stress 2'. The simulation results presented in Figure 6.2 show a concentration of high fibre stress in the indicated regions. The experimental component showed evidence of resin squeeze-out in the same region. The results of the investigations showed that the predictions made by Aniform are valid. The use of Aniform to predict the formability of geometries in this research was well grounded.

The simulation results in the body of this document are presented under the headings 'Shear Angle', 'Fibre Stress 1' and 'Fibre Stress 2'. The results of interest are included in the main report and the full set of results have been placed in the Appendix.

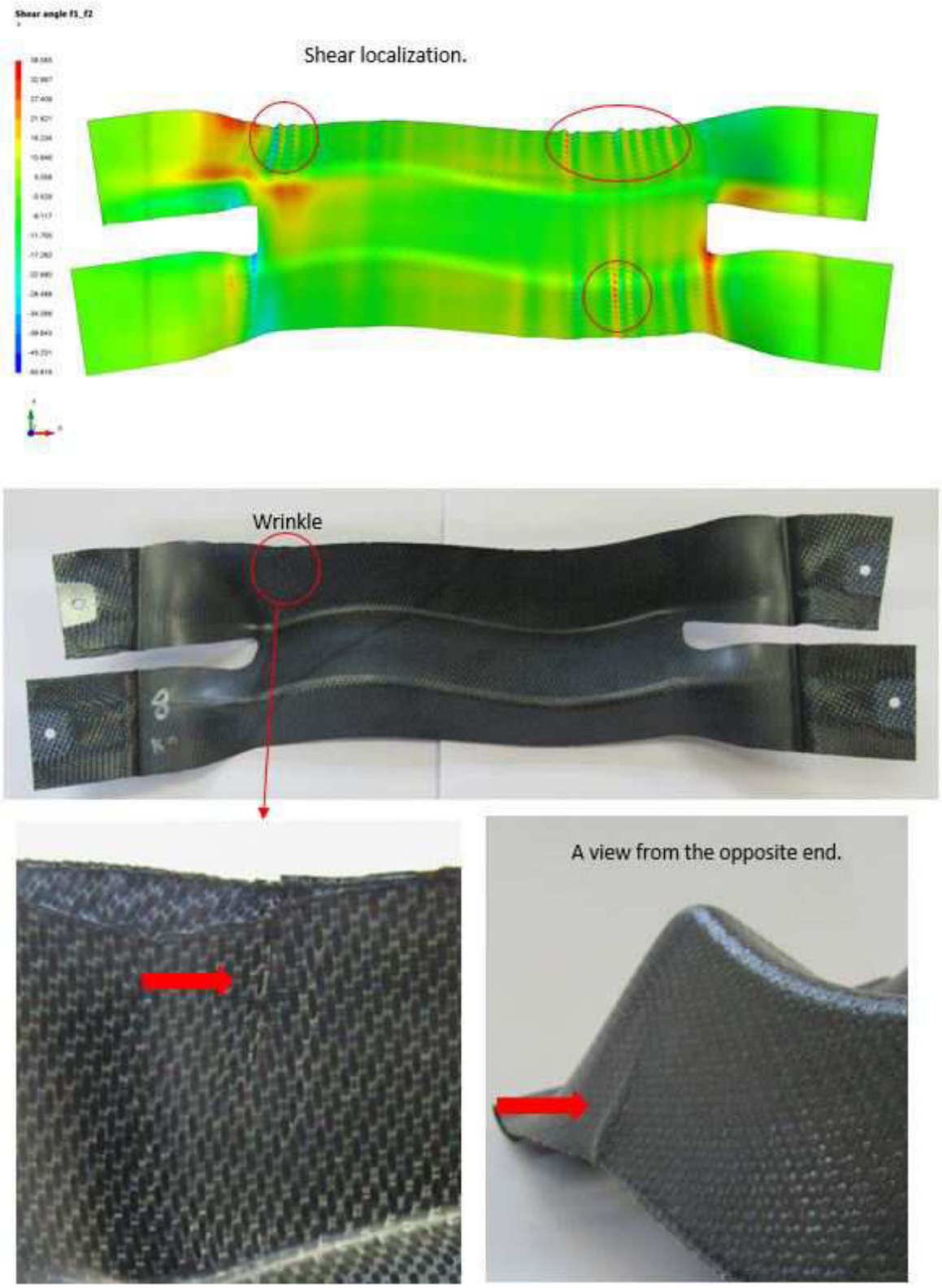


Figure 6.1: A comparison of the shear angle prediction by Aniform to experimental results.

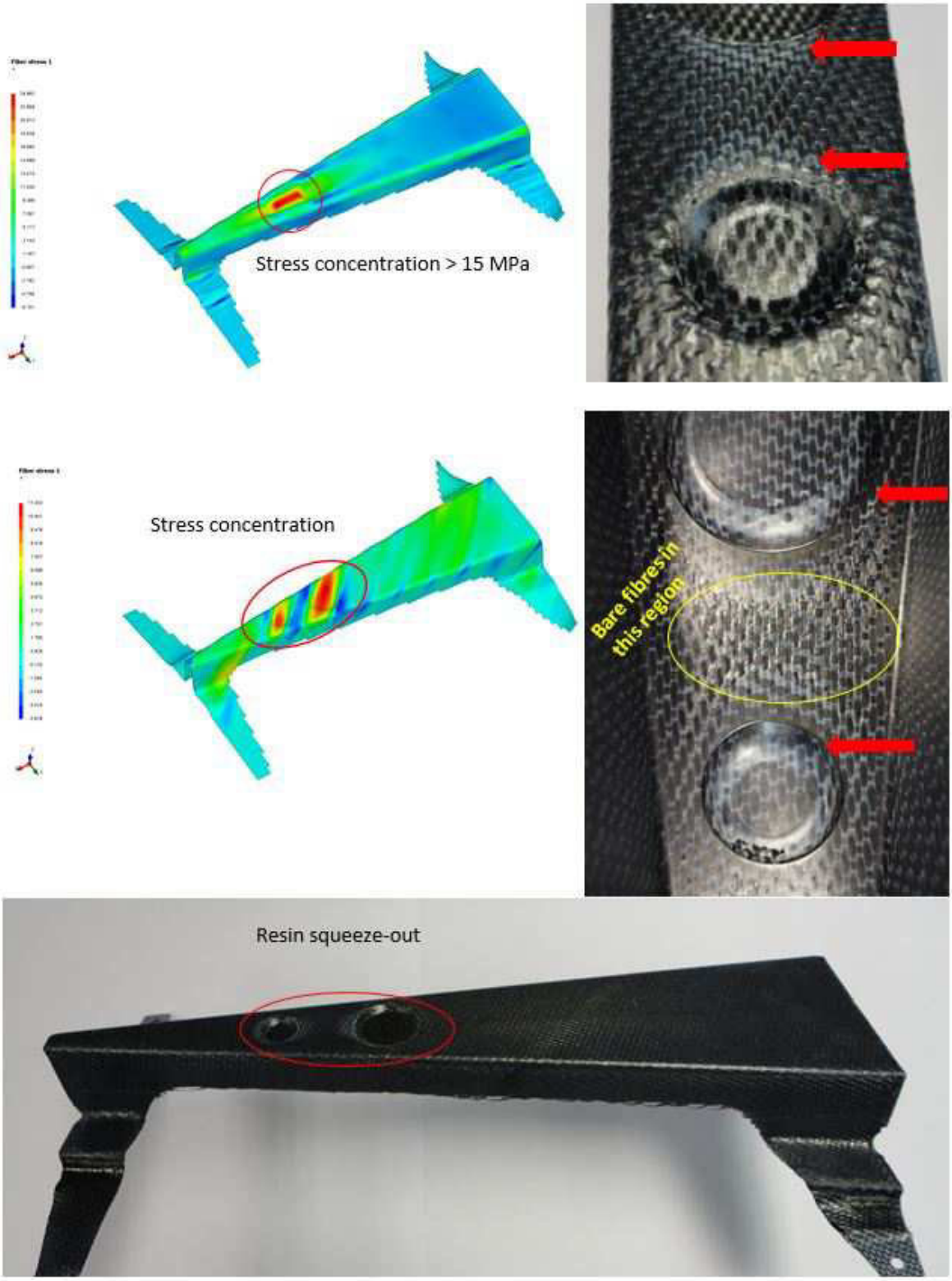


Figure 6.2: A comparison of the fibre stress prediction by Aniform to experimental results.

7 Development of CFRTP Forming Principles

7.1 Introduction

This section of the document is presented in the form of individual investigations, each investigation focusing on a unique objective. The investigations make reference to the different components that were used to conduct the research. The components are introduced here so that the reader can be familiar with their geometry and composition in the succeeding sections.

- **Lower Connection Unit.**

  The lower connection unit (LCU) is a component with geometry that is regarded as complex because it has varying degrees of double curvature. The component is 1700 m long requiring continuous fibres to span the entire length whilst mapping the complex geometry.

  The LCU was manufactured from a glass-polyetherimide composite called TenCate Cetex Premium, the data sheet for this material can be found in Appendix A. The material consists of 5 plies, each with a thickness 0.23 mm, giving a laminate thickness of 1.15 mm. Each of the plies comprises a balanced woven fabric with fibres oriented in the 0°/90° directions. Figure 7.1 shows the LCU and the material orientation.

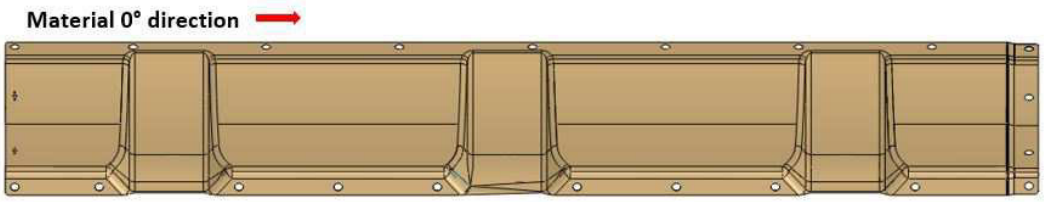


Figure 7.1: LCU geometry and material direction.

- **Rudder components.**

  The rudder was designed as a technology demonstrator for Aerosud Aviation. Its design was adopted from an aluminium rudder and was optimised for manufacturing using CFRTP and other novel technologies such as additive manufacturing and induction welding. The rudder was structurally tested to benchmark the use of these novel technologies against the aluminium structure and traditional joining techniques. The rudder assembly is shown in Figure 7.2.

  The ribs, spar, leading edge and the cleats were all manufactured using the rubber-die forming process. The components were manufactured from a carbon-polyphenylene sulfide composite called TenCate Cetex PPS. The data sheet for this material can be found in Appendix A. The material comprised 4 plies, each of the 5 harness satin woven plies was 0.31 mm thick giving a laminate thickness of 1.24 mm. The fibres in the two outer plies were oriented in the $0°/90°$ directions and the fibre in the two inner plies in the $\pm 45°$ directions. The $0°$ direction of the material was aligned with the axis of symmetry for all the components.

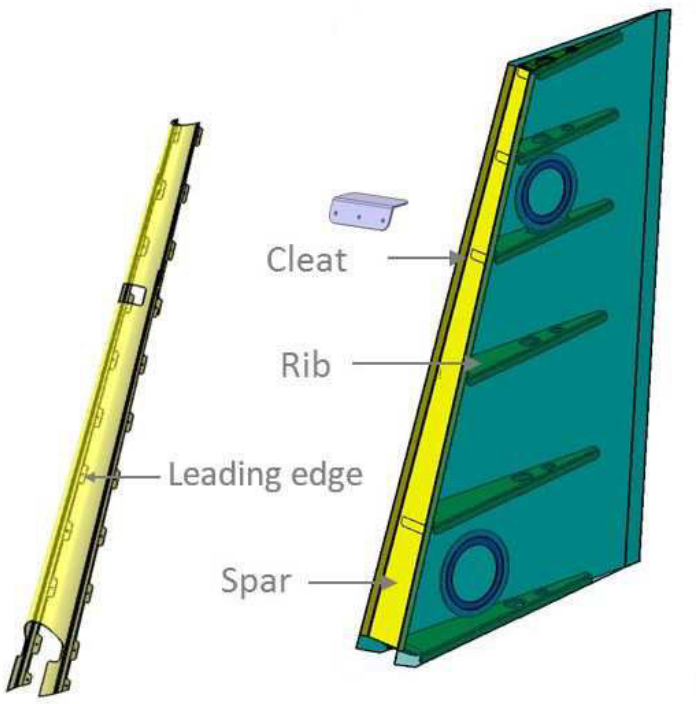


Figure 7.2: Rudder assembly.

- **C-section and Z-section.**

  The range of geometry types that are manufactured using CFRTP is very large. The C and Z sections were chosen because they are typical of the geometry of clips and brackets used in aircraft structures. The bend-lines for the C-section were curved and those of the Z-section took the shape of an S curve. The models for these components are shown in Figure 7.3 and the drawings in Figure 7.4.

  The forming tools for the LCU and rudder components preceded this research so the development of these components (C and Z-section) offered the opportunity to design forming tools in parallel with Aniform's formability prediction studies. These components were developed to further test the forming guidelines that were developed.

  These components were manufactured from the same Carbon-Polyphenylene Sulfide material used for the rudder components. The material comprised 4 plies, each of the 5 harness satin woven plies was 0.31 mm thick giving a laminate thickness of 1.24 mm. The fibres in the two outer plies were oriented in the $0°/90°$ directions and the fibre in the two inner plies in the $\pm 45°$ directions. The $0°$ direction of the material was aligned with the long dimension of the blank.

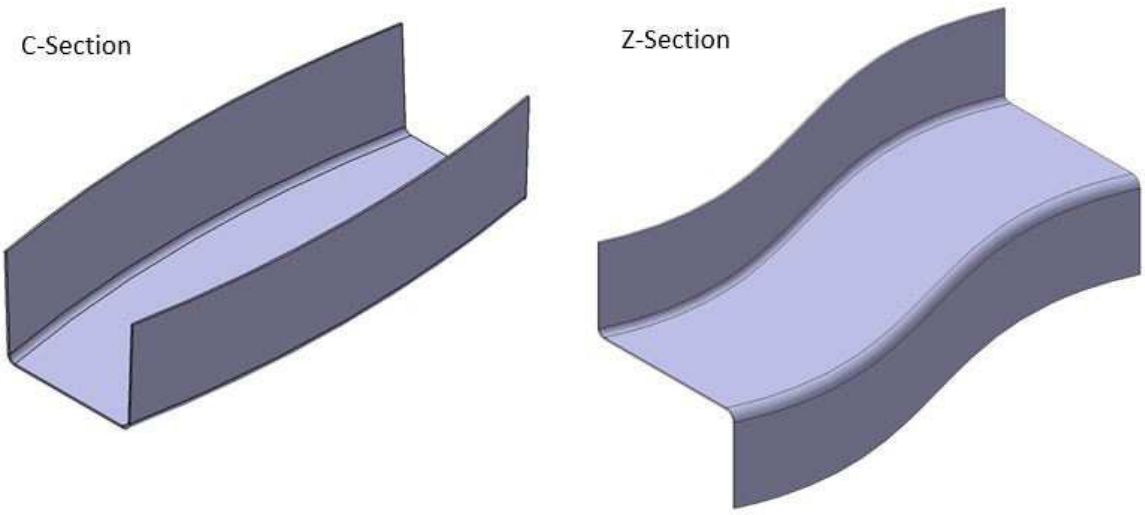


Figure 7.3: Z-section and C-section geometry.

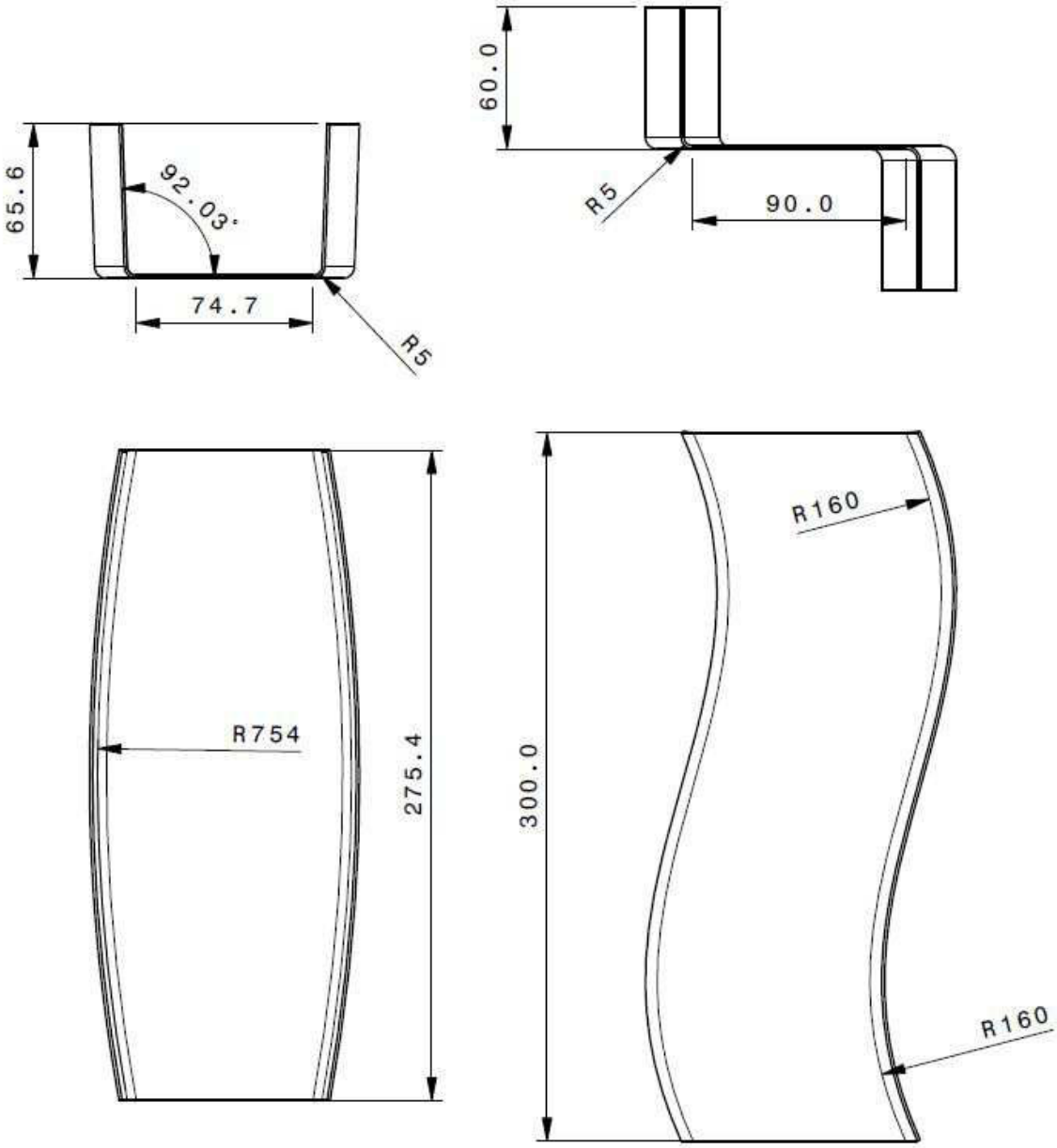


Figure 7.4: Z-section and C-section drawings.

7.2 Investigation 1: Tool Design Considerations

7.2.1 Tool Configuration

There are two main configurations for CFRTP press forming tools, a rigid-rigid pair (male and female) or a rigid-nonrigid pair. The rigid-rigid tool is suitable for manufacturing simple components, it can be effectively used to produce geometries that result in small changes in

laminate thickness after draping. This means that the geometry must require minimal intra-ply shear to be formed, this restricts the application to geometries with single curvature only i.e L, C and Z sections with straight bend-lines. If the laminate has significant thickness variations after being draped into the final geometry, then these variations in thickness must be incorporated into the geometry of the rigid tool. If this is not done, the tool will stop closing when it consolidates the thickest region. This then prevents the thinner regions from being consolidated since they do not experience the required pressure. This makes rigid-rigid tools unsuitable for manufacturing complex geometries with double curvature. The tools used in the investigations for this study were the rigid-nonrigid type.

Figure 7.5 shows the prediction of the shear angle and thickness distribution for the Z-section geometry. This result shows that the change in ply thickness is directly related to the intra-ply shear taking place in the ply during forming. The non-rigid tool in the rigid-nonrigid configuration solves the thickness variation problem by accommodating the changes in laminate thickness. This allows the laminate to assume its draped thickness distribution while still ensuring that the entire laminate is in full contact with both tools and is exposed to the full forming pressure. The flexibility of the non-rigid tool also ensures a uniform pressure distribution within the geometry. In this configuration, the female rubber tool is designed to sit in a container. The container secures the rubber tool as it is pressurized by the rigid male tool. The male tool also acts as a lid to the container preventing the extrusion of the rubber as pressure is applied. The tool must be mounted onto the press with the metal tool at the top and the rubber tool at the bottom. Reversing the arrangement would leave the rubber tool unsecured as it becomes soft due to the heat from the rigid tool and laminate. It would also require the rubber tool to be the one that moves up and down during the pressing cycle. The rubber tool could fall out of the open container. An image of the rigid-non rigid tool is shown in Figure 7.6.

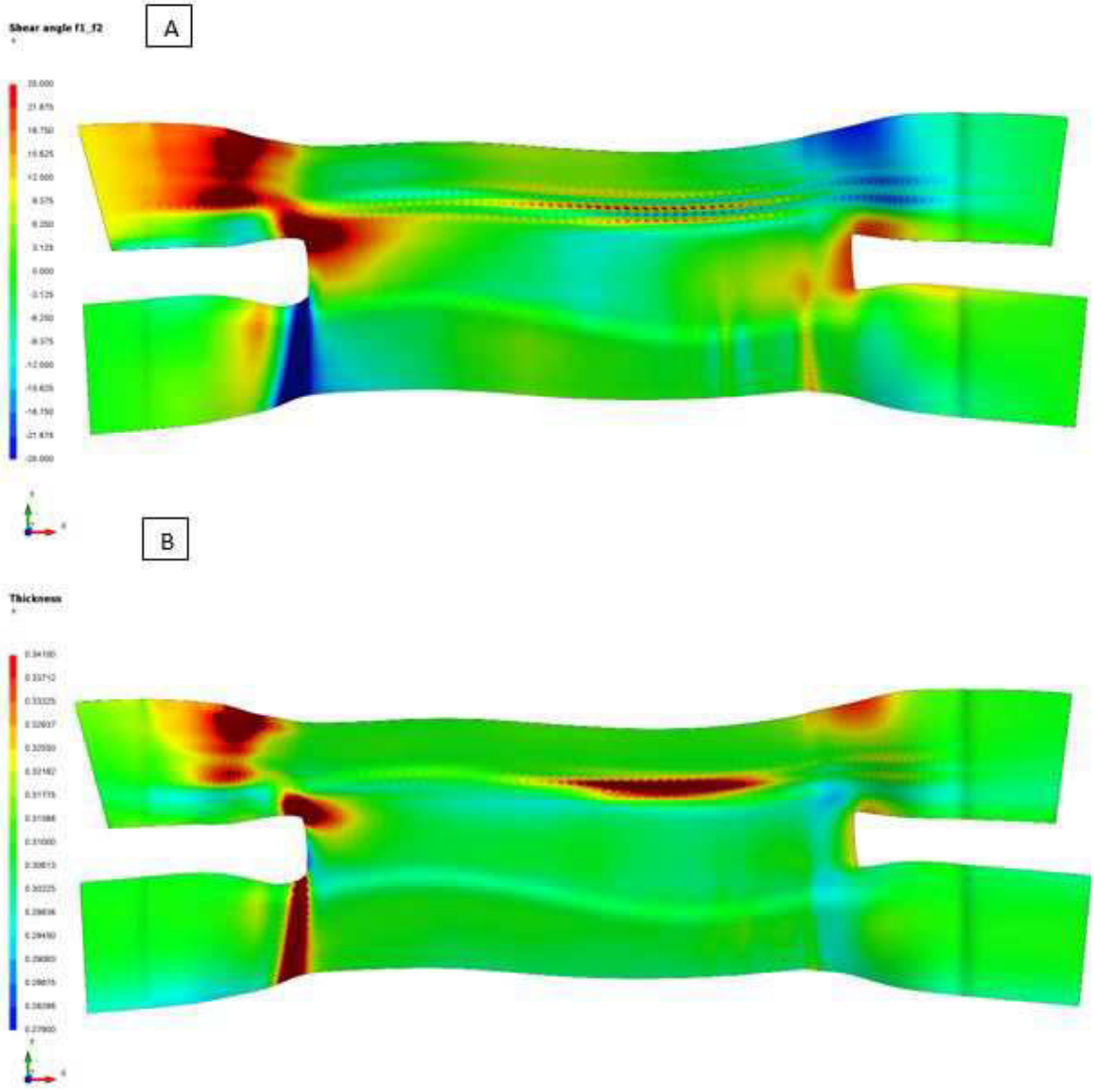


Figure 7.5: (A)Shear angle distribution, (B) Thickness distribution.

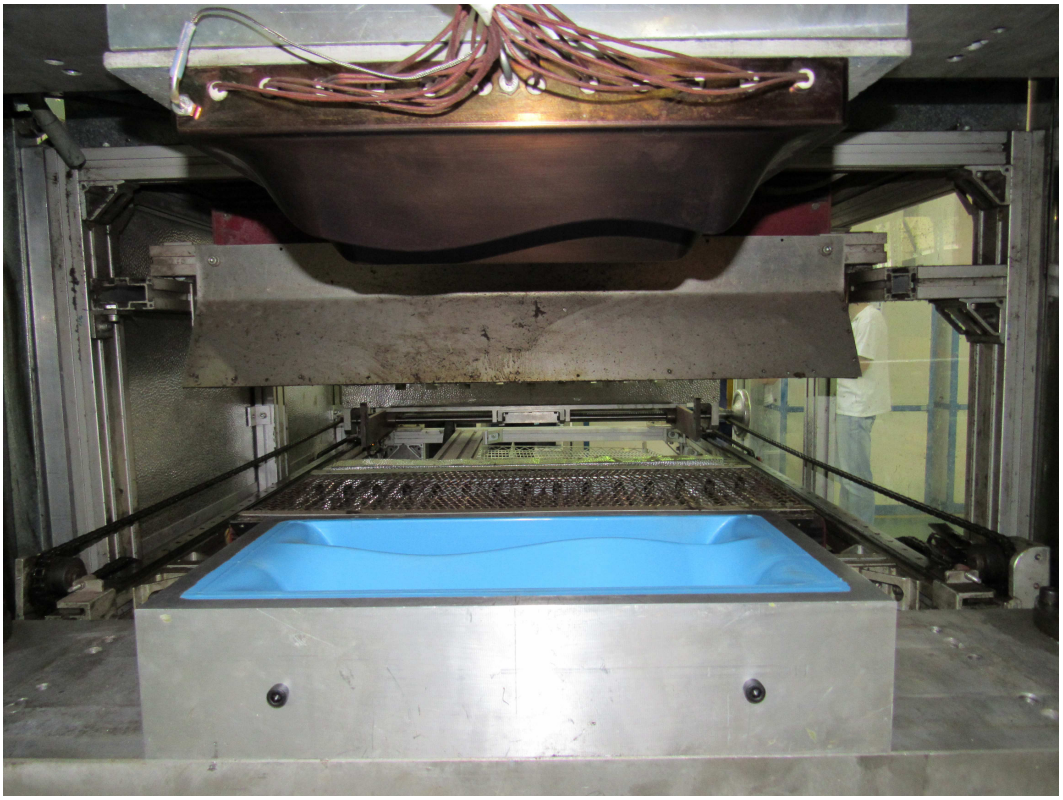


Figure 7.6: Metal-rubber tool.

7.2.2 Tool Design

7.2.2.1 Problem Background

The tools for the rudder components were manufactured before the forming concepts presented in this document were developed. Consequently, the details of the behaviour of the blank during forming were not factored into the design of the tools for the rudder components. Consider the tool for the leading edge for example; the blank for the leading edge was designed with longitudinal tags to stop it from sagging excessively but the tool geometry did not have allowance to accommodate the tags. This resulted in a tool-blank combination that was not in agreement. During forming, the outer ply was sheared off from the laminate (Figures 7.7 A and B) and the longitudinal tags suffered fibre breakage (Figures 7.7 C and D).

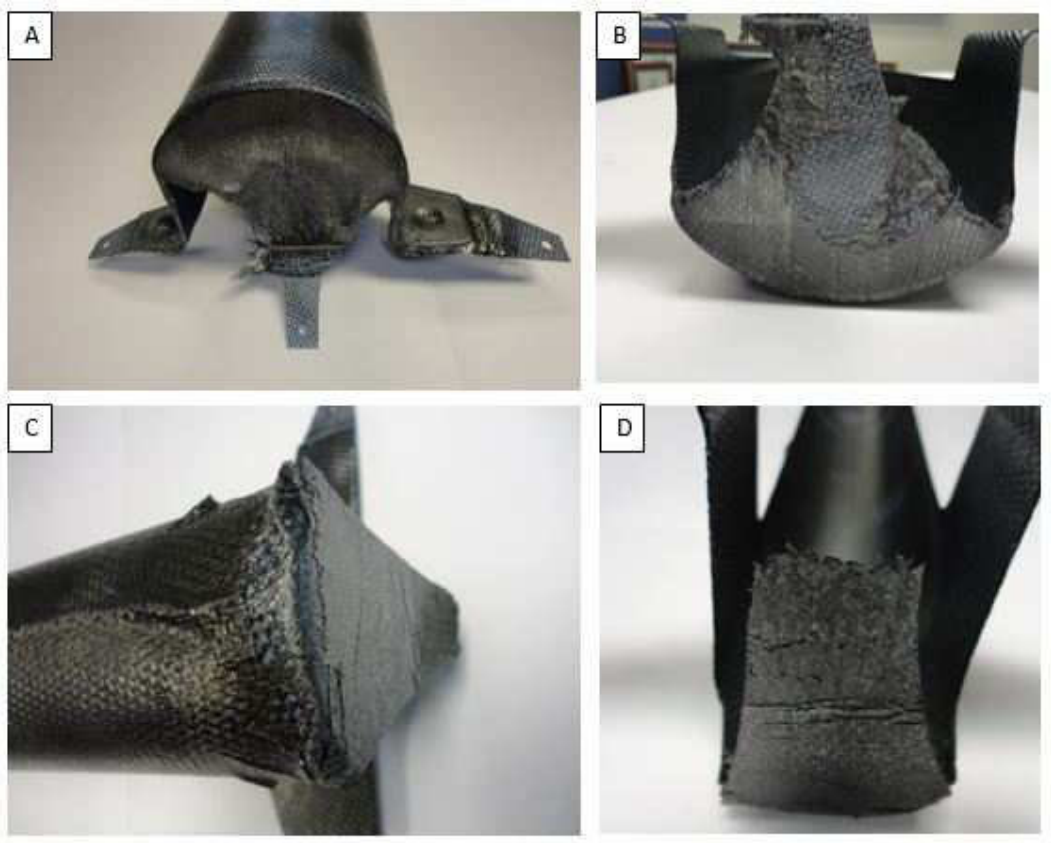


Figure 7.7: Leading edge results.

7.2.2.2 Identification of cause of problems and proposed solution

The cause of the problem shown in Figure 7.7 was mainly due to the fact that the tool was fabricated before the blank design for the geometry was considered. The tool had the surfaces required to manufacture the component but the interaction of the blank geometry with the tool was not considered. In Section 7.4, different blank designs were considered for the manufacturing of the C and Z-sections. Each of the blanks imposes criteria that must be considered in the design of the tool.

The initial stages of the investigation of the formability of geometry in AniForm are executed using moulding tools consisting only of the surfaces required to drape the desired geometry. The investigations regarding tool orientation, blank geometry and BRM stiffness optimisation can be carried out using these simple surface tools. These investigations need to be completed before the tool surfaces are developed further to the complete tool geometry. This is because they have significant influence on the design of the rest of the tool. This is the approach that was taken in the design of the C and Z section tools.

7.2.2.3 Methodology

The problem presented here was taken from the tool of leading edge. The proposed solution was implemented to the design of the C and Z-section. This investigation covers the design of the Z-section tool. The forming surfaces used to perform the initial investigations of the production of the Z-section geometry are shown in Figure 7.8 A. These surface elements were then modified to create the final tool geometry presented in Figure 7.8 B. This geometry needed to be able to form blanks 2 and 3 for the Z-section presented in Section 7.4, Figure 7.28.

The tool geometry was modelled such that it does not impede the forming process. This mostly focuses on the design of the surfaces that channel the tags to the exterior of the tool design to avoid the problem that was shown in Figure 7.7. This region has been marked with a red ellipse in Figure 7.8 B. Obstruction of the tags could prevent the BRM from being effective in the application of the tensile force to the blank. Simulations were performed using both the development tool surfaces and also using the completed tool geometry of the Z-section tool. The simulations were performed using blank 2 with a BRM stiffness of 0.09 N/mm.

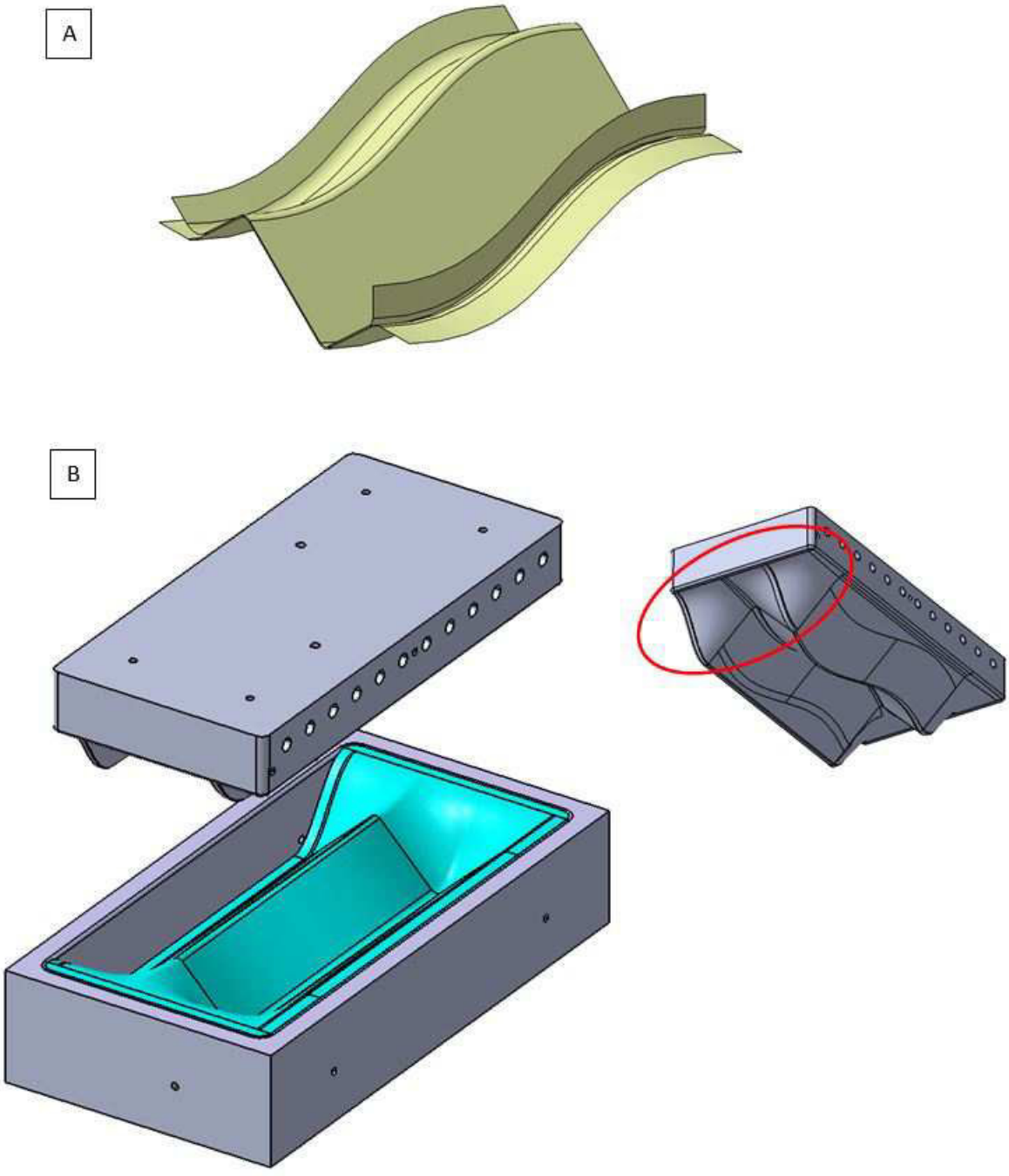


Figure 7.8: (A) Surfaces used for blank development, (B) Final tool design.

7.2.2.4 Results

Figure 7.9 presents the Z-section blank immediately after forming. The relation between the tool and the blank can be seen. The tool geometry has been modelled to allow the tags to 'flow' from the body of the blank to the exterior of the tool where they attach to the BRM. Figures 7.10 and 7.11 show the shear angle results (ply 1 and 2, respectively) of the two phases of the Z-section tool.

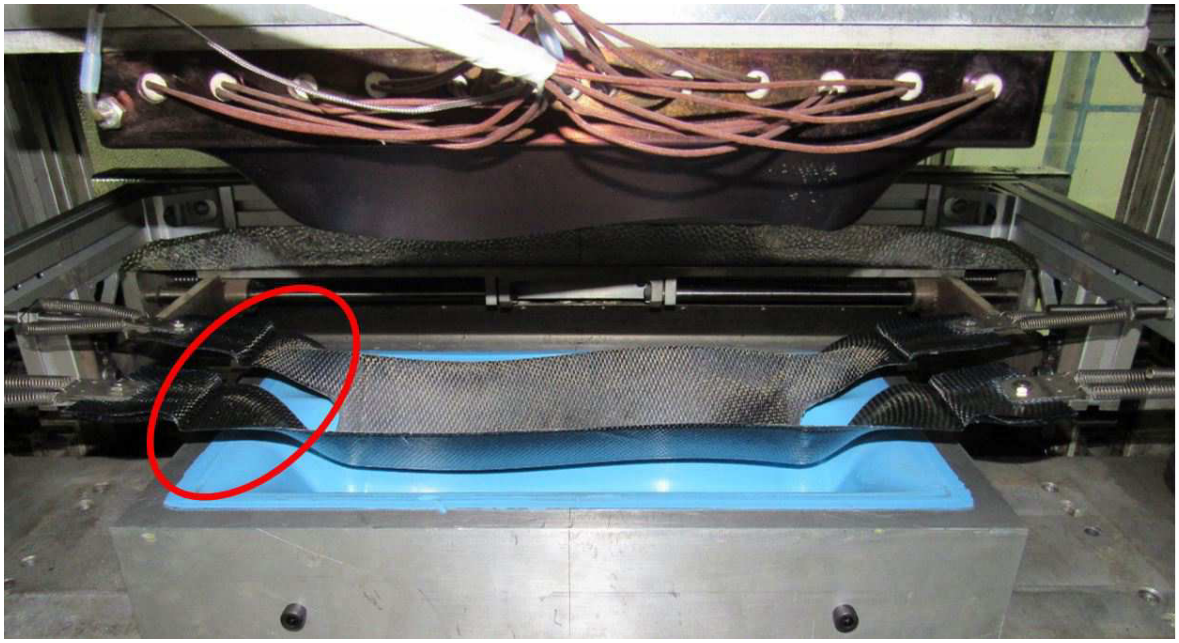


Figure 7.9: Z-section tool design and Z-section blank design relation.

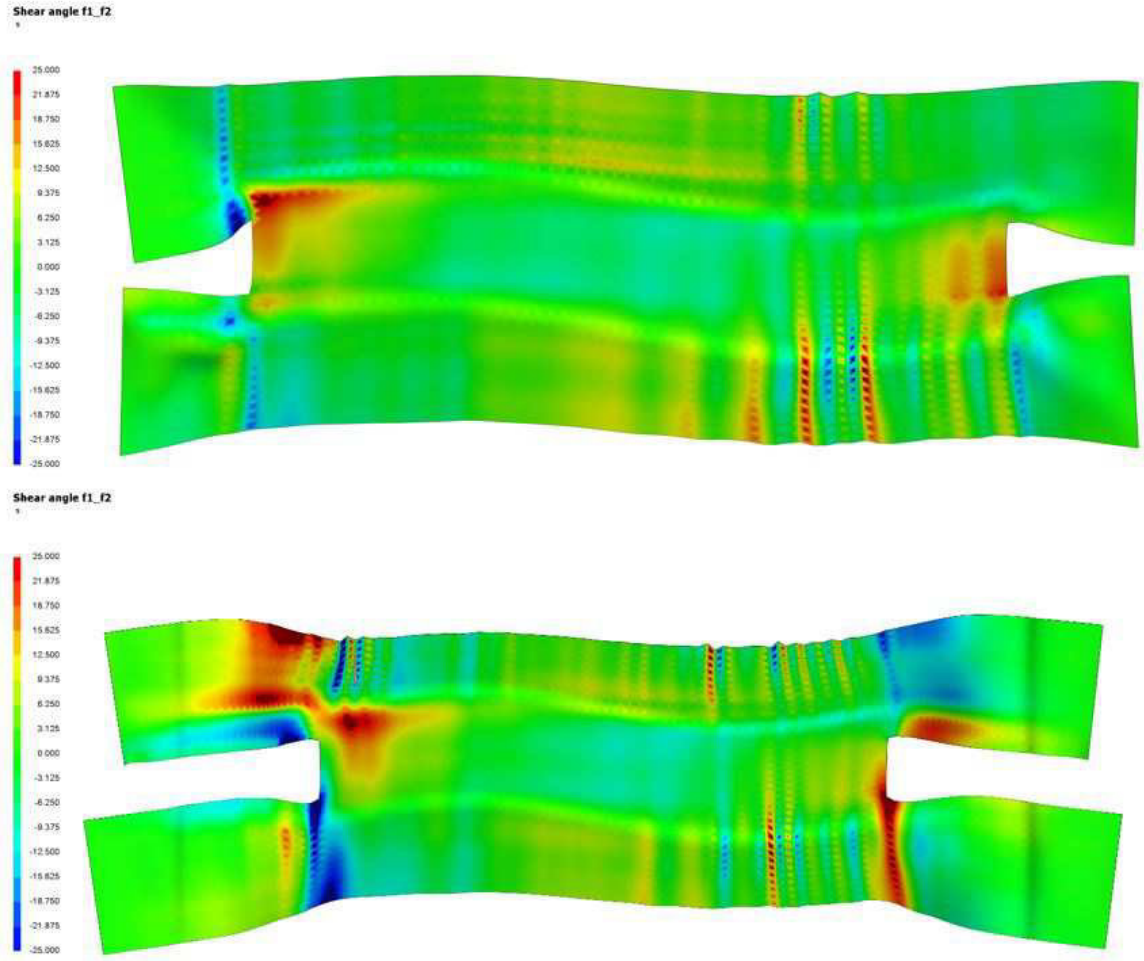


Figure 7.10: Shear angle results for ply 1, forming surfaces only (top) and completed tool (bottom).

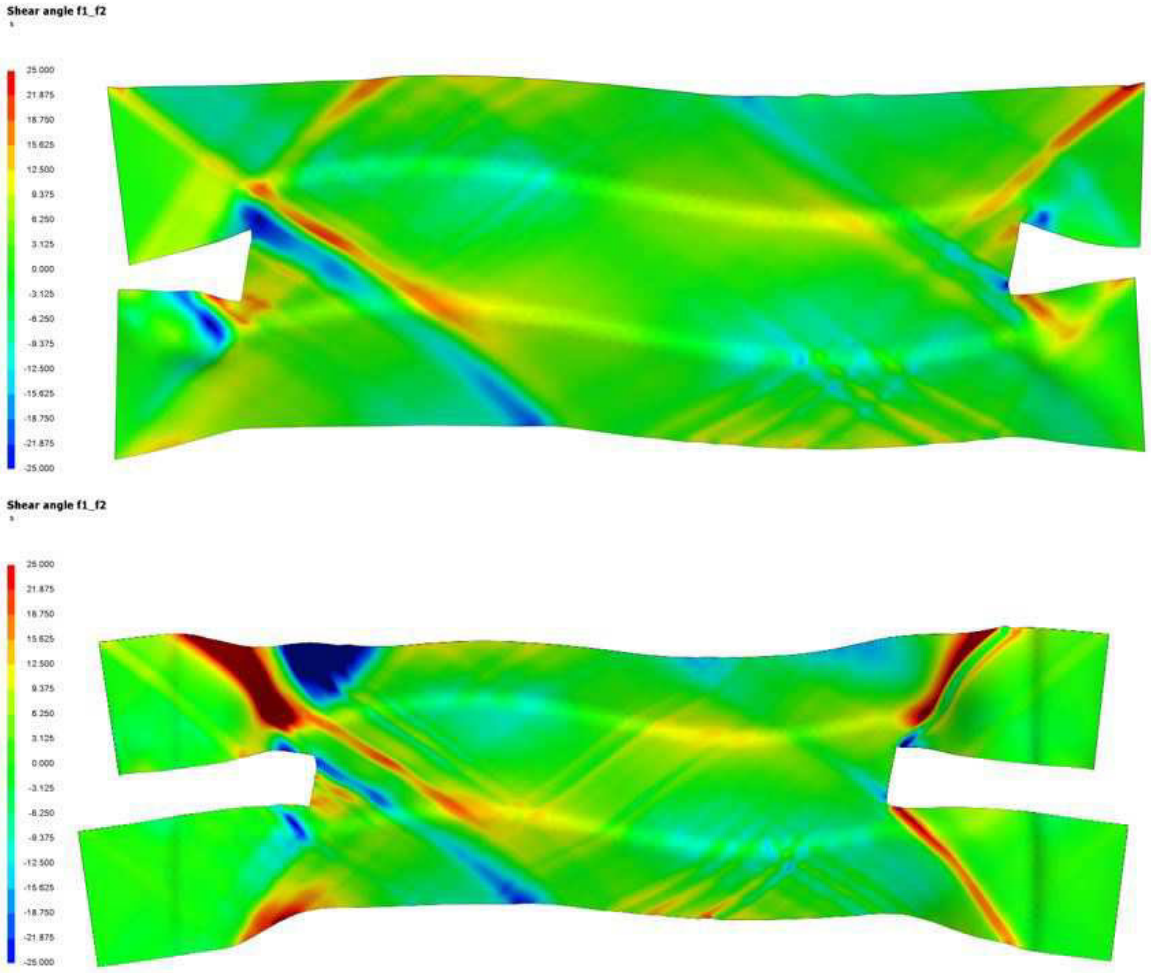


Figure 7.11: Shear angle results for ply 2, forming surfaces only (top) and completed tool (bottom).

7.2.2.5 Discussion

Figure 7.8 A shows the surfaces that were used in the early development stages of the Z-section geometry. These surfaces were used to perform the investigations required to develop a manufacturing solution for the geometry. The blank design was carried out using these surfaces, the simulation results of Z-section blank 2 formed using these surfaces have been presented in Figures 7.10 (top) and 7.11 (top). The results show the shear angle required to form the geometry.

After the acceptance of blank 2 as a suitable candidate to manufacture the geometry, the surface tools must be modelled into a complete tool. The tool that was produced for the Z-setion was presented in Figure 7.8 B, it consists of the upper tool (rigid) and the lower tool consisting of the non-rigid rubber tool and its rigid container. The forming surfaces that were extracted from this model contained the surfaces required to form the geometry and additionally the surface elements required to make a practical tool for the practical experiment.

The incorporation of these additional surfaces has an effect on the manner in which the blank deforms. These surfaces must be contoured in a way that facilitates the forming of the geometry. The final tool design must be evaluated to determine whether the formability of the geometry is still acceptable. The blank design may also need to be updated to accommodate the changes. In the case of the Z-section blank 2, the tags of the blank had to be lengthened to ensure that the BCM clamps do not collide with the tool when the blank is drawn in for the Z-section blank.

The shear angle results for Z-section blank 2 formed using this complete tool has been presented in Figures 7.10 (bottom) and 7.11 (bottom). These results show an increase in shear angle localization in ply 1 (Figure 7.10) and a general increase the shear angles required to form the geometry in ply 2 (Figure 7.10), this marks degradation of formability of the geometry in the final tool simulation in comparison to that of the developmental surfaces.

The relation between the design of the blank and the design of the tool was presented in Figure 7.9. The figure demonstrates how the tool was contoured such that the tags can transition from the junctions to the body of the blank in the tool to the BRMs in the exterior of the tool. The shape of the tool allows the BRMs to apply a tensile force to the blank without obstructions during forming. The defects that were presented in Figure 7.7 can be avoided by developing the blank and tool in a parallel process. This illustrates that the design of the tool can have a significant effect on the formability of a geometry. The discussion presented here reveal the reason that Z-section blank 1 (Figure 7.28) could not be manufactured in

practice using this tool. The blank had it tags running across the length of the tool and there was no allowance for this in the design of the tool.

7.2.2.6 Conclusions

- The design of a tool has an effect on the formability of a geometry.
- The tool must be designed in conjunction with the blank to ensure that the formability of the geometry is maintained.

7.3 Investigation 2: Lower Connection Unit study

7.3.1 Problem Background

An analysis of the existing manufacturing practices at the Aerosud Aviation facility was conducted to identify the impact of these practices on the formability of components. This investigation focuses on the manufacturing process of the Lower Connection Unit (LCU). The component was found to be difficult to form without the occurrence of forming defects as it is a complex geometry.

The component was prone to developing wrinkles shown in Figures 7.12 E and F at random places on the entire body of the part. These wrinkles occurred on different locations on components which were manufactured under the same conditions. The LCU had folds and wrinkles on the regions marked B, C and D, these are shown in inserts Figures 7.12 B, C and D.

The components also suffered an insufficient geometric definition in the region shown in Figure 7.13. The laminate profile bridged along the red curve connecting the two corners instead of draping onto the geometry of the tool. The fibres in this region clearly experience high tensile loads and display further evidence of this in that fibre bunching is visible which gave the region a rough surface texture.

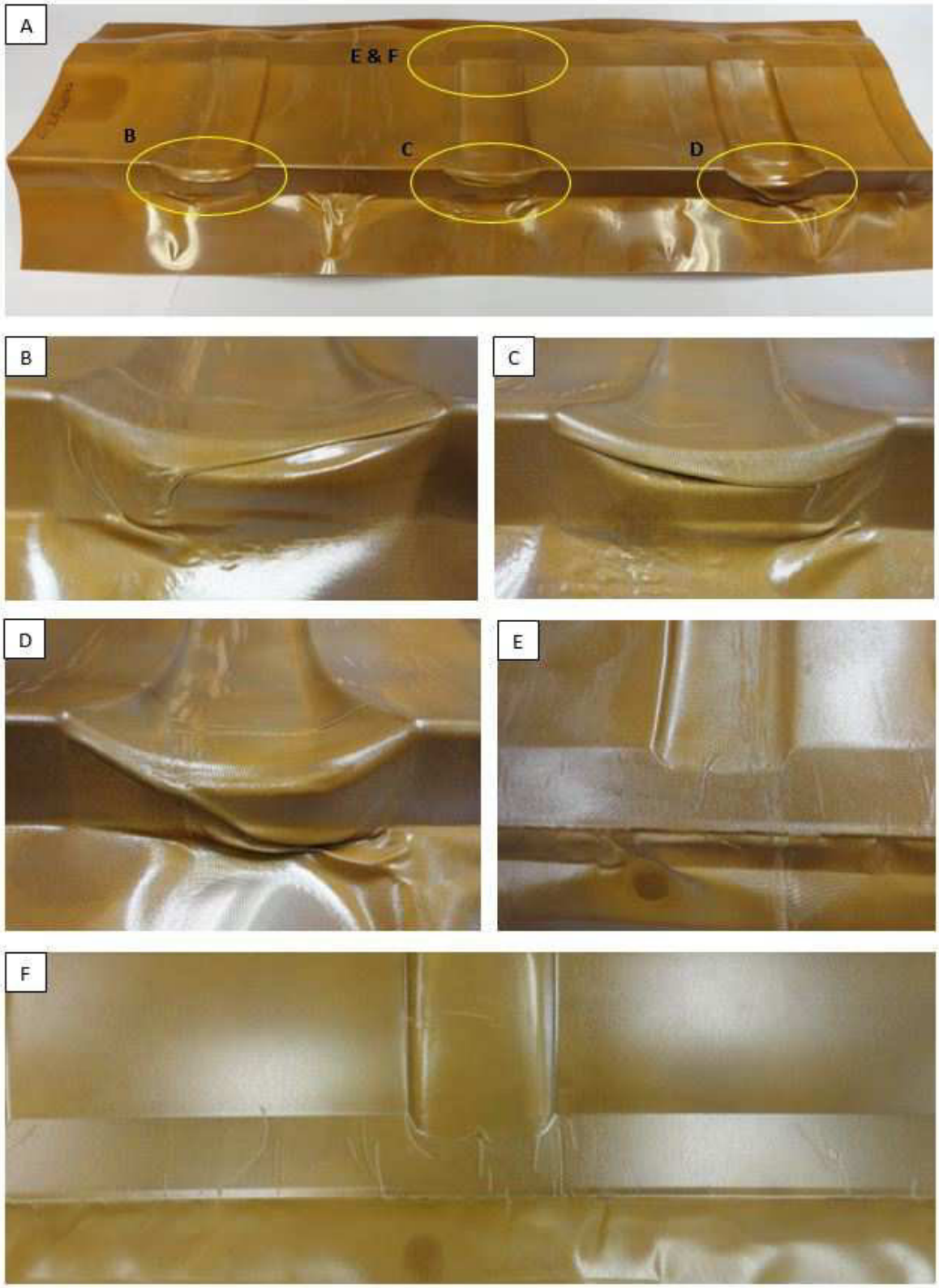


Figure 7.12: Defects on the LCU

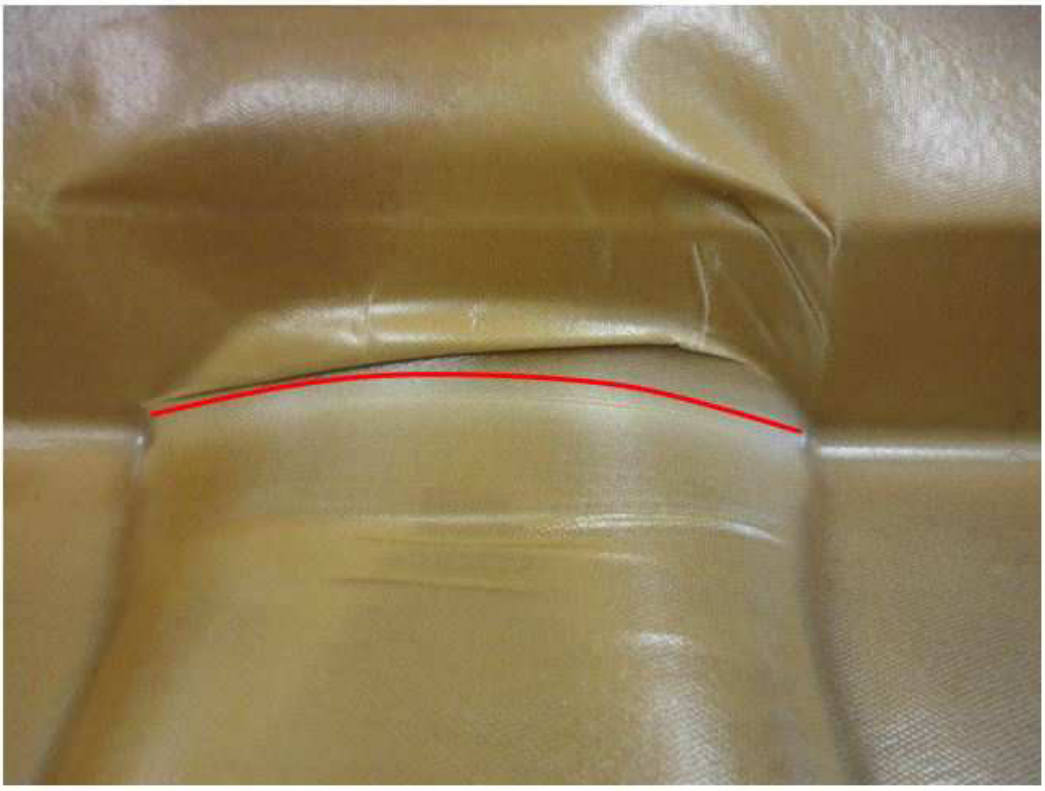


Figure 7.13: Fibre stretching and laminate bridging.

7.3.2 Identification of cause of problems

The LCU blank was not firmly secured during forming. The blank would be released from its supporting frame as it was acted upon by the tool. The problem brought about by this set-up can be explained in terms of energy. During the pressing stroke the restrained blank stores energy as the fibres straighten and strain and the blank deforms. The sudden release of the blank results in this stored energy being dissipated. The dissipation of this energy causes an instability in the geometry of the blank and it forms wavy undulations that result in wrinkles in the final component. The wrinkles and folds resulting from this scenario would be random and unpredictable as was observed in the forming of the LCU.

The blank for the LCU was much larger than it was required to be. A comparison between the blank and the trimmed component is presented in Figure 7.14 showing the position of the trim lines. The excess material on the oversized blank contained fibres that extended within the trim-line (since the fibres are continuous). The use of an oversized blank meant the material that would be trimmed away was affecting the formability on the component. The excess material could buckle and serve as an originating site for folds and wrinkles which can propagate to the useful region of the blank. The action of the laminate folding over itself in the complex region was evidence that the laminate was buckling in those specific regions during forming.

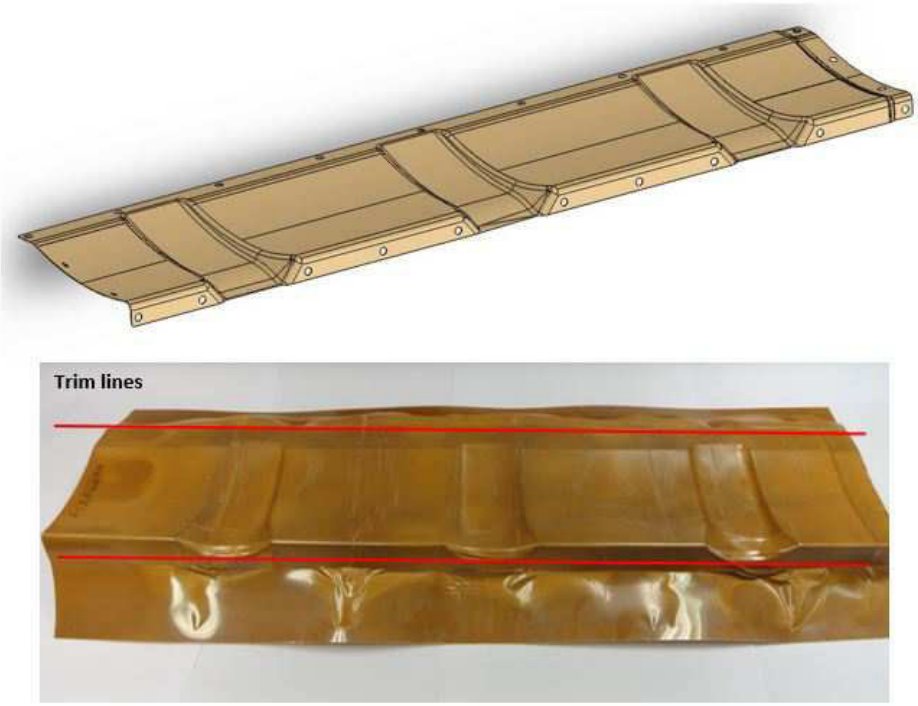


Figure 7.14: (Top) Trimmed component and (Bottom) Oversized blank.

Referring to geometry of the LCU in Figure 7.15 and considering points A and B, there are fibres at both these points running along the entire length of the blank in the 0° direction. The geometry that the fibre at A must map is complex compared to that of the fibre at B. The length of fibre required to map the geometry at A is longer than that needed at B because of the path it must track. Since the initial shape of the blank is flat, this can then be viewed as fitting the same length of fibre to paths A and B. This would result in large fibre stresses along path A.

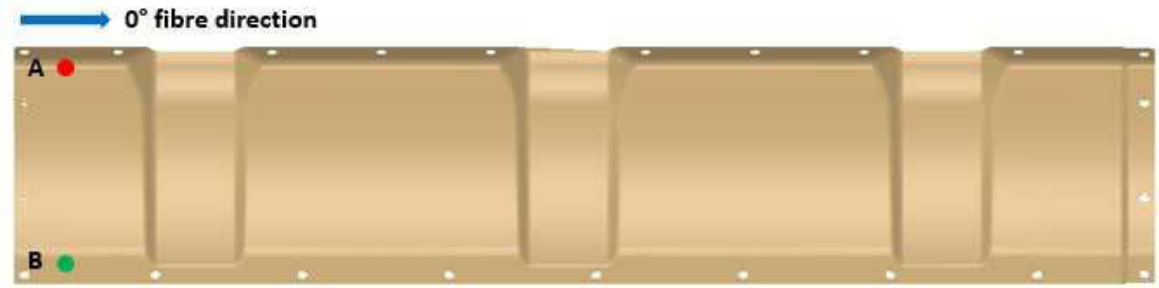


Figure 7.15: LCU geometery.

The lack of geometric definition in the component occurs as a result of laminate bridging. Bridging occurs when the laminate fails to drape onto the metal tool as a result of the rubber failing to press the blank onto the metal tool when the tool set is in its closed position. The diagram in Figure 7.16 shows the tool before the cavity is closed. This figure represents a part of path A discussed in the previous paragraph. The forces that strain the fibres as the tool closes are labelled F in Figure 7.16, these forces load the fibre in this region in tension. The tension in the fibres makes the laminate taught, consequently the laminate compresses the hump on the non-rigid tool preventing the cavity between the tools from being filled when the tool is closed. The side of the laminate adjacent to the rigid tool will not be in contact with the tool in this region. As a result, the laminate does not attain the required geometry. The large fibre stresses generated by this phenomenon exacerbates the wavy undulations (the over and under property of the weave) of the orthogonal fibres giving the region the rough texture.

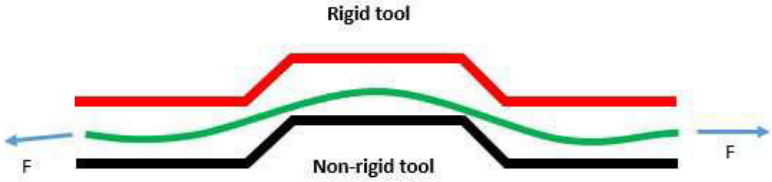


Figure 7.16: Laminate bridging.

7.3.3 Proposed solution

7.3.3.1 Blank Boundary Control

A solution that addressed the release of the blank during forming was required. A restraint system that supports the blank as it is formed was consequently designed. The restraint system was required to prevent the blank from being released without restricting the mobility of the blank, the blank must remain free to move and deform when acted on by the tool. Fully constraining the blank would inhibit the forming mechanisms from taking place as the component is formed. The continuous fibre property of the material creates a system where fibre restrictions at one point can have effects on another region sharing the same fibres.

The restraint of blanks in CFRTP forming is usually achieved by the use of springs or blank holders that restrain the blanks using friction. The spring method was found to be better suited to the requirements of this investigation. This method of restraining the blank could be used with the existing forming tools. The frictional approach would have required completely new tools to be designed specifically for use with this method of blank restraint.

A blank restraint mechanism (BRM) was designed for the CFRTP manufacturing process. The mechanism consisted of several clamps each made from 3 plates that were secured to the blank using a bolt and nut. The clamp assembly was attached to a frame using springs, and the frame was mounted onto the shuttle that moves the blank to the desired stations on the press. An illustration of the BRM and the frame set up are shown in Figures 7.17 (A) and (B).

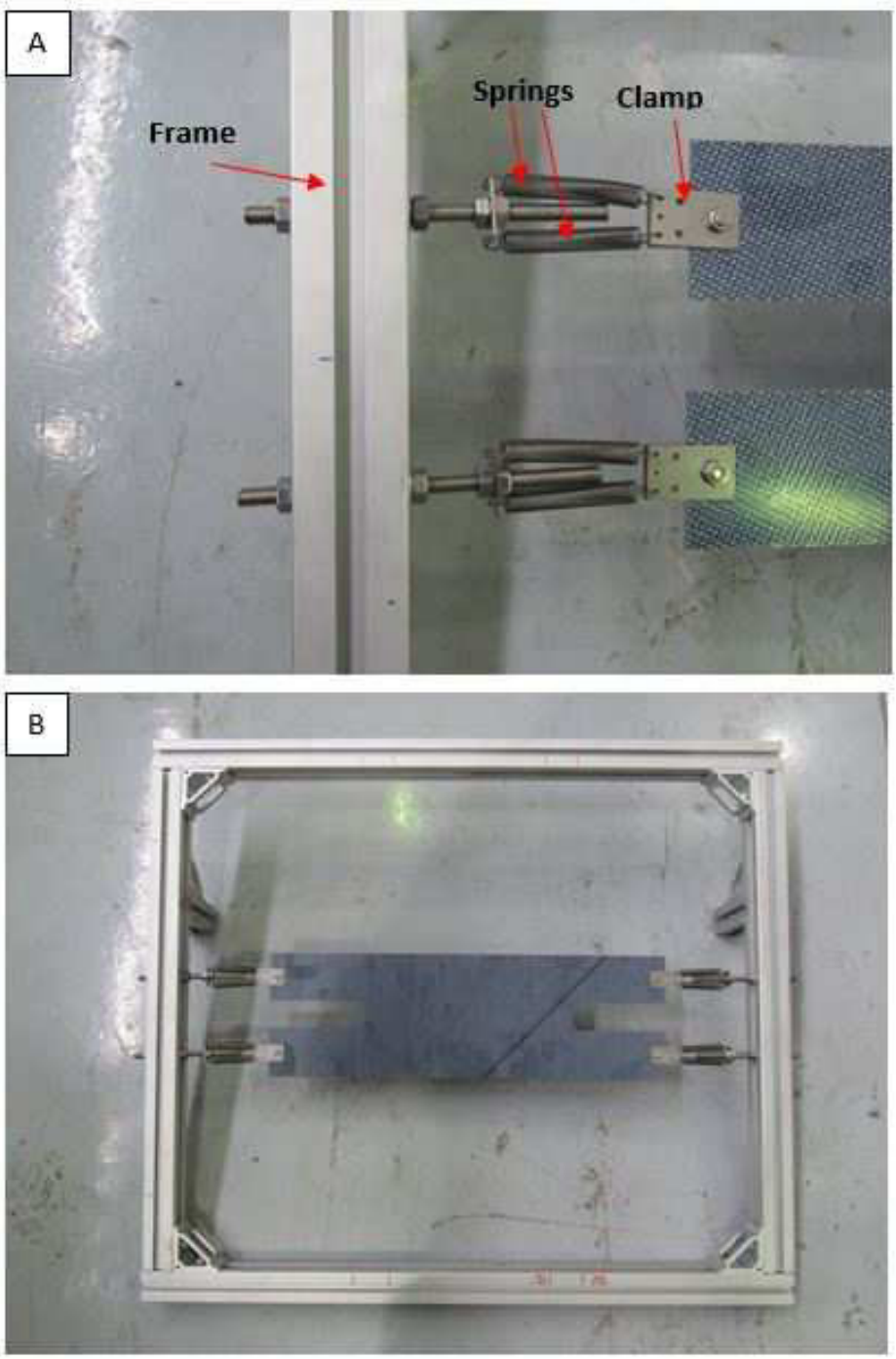


Figure 7.17: (A) Clamp & springs, (B) Frame & blank

7.3.3.2 Blank Geometry Optimization

Principles for the design of CFRTP blanks were then formulated. These principles follow directly from the establishment of the BRM described Section 7.3.3.1. The blank design principles relate to the method chosen to restrain the blank i.e. the spring BRM. The design of a blank to be used with a friction based restraint method would undoubtedly lead to a different blank design philosophy.

The design of the blank was carried out as follows:

The blank was shaped to mimic the basic outline of the geometry required to manufacture the component, with sufficient additional material (20-30 mm) to allow for trimming of the edges to produce the final geometry. This removed the excess material from the blank that would be trimmed away in any case. Tags were added to the basic shape, the tags were used to attach the BRMs to support the blank. The tags were positioned such that the tension generated by the BRM would prevent the laminate from buckling and folding in the regions where folds occurred. The design of the optimized LCU blank is shown in Figure 7.18.

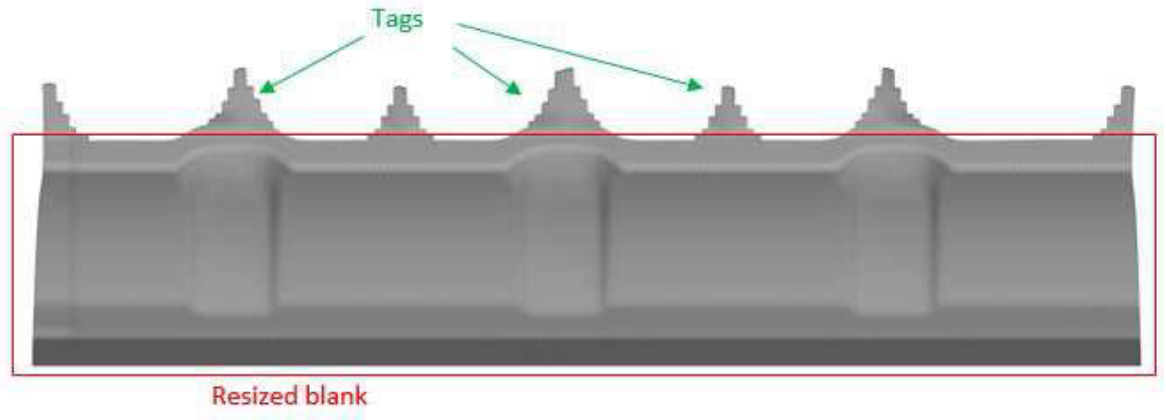


Figure 7.18: Optimized LCU blank.

Figure 7.19 presents the proposed set-up for forming the optimized LCU blank. The blank was supported by the BRMs on the edge with tags and was firmly clamped directly to the frame on the opposite edge.

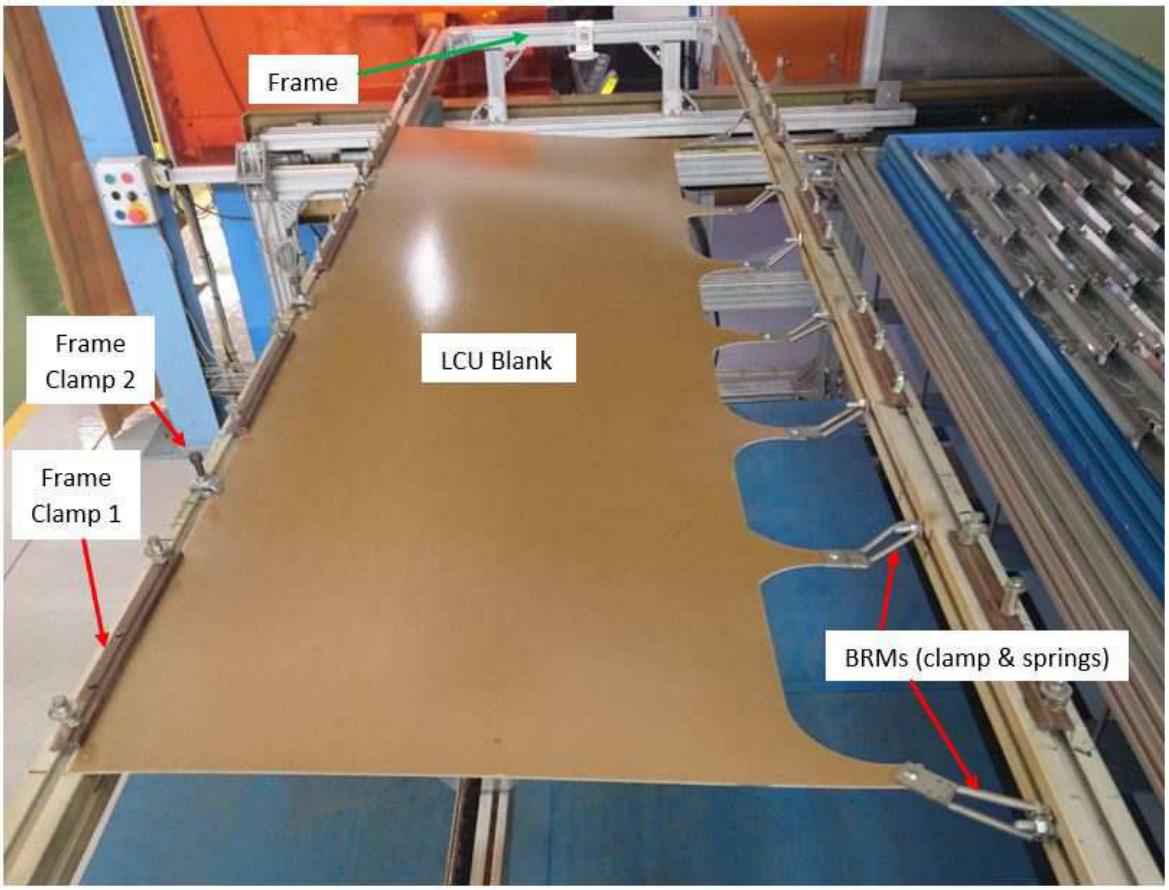


Figure 7.19: Proposed LCU forming set-up.

7.3.3.3 Blank Pre-Draping

As the blank is heated in the oven, the thermoplastic melts and the blank begins to sag under its own weight. If the sag of the blank is not anticipated it can lead to undesired results. Figure 7.20 shows the sag of the blank for the rudder rib under heating, this blank sagged low enough to collide with the bottom tool when the shuttle moved to the pressing station. A ramp was attached to the bottom tool to guide the blank into the press position without colliding with the tool. This was not an adequate solution because the contact between the blank and the ramp quenches the blank, therefore dropping its temperature before it is formed. The amount of sag experienced by a blank needs to be monitored. The degree of sag depends on the shape of the blank, particularly on the arrangement of the tags on the blank and the stiffness of the springs used on the BRMs.

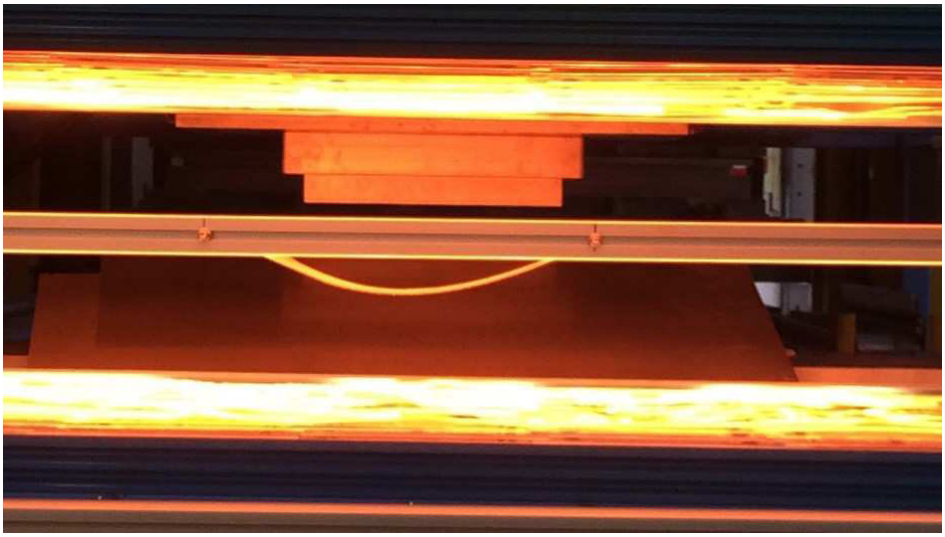


Figure 7.20: Blank sag during heating.

The blank sagging phenomenon was utilized in the forming of the LCU in an attempted to improve the drapability of the LCU. The tags on the blank were arranged such that the natural sag of the molten blank mimicked the geometry of the LCU (see Figures 7.18 and 7.21). The BRM was equipped with springs with a stiffness of 0.09 N/mm, the low stiffness allowed the BRM to generate a small restraining load allowing the blank to sag. This process of pre-conditioning the laminate to mimic the target geometry was referred to as pre-draping. The intention behind pre-draping the blank was to increasing the length of the fibre available to drape onto path A (see Figure 7.15). This would reduce the tension experienced by the fibres along path A with the intention of eliminating their bridging along the path.

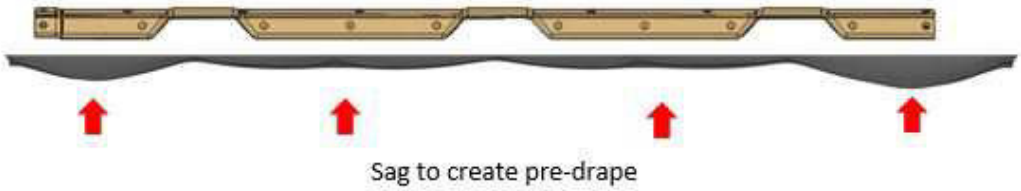


Figure 7.21: Pre-draped LCU blank.

The section of the LCU along path B is mostly flat and simple to form. Applying the pre-drape concept here meant that the edge along path B needed to be kept straight. This edge was consequently pinned directly to the frame without the use of the springed BRM meaning that it was effectively fixed to the frame. This could be done because the amount of intra-ply shear required in this region was small due to the flat geometry.

7.3.4 Results

Figure 7.15 shows the simulated manufacturing set-up for the LCU. In this image, the upper tool is roughly midway to its fully closed position. It shows the use of the BRMs and the optimized blank to manufacture the LCU.

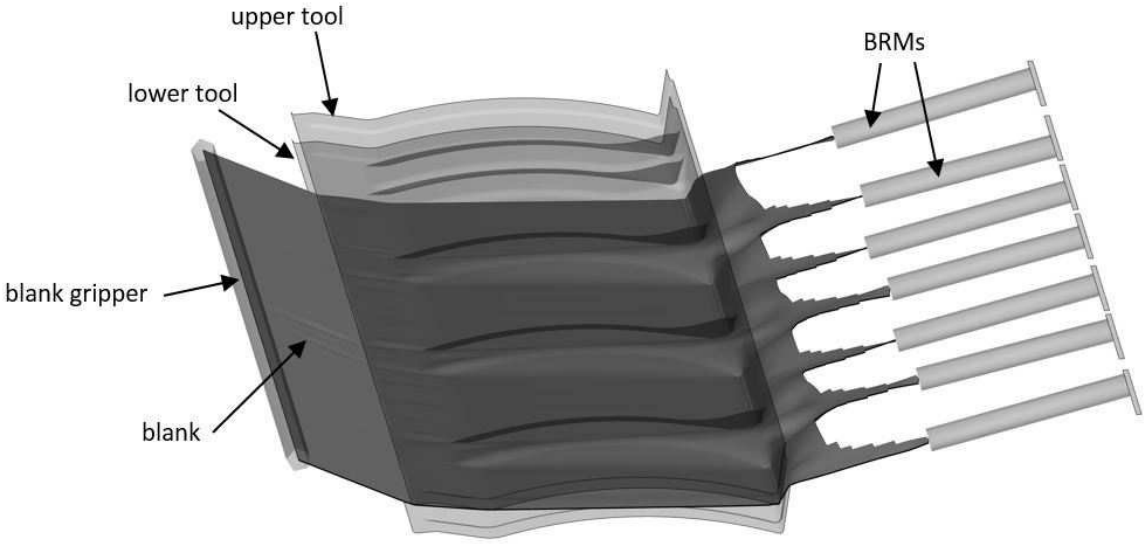


Figure 7.22: Forming simulation of the LCU during tool closure, also showing the simulation set-up.

Figure 7.23 shows simulation results of the deformation of the blank as the tool closes. The view shown is from the front of the tool, with reference to Figure 7.22, this is the view of the tool from the side with the BRMs. This shows how the pre-draping aids with draping the blank into the final geometry, most notably along path A where the fibres must map the complex tool definition.

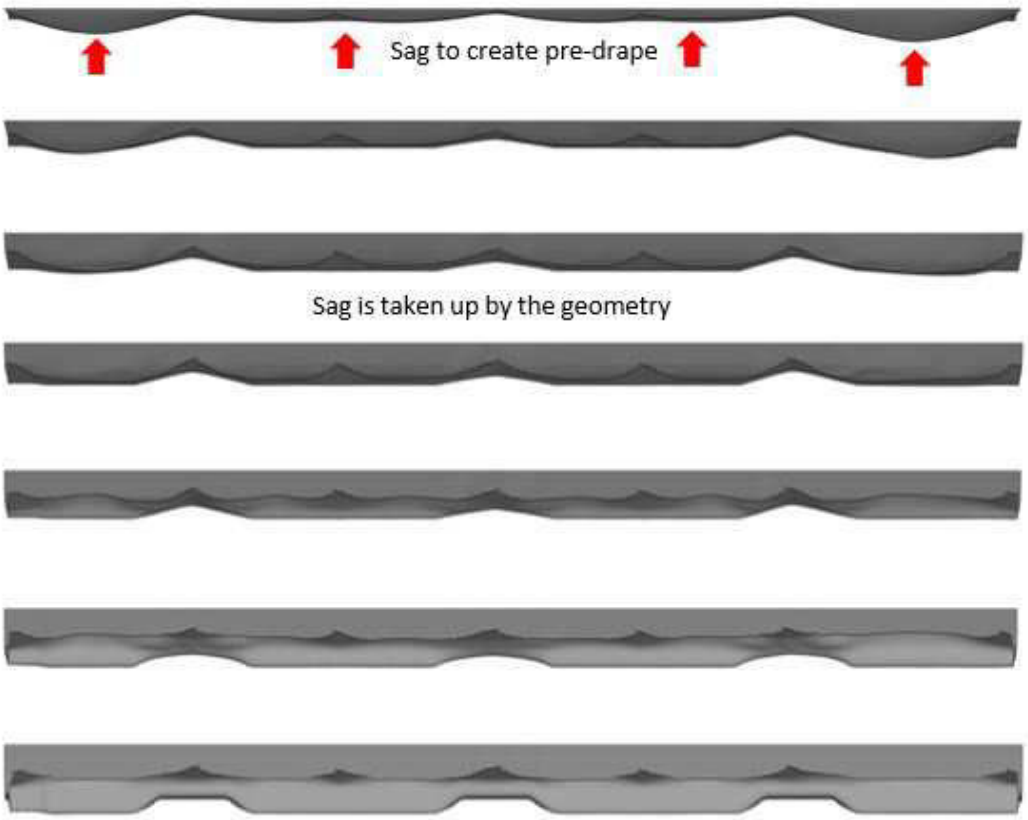


Figure 7.23: Simulated progression of LCU deformation

Figure 7.24 shows the shear angle and fibre stress results obtained from the simulated forming of the LCU. All the plies in the laminate comprised of fibres in the 0°/90° directions. Due to this, the results for all 5 plies are virtually identical and so only one set of results is presented.

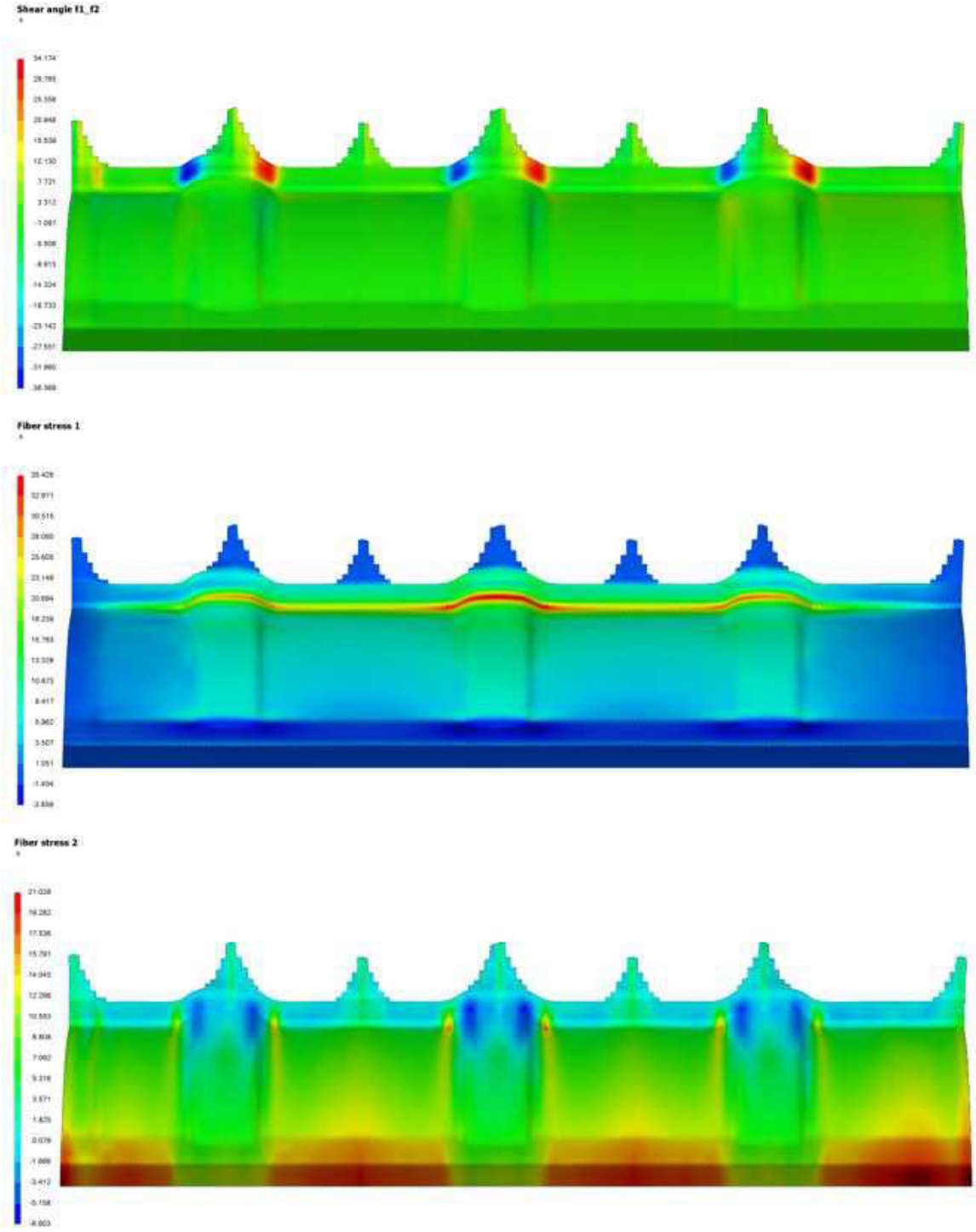


Figure 7.24: Simulation results for the LCU formability study.

Figure 7.25 shows the results from the practical LCU experiment with the optimized blank.



Figure 7.25: Experimental results for the LCU manufactured with the BRM and optimized blank.

7.3.5 Discussion

The results for the prediction of the formability of the optimized LCU are presented in Figure 7.24. The shear angle results show regions of shear angle concentrations along path A owing to the complexity of the region, the largest shear angle required to drape onto the geometry in this region was 34°. The rest of the geometry required a shear angle of 5° in order to be successfully draped. This supports the decision to fix the blank along path B. The simulation on the fibres stress in the longitudinal direction predicted that the fibres running along path A will experience large fibre stresses (35 MPa) in comparison to the rest of the blank. The simulation on the fibres stress in the transverse direction predicts compressive regions along path A, this is in the region when folds occurred in the original blank.

The results of the optimized LCU practical experiment are presented in Figure 7.25. It is difficult to single out the effect that can be solely attributed to the reduction of the size of the blank. It is theorized that reducing the size of the blank by removing unnecessary excess material eliminated the possibility of introducing defects originating from the excess material. The reduction of the size of the blank can improve the ability of the material to drape onto the geometry as a result of there being less material to form. Reducing its size focuses the forming effort onto the component.

The images of the formed component shown in Figure 7.25 where taken immediately after forming, following this, there is a trimming operation to produce the final component. Please refer to Figure 7.14 for the position of the trim lines and a model of the final geometry. The wrinkled portion of the formed blank on the side opposite to the tags (see Figure 7.25) does not form part on the final component. This portion appears wrinkled largely because it does not get consolidated during forming, and not that it is developing wrinkles. This portion remains outside of the forming tools during forming, this can be seen in Figure 7.22. This portion could have been reduced by decreasing the width of the blank. This was not done because it would have required the design of the frame that supports the blank to be altered. The region on the component that is adjacent to this unconsolidated portion requires small intra-ply shear (±5°) to be formed, so it is able to be draped without the occurrences of forming defects as shown in Figure 7.25.

The tags were placed such that together with the BRM, they prevent the development of the compressive stress in the fibres in the 2 direction. This prevented the laminate from buckling and folding. The lack of folds along path A can be seen in Figure 7.25. This redesigned blank was used together with the BCM to improve the formability of the LCU along path A. The occurrence of random wrinkles on the LCU also ceased following the implementation of the BRM to support the blank. No evidence of wrinkles is visible in Figure 7.25.

The BRM and blank design can also be utilized as a tool to manipulate the blank to control the sag profile of the blank when it has been heated. The LCU geometry requires great amounts of material draw in and mobility to enable the material to drape the geometry. By bringing the molten blank to a state that resembles the final formed geometry. The amount of deformation that the laminate must experience under the action of the closing tool is reduced. Taking into account that the laminate cools down rapidly after contact with the tool, this inhibits the forming mechanism from taking place, the pre-draped blank improved the formability prospects of the geometry. Figure 7.23 shows how the pre-draped blank deforms into the target geometry during forming. The pre-drape shape can be managed by the blank design and the BRM.

The spring stiffness determines the load exerted by the BRM as the blank deforms and the spring extends. Considering the stiffness is the most important specification when specifying the spring. The spring's maximum extension must be considered to ensure the spring is used within its design limit. The material used to manufacture the springs must also be considered as they are used in an environment with elevated temperature. The springs are subjected to heating and cooling cycles in the production environment and so the material must perform well under these temperature loads. It was noted that the BRM was cumbersome to use during experimentation. The clamping mechanism should be redesigned to a mechanism that is friendly for use in a production setting. This would help keep the manufacturing cycle times low, further reinforcing this advantage of thermoplastics.

7.3.6 Conclusions

1. The blank should never be fully constrained, it must have the freedom to deform when acted on by the tool but it should also never be released during forming.

2. The design of the blank has an influence on the formability of a geometry. The blank must be designed in a manner that facilitates draping into the required geometry.

3. The blank can be manipulated to improve formability of a component by the using the BRM to prevent the laminate from folding over itself during forming.

4. The sag of the blank can be utilized to improve the draping of the blank, this is done by pre-draping the blank using the design of the blank and the BRM to attain the desired pre-drape shape.

5. The implementation of the points listed above resulted in a significant improvement in the formability of the LCU.

7.4 Investigation 3: The effect of blank design

7.4.1 Problem Background

The typical components that are manufactured by the CFRTP facility are in the form of L, C and Z sections. Just as was the case with the LCU, there were no standard CFRTP rules employed in the interest of ensuring the formability of the components. The concepts that were developed in Section 7.3 had to be applied to the manufacturing of the L, C and Z sections. This section documents the investigations performed in the development of the blank designs for the C and Z sections.

7.4.2 Objective

The purpose of this experiment was to establish standard blank designs that can be used as a template for manufacturing C and Z section components.

7.4.3 Proposed solution

An investigation was carried out to determine the suitability of different blank designs for manufacturing C and Z section components. By evaluating the performance of the blanks, a single blank design can then be selected as a template for forming that particular geometry.

7.4.3.1 C-Section

Figure 7.26 shows the different blank designs that were evaluated to manufacture the C-section geometry. Since the shape assumed by the blank (pre-drape) was known to affect the formability of a component, the simulated pre-drape shape for the blanks is shown in Figure 7.27. The red represents the high areas and the blue the low areas of the blank in its simulated state of sag. The simulations all assumed that the blanks were secured using BRM's with spring of stiffness 0.09 N/mm.

- Blank 1 assumed a semi-cylindrical shape but the axial direction of the shape was perpendicular to the tool geometry.
- Blank 2 remained relatively flat after the laminate was melted.

- Blank 3 assumed a semi-cylindrical shape but with the axial direction of the shape aligned with the orientation of tool.
- Blank 4 was designed such that the tags are oriented in the direction of the fibres in the 45° plies.

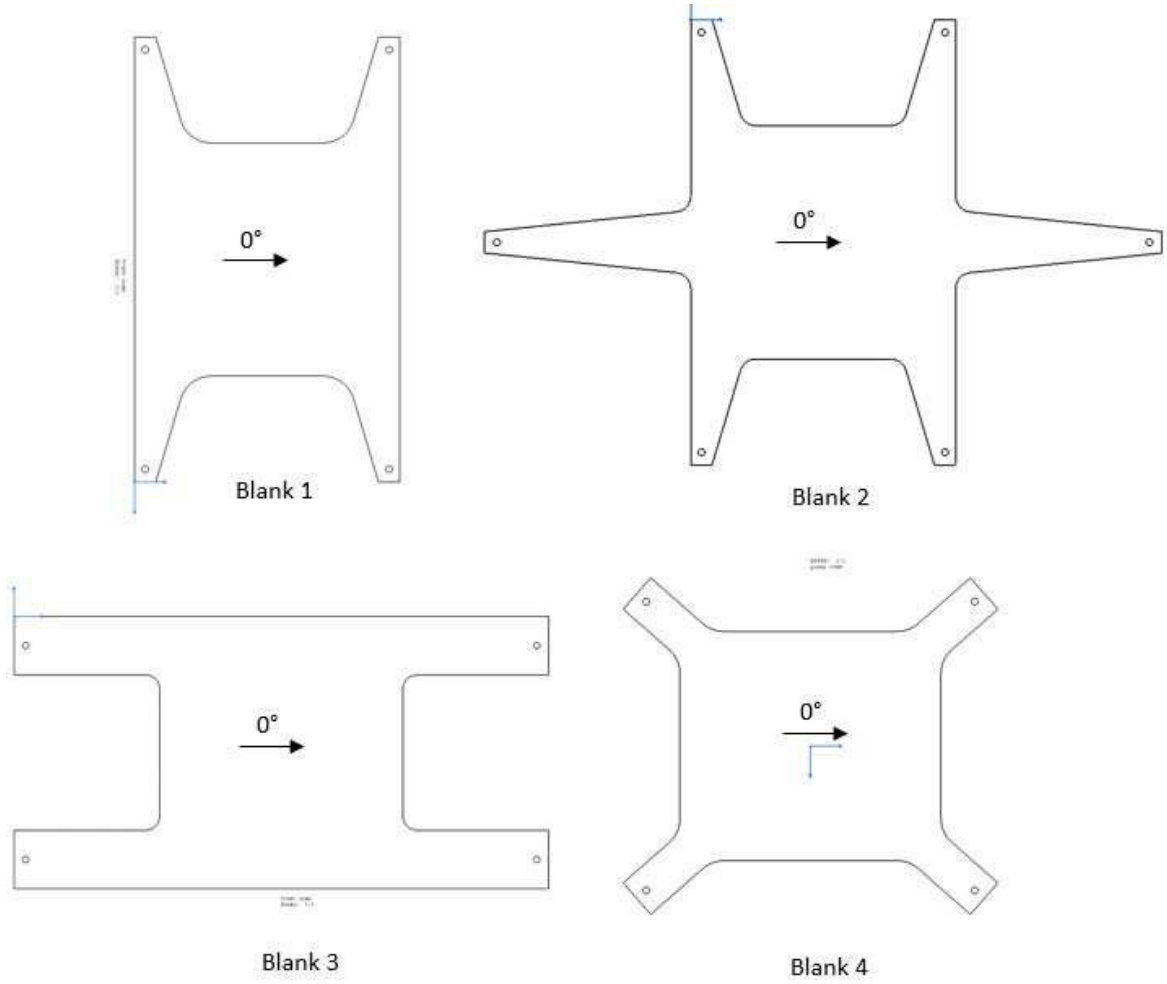


Figure 7.26: Blank designs for the C-section geometry.

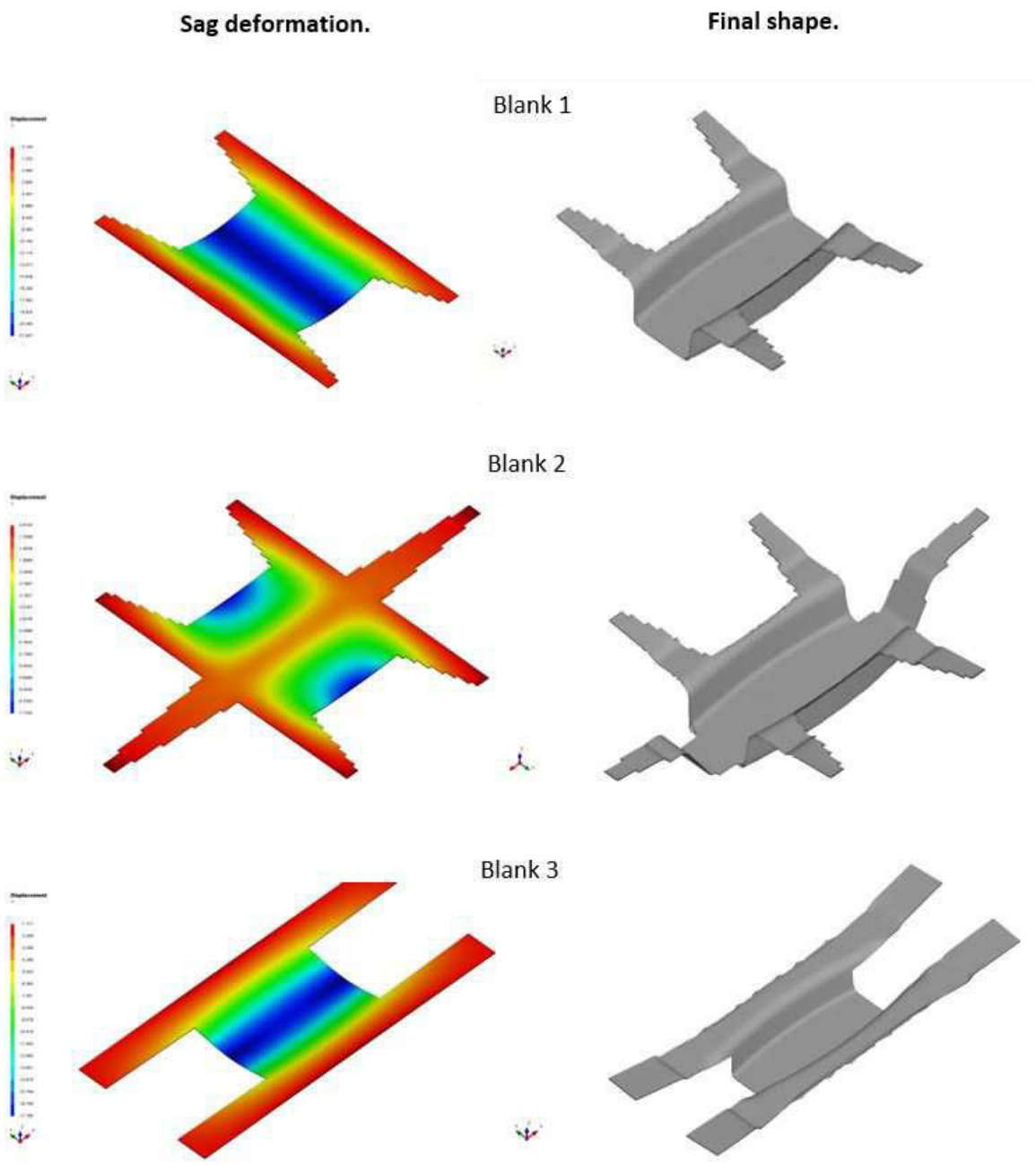


Figure 7.27: Blank sag for different blank designs.

7.4.3.2 Z-Section

Figure 7.28 shows the blank designs that were evaluated to manufacture the Z-section geometry. It was assumed that the blanks were all secured using BRM's with spring of stiffness 0.09 N/mm.

- Blank 1 had tags oriented to pull across the length of the component.
- Blank 2 had tags that pulled along the bend-lines of the component.
- Blank 3 had tags that pulled along the web and flanges of the component.

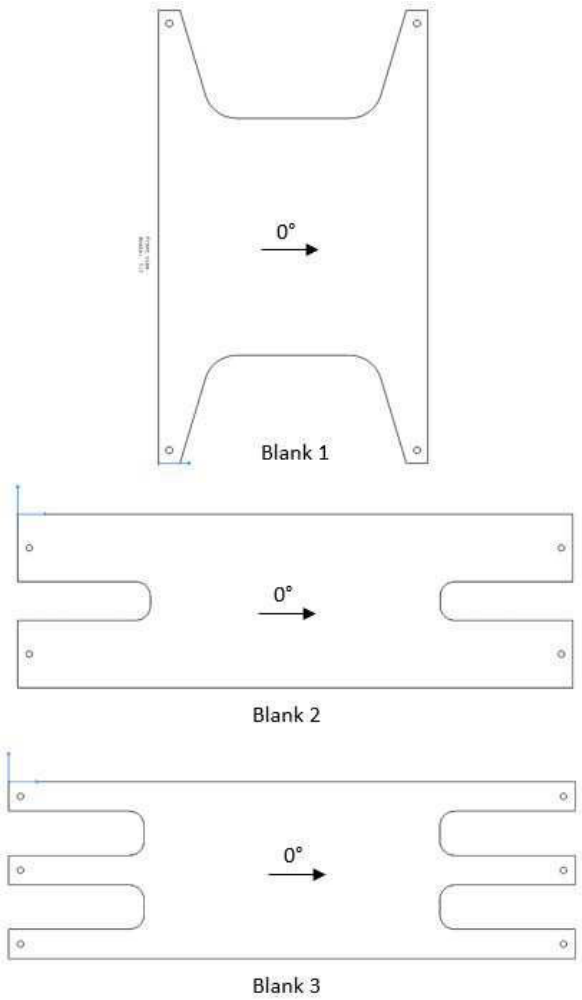


Figure 7.28: Blank designs for the Z-section geometry.

7.4.4 Results

This section presents the results of the blank evaluation study for the C-section. The simulation results for the two unique plies that make up the laminate are shown. Following this, is a presentation of the sag experienced by the blank during heating showing the pre-drape shapes for the different blanks. Lastly, the results of the blanks formed experimentally are presented at the end of the section.

7.4.4.1 C-section: Simulated Results

The state of the blanks 1, 2 and 3 moment before full tool closure are presented in Figure 7.29. Thereafter the shear angle results for the first and second (top and bottom respectively) plies of the fully formed components are presented. Please refer to Appendix D.2 for the full set of results.

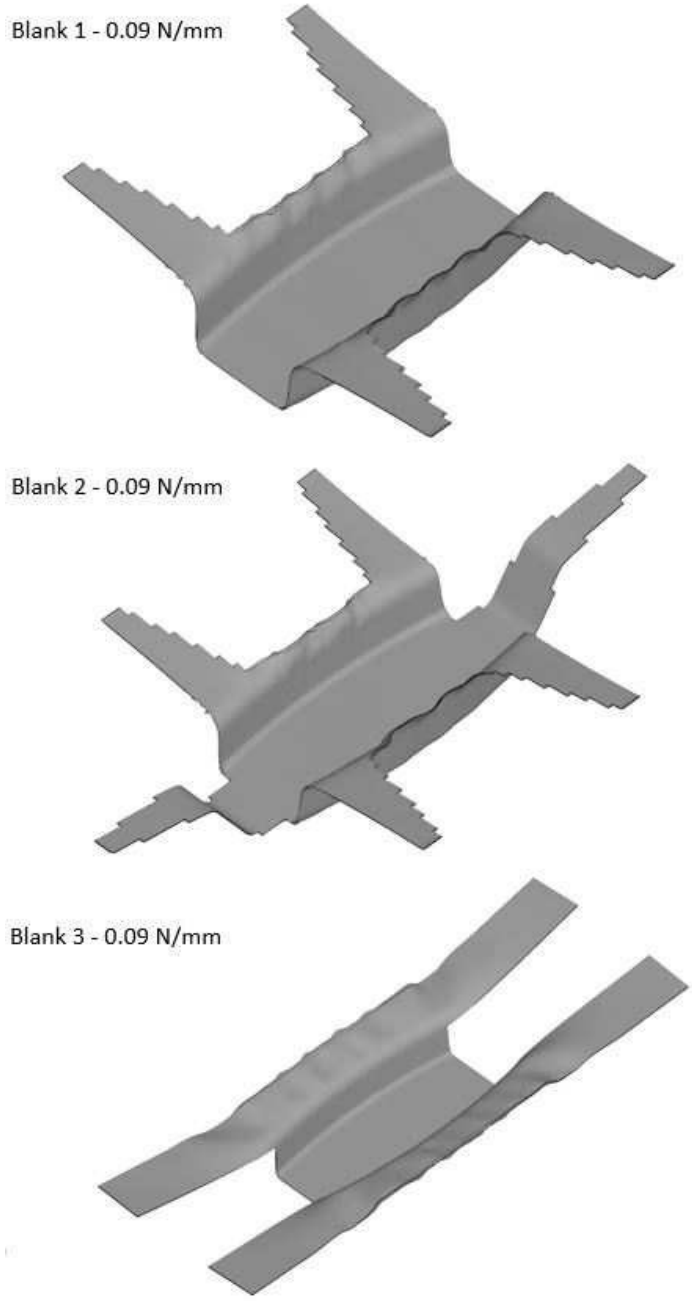


Figure 7.29: Deformation of blanks 1,2 and 3 before full tool closure.

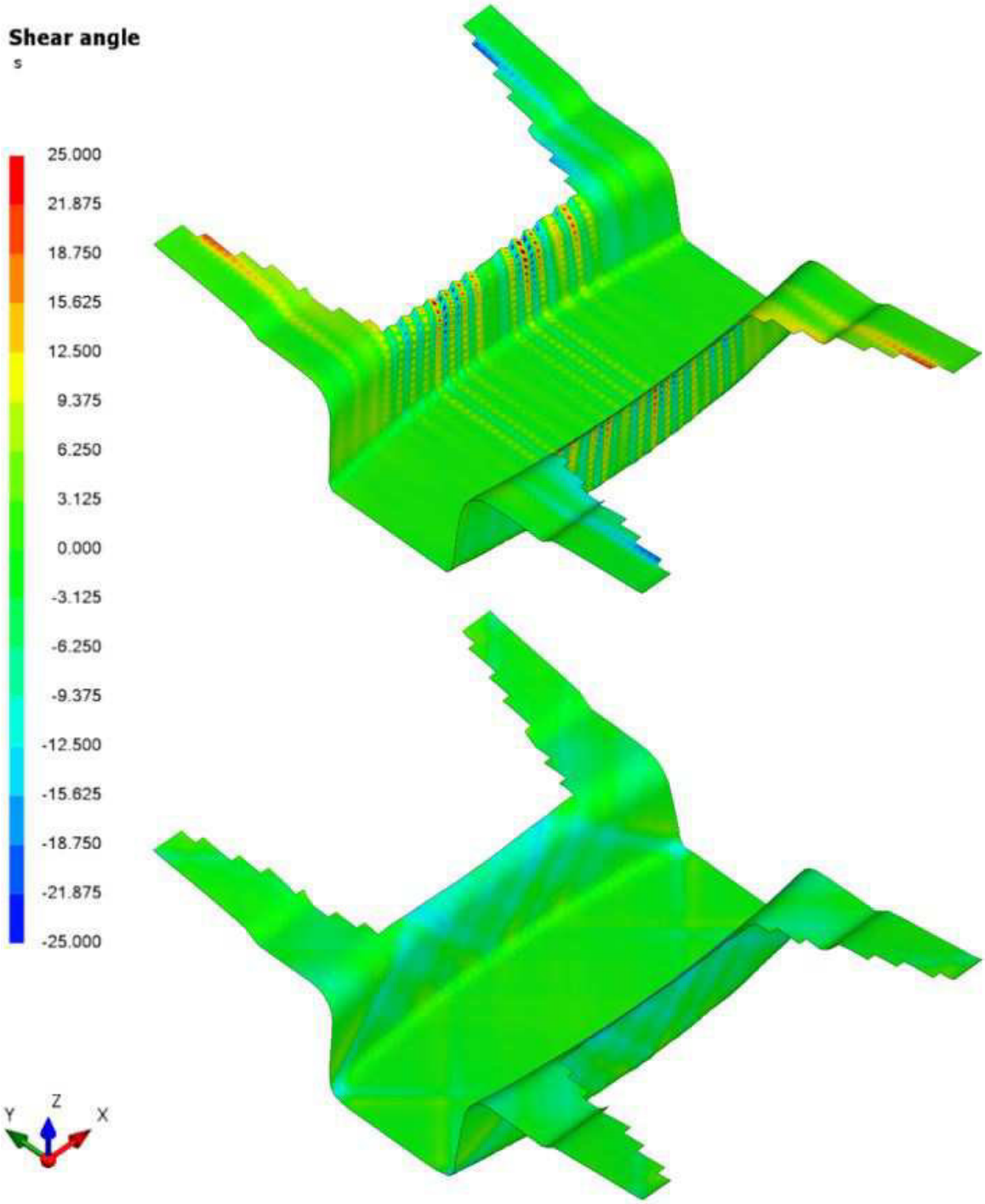


Figure 7.30: C-section blank 1 results, ply 1 above and ply 2 below.

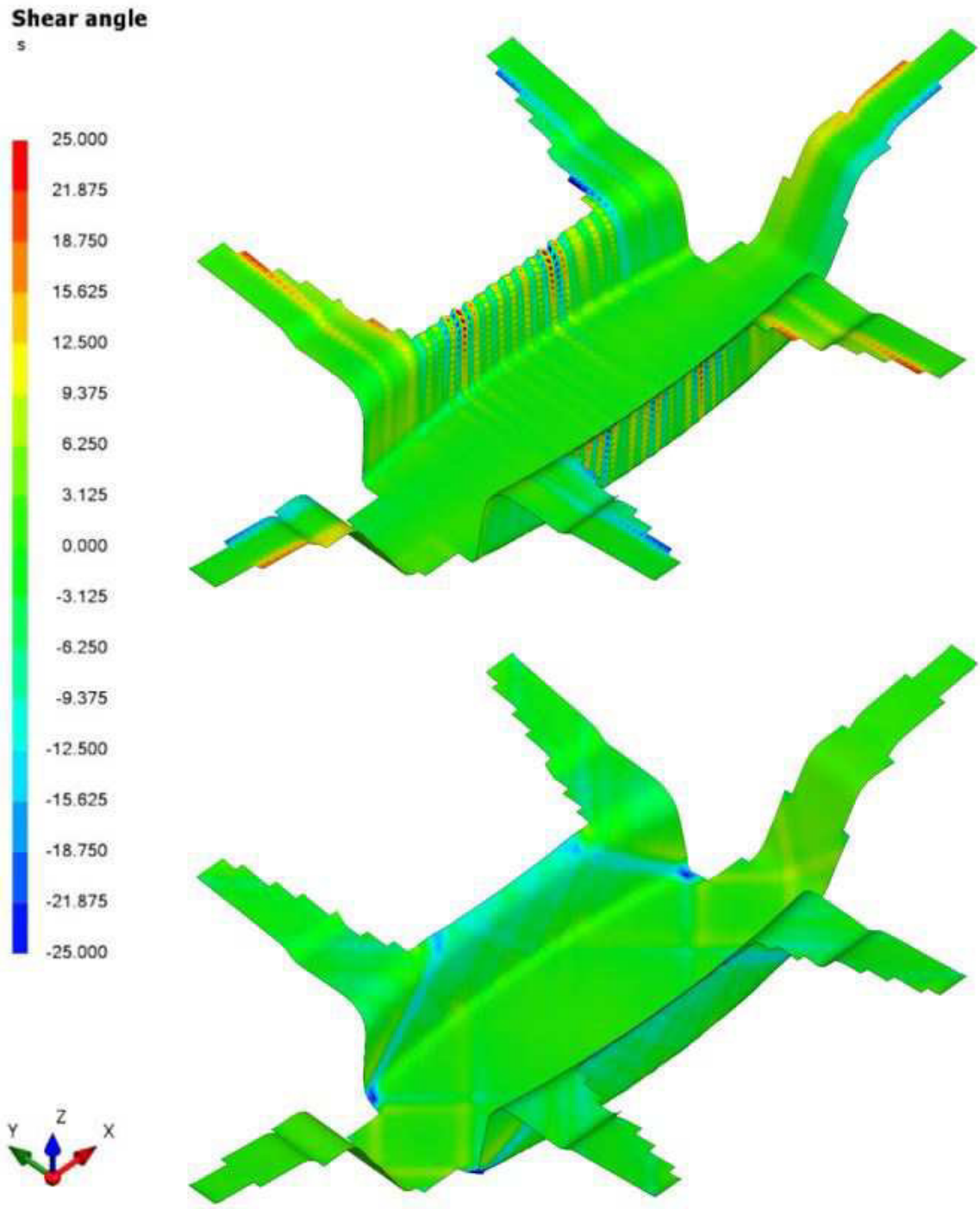


Figure 7.31: C-section blank 2 results, ply 1 above and ply 2 below.

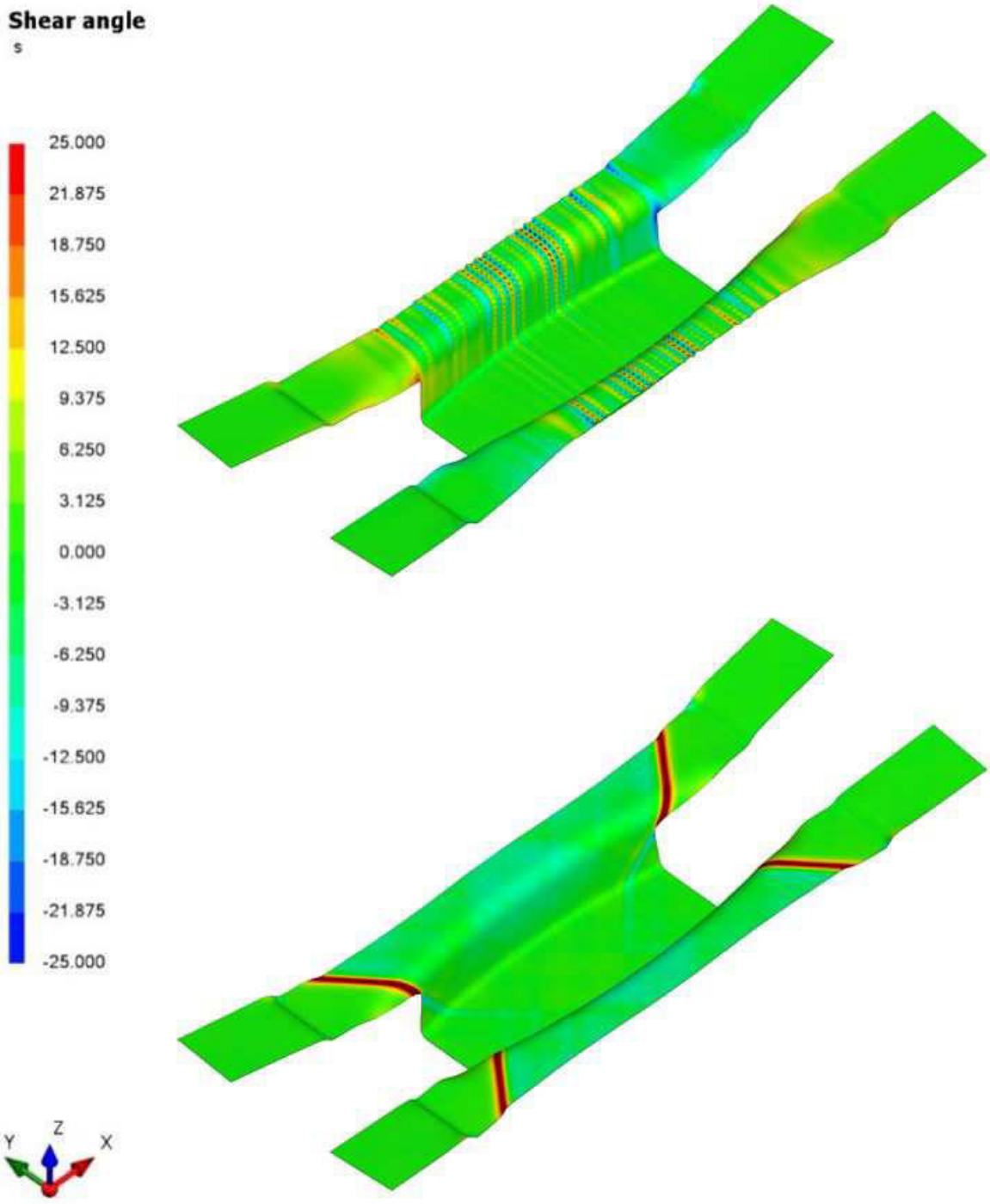


Figure 7.32: C-section blank 3 results, ply 1 above and ply 2 below.

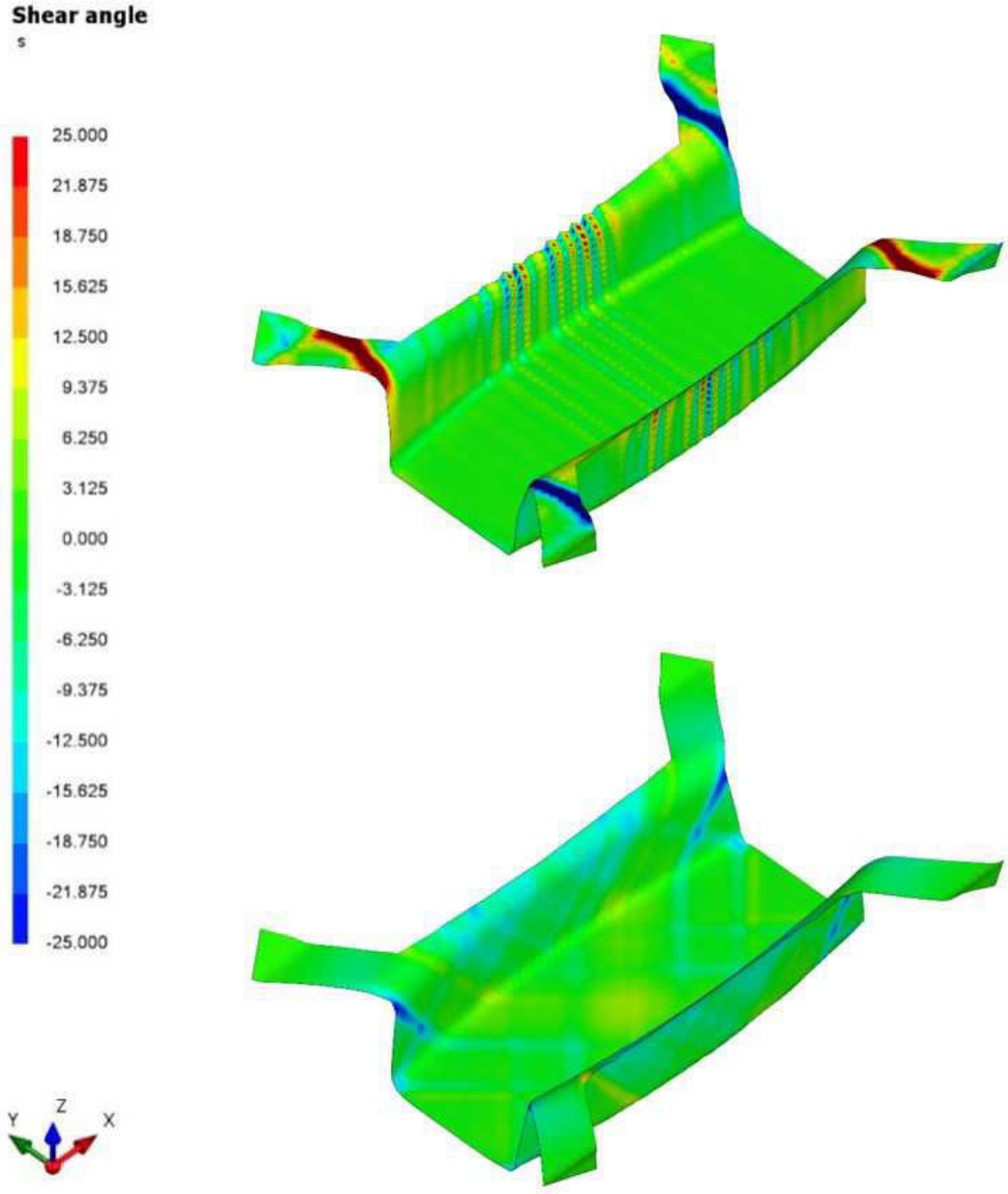


Figure 7.33: C-section blank 4 results, ply 1 above and ply 2 below.

7.4.4.2 C-section: Experimental Results

Figure 7.34 presents the pre-drape shape and the points of first contact for blanks 1, 2 and 3.

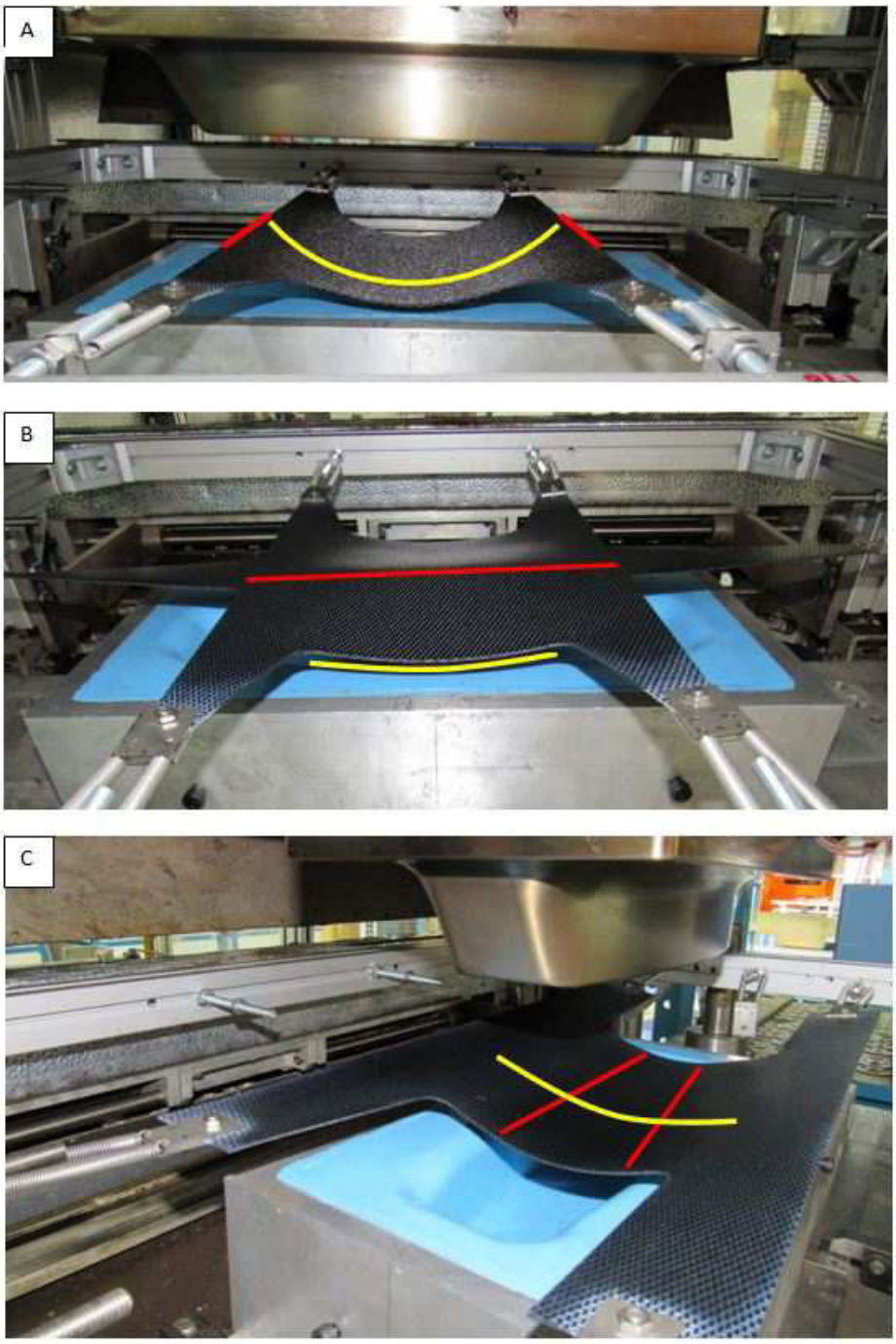


Figure 7.34: Pre-drape shape for (A) blank 1, (B) blank 2 and (C) blank 3. The yellow markers denote the curvature of the blank sag and the red lines denote the lines of first contact with the tool.

Figure 7.35 shows the sag of blank 4 during heating. The bottom ply separated from the rest of the laminate falling under its own weight.



Figure 7.35: Pre-drape shape for blank 4

The results presented in Figures 7.36, 7.37 and 7.38 are of the components manufactured from the blanks. Blank 4 was not formed due to the occurrence of the ply separation, this revoked the blank candidacy for manufacturing the geometry. The region that developed defects have been marked with ellipses and close ups showing the defects marked by red arrows. In all the cases the red arrows point to wrinkles that occurred on the flange of the components.

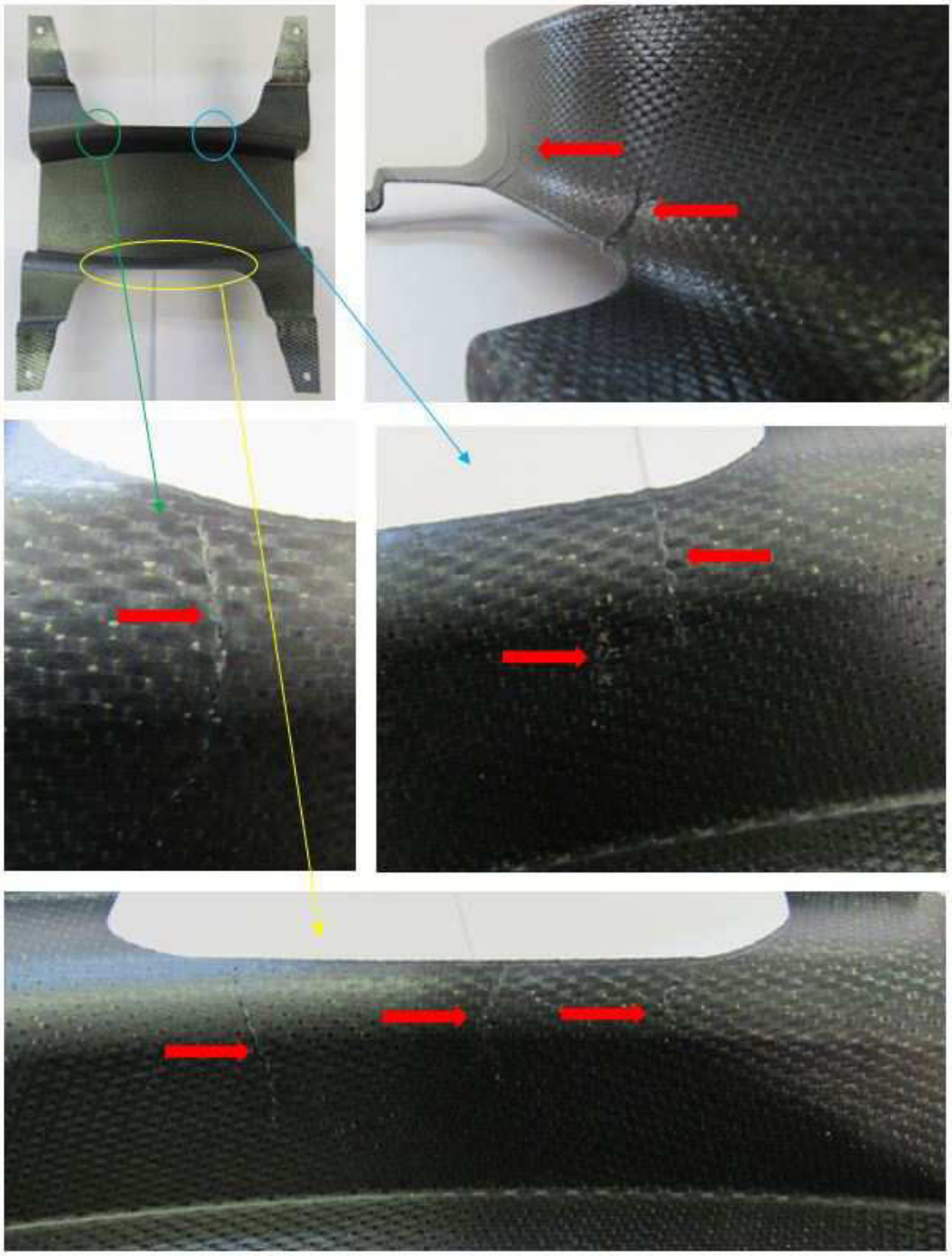


Figure 7.36: Results for C-section manufactured from blank 1. Spring stiffness - 0.09 N/mm.

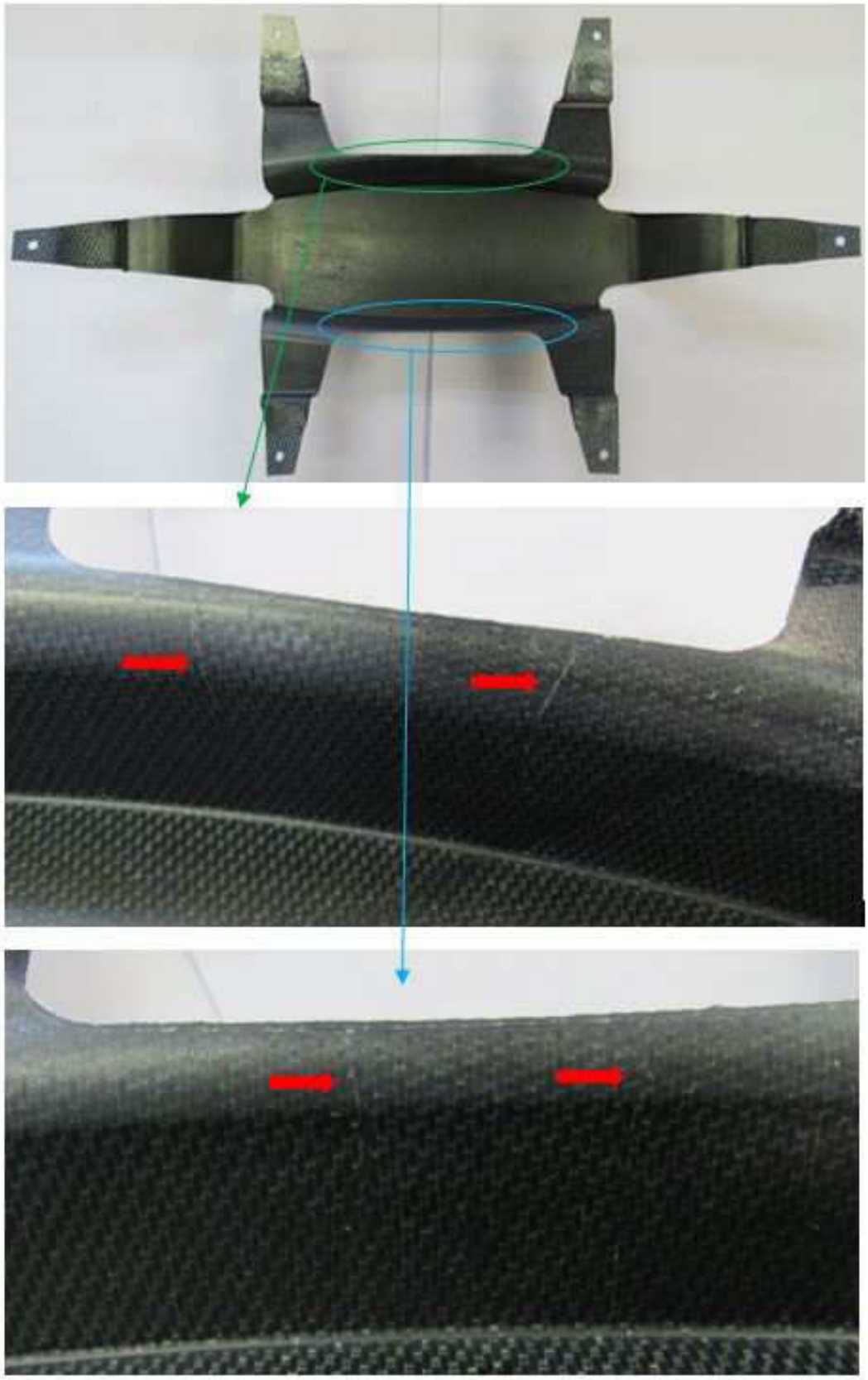


Figure 7.37: Results for C-section manufactured from blank 2. Spring stiffness - 0.09 N/mm.

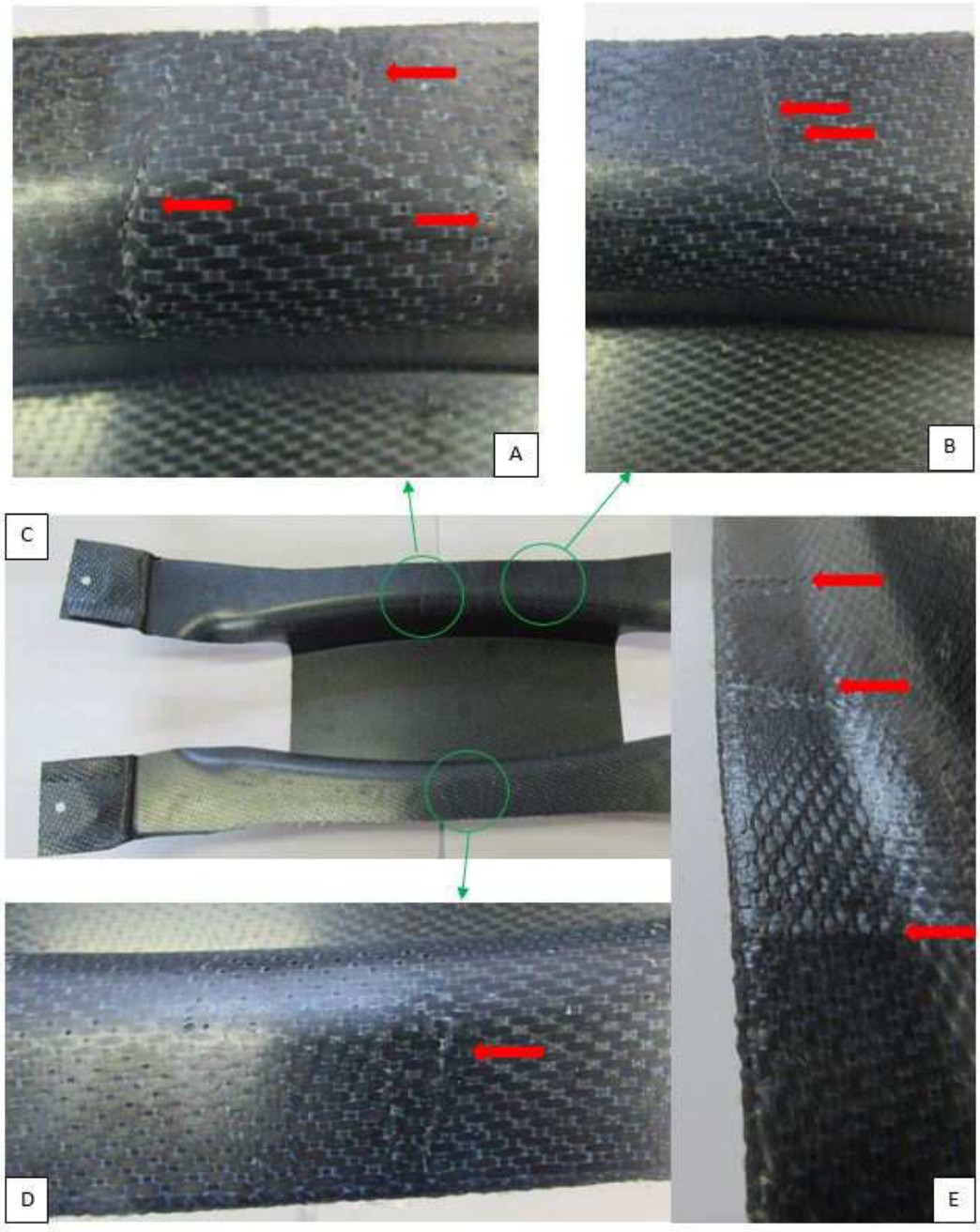


Figure 7.38: Results for C-section manufactured from blank 3. Spring stiffness - 0.09 N/mm.

7.4.4.3 Z-Section: Simulated Results

Figures 7.39, 7.40 and 7.41 show the shear angle simulation results for the blanks that were evaluated for the Z-section geometry. The results shown are of ply 1 and 2, representing the two unique plies that make up the laminate. In addition, Figures 7.39 and 7.40 also show the state of deformation of the blank moments before the tool is fully closed (the shear angle results are at full tool closure).

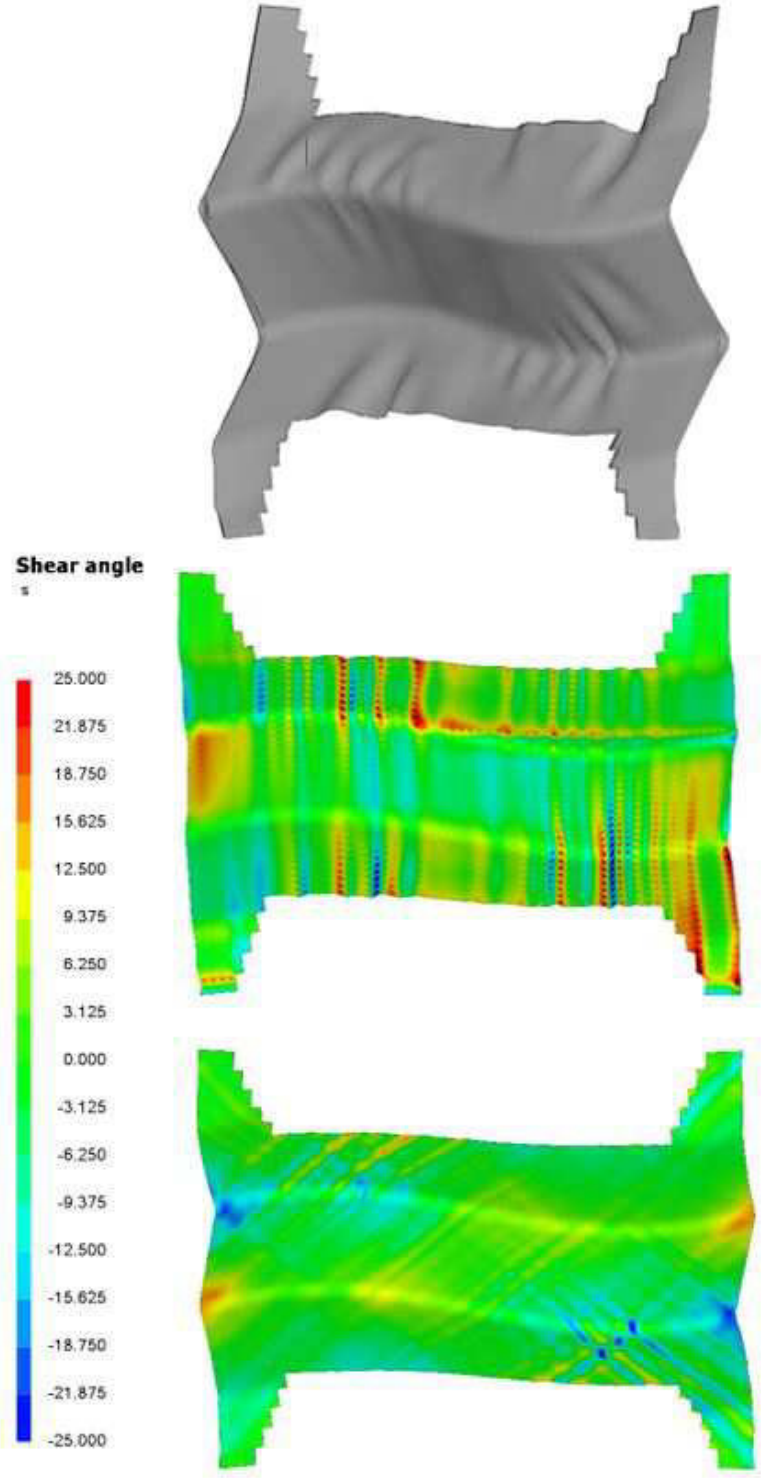


Figure 7.39: Z-section blank 1 results. Deformation before tool closure (top) and the resulting shear angle distribution at full tool closure for ply 1 (middle) and ply 2 (bottom). Spring stiffness - 0.09 N/mm.

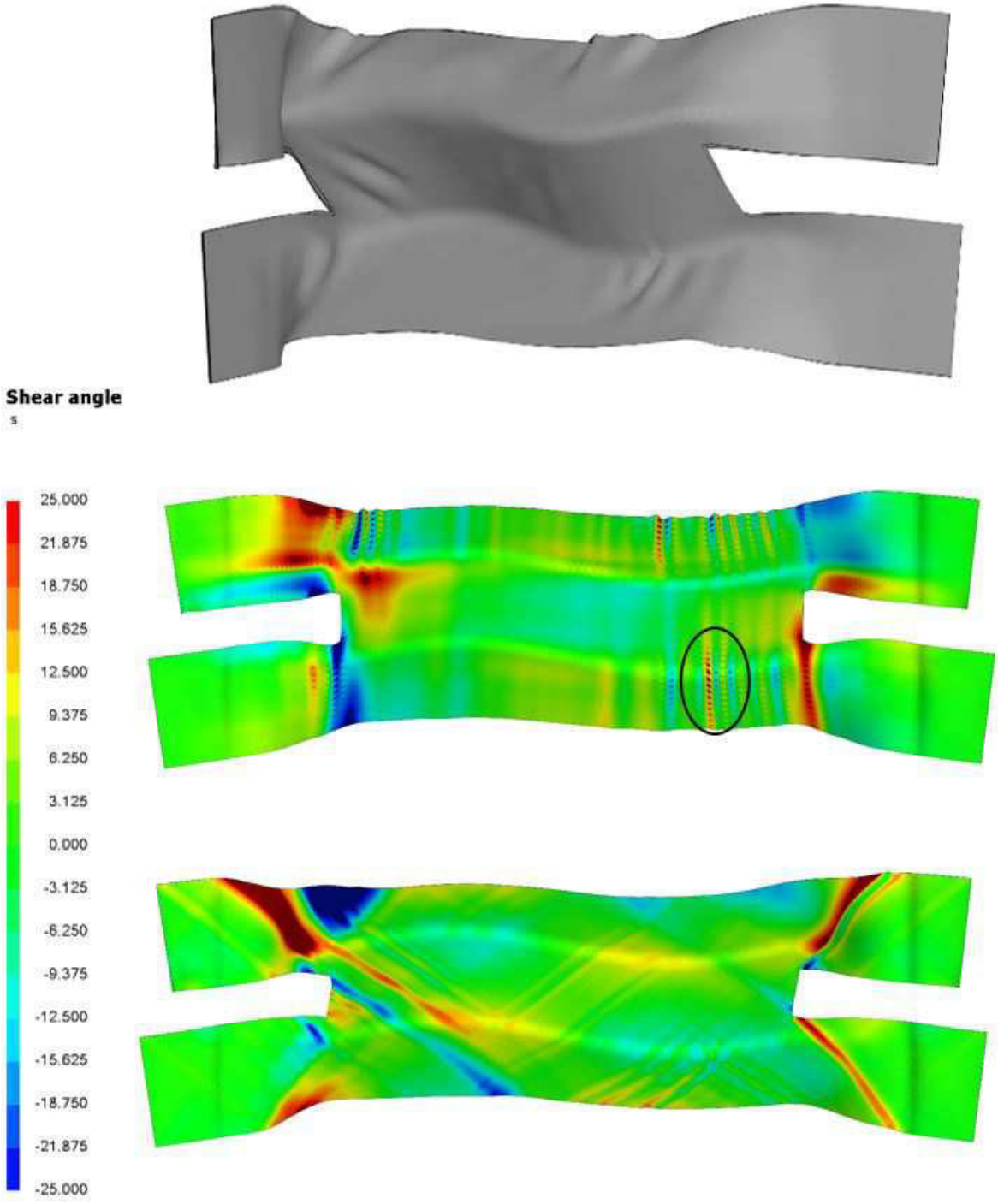


Figure 7.40: Z-section blank 2 results. Deformation before tool closure (top) and the resulting shear angle distribution at full tool closure for ply 1 (middle) and ply 2 (bottom). Spring stiffness - 0.09 N/mm.

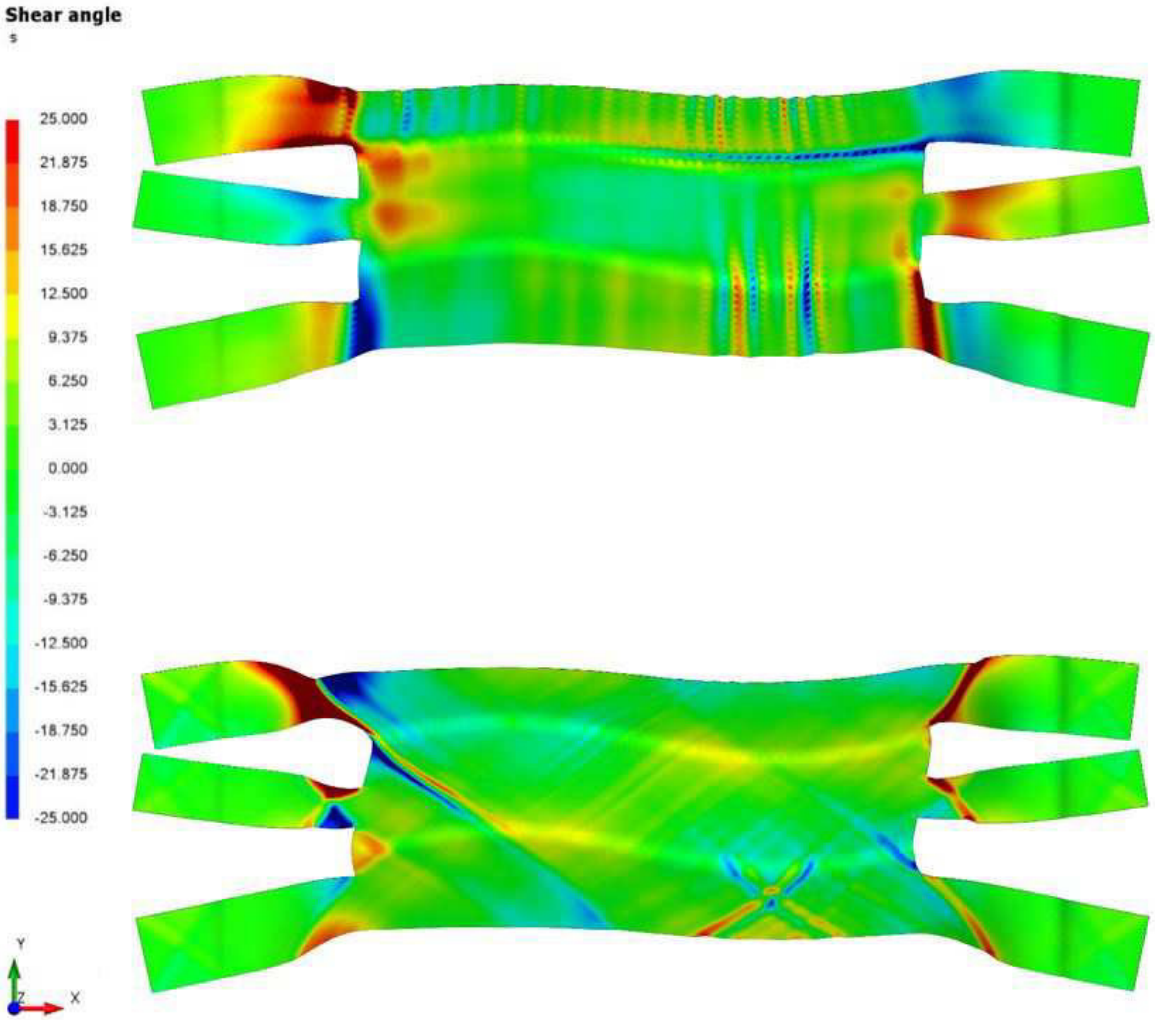


Figure 7.41: Z-section blank 3 results. Shear angle distribution at full tool closure for ply 1, above and ply 2, below. Spring stiffness - 0.09 N/mm.

Figures 7.42 and 7.43 show the Fibre Stress 1 results for blank 2 and 3 respectively. The equivalent results for blank 1 can be found in Appendix D.3.

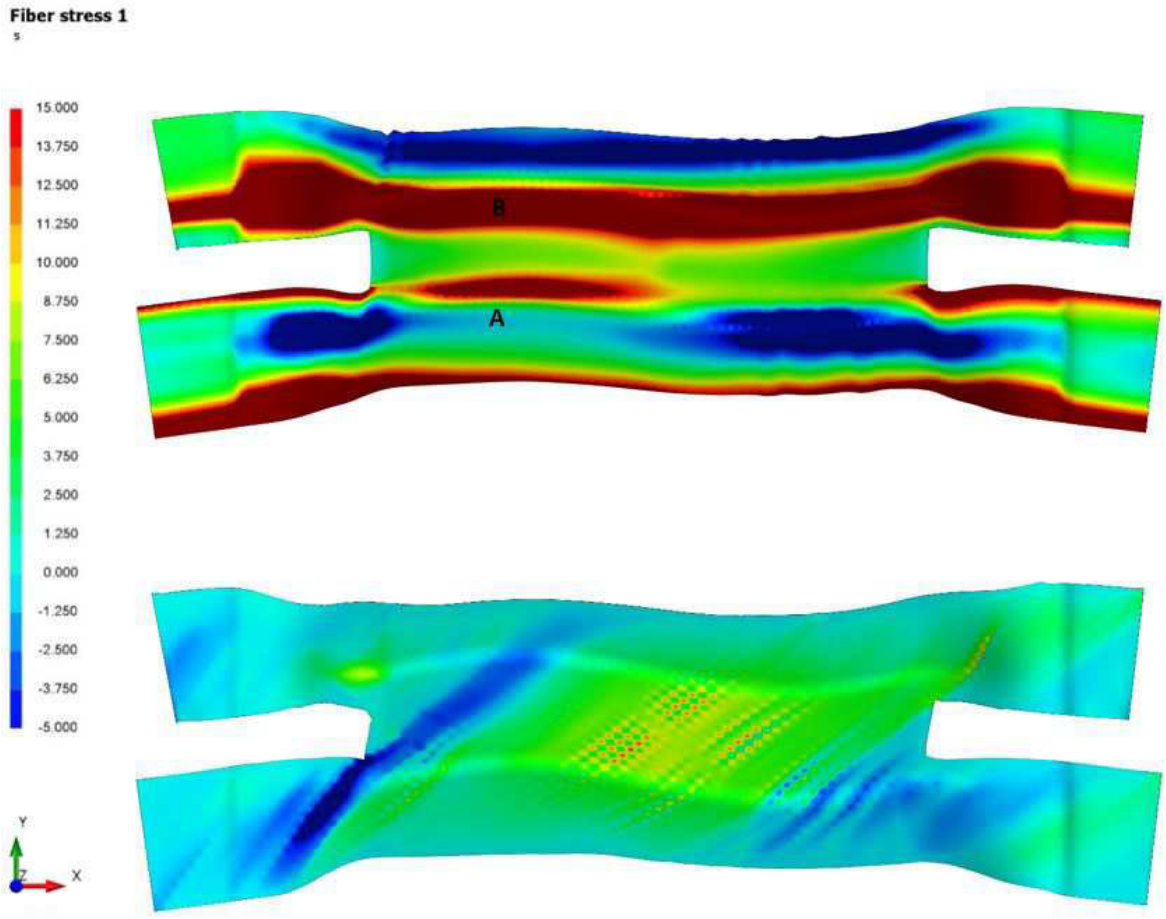


Figure 7.42: Z-section blank 2 fibre stress 1 results. Ply 1 above and ply 2 below. Spring stiffness - 0.09 N/mm.

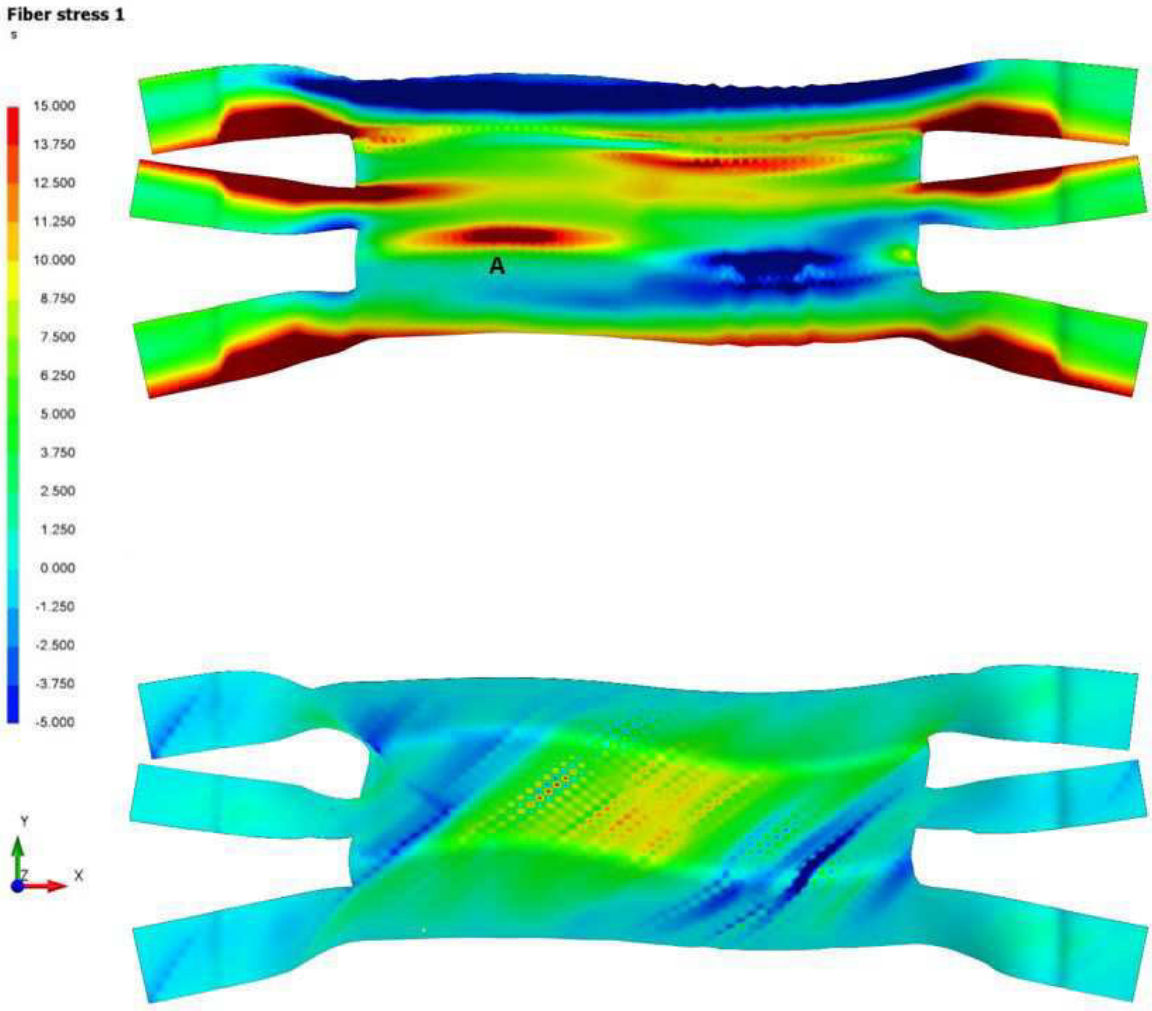


Figure 7.43: Z-section blank 3 fibre stress 1 results. Ply 1 above and ply 2 below. Spring stiffness - 0.09 N/mm.

7.4.4.4 Z-Section: Experimental Results

Figures 7.44 and 7.45 show the components of the blanks manufactured from blanks 2 and 3. Blank 1 was not manufactured because of a limitation of Z-section tool. The design of blank 1 required a unique tool to be formed. This reinforces the relationship between the design of the tool and the blank that mentioned in an earlier investigation. The green circles in Figure 7.44 show the regions that developed wrinkles which have been marked by the red arrows. The blue ellipses in both Figures 7.44 and 7.45 mark regions that developed resin squeeze-out, this has been marked with the blue arrows.

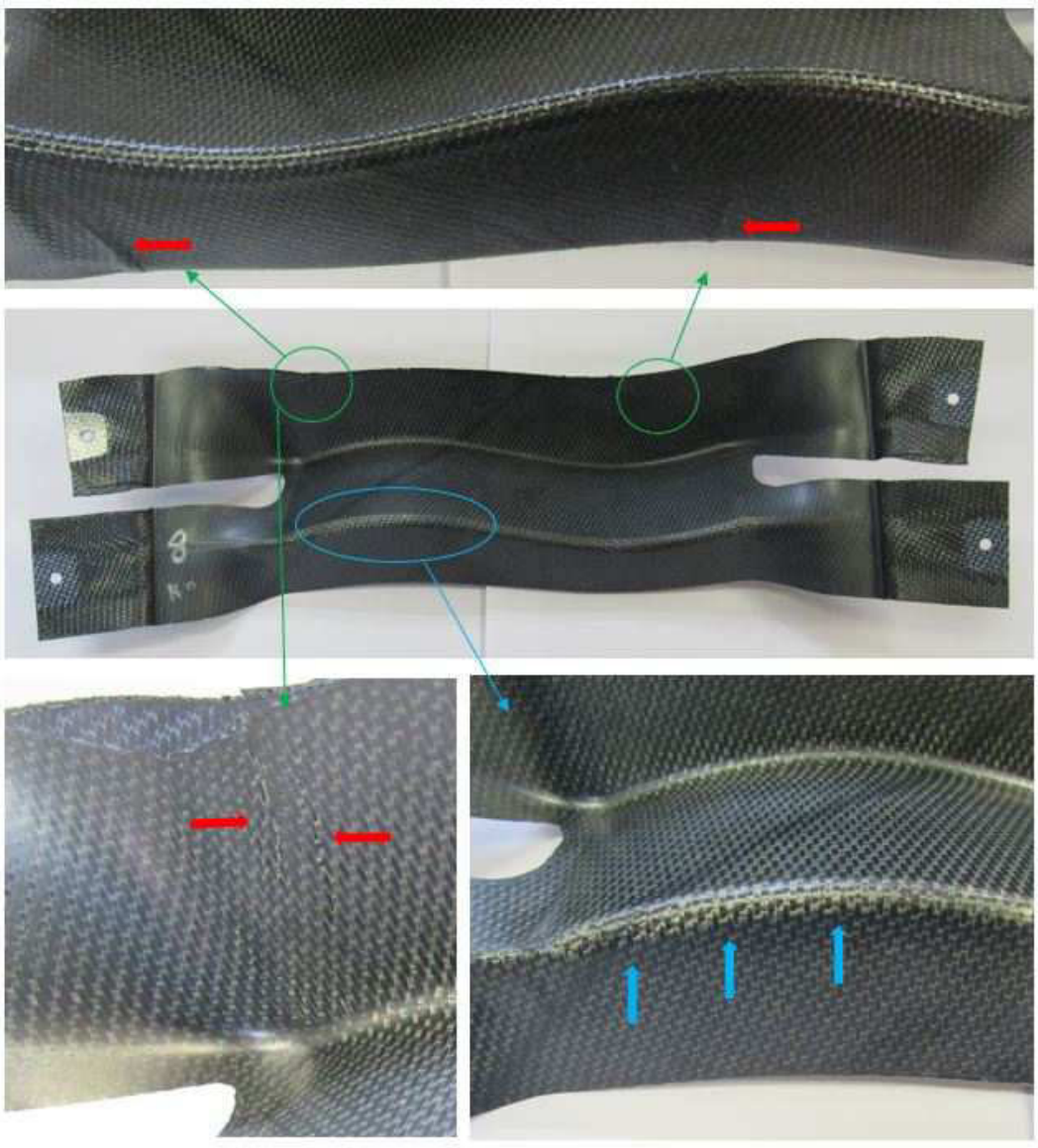


Figure 7.44: Results for Z-section manufactured from blank 2 formed with a spring stiffness of 0.09 N/mm.

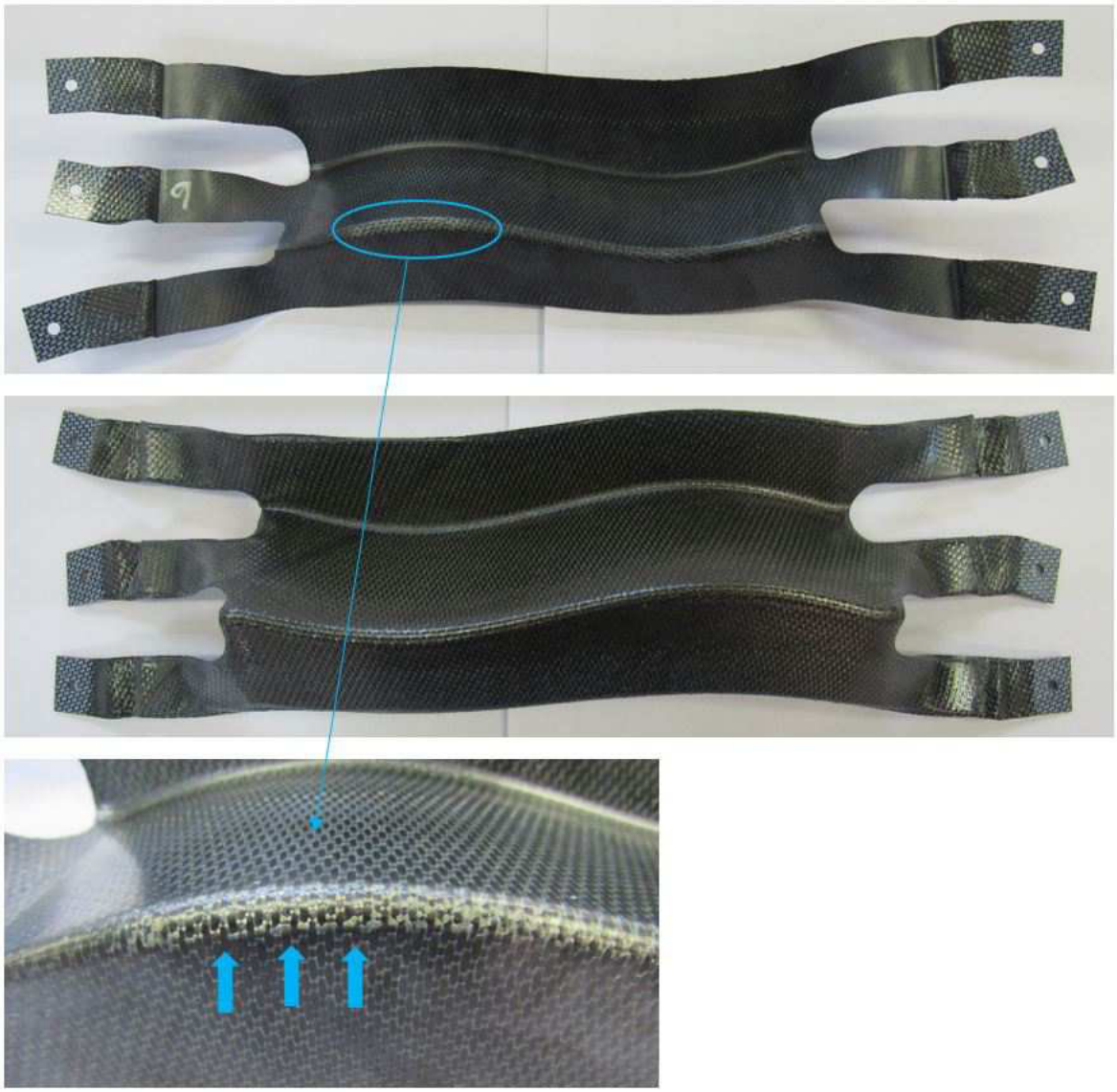


Figure 7.45: Results for Z-section manufactured from blank 3 formed with a spring stiffness of 0.09 N/mm.

7.4.5 Discussion

7.4.5.1 C-section

The pre-draped shape of blanks 1, 2 and 3 in Figure 7.34 correlate with the predictions shown in Figure 7.27. Blank 1 for the C-section geometry is shown in Figure 7.34 A. The red lines denote the points of first contact between the blank and the tool. These lines on the laminate do not move away from each other as the tool closes and flattens the laminate. This resulted in the blank buckling as the tool is closed. The buckled laminate must then follow one of the paths described in Figure 7.46. The results in Figure 7.30 predicted that blank 1 would result in wrinkling along the flanges in ply 1. The results from the experimental sample correlated with the prediction as shown in Figure 7.36, the component had wrinkles on both flanges.

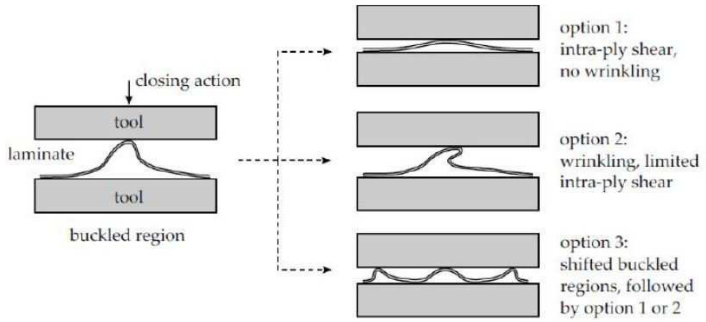


Figure 7.46: The evolution of a buckled region [4].

If the two contact lines are moved away from one another, the laminate would have to shear (intra-ply) less to drape into the same geometry. At the extreme, this would mean that the pre-drape shape would be a flat blank. Blank 2 was intended to represent this scenario (Figure 7.34 B). The simulated results for blank 2 are shown in Figure 7.31, the predicted wrinkling along the flanges in ply 1 meant that blank 2 had no advantage over blank 1. This was supported by experimental results which were presented in Figures 7.36 and 7.37.

The regions that buckled were unaffected by the change from blank 1 to blank 2. Blank 3 was designed with tags positioned to apply tension to the flanges to prevent them from buckling. The position of the tags in blank 3 induced a pre-draped shape that mimicked the geometry of the tool as in Figure 7.34 C. The formability prediction presented in Figure 7.32 showed that blank 3 had reduced wrinkling in the useful portion of the blank. The wrinkling that was predicted occurred on regions outside the trim lines of the final component. Compare the C-section final geometry in Figure 7.3 to the simulated formed blank in Figure 7.32 for a reference on the position of the trim lines. This was corroborated by the experimental results which are presented in Figure 7.38 which show that the wrinkles occurred at the boundary

of the blank. A wrinkle free component could be attained from blank 3 despite the wrinkles at the boundary.

The shear angle results for ply 2 for blanks 1, 2 and 3 in Figures 7.39, 7.40 and 7.41 all predicted good formability. The results show a smooth shear angle distribution across the blank with shear angle concentrations which nonetheless do not display the shear localization characteristic. The regions where the lugs attach to the body of the blank have the highest shear angle. This is due to the fact the $\pm 45^\circ$ fibres in ply 2 are not aligned with the BRM force, the tension created by the force has the effect of splitting the ply. The fibres in the $\pm 45^\circ$ are in the well suited orientation to form the C-section geometry. The strength requirement of component may require fibres in the $0^\circ/90^\circ$ directions so it is usually not always plausible for a component to be specified with $\pm 45^\circ$ plies only.

The pre-drape results for blank 4 were presented in Figure 7.35. The bottom ply of the laminate sagged under its own weight and separated from the stack. The fibres in this ply run in the $0^\circ/90^\circ$ direction whereas the tags were oriented in the $\pm 45^\circ$ direction, this set-up is shown in Figure 7.47. The bottom ply was only supported by the thermoplastic matrix which did not have enough strength to do so in its molten state.

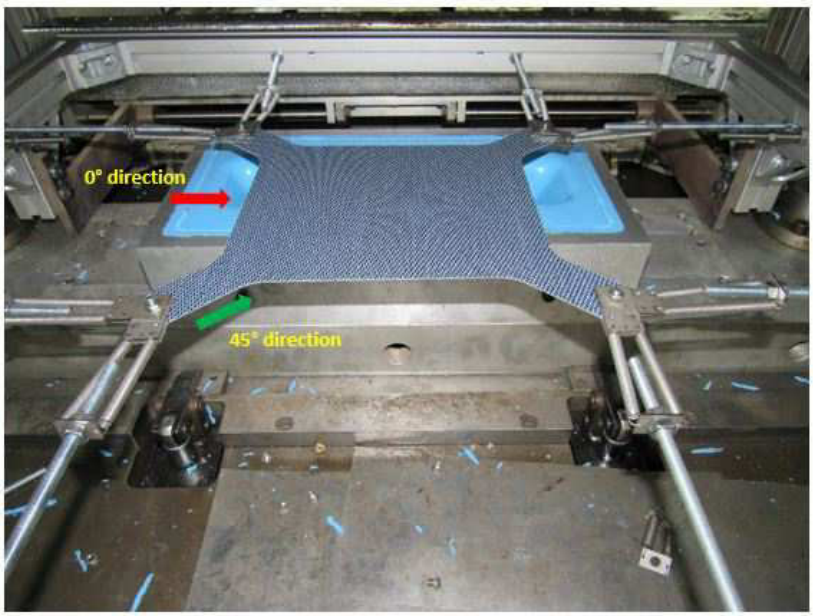


Figure 7.47: Set-up for blank 3.

This ply separation was not predicted by the simulation software marking a deviation from what was observed in the experiment. The contact between plies is modelled using an adhesion model, the model simulates the 'tackiness' between two contact surfaces by specifying a normal pressure that keeps the surfaces together [4]. The simulated gravity load on the

bottom ply did not exceed its 'adhesion pressure' keeping it in contact with the ply adjacent to it. This normal pressure is managed by the specification of a parameter called the 'adhesive tension'. This parameter forms part of the material definition which was acquired from AniForm Engineering BV so it could not be readily changed without supporting material characterisation tests. The simulation results presented for this blank are under the assumption that the laminate remained intact during heating.

The results of this experiment showed the design of the blank has a significant influence on the formability of a geometry. The blank design determines the shape assumed by the molten blank and this shape influenced the behaviour of the blank as it is formed The design of the blank should focus on arranging the tags in suitable positions so that the desired pre-drape is achieved.

Besides their positioning, the tags need to be designed such that they provide sufficient support to the blank without compromising the formability of the component. The BRM clamp serves as a heat shield at the point where it attaches to the tag which prevents the clamped region from melting, ensuring that the blank remains firmly secured. Figure 7.48 shows the varying degrees of melt along the tag. Note the difference in colouration between the melt region and out-of-melt regions. These can be used to identify regions with insufficient melt on the blank itself. The tag must be long enough such that the out-of-melt region is sufficiently distanced from the body of the blank. The tag also needs to be a sufficient length to prevent the clamp from getting caught in the tool as the tag is drawn in during forming.

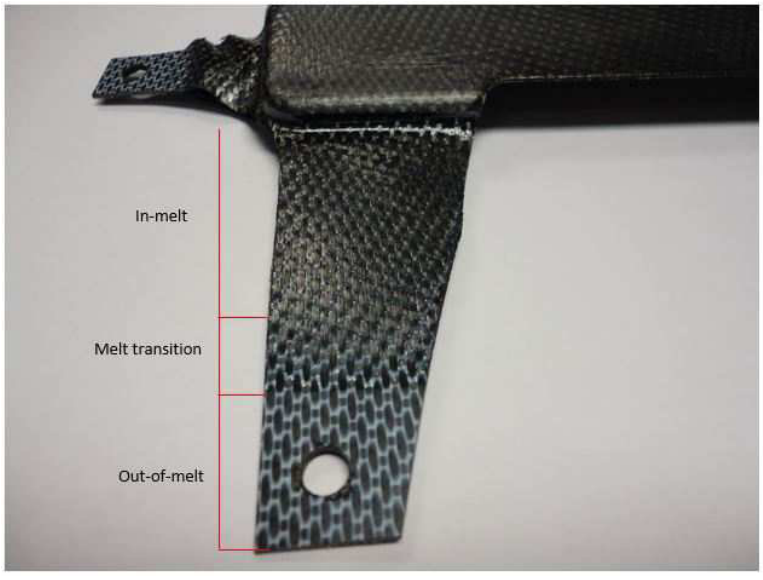


Figure 7.48: Tag showing the melt zones

7.4.5.2 Z-section

The forming predictions for the Z-section blanks 1 and 2 were shown in Figures 7.39 and 7.40 respectively. The state of the deformation of the blank prior to the closing of the tool is shown in the inserts at top of the mentioned figures. Blank 1 presents wavy undulations which are evidence of the laminate buckling. The buckled regions resulted in shear localization in ply 1 as shown in Figures 7.39. This prediction showed that the blank would wrinkle during forming. Blank 1 was not formed experimentally due to tool design limitations.

Blank 2 also presents signs of laminate buckling before full tool closure (Figure 7.40). The severity of the buckling is less in comparison to that observed in blank 1. The buckled regions however, also progressed to develop shear localization in ply 1 in the final geometry. The results for the Z-section manufactured using blank 2 are presented in Figure 7.50. The red markers in the figure indicate the wrinkling, which correlates with the theoretical predictions. The region marked with the black ellipse in the simulation results (Figure 7.40) predicted the development of wrinkling, this was not observed in the experimental result. The experimental sample also presented a region with resin squeeze out along the bend-line, this is marked by the blue markers in Figure 7.50. The simulation model predicted that the fibres in this region would experience large tensile stresses which is shown in Figure 7.42 (marked A). This resulted in fibre bridging over the rubber tool and resin squeeze-out. The texture of the surface of the laminate in this area was rough supporting the notion that the laminate was not in contact with the metal tool in this region. There were no results on the experimental sample that could be linked to the high fibre stress region marked B.

The state of deformation of the blank towards the final stages of tool closure show that laminate buckling can be detected by analysing the blank at this stage of the closing tool. This was the case with blank 1 and 2 for the Z-section geometry as per Figures 7.39 and 7.40. The absence of visible laminate buckling in the blank before tool closure does not necessarily mean that the blank will not form wrinkles as factors such as the size the mesh elements determine how accurately the geometry of the laminate is represented. The blanks for the C-section did not present with definite laminate buckling prior tool closure (Figure 7.29) but they all developed wrinkles after the tool was closed. The susceptibility of the flanges of C-section blanks 1 and 2 could nonetheless be detected. The prime parameter for predicting wrinkling is the shear angle result when the tool is been fully closed.

The prediction for blank 3 showed shear localization, with a slightly lower susceptibility to wrinkling in comparison to blank 2. This was attributed to the fact that this blank had 6 tags with 6 BRMs as opposed to the 4 for blank 2. This created a larger tensile load in the fibres, reducing the tendency of the blank to buckle and develop wrinkles. The experimental results

were presented in Figure 7.45, where it can be seen that the component did not develop any wrinkles. This is contrary to the prediction returned by the simulation results which showed shear localization.

7.4.6 Conclusions

1. The design of the blank, particularly the position of the tags determines the shape which the blank assumes when melted.

2. Blank 3 for the C-section was best suited to forming this geometry because it could be pre-draped to the final geometry.

3. Blank 3 of the Z-section produced the best formability for the geometry.

4. Analysing the deformation of the blank prior to the tool completely closing and consolidating the blank provides an image of the regions that buckle. It also indicates and how they buckle so the blank can be redesigned to address the buckling problem.

7.5 Investigation 4: The effect of spring stiffness

7.5.1 Problem Background and Identification of Cause

The experimental results for the C-section blank 3 and Z-section blank 2 were presented in Sections 7.4.4.2 and 7.4.4.4 respectively. These results have been presented again in Figures 7.49 and 7.50 on the pages that follow. Both these results show the occurrence of wrinkles on the components marked with the red arrows. These wrinkled components were adopted as the problem to this investigation. The purpose of this investigation was to improve the formability of the two blanks. The design of the blanks was taken as fixed and another parameter had to be employed to affect the formability of the blanks.

It was hypothesized in Section 7.4.5 that the wrinkling in both the blanks was caused by laminate buckling as the laminate was draped into the required geometry. In the case of the Z-section geometry, the laminate buckling was identified by looking at the simulated deformation of the blank before the tool was fully closed. The buckled regions resulted in shear localization in the laminate when the tool progressed to its closed state. These results were presented in Figure 7.40. The region with shear localization coincided with the wrinkles on the experimental component.

7.5.2 Proposed solution

The proposed solution was to increase the stiffness of the BRM springs. It was hoped that a higher stiffness would increase the tensile load in the fibres thereby reducing laminate's tendency to buckle as the tool closed. The stiffness of the springs was accordingly increased from 0.09 N/mm to 0.23 N/mm to test this.

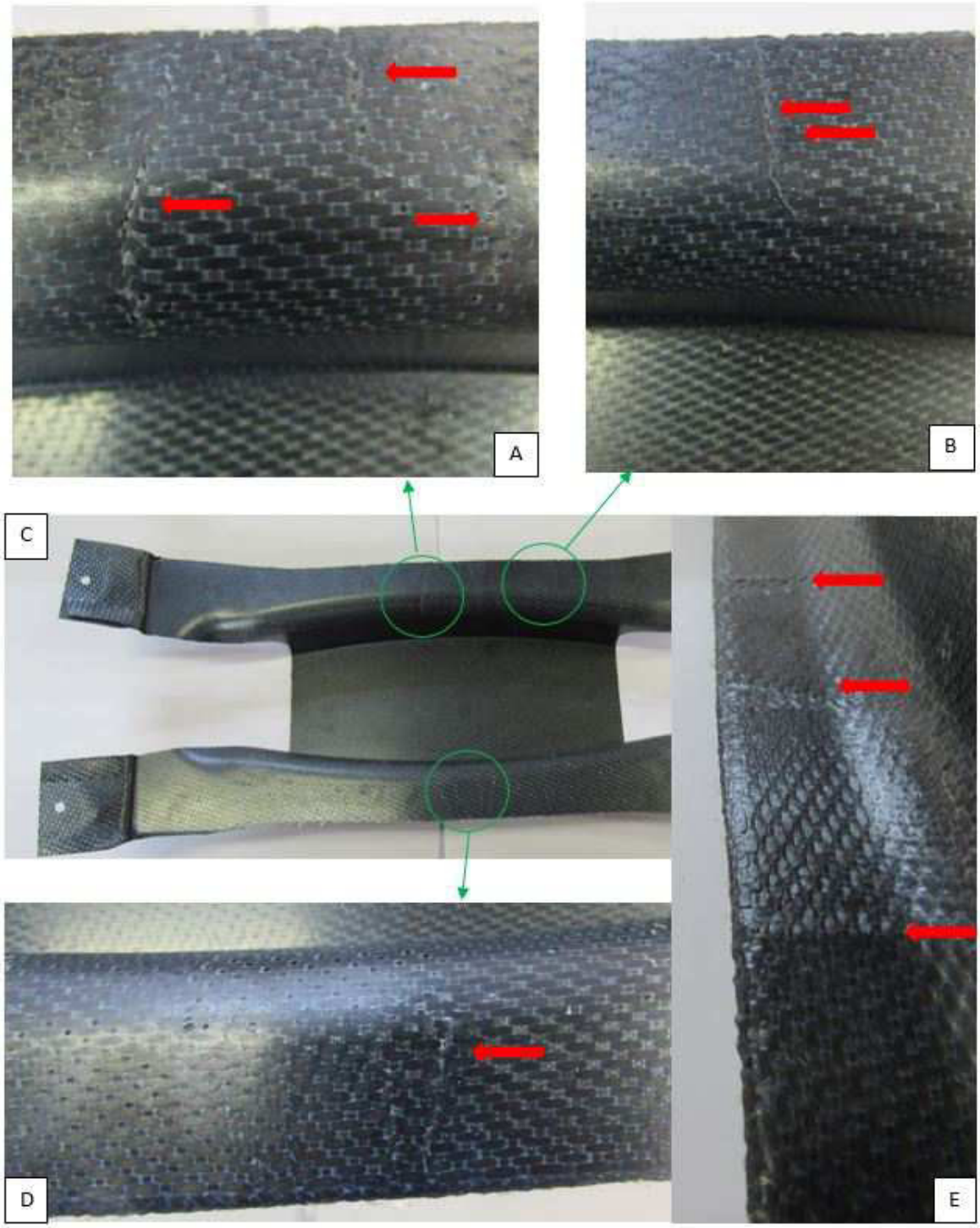


Figure 7.49: C-section blank 3 spring stiffness - 0.09 N/mm

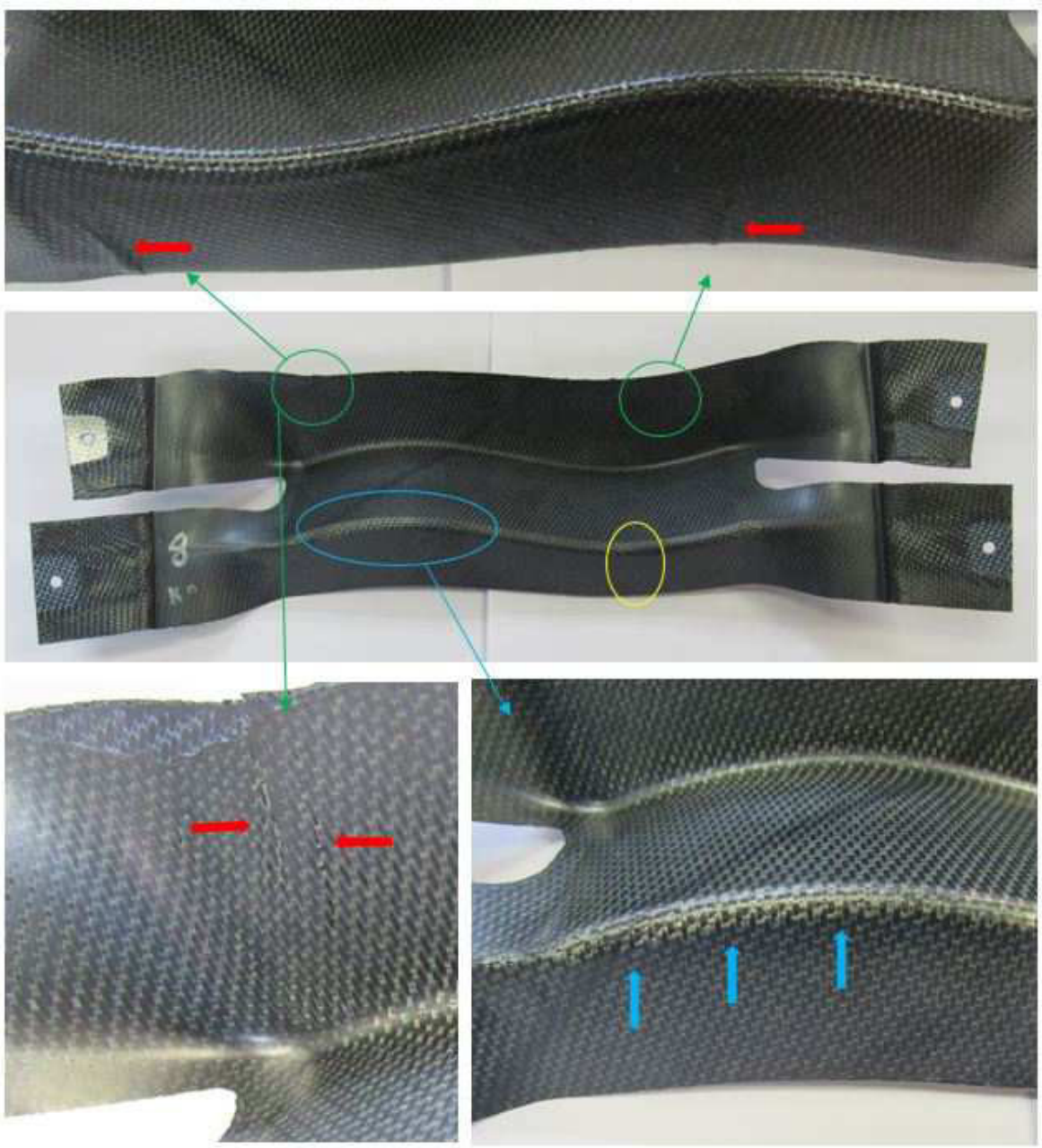


Figure 7.50: Results for Z-section manufactured from blank 2 with a spring stiffness of 0.09 N/mm.

7.5.3 Results

This section present the results for the C and Z-section geometries formed with a BRM spring stiffness of 0.23 N/mm. The simulation results are presented, followed by the results of an assessment of the effect of the increase in spring stiffness on the simulation results. Only the shear angle results are shown since the shear angle is the parameter used to identify the susceptibility to wrinkling. Lastly the experimental results of the manufactured component are presented.

7.5.3.1 C-Section: Simulated results

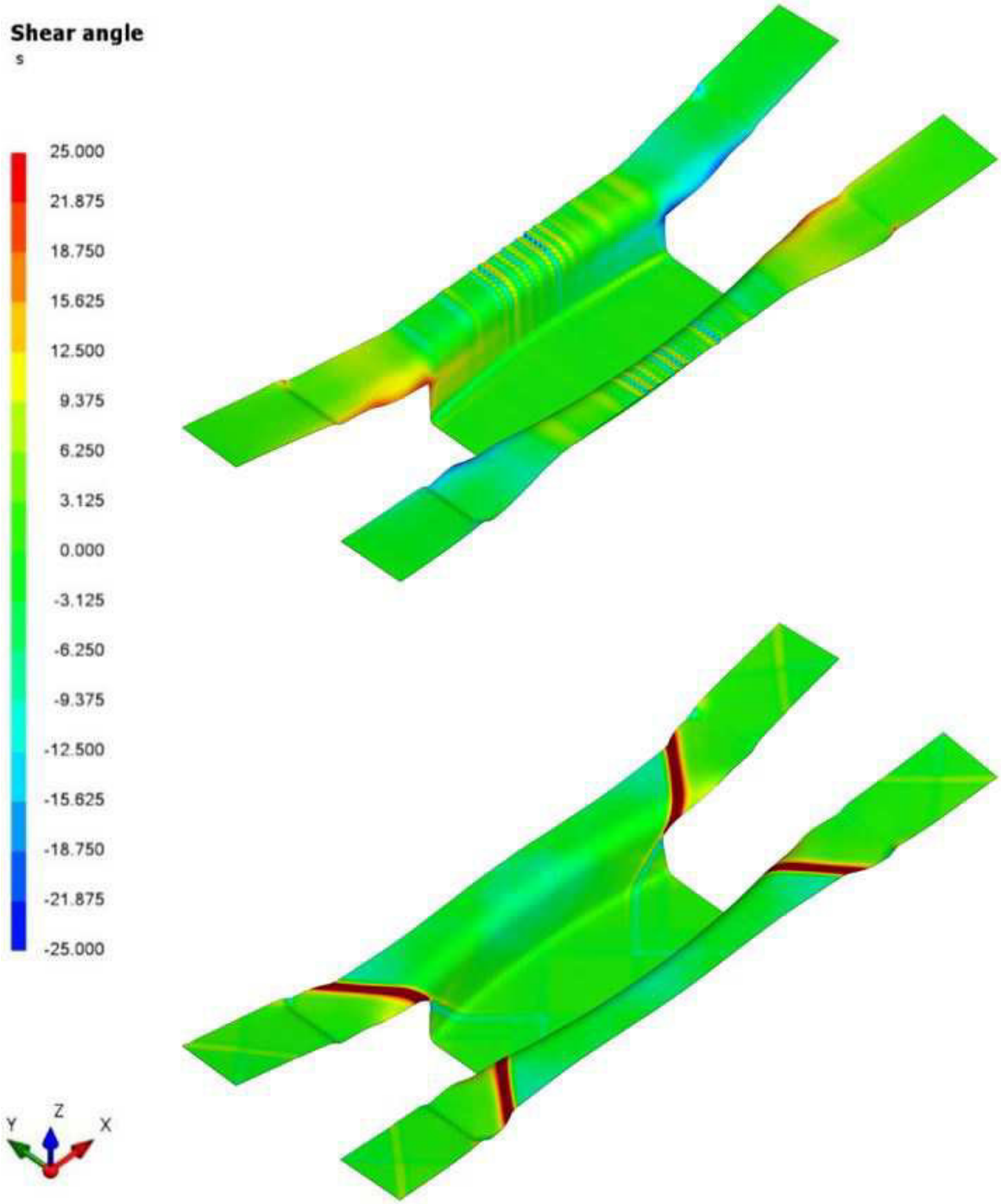


Figure 7.51: C-section blank 3 shear angle simulation results with a 0.23 N/mm spring stiffness. Ply 1 above and ply 2 below.

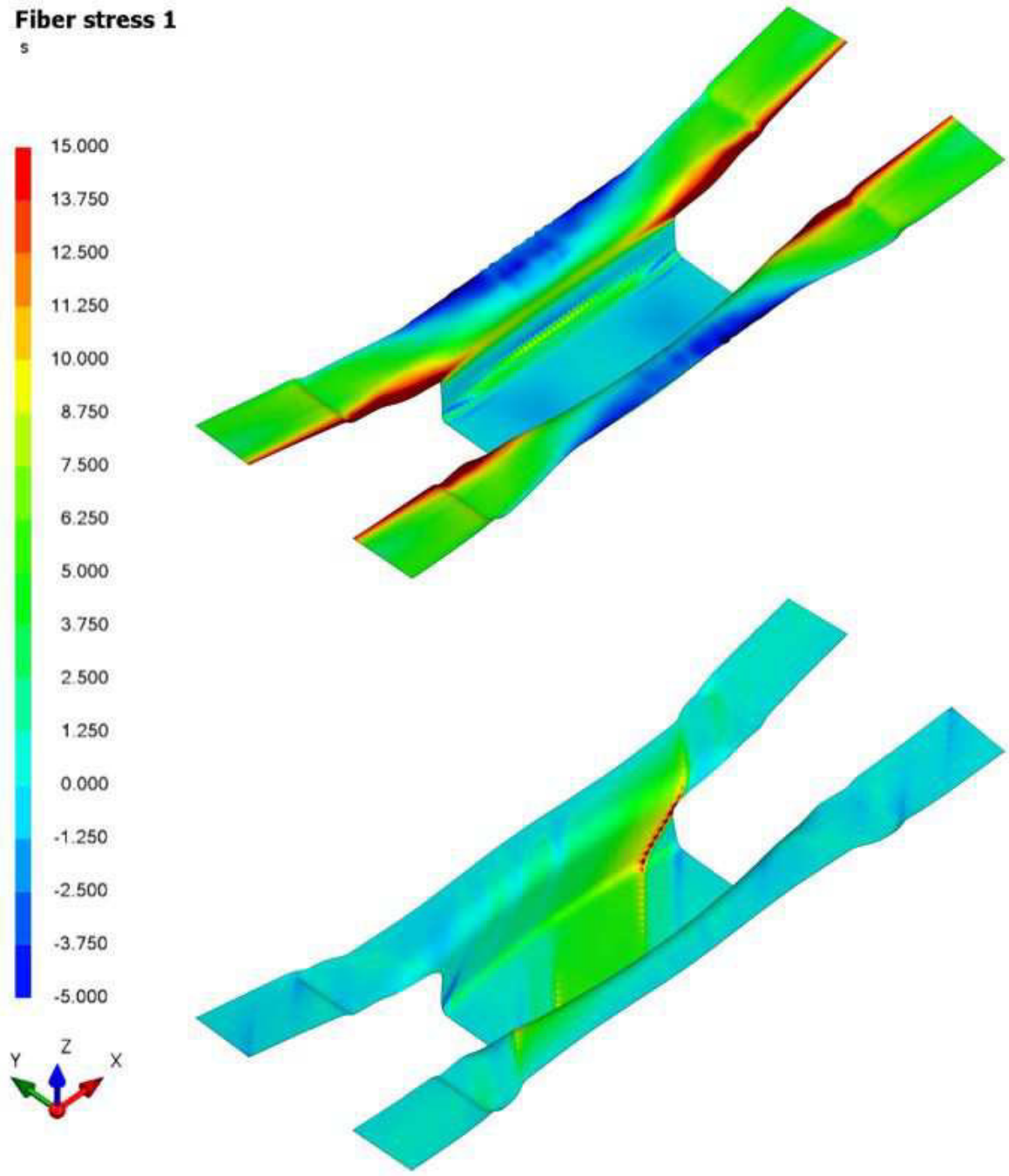


Figure 7.52: C-section blank 3 fibre stress 1 simulation results with a 0.23 N/mm spring stiffness. Ply 1 above and ply 2 below.

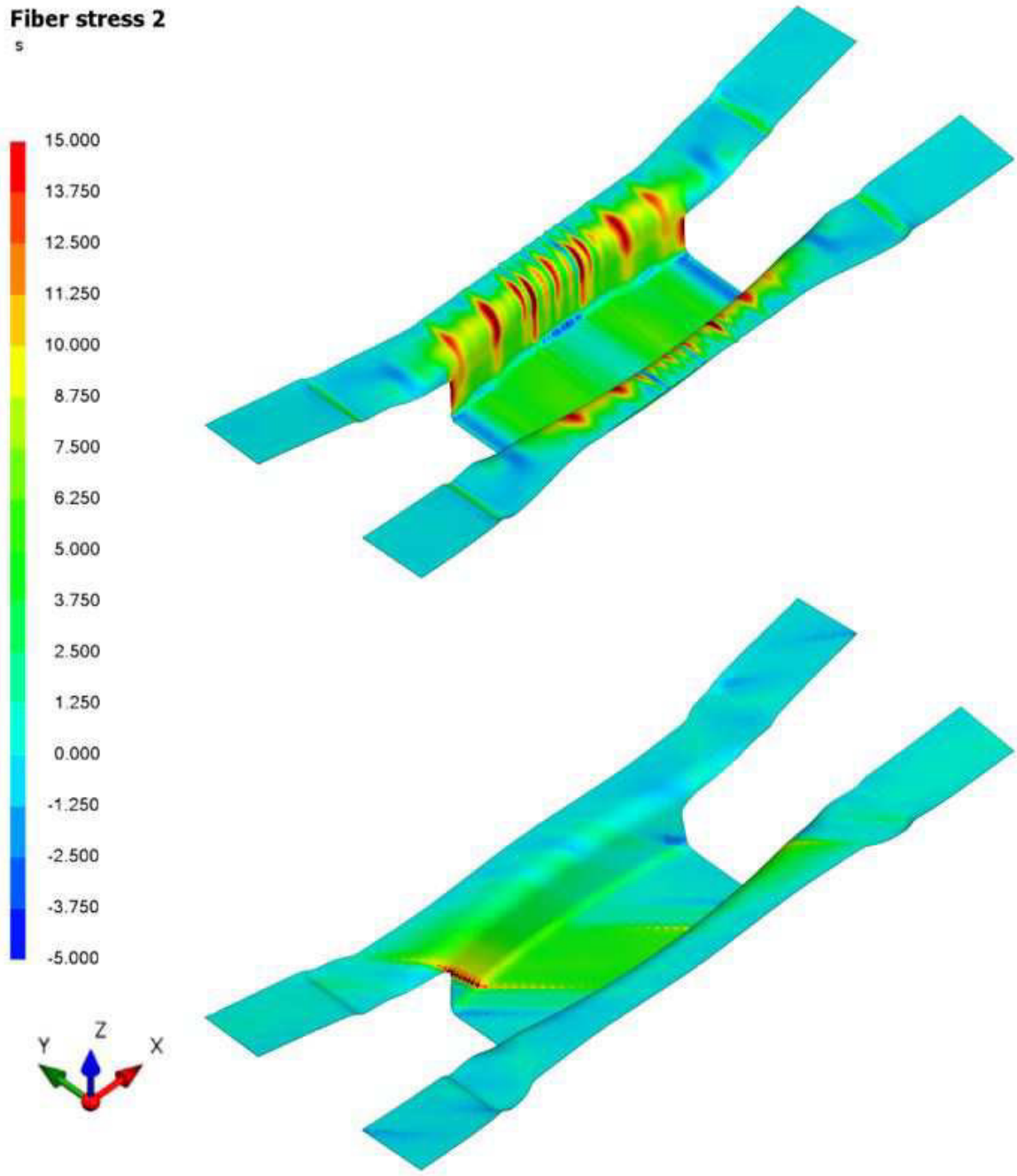


Figure 7.53: C-section blank 3 fibre stress 2 simulation results with a 0.23 N/mm spring stiffness. Ply 1 above and ply 2 below.

An assessment of the effect of the increase in spring stiffness on the simulated results was carried out. This is essentially a comparison of the predictions presented in Figure 7.32 to those in Figure 7.51. The responses of the shear angle and fibre stresses were determined for each of the plies. The terminology is used to document this in Table 7.1 has been detailed below. The effect of the response of the formability of the ply is also documented in the table. The formability of the plies was assessed by considering the appearance of the parameters. The implications of the nature of the shear angle and fibre stress distributions was presented in Section 4.3 (see Figure 4.7).

The terminology used in the table is defined as follows:

- 'increase' and 'decrease' under shear angle refers to the overall behaviour of the absolute value of the shear angle in the ply.
- 'increase' under fibre stress means both the maximum and minimum stresses in the ply increased.
- 'decrease' under fibre stress means both the maximum and minimum stresses in the ply decreased.
- 'diverge' describes behaviour where the maximum increased and the minimum decreased
- 'converge' describes behaviour where the maximum decreased and the minimum increased

The terms for the description of the fibre stress results have been illustrated in Figure 7.54. The 0.09 N/mm bar is the reference for all the responses.

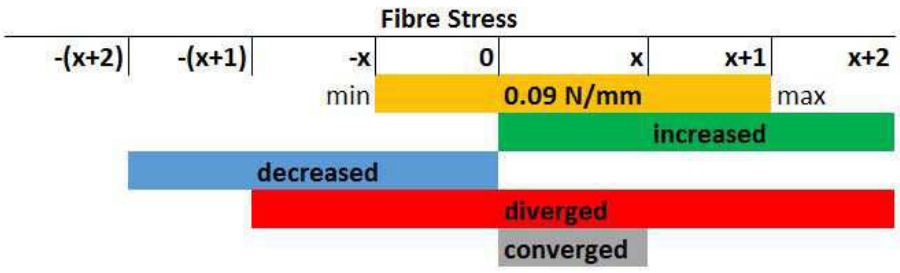


Figure 7.54: Fibre stress response guide.

Table 7.1 presents the results of the assessment of the simulation results of the C-section when the BRM stiffness is increased from 0.09 N/mm to 0.23 N/mm.

Table 7.1: C-Section results for increasing BRM stiffness from 0.09 N/mm to 0.23 N/mm.

Ply		**Shear Angle**	**Fibre Stress 1**	**Fibre Stress 2**
1	**Response:**	Decreased	Increased	Converged
	Formability:	Improved	Improved	Improved
2	**Response:**	Increased	Diverged	Diverged
	Formability:	No effect	No effect	No effect
3	**Response:**	Increased	Diverged	Diverged
	Formability:	No effect	No effect	No effect
4	**Response:**	Decreased	Increased	Decreased
	Formability:	Improved	Improved	Improved

7.5.3.2 C-section: Experimental results

Figure 7.55 shows the experimental results of C-section manufactured using the 0.23 N/mm springs. The component did not have any wrinkles, it presented an improvement over the component manufactured using the 0.09 N/mm springs.

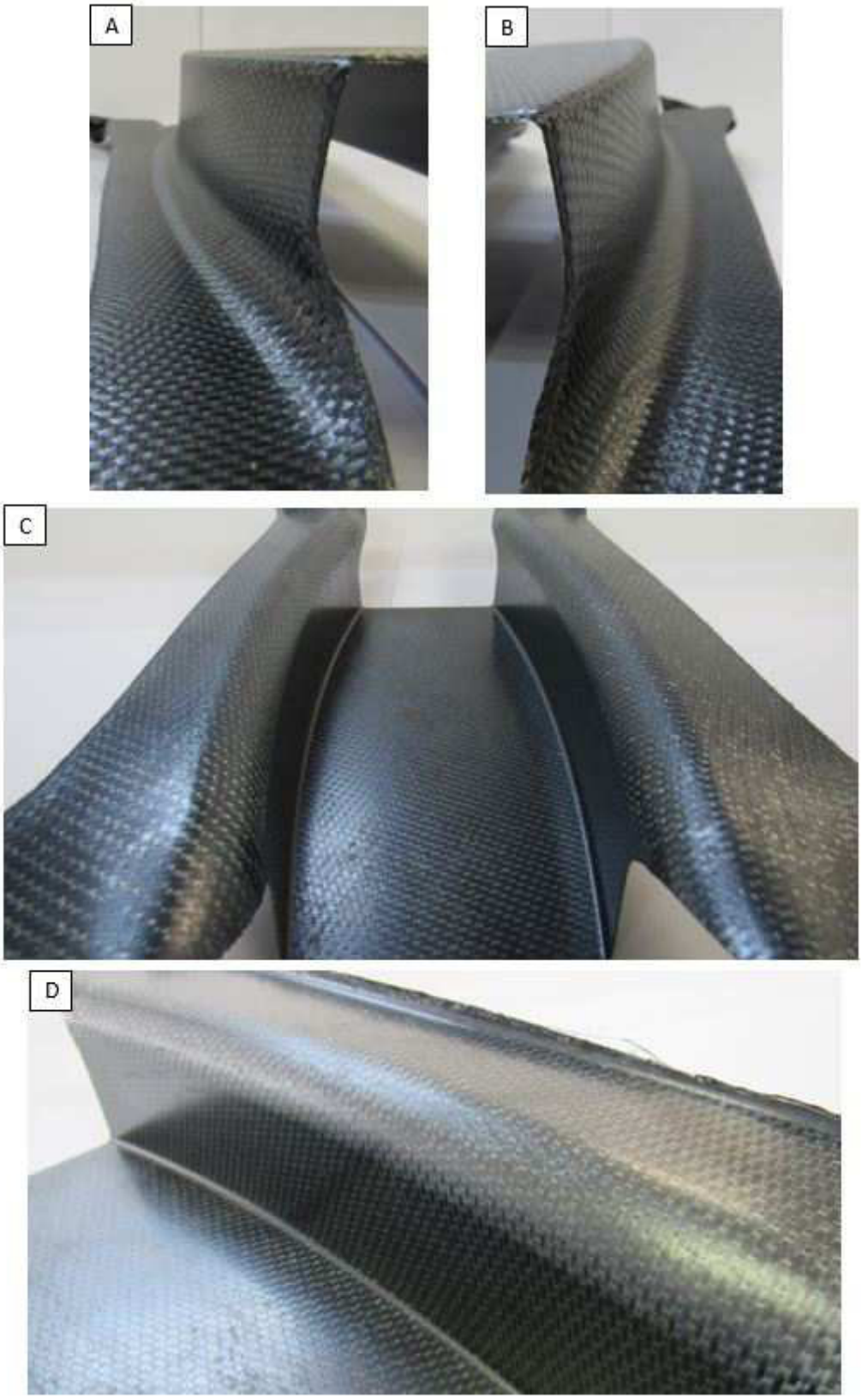


Figure 7.55: C-section spring stiffness - 0.23 N/mm

7.5.3.3 Z-section: Simulated results

Figure 7.56 presents the shear angle results of the Z-section simulation formed with a BRM stiffness of 0.23 N/mm. The ellipse marks a region that displays shear localization. Figure 7.57 presents the fibre stress 1 results of the Z-section simulation formed with a BRM stiffness of 0.23 N/mm. Figure 7.58 presents the fibre stress 2 results of the Z-section simulation formed with a BRM stiffness of 0.23 N/mm.

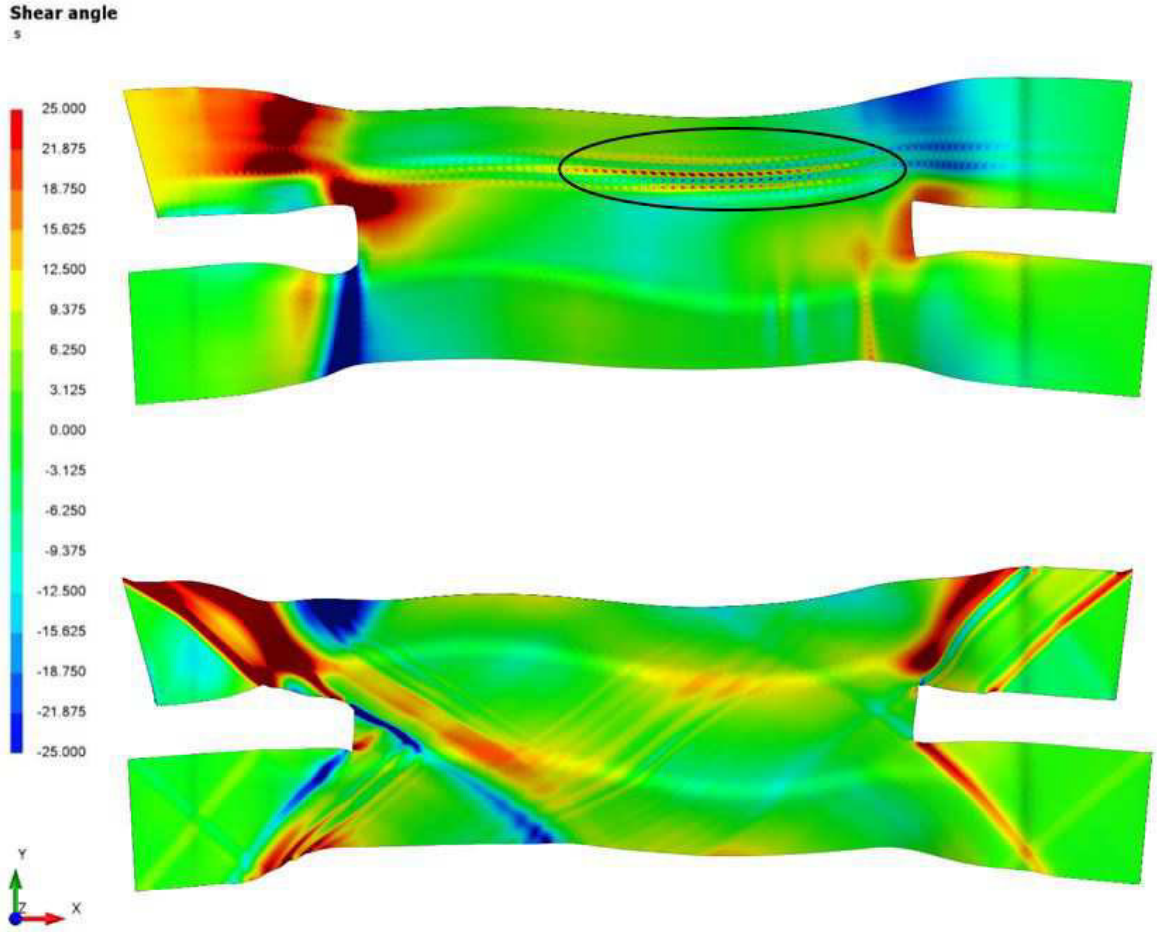


Figure 7.56: Shear angle Z-section results, spring stiffness - 0.23 N/mm. Ply 1 above and ply 2 below.

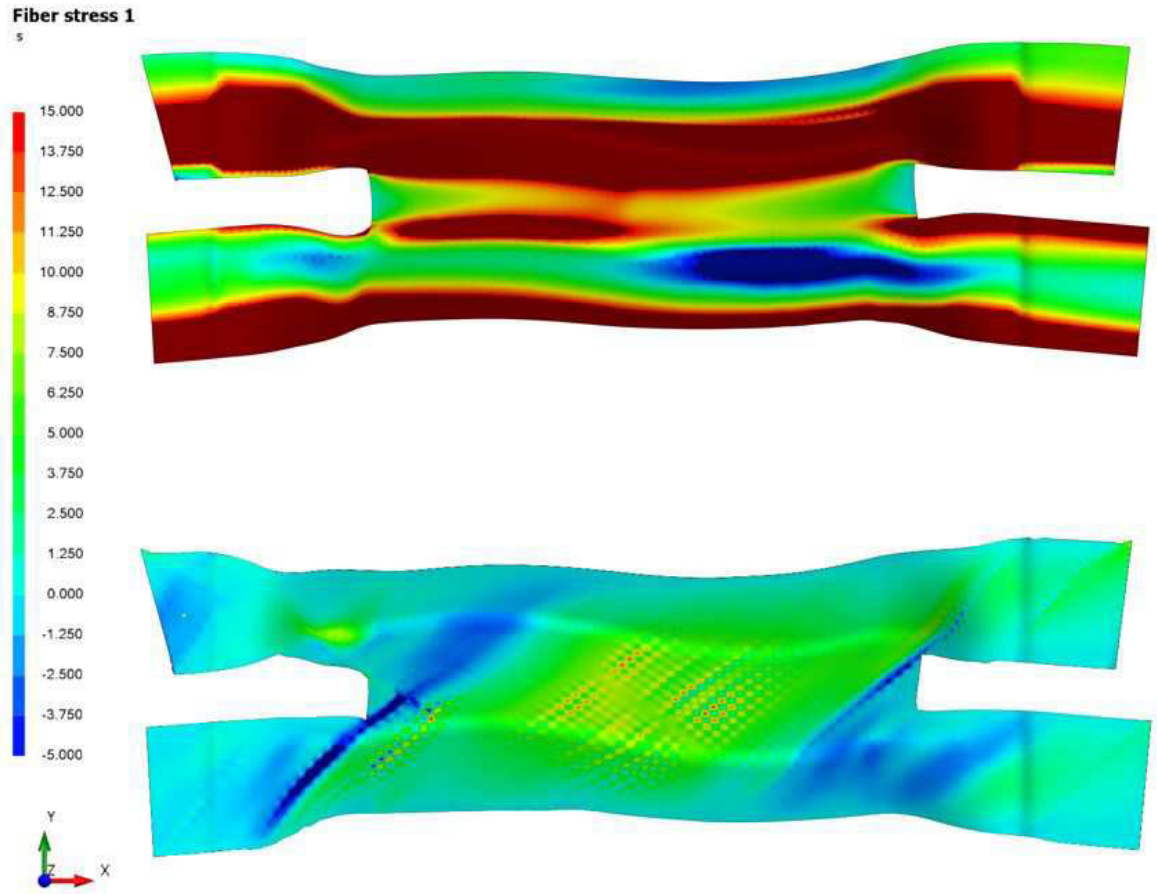


Figure 7.57: Fibre stress 1 Z-section results, spring stiffness - 0.23 N/mm. Ply 1 above and ply 2 below.

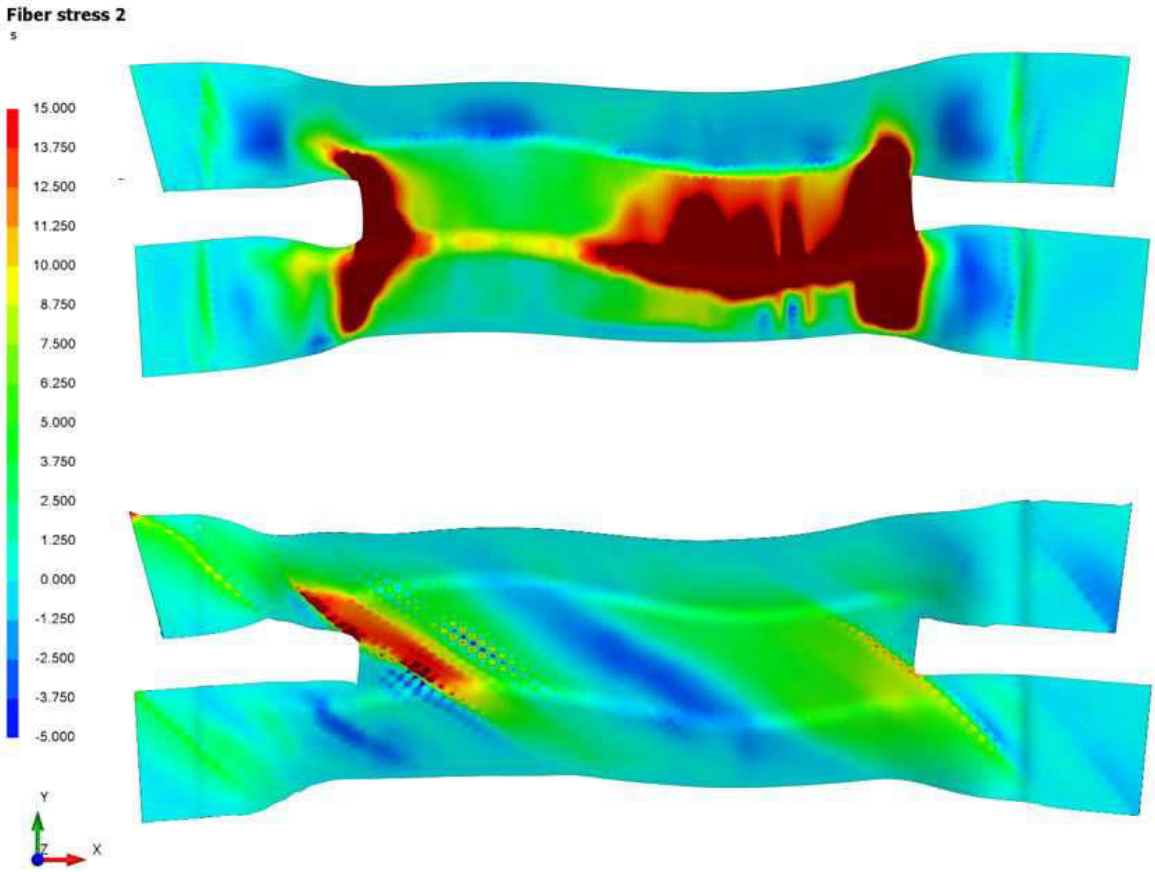


Figure 7.58: Fibre stress 2 Z-section results, spring stiffness - 0.23 N/mm. Ply 1 above and ply 2 below.

Table 7.2 presents the results of the assessment of the simulation results of the Z-section when the BRM stiffness is increased from 0.09 N/mm to 0.23 N/mm.

Table 7.2: Z-Section results for increasing BRM stiffness from 0.09 N/mm to 0.23 N/mm.

Ply		**Shear Angle**	**Fibre Stress 1**	**Fibre Stress 2**
1	**Response:**	Increased	Increased	Converged
	Formability:	Improved	Improved	Improved
2	**Response:**	Increased	Decreased	Increased
	Formability:	No effect	No effect	No effect
3	**Response:**	Increased	Decreased	Increased
	Formability:	No effect	No effect	No effect
4	**Response:**	Increased	Increased	Converged
	Formability:	Improved	Improved	No effect

7.5.3.4 Z-section: Experimental results

Figure 7.55 shows the experimental result of Z-section manufactured using the 0.23 N/mm springs. The component did not have any wrinkles, it presented an improvement over the component manufactured using the 0.09 N/mm springs.

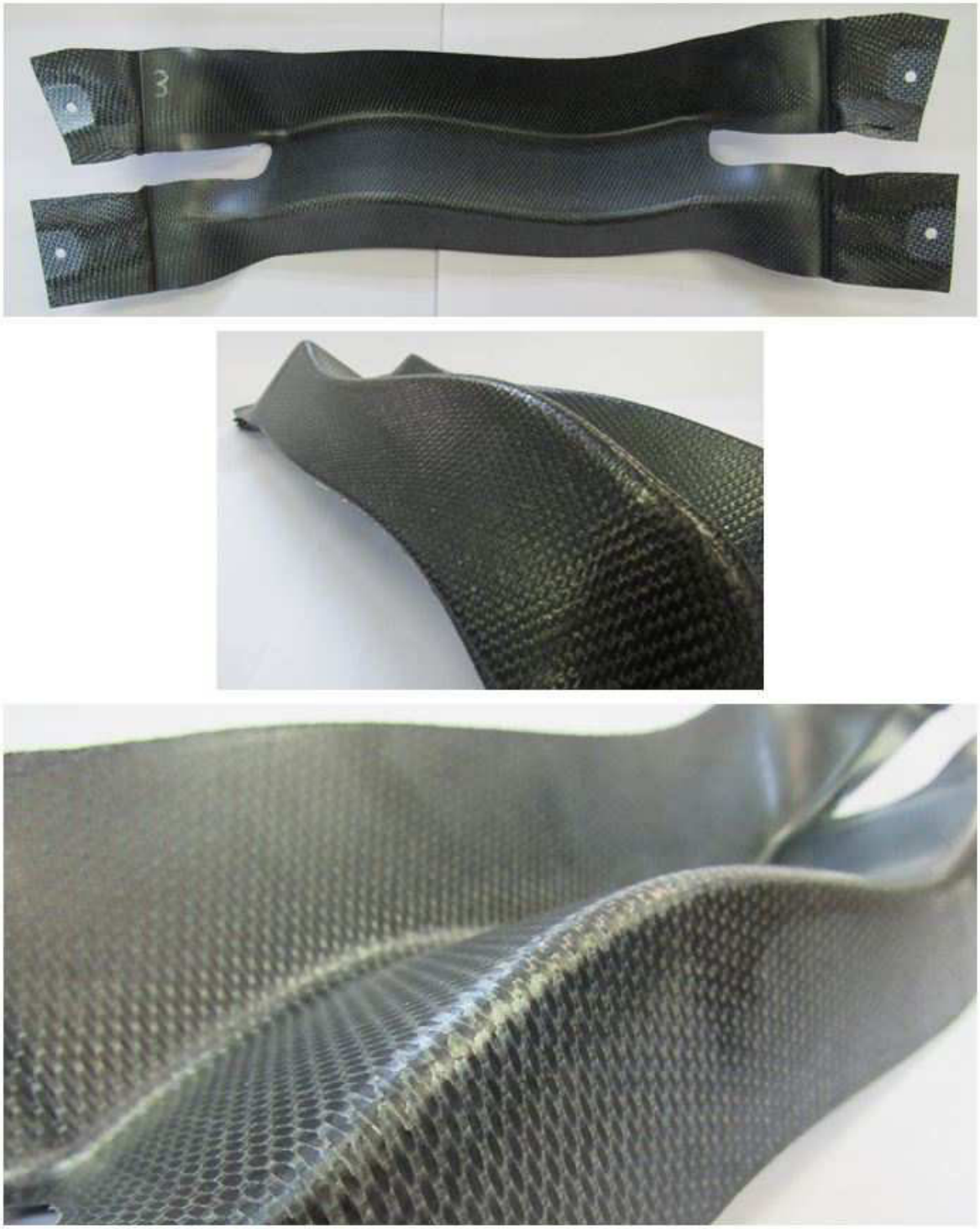


Figure 7.59: Z-section results, spring stiffness - 0.23 N/mm.

7.5.4 Discussion

7.5.4.1 C-section

Shear Angle

The simulated shear angle results presented in Figure 7.55 (0.23 N/mm) present a shear distribution similar to that presented in Figure 7.32 (0.09 N/mm). The increase in BRM stiffness had the effect of decreasing the shear localization at the regions where wrinkles were predicted. The following minimum/maximum shear angle values were recorded; $-34°/36°$ for the 0.09 N/mm simulation and $-32°/23°$ for the 0.23 N/mm simulation. The shear angle required to drape ply 1 to the geometry decreased and thus the formability of the ply was improved. This result has been documented likewise in Table 7.1.

The shear angle results for ply 2 show that the minimum and maximum shear angles for the 0.09 N/mm and 0.23 N/mm simulations fall into the same range ($-12°/12°$) on the legend to the graph. But the distribution of the shear angles is slightly different with the 0.23 N/m presenting more of the minimum and maximum shear angles. There was no discernible change in the formability of the ply. This is due to the fact that ply 2 has fibres aligned at 45° to the force applied by the BRM. The force has the effect of splitting the ply, this supported by the large shear angles where the tags meet the body of the blank. This isolates the body of the blank from the applied force. The slight increase in shear angle can be attributed to the fact that wrinkling has been eliminated in ply 1 and thus improved the formability of the blank. When a ply in a laminate wrinkles, the intra-ply shear mechanism becomes very limited because the mobility of the fibres become compromised. The elimination of wrinkling in the laminate by increasing the BRM stiffness offers the fibres of ply 2 improved mobility, increasing that ability to shear.

The simulation results show that increasing the spring stiffness had a positive effect on the formability of the geometry. The stiffer springs produced a greater force in the fibres preventing the laminate from buckling and reducing the laminate's susceptibility to wrinkling. Plies 2 and 3 do not contain any fibres in the direction of the force applied by the springs which means that the springs have only a very limited influence on the forming mechanisms taking place in these plies.

Fibre Stress 1

Fibre stress 1 denotes the stress in the fibre aligned to direction 1 which runs along the length of the component in ply 1 (x-direction). The increase of the BRM stiffness increased the fibre stresses in direction 1. This direction was aligned with the BRM force and therefore the load

introduced was easily transmitted along the blank by the continuous fibres. This had the effect of increasing the stresses of regions that were in compression and had buckled with the use of the 0.09 N/mm BRM. The mitigation of the buckling presented as an improvement to the formability of the ply.

The increase in spring stiffness had the effect of 'diverging' the fibre stresses in ply 2. The following minimum/maximum fibre stress values were recorded; $-2/21$ MPa for the 0.09 N/mm simulation and $-3/22$ MPa for the 0.23 N/mm simulation. The regions that were in tension experienced an increase in fibre stresses while the regions that were in compression recorded a decrease in fibre stresses. This change though, was too small to have a discernible effect on formability of the ply. Fibre direction 1 runs at 45° to the BRM force therefore the load introduced to the blank is not effectively transferred to blank body. The BRM has limited influence on the formability of ply 2.

Fibre Stress 2

Fibre stress 2 denotes the stress in the fibres aligned to direction 2 which runs across the length of the component in ply 1. The following minimum/maximum fibre stress values were recorded; $-7/130$ MPa for the 0.09 N/mm simulation and $-5/20$ MPa for the 0.23 N/mm simulation. The results presented a decrease in maximum fibre stresses which predicts an improvement in formability of the ply. The fibres in the direction 2 are orthogonal to the applied BRM force but they interact directly with the fibres in direction 1 since they are woven together to create the ply. The increase in fibre stress in direction 1 straightens the fibres in direction 1 which in turn increases the waviness of the fibres in direction 2, this has the effect of decreasing the fibre stresses in direction 2. The minimum fibre stress presented an increase in fibre stress and this was also perceived as an improvement in formability since it implies that the regions in compression had less compressive strain as a result of the increase in tension.

In ply 2, the following minimum/maximum fibre stress values were recorded; $-2/19$ MPa for the 0.09 N/mm simulation and $-3/22$ MPa for the 0.23 N/mm simulation. These results presented a decrease in the minimum fibre stress and an increase in the maximum fibre stress. This placed the compressive region in a worse state and also worsens the high stress concentrations in the ply. This means that, with reference to the fibre stress 2 in ply 2, the formability of the laminate is being deteriorated by the increase in BRM stiffness. The change though, was too small to record a discernible difference between the formability of the plies under the two BRM stiffnesses.

This discussion only covered the results of ply 1 and 2, a complete summary of the results has been presented in Table 7.1. Plies 1 and 2 represent the unique fibre orientations in the

laminate. The results for plies 3 and 4 mirror the results plies 2 and 1 respectively, excluding the fibre stress 2 results for ply 1. The minimum fibre stress 2 in ply 1 increased whereas the minimum fibre stress 2 in ply 4 decreased.

In summary, the simulation predicted that the increase of the BRM stiffness will have the effect of improving the formability of the geometry.

Experimental Results

The experimental result for the C-section component formed using BRMs with a stiffness of 0.23 N/mm were presented in Figure 7.55. The component was free from wrinkles presenting an improvement over the component formed using the 0.09 N/mm BRMs (see Figure 7.49). This results corroborated the prediction that was reach in the simulation study. The formability of a geometry can be influenced by the stiffness of the BCM springs.

7.5.4.2 Z-section

Shear Angle

The simulated shear angle results presented in Figure 7.56 (0.23 N/mm) must be compared to the results presented in Figure 7.40 (0.09 N/mm) to assess the impact on increase in BRM stiffness. In ply 1, the increase in BRM stiffness had the effect of removing the shear localization that was predicted in 3 regions on the blank. Two of the these regions had developed into wrinkles in the experimental component (see the green circles in Figure 7.50). These wrinkle appeared across the length of the component, the increase in BRM stiffness cleared the prediction of these wrinkles but predicted to susceptibility to a wrinkle running along the length of the component. The wrinkle has been marked with the ellipse in Figure 7.56. The following minimum/maximum shear angle values were recorded; $-51°/39°$ for the 0.09 N/mm simulation and $-39°/42°$ for the 0.23 N/mm simulation. It was concluded that the prediction using the 0.23 N/mm represents an improvement since it predicts the occurrence of wrinkling in 1 region versus the 3 in the 0.09 N/mm prediction.

In ply 2, the following minimum/maximum shear angle values were recorded; $-51°/39°$ for the 0.09 N/mm simulation and $-39°/42°$ for the 0.23 N/mm simulation. This presents an increase in shear angle in the ply. The results presented a similar shear angle distribution for the two simulations. The change in formability between the two BRM stiffness was not discernible. The influence of the increase in BRM stiffness is marginal in this ply due to the fact that both fibre directions in the ply run at 45° to the BRM force.

Fibre Stress 1

The fibre stress 1 is the the stress of the fibres in direction 1, in ply 1 these fibres run along the length of the component. The following minimum/maximum fibre stress values were recorded; $-20°/77°$ for the 0.09 N/mm simulation and $-8°/99°$ for the 0.23 N/mm simulation. This presented an increase in fibre stress 1 in the ply, the fibres in direction 1 are aligned with the force introduced by the BRM so increase in stiffness has a major impact on the fibre stress. The increase in fibre stress was documented to have a positive effect on the formability of the ply since the regions that were in compression would then have reduced susceptibility to buckling.

In ply 2, the following minimum/maximum fibre stress values were recorded; $-10°/20°$ for the 0.09 N/mm simulation and $-9°/17°$ for the 0.23 N/mm simulation. The result presents a decrease in the fibre stress 1. This was attributed to the theory that the buckling and wrinkling in the blank formed using the 0.09 N/mm BRM stiffness constrains the fibres, limiting their mobility leading to higher fibre stresses. These fibres run at 45° to the force applied by the BRM, therefore they are not directly influenced by the BRM force.

Fibre Stress 2

The fibre stress 2 is the the stress of the fibre in direction 2, in ply 2 these fibres run across the length of the component. In ply 1, the following minimum/maximum fibre stress values were recorded; $-21°/55°$ for the 0.09 N/mm simulation and $-3°/51°$ for the 0.23 N/mm simulation. The minimum stress increased marking a reduction in the compressive regions and the maximum stress reduce. This was documented as an improvement in the formability of the ply due to the reduction in the susceptibility to buckling.

In ply 2, the fibre stresses in the 2 direction increased. The following minimum/maximum fibre stress values were recorded; $-10°/23°$ for the 0.09 N/mm simulation and $-10°/31°$ for the 0.23 N/mm simulation. The minimum stress remains the same and the maximum stress increased. The increase did not have a discernible impact on the formability of the ply.

Experimental Results

The experimental results presented in Figure 7.59 show that increase in stiffness from 0.09 N/mm (Figure 7.50)to 0.23 N/mm had a positive effect on the formability of the Z-section. The wrinkles circled green in Figure 7.50 did not occur in the specimen produced with the higher BRM stiffness. This improvement in formability corroborated the predictions made by the simulation software.

Summary

The response of the shear angle to the increase in spring stiffness was found to be different for the C and Z-section geometries. The C section recorded an decrease in shear angle whereas an increased was recorded for the Z-section. Besides this difference, the formability of both the components was improved. Wrinkling is identified by shear localization and not just the presence of large shear angles. Wrinkles that occur due to buckling of the laminate can occur at lower shear angles (lower than required for the laminate to drape the geometry) and the wrinkle itself will be a site of shear localization. Applying tension to the laminate prevents if from buckling and thus allowing the intra-ply shear mechanism to continue uninhibited, in this case the laminate can attain higher shear angles. The laminate can continue to shear in this manner whilst maintaining good formability until the shear locking angle of the material is reached (Figure 2.5). Wrinkling caused by the buckling of the laminate causes premature wrinkle in comparison to a fabric being sheared on a flat surface.

7.5.5 Conclusions

- The force applied by the springs has a direct influence on plies 1 and 4 due to the fact these plies have fibres aligned with the direction of the applied force.
- It is not possible to link the nature of the response of the parameters (increase/decrease) to the change in formability.
- The only way to determine the change in formability is by assessing the distribution plots of the parameters.
- The shear angle and fibre stresses responded to the change in stiffness in different ways ways for the two geometries.
- Though it may be difficult to match the parameter behaviour to formability it is clear that the increase in the spring stiffness improved the formability of both the C and Z-section geometries.

7.6 Investigation 5: The effect of material orientation

7.6.1 Background and Objective

The woven material results in different properties in the two fibre directions. The terms warp and weft are used to refer to the fibre tows in the two orthogonal directions. The orientation of the material relative to the component geometry is usually determined by considering the mechanical loads that the component will be exposed to. In a fabric that has an equal number of warp and weft fibre, the fibres in the warp direction usually display better tensile strength in comparison to the weft. The higher tension in the warp fibres (a result of the weaving process) induces crimp in the weft fibres which reduces their tensile strength.

The purpose of this investigation was to determine the effect of material orientation on the formability of a geometry. This would add to the factors that should be considered when specifying the material lay-up for the component.

7.6.2 Methodology

Two C-section blanks were prepared with the warp and weft directions interchanged. The C-section blank 2 design (Figure 7.26) was chosen for this investigation . The orientation of the warp and weft tows relative to the component's geometry is shown in Figure 7.60. The blanks were processed using the same manufacturing parameters, they were formed using a spring stiffness of 0.23 N/mm. The simulation results for specimen 1 (Figure 7.60) were presented in Figures 7.56, 7.57 and 7.58 and the experimental results for the processed blank in Figure 7.55.



Figure 7.60: Material orientation for specimens 1 and 2.

7.6.3 Results

The results for specimen 2 are presented in Figure 7.61. The laminate developed fibre buckling in the regions marked A and B. The fibre buckling was present in the top ply (reference to Figure 7.61), but was not present in the bottom ply. Specimen 1 did not develop any fibre buckling issues.

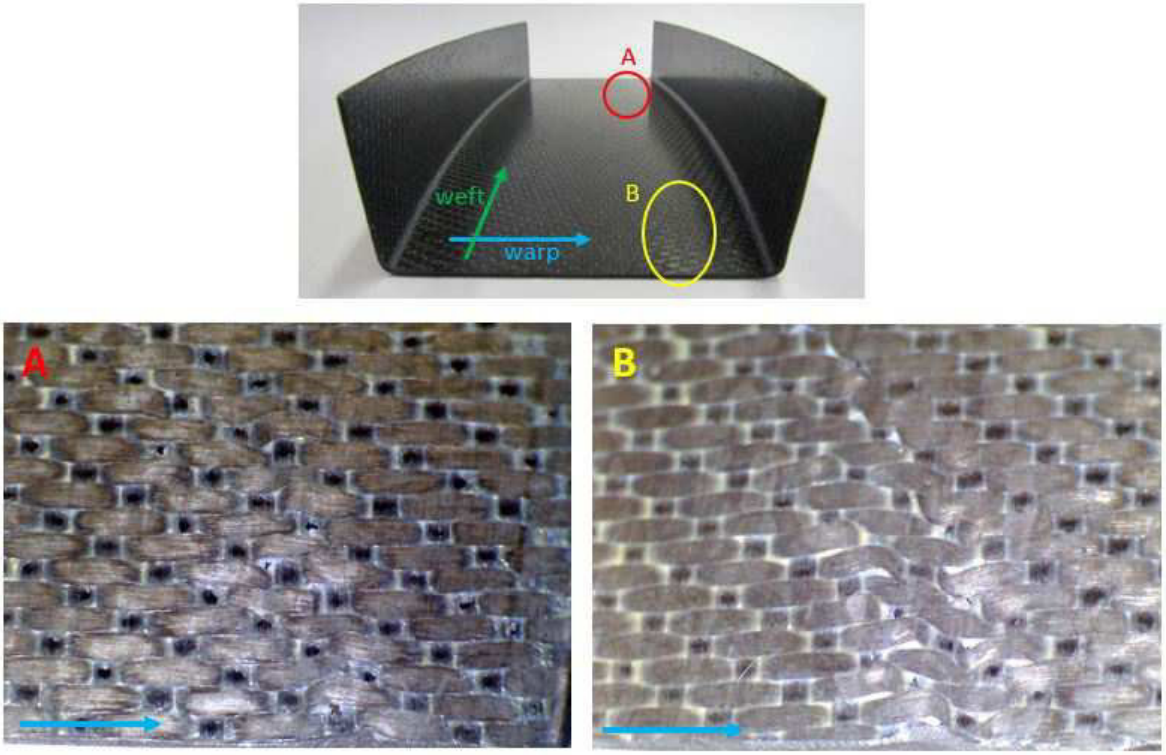


Figure 7.61: Fibre buckling in regions marked A and B.

7.6.4 Discussion

Figure 7.62 presents a diagram of the weaving set up for the production of woven fabric that are used as the plies for the laminate. The fabric consists of tows of fibres that are interlaced to produce the woven fabric. The Tencate Cetex PPS material was woven using a 5 harness satin weave, this implies that the fibres are woven in a 4 over 1 pattern. During weaving the warp fibres are held in tension and weft fibres are inserted between the warp fibres in the 4 over 1 pattern. The weft fibres are left relatively un-tensioned in comparison to the warp fibres. As a result of this, the woven ply will display different properties in the warp and weft directions. The warp fibres are straighter in comparison to weft fibres. This makes them more prone to localized buckling than the weft fibres which are already bent and can more readily accommodate the shortening requirements imposed by compressive loads on the fibres of the ply.

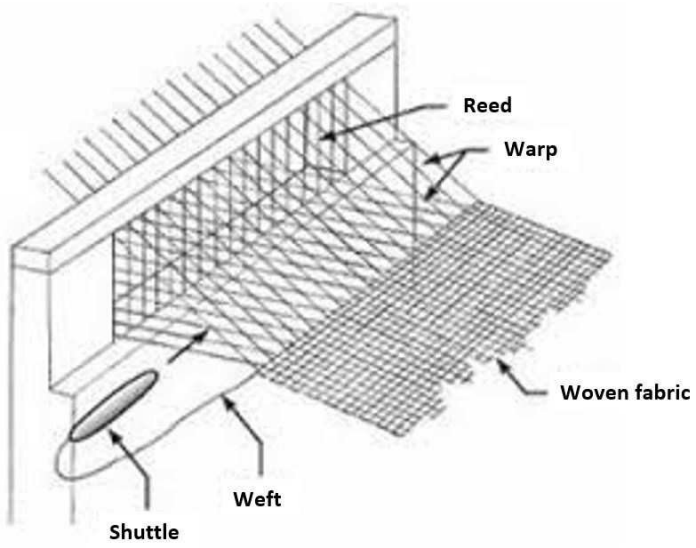


Figure 7.62: Weaving of the fabric showing the warp tows in tension and the weft tows un-tensioned [33].

In order to be draped on to the C-section geometry, the fibres oriented across the component (weft in specimen 1 and warp in specimen 2 - see Figure 7.60) must go around the two bends of the C-section. The bending of the laminate places the inner plies in compression. In specimen 1, the weft fibres are aligned to this direction and the component can be formed without any defects. In specimen 2, the warp fibres are aligned to this direction, the result was the local fibre buckling presented in Figure 7.61. The fibre buckling occurred in ply 1 which is on the inner side of the component, ply 4 on the outside which has the same fibre directions as ply 1 did not present with this fibre buckling phenomenon. The reduced formability of the warp direction when placed in compression must be considered when making decisions on the orientation of the material on a part.

7.6.5 Conclusions

- Material orientation has an effect on the formability of geometry, the warp fibres are more susceptible to fibre buckling when placed under compression during forming.
- The woven material may have a 'preferred' forming orientation that depends on the properties of the weave and the geometry that is being formed.

7.7 Investigation 6: The effect of tool temperature

7.7.1 Problem Background

The Z and C section tools were equipped with a heating system, the design details for this system can be found in Appendix B. The allowable tool temperature for forming the Carbon-PPS material is 200°C ±20. After the design of the Z-section tool, the first component was manufactured with the tool set to a surface temperature range of 200 to 220°C. The results of that experiment are shown in Figure 7.63. Inserts B and C show evidence of burnt resin on the part, the resin turned brown in colour. The side of the part that was in contact with the rubber is shown in insert D for comparison. The texture of the surface of the part tool side was also rough due to the resin burn. The metal tool was left coated with resin residue after pressing the part, this is shown in insert A.

The tool temperature was controlled by setting a target temperature for the thermocouple. The thermocouple did not measure the temperature directly on the mating surface of the tool. This meant that the thermocouple temperature had to be related to the temperature of the mating surface. The thermocouple had to be set to 250°C to attain the 200 to 220°C mating surface temperature.

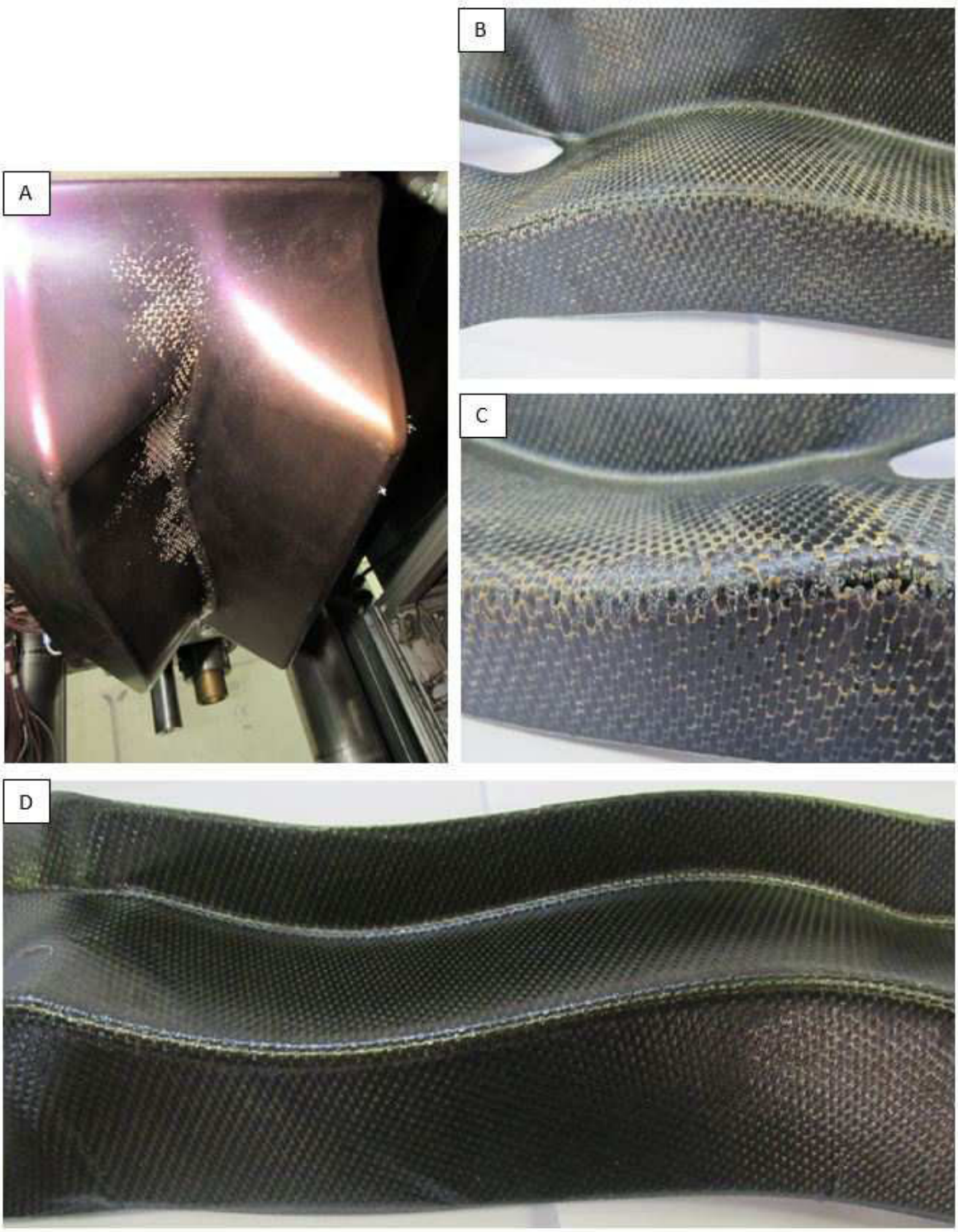


Figure 7.63: (A)Thermoplastic residue on the tool, (B) & (C) resin burn on tool side and (D) rubber side for reference.

7.7.2 Objective and proposed solution

An appropriate tool temperature had to be established since the allowable range provided a 40°C band. The thermocouple setting was decreased by 20°C and the surface temperature of the tool was monitored. When the temperature had stabilized again, a new component was pressed. This was repeated until a suitable temperature setting was reached.

7.7.3 Results

The thermocouple setting was dropped to 230°C which resulted in unsatisfactory results and then to 210°C which was found to be an acceptable setting. The results of these thermocouple settings are shown in Figure 7.64.



Figure 7.64: Z-section component manufactured with a tool setting of 230°C (above) and on the right to 210°C (below).

Figure 7.65 shows a comparison of the original component (250°C) with parts pressed at a thermocouple setting of 230 and 210°C.

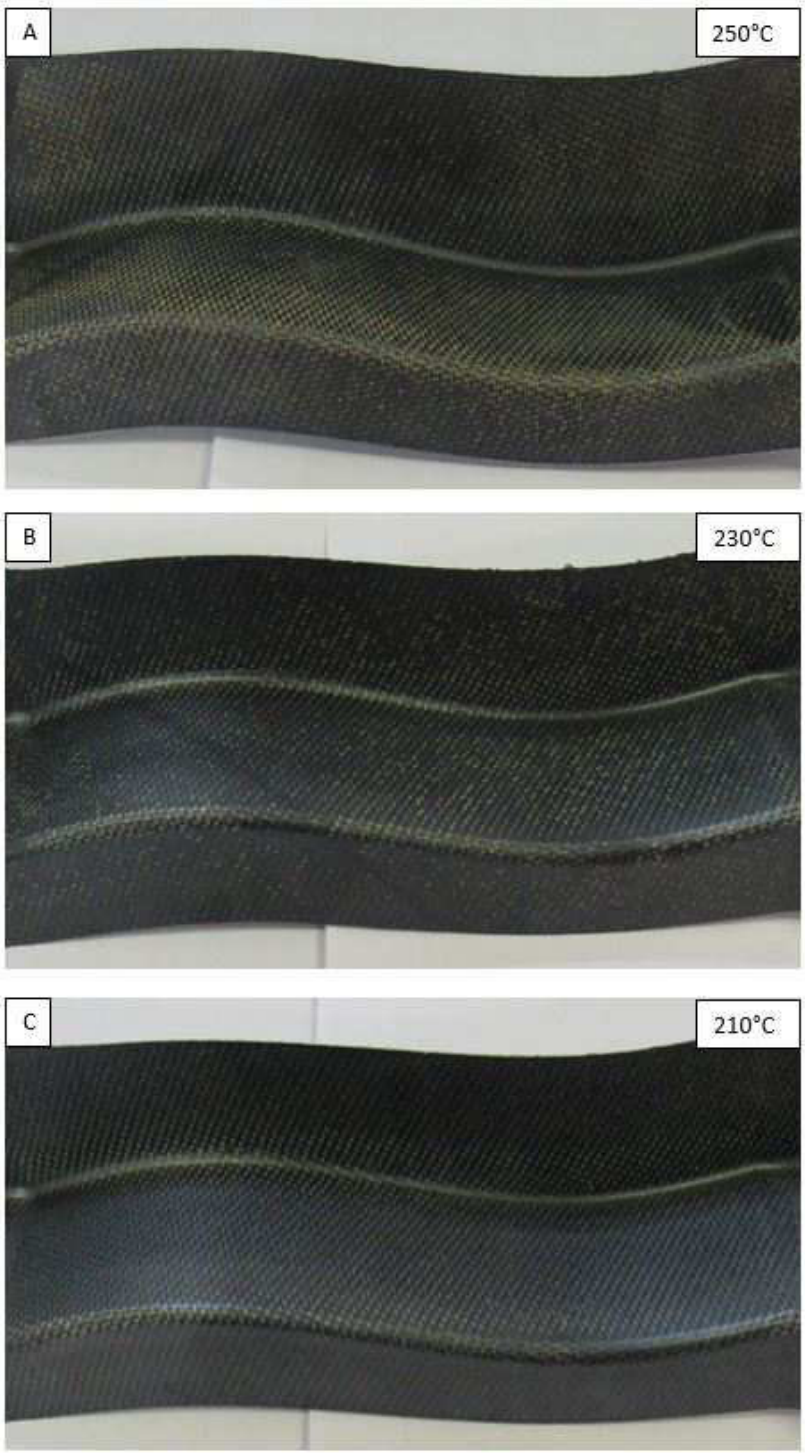


Figure 7.65: Effect of tool temp on forming.

An infra-red camera was used to monitor the temperature distribution on the tool and a probe thermometer was used to confirm the readings. Figure 7.66 presents the heat distribution of the tool with the thermocouple set to 210°C. The temperature probe gave readings ranging from 175°C to 190°C at this setting.

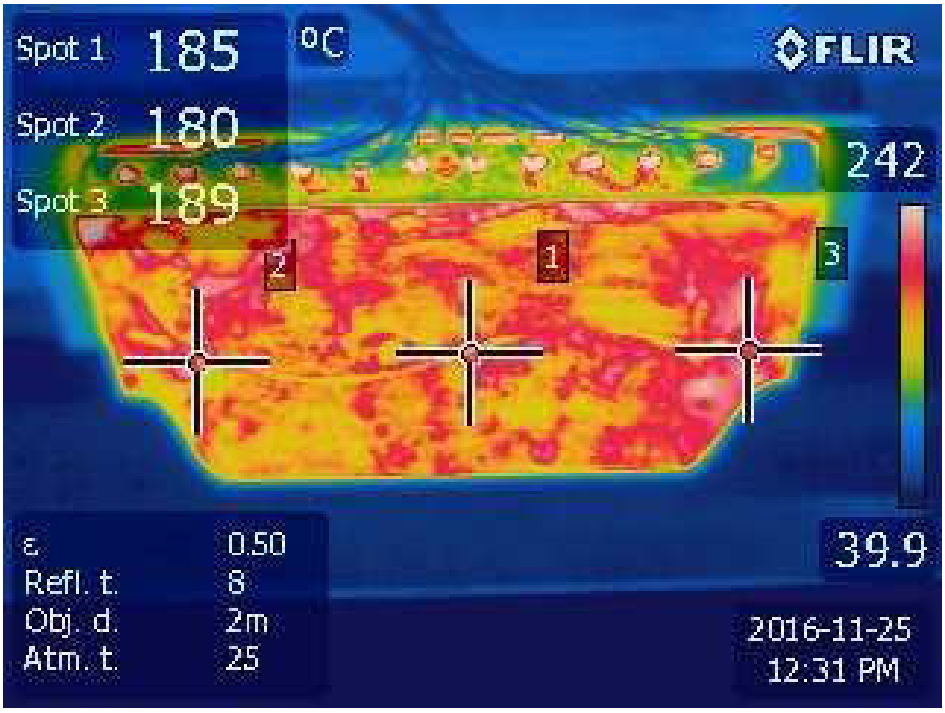


Figure 7.66: Heat distribution of the Z-section tool.

7.7.4 Discussion

Figures 7.64 and 7.65 show the results of the different temperature settings. The results for the 230°C showed an improvement over the initial 250°C setting but the component still had some burnt resin. The resin burn was not present on the component from the 210°C setting. The severity of the resin burn defect was directly proportional to the temperature of the tool. The 210°C setting correlated with a surface temperature of 175°C to 190°C (182.5°C ±7.5°C). This temperature distribution positions the tool at the lower end of the 200°C ±20°C stipulated tool temperature for this material.

The blank is heated to 330°C to melt it, therefore the 200°C tool temperature is well below the temperature of the blank. Contact between the blank and the tool results in rapid cooling of the blank, which has a negative impact on draping. The lower temperature of the thermoplastic increases its viscosity, reducing the mobility of the fibres and the effectiveness of forming mechanisms. The results of this experiment showed that the tool temperature has an upper limit, a surface temperature of 210°C ±10°C resulted in severe resin burn even though this occurred within the recommended tool temperature specification of 200°C ±20°C.

The components formed from the three temperature settings presented similar levels of formability. The effect of the temperature setting on formability of the component with reference to forming mechanisms could not be deduced from the 210°C, 230°C and 250°C settings. The temperature of the tool at these settings is on average within range of the maximum and minimum allowable temperatures for the material. A greater temperature range would have to be tested to evaluate the effect of the tool temperature. The primary objective of this experiment was to establish a suitable temperature within the specified recommended range of the material.

7.7.5 Conclusions

- The appropriate tool temperature for forming the TenCate Cetex PPS was found to be 182.5°C ±7.5°C.
- Tool temperatures of 210°C ±10°C resulted in resin burn, this phenomenon was eliminated by a reduction in tool temperature.
- The effect of tool temperature on forming with respect to the forming mechanisms was not established.

7.8 Investigation 7: The effect of blank heating

7.8.1 Problem Background

The blank can only be successfully draped into the desired geometry if it has been sufficiently heated and melted to ensure that the fibres and resin experience minimal resistance as they migrate during the forming process. The heating of the blank is a critical component of the forming process.

The material specification requires the blank to be heated to 330°C±15°C. The heating setting for the oven has been determined experimentally for various materials and thicknesses by Aerosud. Materials with higher melting points require higher heat settings and the heat setting is reduced as material thickness increases to allow the heat to be conducted to the centre of the laminate without scorching the outer plies. The degree of melt can also be controlled by altering the length of time the material spends in the oven after the manufacturing temperature has been reached. The time span is referred to as the soak time. Each blank design of different size, shape and thickness requires a unique heat setting and soaking time [1].

The larger blanks (spar and leading edge) that were melted in the oven showed evidence of regions with insufficient heating. This is shown in Figure 7.67, the red markers point out the grey areas which were regions with undesirable melt. Figures 7.67 B and C show that the unmelted laminate folded around the end of the tool in a manner that a solid homogeneous material would, mechanisms such as intra-ply shear did not occur.

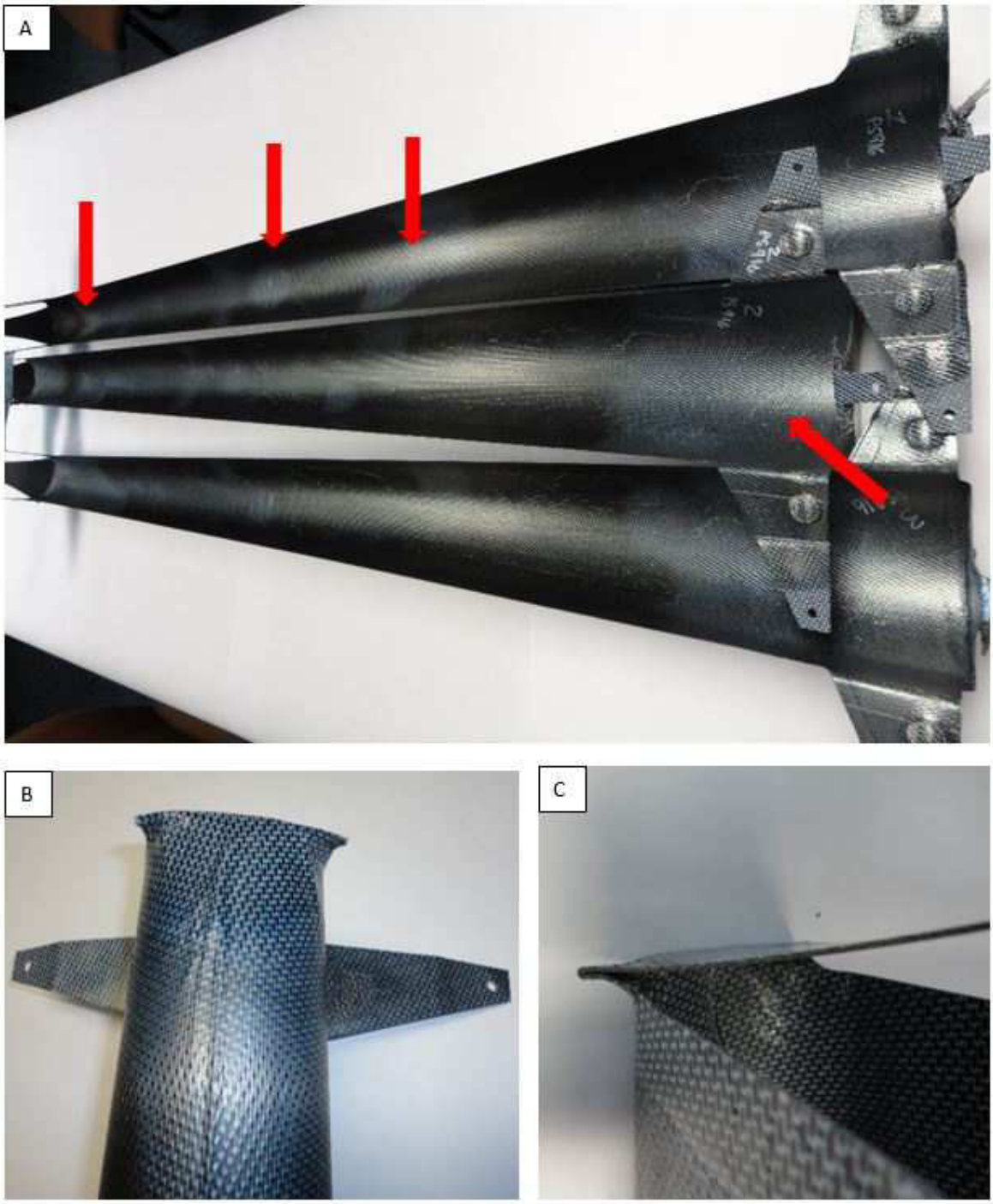


Figure 7.67: Insufficient blank heating.

7.8.2 Identification of cause of problems and proposed solution

The regions with undesirable melt on the blank show that the oven did not produce a uniform heating profile. This could have been caused by faulty or non operational heating elements. The infra-red heating elements in the oven are controlled by emissivity sensors which monitor the temperature of the blank and use that to determine the amount of heat that should be supplied. The sensors are prone to dust collection which obscures readings. Extreme sagging of a blank can also lead to faulty readings because the sensors are designed to operate perpendicular to the material. Exposing the oven to air drafts reduces the effectiveness of the oven.

The heating profile of the oven and the correct reason behind the cold spots need to be determined. This would form an entire project on its own so a temporary solution to the problem was sought. The soak time for the blanks was increased until the regions received enough heat to successfully melt the blank. The doors to the workshop were kept closed to prevent drafts of wind from interfering with the heating process.

7.8.3 Results

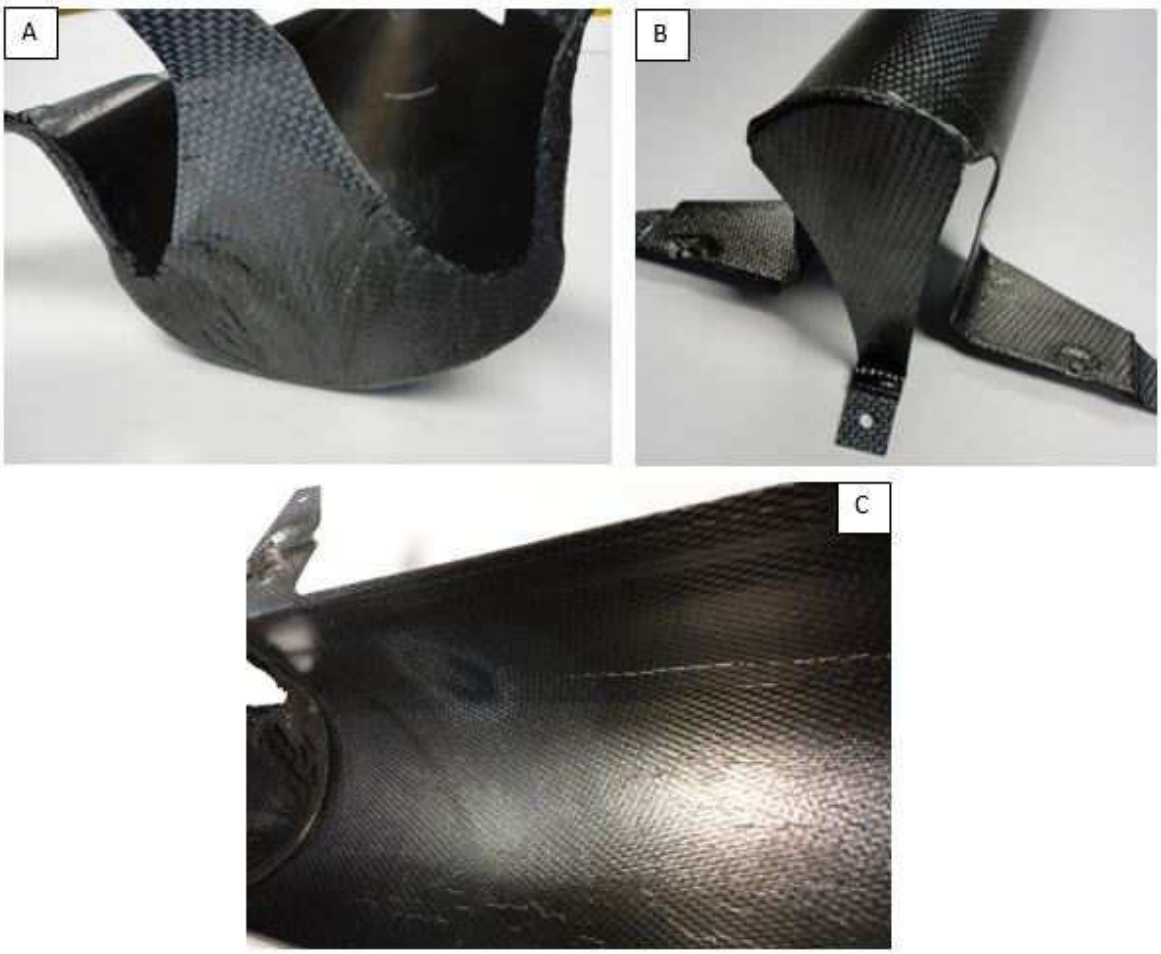


Figure 7.68: Effect of blank heating on forming.

7.8.4 Discussion

Increasing the soak time resulted in a successful heating of the blanks. The soak time form the blank had to be increased from 50 seconds to 70 seconds to obtain a full melt on the entire blank. Figure 7.68 shows improvement of the melting of the blank. Inserts A and B show that the melted region extends well into the tags, the laminate now drapes onto the geometry using the mechanism required for the draping of a woven laminate.

7.8.5 Conclusions

- The blank needs to be sufficiently melted for the forming mechanisms that are required to drape the blank onto the geometry to take place.

7.9 Investigation 8: Simulated study of the effect of tool inclination

7.9.1 Background

It was shown in sections 7.4 and 7.5 that the design of the blank and the stiffness of the BRM can be effectively used to affect the formability of a geometry. The focus of those investigations was on the blank and the forming process itself. This study investigates the effect of a factor that relates to the design of the tool. This design of a tool that facilitates the forming of a geometry can eliminate the need for special forming techniques.

7.9.2 Objective and Methodology

The purpose of this investigation was to determine the effect of the angular position of the forming surfaces relative to the blank for the Z-section geometry. Considering that it was not practical to physically do this experiment, the experiment was performed through simulation. Two simulations were performed with the tools at different inclinations. The one tool was set-up at the default inclination of 0° and the other tool was rotated by 30° counter-clockwise (about the axis normal to the page - refer to Figure 7.69). The simulations were performed using Z-section blank design 2 with a BRM stiffness of 0.09 N/mm.

7.9.3 Results

Figure 7.69 presents the results of the deformation of the blanks for the experiments. The shear angle and fibre stress results for both the tool arrangements are presented in Figures 7.70, 7.71 and 7.72. The complete set of results for this experiment can be found in Appendix E.1. The results are summarised in Table 7.3.

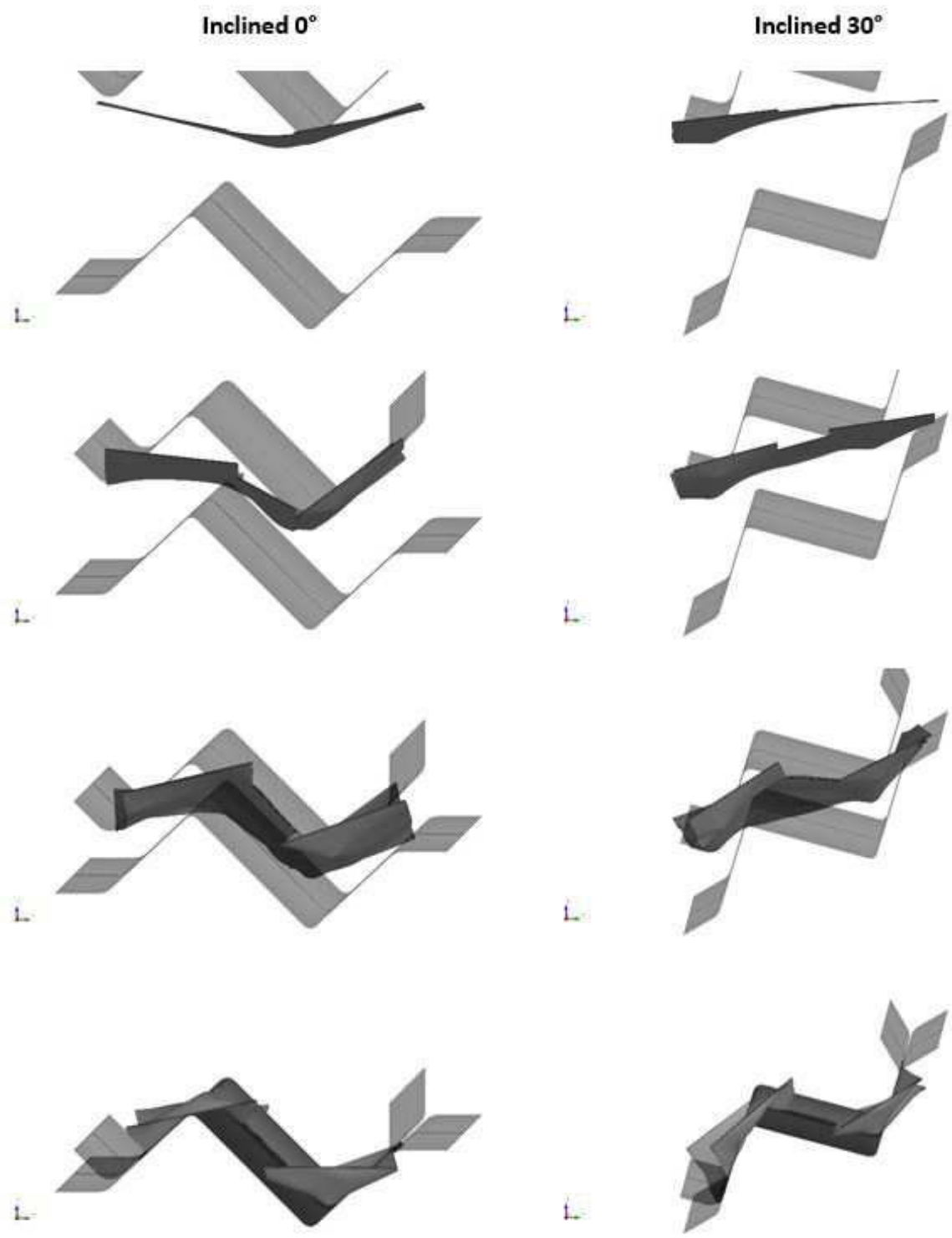


Figure 7.69: Blank deformation sequence for two tool orientations.

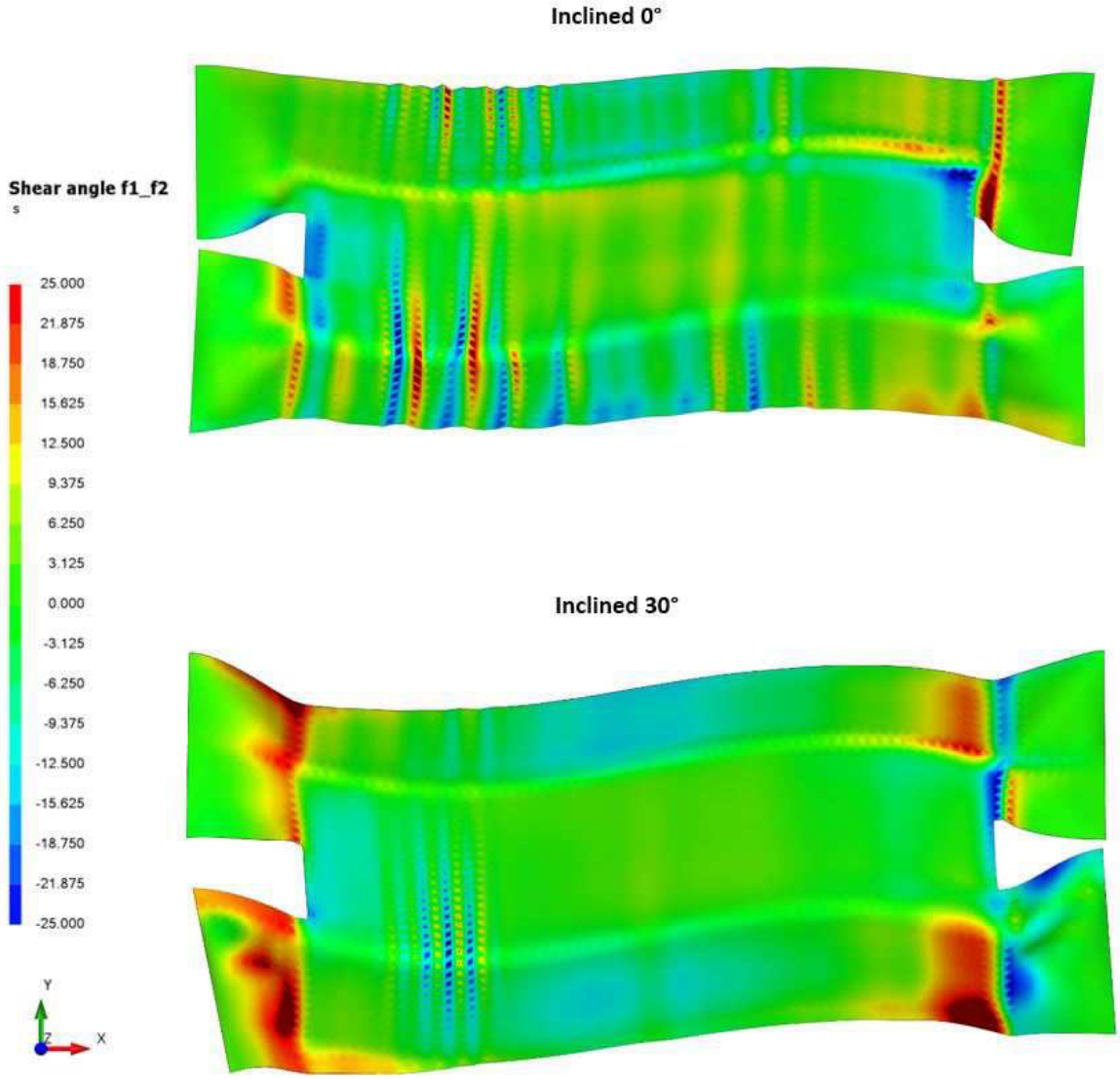


Figure 7.70: Ply 1 shear angle results for the tool inclined through 0° and 30°.

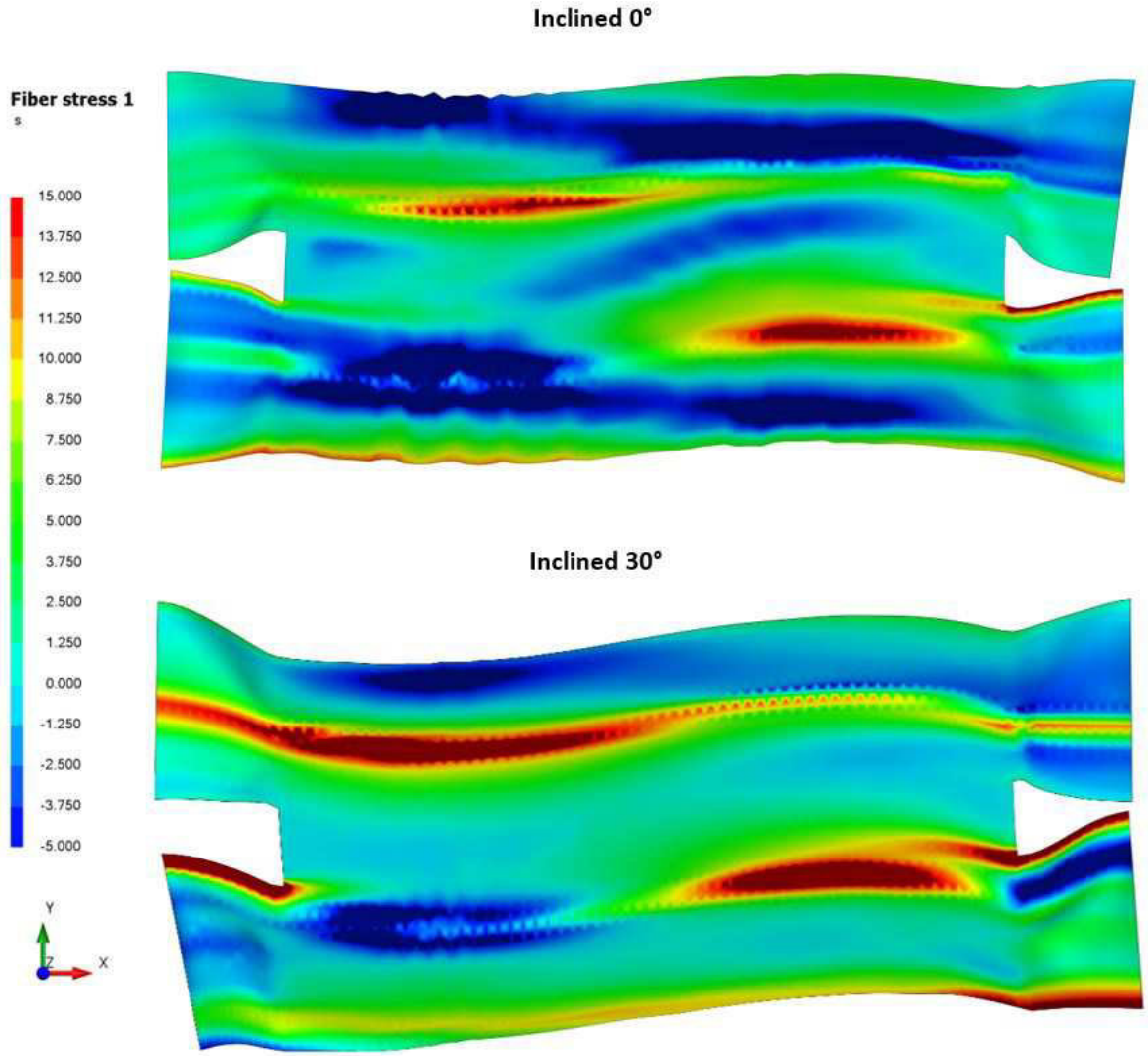


Figure 7.71: Ply 1 fibre stress results in direction 1 for the tool inclined through 0° and 30°.

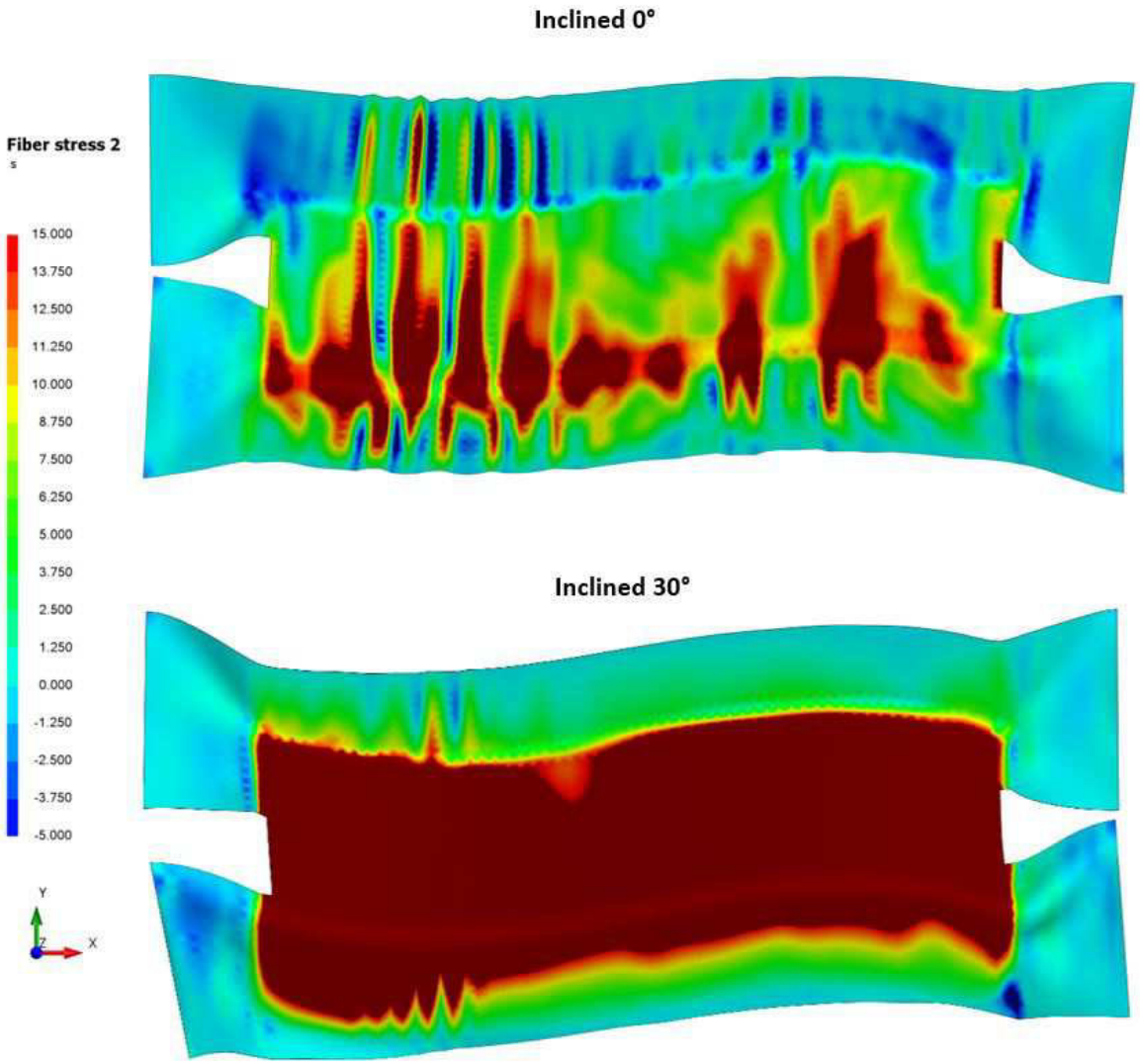


Figure 7.72: Ply 1 fibre stress results in direction 2 for the tool inclined through 0° and 30°.

Table 7.3: The effect of rotating the tool by 30° on the formability of the plies.

Ply	**Shear Angle**	**Fibre Stress 1**	**Fibre Stress 2**
1	Improved	Improved	Improved
2	Improved	Improved	Improved
3	Improved	Improved	Improved
4	Improved	Improved	Improved

7.9.4 Discussion

Changing the inclination of the tool surfaces altered the interaction between the blank the tool. This can be seen in the deformation sequence shown in Figure 7.69. The results show that the tools make initial contact with the laminates at different places. The steps that follow show that the sequence in which the blank deforms to into the final geometry is also different, resulting in different shear angle and fibre stress distributions.

The ply 1 shear angle results for the two arrangements have been presented in Figure 7.70. The shear angle results of the tool rotated through 30° predicted better formability of the geometry, they present a reduction in in shear localization over the 0° tool arrangement. The ply 1 fibre stress results in direction 1 which is aligned with the x-axis have been presented in Figure 7.71. Of the two tool arrangements, the tool rotated through 30° predicted better formability. This arrangement presented a reduction in the regions that display compressive fibres stresses (blue regions), this means a reduction in the laminates susceptibility to laminate buckling. The ply 1 fibre stress results in direction 2 which is aligned with the y-axis have been presented in Figure 7.72. The fibre stress results in direction 2 also predicted that the tool rotated through 30° is a better arrangement for forming the geometry. It presented no regions in compression on the component. A complete set of results of this study can be found in Appendix E.1. A summary of the results of the formability of all the plies was presented in Table 7.3. The shear angle and fibre stress results predicted that the tool rotated through 30° improved the formability of the Z-section geometry.

Despite this finding, the experimental tool was produced using the forming surfaces rotated through 0°. The tools for the C and Z-section were designed as parts of a single modular tool. The tool had to also be designed to be compatible with an existing tool die set. These design constraints resulted in the 0° tool arrangement being chosen to manufacture the tool. The tool also enabled experiments such as the effect of BRM stiffness on the formability of geometry to be carried in an attempt to improve the formability of a component.

The results of this experiment shows that the Z-section could have been produced free of wrinkles with a BRM stiffness of 0.09 N/mm if the forming surfaces were rotated through 30° as depicted in Figure 7.69. Whereas, with the in the 0° arrangement a BRM stiffness of 0.23 N/mm had to be employed to achieved a wrinkle free component (see Section 7.5). The results of this investigation present a consideration that must be looked into when designing CFRTP tools.

7.9.5 Conclusions

- The orientation of the tool relative to the blank determines the sequence with which the blank is draped into the target geometry.
- The orientation of the tool surfaces has an affect on the formability of a geometry.
- The most suitable orientation should be determined as part of the tool design optimization task.

7.10 Investigation 9: Simulated study of the effect of forming speed

7.10.1 Background

When the heated blank is removed from the oven it starts cooling rapidly and when it makes contact with the tool, the cooling rate is exacerbated. There is an interest in keeping the time period from when the laminate leaves the oven to the point where it has been draped and is under pressure to a short time period. The typical specification for this time interval is 5 seconds. Two motions take place within this period, the shuttle transfers the blank from the oven to the tool and the tool closes to form the geometry. The parameter under investigation in this particular experiment was speed of the closing action of the tool. This is referred to as the forming speed. Increasing this speed decreases the time interval so that the specified time for the interval is realised. The 5 seconds specification for this interval is defined to ensure that the resin remains molten, thereby allowing unimpeded forming to take place. It is believed that increasing the speed also means that the viscous forces in the laminate increase which may result in forming problems.

7.10.2 Objective and Methodology

A theoretical investigation was conducted to determine the effect of forming speed on formability. The CFRTP press at the facility can be operated at two speeds, the ram of the press is dropped at 200 mm/s from its set holding position and is then braked to a speed of 50 mm/s as the tool closes. The upper tool usually makes contact with the blank at 50 mm/s. This depends on the position of the blank relative to the bottom tool which in turn depends on the sag experienced by the blank during heating. The two forming speed are hard coded into a program that controls the press and could not be altered at will, so this experiment could not be performed in practice. The 50 mm/s speed, which is the closing speed at the later stage of the forming stroke when the blank is actually being formed, was used in all the investigations prior to this one. The simulations for this investigation were conducted at forming speeds of 25, 50 and 150 mm/s. The Z-section geometry blank 2 with a BRM stiffness of 0.23 N/mm was used to perform the investigation.

7.10.3 Results

The complete set of results can be found in Appendix E.3 and a summary of the findings has been presented in Table 7.4. The table summarises the comparison of both the increases from 25 to 50 mm/s and from 50 to 150 mm/s. Where a contradictory result was obtained for the comparisons (i.e from 25 mm/s to 50 mm/s and from 50 mm/s to 150 mm/s), the result has been marked as inconclusive.

Table 7.4: The effect of increasing forming speed on the formability.

Ply	**Shear Angle**	**Fibre Stress 1**	**Fibre Stress** 2
1	Degraded	Degraded	Degraded
2	No effect	Degraded	Degraded
3	No effect	Degraded	Degraded
4	Degraded	Inconclusive	Improved

7.10.4 Discussion

A summary of the results has been presented in Table 7.4. Refer to Appendix E.3 for the plots. The results show that an increase in forming speed had a negative effect on the formability of the geometry. The results of the increase for 25 mm/s and 50 mm/s showed a deterioration of formability but both simulations predicted that the parts would have no defects, whereas that of the 150 mm/s speed revealed a possibility of wrinkling.

The mobility of the fibres during intra-ply shear and the mobility of the plies during inter-ply shear are dependent on the viscous effects of the molten thermoplastic. The lower forming speeds result in lower viscous forces which minimizes the material's resistance to forming, thereby improving the formability [14]. This behaviour is in line with the experimental data that was presented in Section 2.6. The experimental data that was presented in Section 2.6 is for a different PPS resin to the product used in the investigation but the behaviour is expected to be similar. Even though the higher forming speeds reduce the melt viscosity of the resin because of the higher shear rates, the higher velocity tends to increase the viscous forces within the material, thereby reducing the ability to form the material.

The parts that were manufactured during the course of this research were all formed at 50 mm/s. This speed was rapid enough to circumvent the blank heat loss issues without introducing defects associated with high forming speeds.

The simulation software assumes that the material is isothermal during forming, so the effect of the cooling resin has been omitted from this investigation. The viscous forces on the fibres

are then dependent on the velocity at which forming takes places and the properties of the resin at the initial forming temperature. In practice the properties of the resin changes as the laminate cools creating an environment that is unfavourable for the forming mechanisms to take place.

7.10.5 Conclusions

- (Action 15 and 16)There is a need to the close the forming tool rapidly so that the laminate is processed at the resin melt temperature. High forming speeds have a negative impact on the formability of components due to the increase in the viscous forces on the fibres.
- The forming speed needs to be a trade-off that circumvents the effects off both slow and rapid forming between the two effects. The tool must be closed rapidly enough to ensure the blank is formed at an acceptable temperature but not too rapidly to invoke the development of large viscous forces because of the drop in resin melt viscosity.

7.11 Investigation 10: The effect of forming pressure

7.11.1 Background

The TenCate Cetex PPS processing instructions require the material to be formed at a pressure of 30 bar±10 bar to ensure that the final geometry has been consolidated. The applied forming pressure is required to re-consolidate the laminate after draping it into the target geometry. Insufficient pressure on the part can lead to non-consolidation issues. The forming pressure can also be used to influence the definition of the geometry in areas where bridging may occur such as bends and corners. Bridging occurs when the pressure generated in the rubber fails to drape the laminate onto the metal tool.

7.11.2 Objective and Methodology

The purpose of this investigation was to determine the effect of forming pressure on the consolidation of the laminate and the definition of the geometry. The C-section was manufactured at 25, 30 and 35 bar and the Z-section at 25 and 30 bar. The C-section blank 3 and the Z-section blank 2 were used to manufacture the specimens. Both the geometries were manufactured using a BRM stiffness of 0.23 N/mm. The articles were inspected using a non-destructive inspection (NDI) technique to determine the consolidation of the laminates.

An instrument called an A-scan was utilized, the instrument estimates the size of discontinuities in the material by measuring the amount of ultrasonic energy reflected by the material. The facility that was used is contracted by Aerosud to perform NDI tests for components for Airbus. The equipment is calibrated to process the specific material and the components were tested according to Airbus acceptance criteria for CFRTP clips.

7.11.3 Results

The results for the NDI can be found in Appendix F. The components all recorded a signal attenuation no greater than -6 dB. This means that there was no detection of voids or non-consolidation regions that exceed the allowable threshold as defined by the Airbus Acceptance Criteria specification.

The C-section articles all presented similar levels of definition with no occurrence of bridging. Figure 7.73 shows the bend-lines on the Z-section geometry for the 25 and 30 bar pressures.

The equivalent simulation results for these experiments can be found in Section 7.5, Figures 7.51, 7.52 and 7.53 for the C-setion and Figures 7.56, 7.57 and 7.58 for the Z-section.

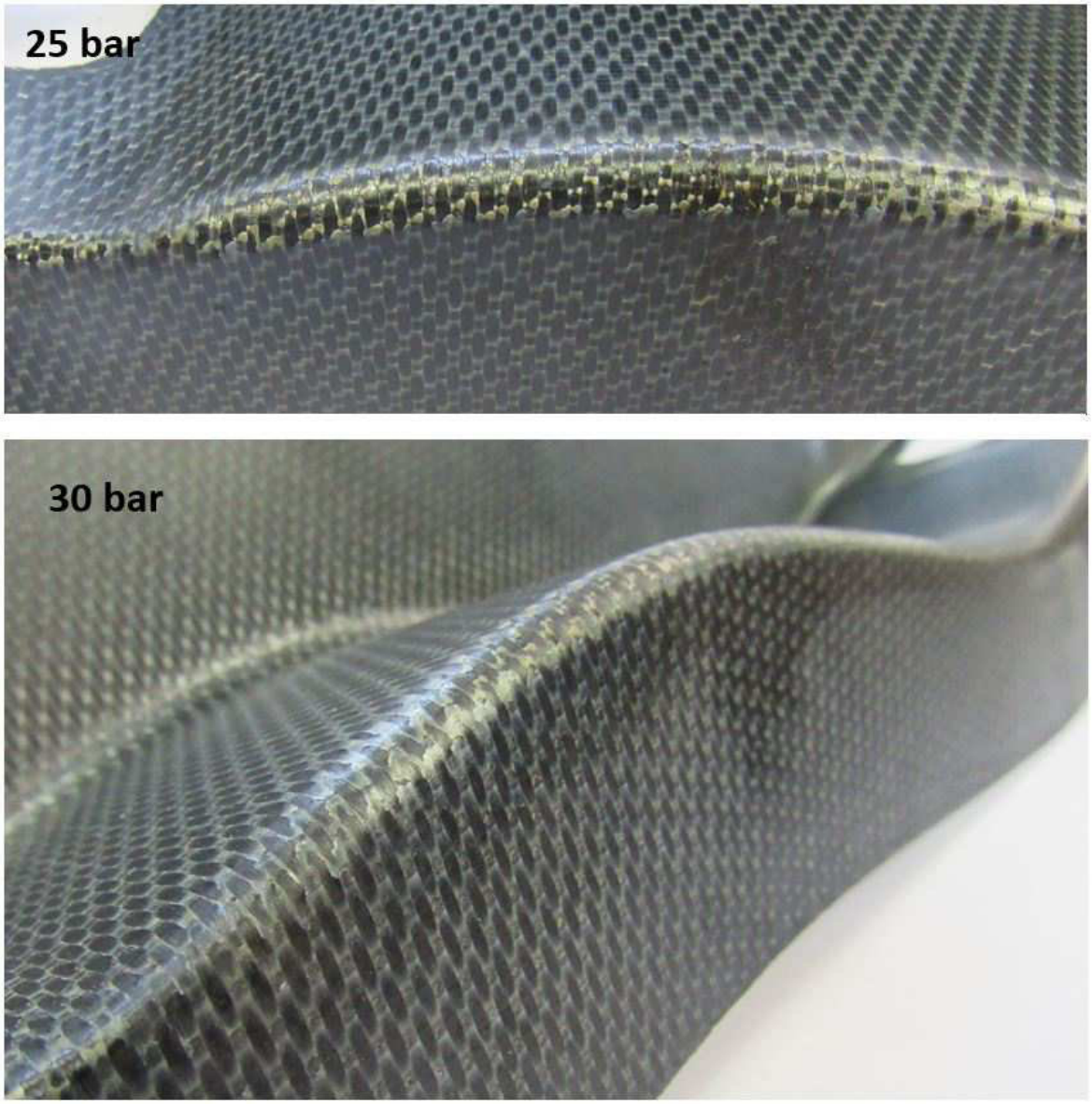


Figure 7.73: Geometry definition for the 25 bar sample (top) and the 30 bar sample (bottom) for the Z-section.

7.11.4 Discussion

The results obtained from the NDI exercise only provided information on whether the -6dB threshold had been exceeded. As a result, a consolidation trend for the various pressures could not be determined. All three pressure settings provided adequate pressure to satisfy the Airbus consolidation criteria.

The variation in form pressure was found to have an influence on the formability of the geometry in the region of the bend-curve. The result for the 25 bar specimen shows resin squeeze-out on the bend-curve, the resin coalesced on the surface showing that the laminate was not in contact with the tool in this region. The region with resin squeeze-out and bridging coincides with a region of high fibre stress in Figure 7.57. Increasing the forming pressure to 30 bar ensured that the pressure generated in the rubber tool was enough to overcome the laminate bridging and the resin squeeze-out. The defects predicted in Figure 7.57 only occur when the forming pressure is low. The simulation results do not enable the prediction of the difference in formability between the different pressures.

7.11.5 Conclusions

- All the articles shown presented acceptable consolidation. The degree of consolidation relative to the forming pressure could not be established.
- Forming pressure has an effect on the accuracy of the definition of the geometry of a component because it regulates the extent to which the laminate is forced to map the metal tool defining the geometry.
- Resin squeeze-out phenomenon occurs as a result of fibre bridging and large fibre stresses. An increase in the forming pressure eliminated the fibre bridging and the associated resin squeeze-out.

8 Final Discussion

The manufacturing process for CFRTP components consists of many segments that have a significant influence on the production of a successful component. The fact that a fabric can be shown to successfully drape a particular geometry is not enough to ensure the production of a successful part. The entire manufacturing process must be analysed to ensure that there is a solution for every process involved, that satisfies the geometry in question. The investigation into the parameters involved in the manufacturing process resulted in the identification of the following as key process parameters;

1. The geometry being formed, and consequently the design of the blank.
2. The boundary conditions that the blank is subjected to during forming.
3. The design of the forming tool.
4. The tool temperature.
5. The forming pressure.
6. The forming speed.
7. The blank heating.

These process parameters all serve as inputs to a system where the output is the formability of the geometry. The failure to address any shortcomings regarding these process parameters will impact negatively on the formability. The forming mechanisms that take place when a geometry is draped are of great importance. The mechanisms that are required to drape a particular geometry depend on the geometry. The AniForm simulation software uses knowledge of the material behaviour to described the manifestation of the forming mechanism in order to predict the formability of geometries. Geometry that has double curvature requires the intra-ply shearing mechanism in order to be draped. Unsuccessful drapes can be related to failure of the intra-ply shearing mechanism. This is identified as shear angle localization in

AniForm. The occurrence of high fibre stress shows susceptibility to laminate bridging and resin squeeze out where compressive fibre stress reveal a susceptibility to laminate buckling which can result in ply wrinkling. Monitoring these parameters which rely on the mechanisms that occur in the laminate provides knowledge that enables the prediction of the formability of geometries. A good correlation was obtained between the predicted formability using AniForm and the results of the practical experiments. Besides assumptions in the theoretical model such as the rigid-rigid tooling and the isothermal behaviour of the blank, the software was successful in determining the behaviour of the constituents of the laminate and predicting the occurrence of forming defects.

The design of the blank was found to greatly affect the formability of geometries. In the investigation of the forming of the LCU, the blank was redesigned to improve the formability of the component. It was found that a reduction in the size of the blank had a positive impact on the formability of the component. Reducing the size of the blank removed material that was prone to developing wrinkles, this material would in any case be trimmed away to produce the final component. The blank for a component needs only to be made marginally larger than the part itself. Tags that are used to support the blank were incorporated into the design of the blank. The placement of the tags determines the shape that is assumed by the blank as it sags during the heating cycle. The shape of the molten blank must be considered because it influences the manner in which the blank is draped into the final geometry which affects formability. Good forming was achieve by ensuring that the molten shape of the blank mimics the target geometry, this is referred to as 'pre-draping'. The manufacture of the C-section using blank 1 and 3 showed that the blank that displayed the pre-drape principle achieved better results. The formability of a component can be greatly improved by the design of a blank that considers the geometry that must be formed. The blank must deform into the required geometry in a manner that prevents the development of defects.

The C-section blank 3 and and Z-section blank 2 present the basic approach to blank design for these cross sections. There are limitless variations of the same geometry that can be produced from a single cross section. The component may be longer, wider, or have different lay-up properties, these variations will warrant the blank design to be revised to satisfy the changes brought about by the variation but the fundamental design of the blank will remain.

The investigation of the effect the orientation of the warp and weft fibre directions relative to the geometry was carried out. The orientation of the warp and weft directions is determined by considering the mechanical strength requirements of the components. The investigation showed that the fibres in the warp direction are more susceptible to fibre buckling, this was attributed to the fact they are placed in a state of greater tension during the weaving of the fabric. This must be considered when designing the component as an unsuitable orientation of the warp fibre may result in this forming defect.

The BRM was introduced as a device to secure the blank such that the forming can take place in a controlled fashion. A blank that is released during the forming stroke leads to wrinkles and non-repeatability of results between subsequent components. The blank should not be rigidly supported as this will lead to the development of large fibre stress which cause laminate bridging. The development of the spring actuated BRM allowed the blank to be constrained while enabling it to be easily manipulated by the forming tool. The amount of resistance introduced by the BRM can be simply controlled by the specification of the stiffness of the springs on the BRM. The BRM firmly secured the blank and ensured repeatability of results as every blank was subjected to the same boundary conditions.

Beyond its use as a supporting device the BRM was also used to improve the forming of components that were prone to laminate buckling. It was found that an assessment of the state of the blank moment before tool closure can be used to identify regions that are susceptible to buckling as the blank is formed. Regions on the blank that experienced compressive fibre stresses made the area prone to buckling and developing wrinkles. This tendency to buckle was successfully resolved by orienting the tag such that the tension applied by the springs eliminated the laminate buckling. The BRM stiffness was used to modulate the amount of tension that was applied to the blank during forming. An increase in the stiffness of the BRM springs from 0.09 to 0.23 N/mm in the manufacturing of the C and Z-section, transformed the result from a component with wrinkles to one that was wrinkle free. The use of the BRM resulted in higher fibre stress, this may lead to defects associated with high fibre stresses such as resin squeeze-out and laminate bridging. The lower stiffness did not generate adequate tension to resist the buckling and the higher tension prevented the laminate from buckling without introducing defects.

The design of the tool was found to be critical to the formability of the geometries. The design of the tool is directed primarily by the shape of the final geometry. The C-section tool was found to be simple to design, the orientation of the tool is motivated by the pre-drape shape that can be achieved by the blank using gravity. The Z-section geometry does not have a distinguishable pre-drape that the blank should assume, in fact the blank was designed to remain flat because it gets bent in two opposite direction during forming. This allowed for the experimentation of other tool design parameter that were not applicable to the C-section tool. The mating surfaces of the Z-section tool were rotated by 30°, the simulation results predicted this to have a marked improvement on the formability of the geometry.

It was established that the blank and the tool must be designed to complement each other, the tool must be designed only after a general blank design has been agreed upon because the design of the blank will affect the design of the tool. The blank design may also need to be updated as the design of the tool progresses. If this process is not followed, the result will be a tool that does not facilitate the draping of the blank into the required geometry.

The simulation prediction was used to show that the occurrence of intra-ply shear mechanism is commensurate with changes in the thickness of the plies. Geometry that is considered as complex usually has surfaces of double curvature which require intra-ply shear to be formed. This requires the complex components to be manufactured from a tool that has a rigid punch and a non-rigid die. The non-rigid die accommodates the non-uniform laminate thickness allowing for the thinner regions of the laminate be subjected to the forming pressure. This ensures that the entire blank is well consolidated. Bohler-M200 moulding steel was used for the rigid tool and Smooth-Sil 950 silicone rubber was used for the non-rigid tool.

The investigation into the effect of forming speed using Aniform showed that lower forming speeds result in better draping, this was attributed to the generation of large viscous forces at high forming speeds. There is also an interest to form the blank rapidly before the resin cools down, reducing the mobility of the fibre. A balance must be established between the two interests, the components that were manufactured during this research were all formed at a speed of 50 mm/s with no defects linked to the forming speed. The metal punch was heated to reduced the temperature differential between the the blank and the tool, this minimizes the amount of cooling experienced by the blank as it is formed. It was established that there is an upper limit to the temperature of the tool, high tool temperatures resulted in a scorching of the resin in that laminate, this also left resin residue on the surface of the tool. The optimum tool temperature for forming the TenCate Cetex-PPS was found to be in the range of 175°C to 190°C.

Non-destructive inspections were carried out on C-section components which were formed using different pressures (25, 30 and 35 bar) to investigate the effects of pressure on the formability of components. These pressures all fall within the allowable forming pressure for the material. The results of the investigation showed that the pressures used all resulted in good consolidation in the laminate but a consolidation trend relating the pressure could not be established. However, the forming pressure was effectively used to improve the formability of the Z-section in regions where laminate bridging and consequently resin squeeze-out was experienced These defects are predicted by the presence of the concentration of high fibre stresses in areas where they are most likely to occur such as along bend lines.

9 Final Conclusions

1. Assessment of AniForm as a predictive tool.

   (a) AniForm's predictive capability showed good correlation with experimental results and AniForm can be successfully used to simulate the CFRTP forming process.

2. Definition of key process parameters for the forming process.

   (a) The size of the blank for a component must be designed such that it is slightly larger than required to allow for trimming to final geometry. This eliminates the occurrence of wrinkles in off-cut areas, which can influence the formability of the entire blank.

   (b) The supporting tags for the blank must be arranged such that the pre-drape attained when the blank melts mimics the shape of the final geometry.

   (c) The blank must be firmly secured using BRMs such that it is not released during forming. The BRMs can also be used to prevent the laminate from buckling during forming by applying tension to the laminate.

   (d) The amount of tension applied by the BRM is controlled by the specification of the spring stiffness of the BRMs. A low spring stiffness will render the BRMs ineffective whilst excessively large stiffness introduce large fibre stresses into the laminate.

   (e) The tool for manufacturing complex CFRTP components must be specified to have a rigid punch and a non-rigid tie to accommodate the changes in ply thickness that take place in the laminate during forming.

   (f) The tool must be optimized by considering factors such as the orientation of the mating surfaces of the tool and the forming directions.

   (g) The design of the tool and the blank must take place in conjunction, the interaction between the blank and that tool must facilitate the forming of the required geometry.

(h) The rigid punch of the tool must be fabricated from a metallic material to ensure stability of the tool during forming and non-rigid tool was fabricated from a silicone rubber.

(i) The forming speed must be a balance between avoidance of defects from viscous effects generated by high forming speeds and poor formability due to excessive cooling of the blank as a result of slow forming speeds.

(j) The forming pressure can be used to regulate the level of definition attained by the laminate. This can be used to address phenomena such as laminate bridging and resin squeeze out.

3. Identification of the significance of forming mechanisms on the forming process.

(a) The failure of the manifestation of the intra-ply shear mechanism results in ply wrinkling.

(b) The limited forming potential through fibre strain due to the high fibre stiffness makes the laminate susceptible to large fibre stresses and associated defects.

(c) The fibres in the warp direction are more susceptible to fibre buckling in comparison to the weft, the laminate must be aligned so as to avoid compressive loads in the warp direction.

10 Recommendations

CFRTP components exhibit geometric distortions as the laminate cools down from the manufacturing temperature. This phenomenon is referred to as spring forward, for instance, an L-section component will result in angle section slightly less than 90°. This effect is a result of the anisotropic thermal shrinkage of the composite, which is small in the fibre direction and relatively large in the direction normal to the fibres [36]. The tool is designed with a slightly smaller angle to compensate for this effect. The expected amount of spring forward needs to be known for the tool to be designed correctly. The incorporation of a model that accounts for the thermal effects would add value to the predictive capability of a package like AniForm.

During forming the fibres migrate and there is often a mis-match between the fibre orientation of the manufactured product and the intended orientation. Composite structures rely on the fibre orientations for mechanical properties. The results of a study to compare the fibre orientations predicted by AniForm, those measured experimentally and those intended during design could yield results that could be used to refine the determination of the mechanical properties of components.

11 References

[1] Aerosud-Aviation. CFRTP IR-Oven Manual, 2015.

[2] Airbus Website. http://www.airbus.com/innovation/proven-concepts/in-design/innovative-materials/, 2015.

[3] Allaoui S, Cellard C and Hivet G. *Effect of inter-ply sliding on the quality of multilayer interlock dry fabric preforms,* Composites Part A: Applied Science and Manufacturing 68:336-345, 2015.

[4] AniForm-BV. *Aniform user documentation*, 2015.

[5] AniForm-BV. http://www.aniform.com/news., 2015.

[6] ASM-Materials ASM Alloy Center Database. http://mio.asminternational.org/ac/index.aspx?profileKey=grantami-ac-datasheets., 2016.

[7] Bel S. *Draping simulation - Recent achievements and future trends*, University of Lyon: Laboratoire de Genie Civil et d'Ingenierie Environnementale, 2014.

[8] Bigg DM. *Manufacturing methods for long-fiber reinforced polypropylene sheets and laminates*, Dordrecht:Springer Netherlands:263-292, 1995.

[9] Boisse P, Hamila N, Vidal-Sall E and Dumont F. *Simulation of wrinkling during textile composite reinforcement forming, influence of tensile, in-plane shear and bending stiffnesses,* Composites Science and Technology 71(5):683-692, 2011.

[10] Burkhart A and Cramer D. *Feasibility of CFRTP Tailored Blanks for Automotive Applications*, Society of Plastic Engineers, https://www.4spe.org/Resources/resource.aspx?ItemNumber=25515, 2005.

[11] Cengel Y and Ghajar A. *Heat and Mass Transfer: Fundamentals & Applications*, McGraw-Hill, 2010.

[12] Classle.net. *AB and C-Scan Displays*, https://www.classle.net/book/ab-and-c-scan-displays, 2017.

[13] Covestro. *Covestro CFRTP Brochure*, https://www.cfrtp.covestro.com/, 2017.

[14] de Luca P, Lefbure P and Pickett A. *Numerical and experimental investigation of some press forming parameters of two fibre reinforced thermoplastics: Apc2-as4 and pei-cetex,* Composites Part A: Applied Science and Manufacturing 29(1):101-110, 1998.

[15] ESI-Group. https://www.esi-group.com/software-solutions/virtual-manufacturing/, 2017.

[16] Fokker Website. http://www.fokker.com/, 2015.

[17] Haanappel S and ten Thije R. Multi-Layer Thermoplastic Composites Manufacturing Processes: Simulations and Experiments, University of Twente: Faculty of Engineering Technology, 2011.

[18] Haanappel SP, Ten Thije RH, Sachs U, Rietman B and Akkerman R. *Formability analyses of uni-directional and textile reinforced thermoplastics,* Composites Part A: Applied Science and Manufacturing 56:80-92, 2014.

[19] Kapadia, A. *Non Destructive Testing of Composite Materials*, National Composites Network, https://avaloncsl.files.wordpress.com/2013/01/ncn-best-practice-ndt.pdf., 2007.

[20] Lebrun G, Denault J and Bureau M. *Influence of Consolidation and Forming Parameters in the Moulding of CFRTP Composties*, Industrial Materials Institute-National Research Council, Canada, http://www.temp.speautomotive.com/SPEA-CD/SPEA2002/pdf/b02.pdf., 2014.

[21] Liang B, Hamila N, Peillon M and Boisse P. *Analysis of thermoplastic prepreg bending stiffness during manufacturing and of its influence on wrinkling simulations,* Composites Part A: Applied Science and Manufacturing 67:111-122, 2014.

[22] Lin H, Wang J and Harrison P. *Textile Wrinkling in Composite Forming*, University of Glasgow:School of Engineering http://userweb.eng.gla.ac.uk/philip.harrison/publications/, 2006.

[23] Lin H, Wang J, Long AC, Cliord MJ and Harrison P. *Predictive modelling for optimization of textile composite forming,* Composites Science and Technology 67(15-16):3242-3252, 2007.

[24] Nishi M, Kaburagi T, Kurose M, Hirashima T and Kurasiki T. *Forming Simulation of Thermoplastic Pre-Impregnated Textile Composite,* International Journal of Chemical, Nuclear, Metallurgucal and Materials Engineering 8(8):724-732, 2014.

[25] Nosrat-Nezami F, Gereke T, Eberdt C and Cherif C. *Characterisation of the shear-tension coupling of carbon-fibre fabric under controlled membrane tensions for precise simulative predictions of industrial preforming processes,* Composites Part A:Applied Science and Manufacturing 67:131-139, 2014.

[26] Olympus-IMS. *Instrumententation Introduction*, http://www.olympus-ims.com/en/ndt-tutorials/instrumententation/intro, 2017.

[27] Omnexus. https://omnexus.specialchem.com/selection-guide/polyphenylene-sulfide/, 2017.

[28] Reid R. *Aircraft Structures I - MECN3001* University of the Witwatersrand: School of Mechanical, Industrial and Aeronautical Engineering, 2010.

[29] Robroek L. *An introduction to the rubber forming of thermoplastic composites*, Delft University of Technology, Faculty of Aerospace Engineering, Report LR-683, 1992.

[30] RTPCompany. https://www.rtpcompany.com/products/product-guide/polyphenylene-sulfide-pps/, 2017.

[31] Stackplastics. https://www.stackplastics.com/injection-molding-resin/pps, 2017.

[32] Tencate. http://www.tencate.com/emea/aerospace-composites/products/ thermoplastic/default.aspx., 2015.

[33] Textile-Innovation-Knowledge-Platform. *Weaving Process*, http://www.tikp.co.uk/knowledge /technology/warping-and-weaving/weaving-process/, 2017.

[34] TORAY-Plastics. *Torelina PPS Resin Product Profile*, http://www.toray.jp/plastics/en/ torelina/technical/tec-017.html., 2017.

[35] Wang P, Hamila N and Boisse P *Thermoforming simulation of multilayer composites with continuous fibres and thermoplastic matrix,* Composites Part B: Engineering 52(C):127-2013

[36] Wijskamp S, Lamers E and Akkerman R. *Spring-forward of Woven Fabric Reinforced Composites*, University of Twente: Faculty of Engineering Technology, Production Technology, https://research.utwente.nl/en/publications/spring-forward-of-woven-fabric-reinforced - composites, 2002.

[37] Zhu B, Yu TX and Tao XM. *An experimental study of in-plane large shear deformation of woven fabric composite,* Composites Science and Technology 67(2):252-261, 2007.

Appendix A Material Data Sheets

Page intentionally left blank

TECHNICAL DATA

TENCATE ADVANCED COMPOSITES USA, INC.

CETEX® PPS

PRODUCT TYPE

Polyphenylene Sulfide
Thermoplastic
Resin System

SERVICE TEMPERATURE

212°F (100°C) Continuous

TYPICAL APPLICATIONS

- Primary Aircraft Structures
- Secondary Aircraft Structures
- Engine Nacelles
- Radomes

PRODUCT DESCRIPTION

CETEX® PPS is a semicrystalline polyphenylene sulfide thermoplastic composite offering outstanding toughness and excellent chemical and solvent resistance. The material is inherently flame resistant with low smoke emission. It exceeds 35/35 OSU and is qualified at Airbus and Boeing for multiple structural applications. This material is typically supplied in 12ft by 4ft (3,660mm by 1,220mm) preconsolidated laminates using the customer's designated ply count and orientation. In addition, lightning strike material can be incorporated and the laminates can be textured. By utilizing preconsolidated sheets and avoiding hand lamination, the customer can significantly reduce the cycle time required to produce a finished part. In addition, thermoplastics have the unique capability of allowing parts to be welded, folded, etc., to facilitate lower part count structures.

TYPICAL PROPERTIES OF NEAT RESIN

Specific gravity	1.35 g/cc
Tg	194°F (90°C)
Melt temp	536°F (280°C)
Dielectric constant	3.20 at 1MHz
Loss tangent	0.0013 at 1MHz
Moisture absorption	0.02%
Flammability	V-0
Tensile strength	13.1ksi (90.3MPa)
Tensile modulus	0.551Msi (3,800MPa)
Elongation at yield	3%
Poisson's ratio	0.36
Compression strength	21.5ksi (148MPa)
Compression modulus	0.43Msi (2,965MPa)
Flexural strength	18.1ksi (125MPa)
Flexural modulus	0.54Msi (3,725MPa)
Izod unnotched	94.6ft-lb/in2 (199kJ/m2)
Izod notched	7.4ft-lb/in2 (15.6kJ/m2)
CTE	29ppm/°F (52.2ppm/°C)
Thermal conductivity	0.19 W/m-°K
Outgassing TML	0.04%
Outgassing CVCM	0.00%
WVR	0.00%
Fluid resistance	Excellent

18410 Butterfield Blvd.
Morgan Hill, CA 95037
USA

Tel 408 776 0700
Fax 408 776 0107
www.tencate.com

ISO 9001
AS 9100
Registered

TECHNICAL DATA

TENCATE ADVANCED COMPOSITES USA, INC.

CETEX® PPS

Physical/Thermal (nominal values)	T300 3K 5HS/PPS with double sided Amcor foil					7781/PPS			
Mass of fabric	8.26	oz/yd²	280	g/m²		8.85	oz/yd²	300	g/m²
Mass of fabric + resin	14.33	oz/yd²	486	g/m²		14.01	oz/yd²	475	g/m²
Resin content by volume	50	%	50	%		47.5	%	47.5	%
Resin content by weight	43	%	43	%		37	%	37	%
Moisture pick up	0.1	%	0.1	%		0.1	%	0.1	%
Ply thickness	0.0122	in	0.31	mm		0.0098	in	0.25	mm
Specific gravity	96.7	lb/ft³	1.55	g/cm³		119.8	lb/ft³	1.92	g/cm³
Tg (DSC) (amorphous)	194	°F	90	°C		194	°F	90	°C
Tg (DSC) (crystalline)	248	°F	120	°C		248	°F	120	°C
Tm	536	°F	280	°C		536	°F	280	°C
Mechanical properties -67°F (-55°C) Dry									
Tensile strength warp	114.5	ksi	790	MPa		65.6	ksi	453	MPa
Tensile strength weft	108.7	ksi	750	MPa		64.8	ksi	447	MPa
Tensile modulus warp	7.7	Msi	53	GPa		3.2	Msi	22	GPa
Tensile modulus weft	7.6	Msi	53	GPa		3.0	Msi	20	GPa
Compression strength warp	98.0	ksi	676	MPa		82.1	ksi	566	MPa
Compression strength weft	101.3	ksi	699	MPa		55.7	ksi	384	MPa
Compression modulus warp	7.2	Msi	49	GPa		3.8	Msi	27	GPa
Compression modulus weft	7.2	Msi	50	GPa		3.6	Msi	25	GPa
Flexural strength warp	151.3	ksi	1043	MPa					
Flexural strength weft	120.9	ksi	834	MPa					
Flexural modulus warp	8.6	Msi	59	GPa					
Flexural modulus weft	6.3	Msi	43	GPa					
In plane shear strength	19.0	ksi	131	MPa		15.8	ksi	109	MPa
In plane shear modulus	642.1	ksi	4428	MPa		711.5	ksi	4907	MPa
Open hole tensile strength	41.4	ksi	286	MPa					
Open hole compressive strength	39.5	ksi	273	MPa					
Compression after impact	32.3	ksi	223	MPa					
Bearing strength yield	71.2	ksi	491	MPa					
Bearing strength ultimate	121.5	ksi	838	MPa					
Mechanical properties -73°F (23°C)/50%RH									
Tensile strength warp	109.8	ksi	758	MPa		49.3	ksi	340	MPa
Tensile strength weft	109.4	ksi	755	MPa		48.3	ksi	333	MPa
Tensile modulus warp	8.1	Msi	56	GPa		3.1	Msi	22	GPa
Tensile modulus weft	7.8	Msi	54	GPa		2.9	Msi	20	GPa
Compression strength warp	93.3	ksi	644	MPa		61.6	ksi	425	MPa
Compression strength weft	92.4	ksi	637	MPa		42.8	ksi	295	MPa
Compression modulus warp	7.5	Msi	51	GPa		3.7	Msi	26	GPa
Compression modulus weft	7.5	Msi	51	GPa		3.5	Msi	24	GPa
Flexural strength warp	148.9	ksi	1027	MPa		74.2	ksi	511	MPa
Flexural strength weft	120.5	ksi	831	MPa		56.6	ksi	390	MPa
Flexural modulus warp	8.7	Msi	60	GPa		3.3	Msi	23	GPa
Flexural modulus weft	6.5	Msi	45	GPa		2.9	Msi	20	GPa
In plane shear strength	17.2	ksi	119	MPa		11.6	ksi	80	MPa
In plane shear modulus	585.8	ksi	4040	MPa		538.5	ksi	3714	MPa
Open hole tensile strength	40.4	ksi	278	MPa		23.0	ksi	158	MPa
Open hole compressive strength	37.1	ksi	256	MPa		26.5	ksi	183	MPa
Compression after impact	31.2	ksi	215	MPa		24.8	ksi	171	MPa
Bearing strength yield	65.8	ksi	454	MPa		46.1	ksi	318	MPa
Bearing strength ultimate	122.4	ksi	844	MPa		74.8	ksi	516	MPa

18410 Butterfield Blvd.
Morgan Hill, CA 95037
USA

Tel 408 776 0700
Fax 408 776 0107
www.tencate.com

ISO 9001
AS 9100
Registered

TECHNICAL DATA

TENCATE ADVANCED COMPOSITES USA, INC.

CETEX® PPS

Physical/Thermal (nominal values) — T300 3K 5HS/PPS with double sided Amcor foil — 7781/PPS

Mechanical Properties 80˚C Dry

Tensile strength warp	105.9	ksi	730	MPa	40.5	ksi	280	MPa
Tensile strength weft	93.6	ksi	646	MPa	40.7	ksi	281	MPa
Tensile modulus warp	8.2	Msi	57	GPa	2.9	Msi	20	GPa
Tensile modulus weft	7.6	Msi	53	GPa	2.7	Msi	19	GPa
Compression strength warp	80.9	ksi	558	MPa	43.0	ksi	297	MPa
Compression strength weft	76.3	ksi	526	MPa	29.4	ksi	203	MPa
Compression modulus warp	7.5	Msi	51	GPa	3.2	Msi	22	GPa
Compression modulus weft	7.4	Msi	51	GPa	2.9	Msi	20	GPa
Flexural strength warp	138.4	ksi	955	MPa				
Flexural strength weft	115.1	ksi	794	MPa				
Flexural modulus warp	8.4	Msi	58	GPa				
Flexural modulus weft	6.5	Msi	45	GPa				
In plane shear strength	15.7	ksi	108	MPa	8.6	ksi	60	MPa
In plane shear modulus	384.4	ksi	2651	MPa	247.3	ksi	1705	MPa

Mechanical properties 176˚F (80˚C) conditioned at 158˚F (70˚) and 85%RH

Tensile strength warp	109.6	ksi	756	MPa	41.9	ksi	289	MPa
Tensile strength weft	101.2	ksi	698	MPa	41.8	ksi	289	MPa
Tensile modulus warp	8.2	Msi	56	GPa	3.0	Msi	21	GPa
Tensile modulus weft	7.6	Msi	53	GPa	2.8	Msi	19	GPa
Compression strength warp	83.8	ksi	578	MPa	33.4	ksi	230	MPa
Compression strength weft	77.5	ksi	535	MPa	22.6	ksi	156	MPa
Compression modulus warp	7.5	Msi	52	GPa	3.1	Msi	22	GPa
Compression modulus weft	7.4	Msi	51	GPa	2.9	Msi	20	GPa
Flexural strength warp	141.7	ksi	977	MPa				
Flexural strength weft	107.2	ksi	739	MPa				
Flexural modulus warp	8.7	Msi	60	GPa				
Flexural modulus weft	6.4	Msi	44	GPa				
In plane shear strength	15.1	ksi	104	MPa	9.8	ksi	68	MPa
In plane shear modulus	434.7	ksi	2998	MPa	208.4	ksi	1437	MPa
Open hole tensile strength	39.1	ksi	270	MPa	19.6	ksi	135	MPa
Open hole compressive strength	33.7	ksi	232	MPa	16.0	ksi	110	MPa
Compression after impact	31.6	ksi	218	MPa	0.0	ksi		MPa
Bearing strength yield	59.9	ksi	413	MPa	26.7	ksi	184	MPa
Bearing strength ultimate	121.6	ksi	839	MPa	55.6	ksi	384	MPa

Mechanical properties 212˚F (100˚C) conditioned at 158˚F (70˚) and 85%RH

Tensile strength warp					35.7	ksi	246	MPa
Tensile strength weft					39.6	ksi	273	MPa
Tensile modulus warp					2.8	Msi	20	GPa
Tensile modulus weft					2.6	Msi	18	GPa
Compression strength warp					24.4	ksi	169	MPa
Compression strength weft					16.9	ksi	117	MPa
Compression modulus warp					2.9	Msi	20	GPa
Compression modulus weft					2.5	Msi	18	GPa
In plane shear strength					9.1	ksi	63	MPa
In plane shear modulus					109.0	ksi	752	MPa

Average results according to Mil-R-17; test methods vary

FLAMMABILITY PROPERTIES

	OSU		Flammability			SMOKE (4 min)		TOXICITY						
	Heat Release	Release Rate	Burn Length	After Flame	Drip Flame	Non-flaming	Flaming	HCN	CO	NOx	SO2	HF	HCl	HBr
5 plies of 7781/PEI	14	21	1.9 mm	0sec	N/D									
4 plies of 3k PW/PPS							9.03	9		1	17	1	1	

Flammability & Heat Release - FAR 25.853

Smoke Density & Toxicity - ATS 1000.001

All data given is based on representative samples of the materials in question. Since the method and circumstances under which these materials are processed and tested are key to their performance, and TenCate Advanced Composites USA, Inc. has no assurance of how its customers will use the material, the corporation cannot guarantee these properties. Rev Mar 2009

18410 Butterfield Blvd.
Morgan Hill, CA 95037
USA

Tel 408 776 0700
Fax 408 776 0107
www.tencate.com

ISO 9001
AS 9100
Registered

TECHNICAL DATA

TENCATE ADVANCED COMPOSITES

TenCate Cetex®
Premium

Product Type
Polyetherimide Thermoplastic Resin System

Service Temperature
149°C (300°F) Continuous

Typical applications
- Aircraft Interiors
- Secondary Aircraft Structures

Customer qualifications
- BMS 8-353 (Type 1)
- ABS 5036
- AIMS 003-01
- ASNA 5054

Product Description
TenCate Cetex® Premium is an engineered thermoplastic composite, utilizing polyetherimide resin for outstanding toughness and excellent fire performance. TenCate Cetex® Premium has gained qualification at Airbus, Boeing and many other airframe OEMs and Tier 1 suppliers for use in aircraft interior and secondary structures.
TenCate Cetex® is typically supplied in 3.66m x 1.22m (12ft x 4ft) pre-consolidated laminates (RTL) of varying ply thicknesses, specifically adhering to customer designated fiber selection, orientation and ply count.
The use of Cetex® as an reinforced thermoplastic laminate (RTL) composite significantly reduces the production cycle-time by eliminating the handling and assembly of traditional wet-lay materials, along with the potential for error. In addition, the thermoplastic forming time is calculated in minutes and seconds, not hours. Heating, forming and cooling can take less than 5 minutes for complex 3D geometry, and sandwich panels can now be realized in 15 minutes without the inconvenience of core read-through. Further optimization can be gained in secondary processing, due to the thermoplastic resin. These operations can include welding, folding, painting and printing.

TenCate Cetex® Premium product benefits / features
- Excellent FST performance (OSU <15/15)
- No freezer storage required
- Rapid processing with cycle times <3 min
- Very low moisture absorption
- Good solvent resistance
- Low CTE and CME
- Qualified and certified to OEM specifications
- Optional color grades available

Typical properties of neat resin

Specific gravity	1.27 g/cc
Tg	217°C (423°F)
Dielectric constant	3.15 at 1 MHz
Loss tangent	0.0013 at 1 MHz
Moisture absorption	1.25%
Flammability	V-0
Tensile strength	105 MPa (15.2 ksi)
Tensile modulus	3,276 MPa (0.475 Msi)
Elongation at yield	7%
Poisson's ratio	0.36%
Compression strength	152 MPa (22.0 ksi)
Compression modulus	3,310 MPa (0.48 Msi)
Flexural strength	138 MPa (20.0 ksi)
Flexural modulus	3,450 MPa (0.50 Msi)
Shear strength	103 MPa (15 ksi)
Izod unnotched	1,335 J/m (25.0 ft-lb/in)
Izod notched	53.4 J/m (1.0 ft-lb/in)
CTE	31 ppm/°F (55.8ppm/°C)
Thermal conductivity	0.22 W/m-°K
Outgassing TML	0.40%
Outgassing CVCM	0.00%
WVR	0.06%

TenCate Advanced Composites bv
P.O. Box 9
7443 PV Nijverdal
The Netherlands

Email: info_tcac@tencate.com
Web: www.tencate.com
Tel.: +31 548 633 933
Fax: +31 548 633 299

ISO 9001
AS 9100
Registered

TECHNICAL DATA

TENCATE ADVANCED COMPOSITES

TenCate Cetex®
Premium

(2 of 2)

Physical / thermal properties of prepreg - 7781 PEI

Mass of Fabric	296 g/m2 (8.85 oz/yd2)
Mass of Fabric + Resin	450 g/m2 (13.27 oz/yd2)
Resin Content by Volume	50%
Resin Content by Weight	33%
Moisture Pick Up	0.35%
Ply Thickness	0.24 mm (0.0094 in)
Specific Gravity	1.91 g/cm3 (119.1 lb/ft3)
Tg (DSC) (amorphous)	217°C (423°F)
Tm	310°C (590°F)

Laminate data for 7781 PEI

Property	Condition	Methods	Results	
Tensile Strength 0°	RTD	ISA 527 (type 3) EN 2747 (III)	451 MPa	65.4 ksi
Tensile Modulus 0°	RTD	ISA 527 (type 3) EN 2747 (III)	26.3 GPa	3.8 Msi
Compression Strength 0°	RTD	ASTM D 6641 EN 2850	560 MPa	560 MPa
Compression Modulus 0°	RTD	ASTM D 6641 EN 2850	29 GPa	4.2 Msi
Flexural Strength 0°	RTD	ISO 178	650 MPa	94.3 ksi
Flexural Modulus 0°	RTD	ISO 178	26 GPa	3.8 Msi

Flammability proporties - 7781 FG

Test	Spec	Criteria	2 Plies of 7781/ PEI Resin	5 Plies of 7781/PEI Resin	5 Plies of 7781/ White PEI Resin
Flammability	60 second vertical burn FAR 25.853 (a)	152 mm	PASS	PASS	PASS
Smoke Emisssion	ABD0031 (F)	150/200	PASS	PASS	PASS
Toxicity	ABD0031 (F)	Ds Max 4 min (Flaming/Non-Flaming) = 150	PASS	PASS	PASS
Heat Release	FAR 25.853 (d)	2 min Total HR (kWmin/m2) = 65	10.0	0	3.5
		Peak HR (kW/ m2) = 65	12.0	13.0	14.1

Revised 12/2012

TenCate Cetex® is a registered trademark of Royal TenCate. All data given is based on representative samples of the materials in question. Since the method and circumstances under which these materials are processed and tested are key to their performance, and TenCate Advanced Composites has no assurance of how its customers will use the material, the corporation cannot guarantee these properties.

TenCate Advanced Composites bv
P.O. Box 9
7443 PV Nijverdal
The Netherlands

Email: info_tcac@tencate.com
Web: www.tencate.com
Tel.: +31 548 633 933
Fax: +31 548 633 299

ISO 9001
AS 9100
Registered

NECURON® 651
BOARD MATERIAL - TECHNICAL DATA SHEET

CHARACTERISTICS
- very fine structure
- smooth and paintable surface
- excellent processing properties

APPLICATIONS
- master and copy models
- cubing and data models
- general modelling



TECHNICAL DATA

Colour	brown	visual
Coefficient of thermal expansion	approx. 55 x 10^{-6} K^{-1}	DIN 53752-B
Temperature resistance	approx. 65 °C	ISO 75
Shore D	approx. 70	ISO 868
Compressive strength	approx. 25 N/mm^2	DIN 53421
Flexural strength	approx. 27 N/mm^2	ISO 178
Density	approx. 0.70 g/cm^3	ISO 845
Abrasion resistance (at defined parameters)	approx. - mm^3	DIN ISO 4649
Fire protection classification	B2	
Electrical current resistance	approx. - Ω x cm	IEC 93
Notched impact strength	approx. - kJ/m^2	ISO 179-1
Thermal conductivity	approx. 0.11 W/mk	DIN 52612

- Contains no halogens, plasticizer or solvent
- Manufactured fluorocarbohydrate-free
- Physiologically harmless

DIMENSIONS

1,200	500	130	mm
1,200	500	150	mm
1,500	500	40	mm
1,500	500	50	mm
1,500	500	60	mm
1,500	500	75	mm
1,500	500	100	mm
1,500	500	130	mm
1,500	500	150	mm

Surfaces machined parallel.
Other dimensions on request.

STORAGE/TRANSPORT
NECURON®-boards should be stored on a flat underground and in a dry space at a temperature between 18°C and 25°C. Variations in temperature should be avoided during the transport and storage.

NECUMER GmbH ▪ Industriestraße 26 ▪ D-49163 Bohmte
Tel +49 5471 9502-0 ▪ Fax +49 5471 9502-99 ▪ info@necumer.de ▪ www.necumer.de ▪ Version: 27.07.16

PROCESSING

Adhesive	Colour	Mixture ratio A to B (by weight)	Pot life in minutes at 20°C	Curing time at 20°C
NECURON® K6	brown	1:1	2-3	15-30 min
NECURON® K8N	amber	1:0,5	10	5 hrs

or usual and compatible patternmaking adhesives/resins
We recommend that boards are plane-parallel to ensure good glue joints.

MACHINING

Machining temperature: 20°C - 25°C
Tools: Metal-cutting tools

MILLING PARAMETERS

	ROUGHING	FINISHING
Type of tool	Finishing tools d=80mm	Finishing tools d=80mm
Tool diameter [d] (mm)	80	80
Cutting speed [Vc] (m/sek)	50	50
Speed [n] (1/min)	12000	8000
Feed speed (m/min)	10	7.5
Tooth speed [fz] (mm)	0.21	0.21
Number of teeth [z]	4	4
Cutting depth [ae] (mm)	4	0.5
Cutter mark length [fzeff] (mm)	38	5

NECURON® 651

- This material does not contain any fillers that release harmful dust during machining. Nevertheless the dust content in the air should not rise above 6 mg/m^3. Safety procedures recommended by the vocational co-operative of the chemical industry should be complied with.
- The article is not a regulatory product according to ICC regulations. In accordance with general local and national regulations waste is to be disposed by incineration in authorised places or conveyed to authorised tips (EAK 120105).
- Technical statements and recommendations refer to current standard of technique and are based on our own experience. Further developments and improvements are reserved. Due to the variety of processing possibilities own experiments are recommended to optimise results.
- This data sheet is not legally binding. Actual specifications and / or features may vary.

Smooth-Sil® Series

Addition Cure Silicone Rubber Compounds

www.smooth-on.com

PRODUCT OVERVIEW

Smooth-On **Smooth-Sil®** Platinum Silicones cure at room temperature with negligible shrinkage. With different hardnesses to choose from, **Smooth-Sil®** products offer tremendous versatility and are suitable for making production molds of any configuration, large or small. These silicones exhibit good chemical, abrasion and heat resistance. Materials such as plasters, concrete, wax, low-melt metal alloys or resins (urethane, epoxy or polyester) can then be cast into these silicone rubbers without a release agent.

Smooth-Sil® 945 offers the convenience of a **1A:1B by volume** mix ratio and a fast **6 hour cure time.**

Smooth-Sil® Platinum Silicones are used for rapid prototyping, wax casting (foundries and candle makers), architectural restoration and for casting concrete. Smooth-Sil® 940 is suitable for food related applications. (See separate technical bulletin for usage instructions available at www.smooth-on.com).

TECHNICAL OVERVIEW

	Mixed Viscosity (ASTM D-2393)	Specific Gravity (g/cc) (ASTM D-1475)	Specific Volume (cu. in./lb.) (ASTM D-1475)	Color	Pot Life (ASTM D-2471)	Cure Time	Mix Ratio	Shore A Hardness (ASTM D-2240)	Tensile Strength (ASTM D-412)	100% Modulus (ASTM D-412)	Elongation @ Break % (ASTM D-412)	Die B Tear Strength (ASTM D-624)
Smooth-Sil® 935	40,000 cps	1.18	23.5	Blue	45 min.	24 hrs.	100A:10B by weight	35A	650 psi	170 psi	300%	115 pli
Smooth-Sil® 940	35,000 cps	1.18	23.4	Pink	30 min.	24 hrs.	100A:10B by weight	40A	600 psi	200 psi	300%	100 pli
Smooth-Sil® 945	30,000 cps	1.24	22.3	Purple	25 min.	6 hrs.	1A:1B by weight or volume	45A	700 psi	260 psi	320%	120 pli
Smooth-Sil® 950	35,000 cps	1.24	22.3	Blue	45 min.	24 hrs.	100A:10B by weight	50A	725 psi.	272 psi	320%	155 pli
Smooth-Sil® 960	30,000 cps	1.25	22.2	Green	45 min.	16 hrs.	100A:10B by weight	60A	650 psi.	280 psi.	270%	110 pli

Useful Temperature Range: -65°F to 450°F (-53°C to 232°C)
Dielectric Strength (ASTM D-147-97a)**:** >350 volts/mil

*All values measured after 7 days at 73°F/23°C
Shrinkage* *(in./in.) (ASTM D-2566):* < .001

PROCESSING RECOMMENDATIONS

PREPARATION... Safety – Use in a properly ventilated area ("room size" ventilation). Wear safety glasses, long sleeves and rubber gloves to minimize contamination risk. Wear vinyl gloves only. Latex gloves will inhibit the cure of the rubber.

Store and use material at room temperature (73°F/23°C). Warmer temperatures will drastically reduce working time and cure time. Storing material at warmer temperatures will also reduce the usable shelf life of unused material. These products have a limited shelf life and should be used as soon as possible.

Cure Inhibition – Addition-cure silicone rubber may be inhibited by certain contaminants in or on the pattern to be molded resulting in tackiness at the pattern interface or a total lack of cure throughout the mold. Latex, tin-cure silicone, sulfur clays, certain wood surfaces, newly cast polyester, epoxy or urethane rubber my cause inhibition. If compatibility between the rubber and the surface is a concern, a small-scale test is recommended. Apply a small amount of rubber onto a non-critical area of the pattern. Inhibition has occurred if the rubber is gummy or uncured after the recommended cure time has passed.

Because no two applications are quite the same, a small test application to determine suitability for your project is recommended if performance of this material is in question.

To prevent inhibition, one or more coatings of a clear acrylic lacquer applied to the model surface is usually effective. Allow any sealer to thoroughly dry before applying rubber. Note: Even with a sealer, platinum silicones will not work with modeling clays containing heavy amounts of sulfur. Do a small scale test for compatibility before using on your project.

Applying A Release Agent - Although not usually necessary, a release agent will make demolding easier when pouring into or over most surfaces. Ease Release® 200 is a proven release agent for making molds with silicone rubber. Mann Ease Release® products are available from Smooth-On or your Smooth-On distributor.

Safety First!

The Material Safety Data Sheet (MSDS) for this or any Smooth-On product should be read prior to use and is available upon request from Smooth-On. All Smooth-On products are safe to use if directions are read and followed carefully.

Keep Out of Reach of Children

Be careful. Use only with adequate ventilation. Contact with skin and eyes may cause irritation. Flush eyes with water for 15 minutes and seek immediate medical attention. Remove from skin with waterless hand cleaner followed by soap and water.

Important: The information contained in this bulletin is considered accurate. However, no warranty is expressed or implied regarding the accuracy of the data, the results to be obtained from the use thereof, or that any such use will not infringe upon a patent. User shall determine the suitability of the product for the intended application and assume all risk and liability whatsoever in connection therewith.

Applying A Release Agent - IMPORTANT: To ensure thorough coverage, lightly brush the release agent with a soft brush over all surfaces of the model. Follow with a light mist coating and let the release agent dry for 30 minutes.

If there is any question about the effectiveness of a sealer/release agent combination, a small-scale test should be made on an identical surface for trial.

MEASURING & MIXING...

Before you begin, pre-mix Part B thoroughly to re-disperse pigments that may have settled. ***Using a gram scale***, dispense required amounts of parts A and B into a mixing container and mix for 3 minutes. Scrape the sides and bottom of the container several times. After mixing parts A and B, **vacuum degassing is recommended** to eliminate any entrapped air. Vacuum material for 2-3 minutes (29 inches of mercury), making sure that you leave enough room in container for product expansion.

POURING, CURING & MOLD PERFORMANCE...

For best results, pour your mixture in a single spot at the lowest point of the containment field. Let the rubber seek its level up and over the model. **A uniform flow will help minimize entrapped air.** The liquid rubber should level off at least 1/2" (1.3 cm) over the highest point of the model surface.

Curing / Post Curing - Allow rubber to cure as prescribed at room temperature (73°F/23°C) before demolding. Do not cure rubber where temperature is less than 65°F/18°C. **Optional:** Post curing the mold will aid in quickly attaining maximum physical and performance properties. After curing at room temperature, expose the rubber to 176°F/80°C for 2 hours and 212°F/100°C for one hour. Allow mold to cool to room temperature before using.

Using The Mold - When first cast, silicone rubber molds exhibit natural release characteristics. Depending on what is being cast into the mold, mold lubricity may be depleted over time and parts will begin to stick. No release agent is necessary when casting wax or gypsum. Applying a release agent such as Ease Release® 200 (available from Smooth-On) prior to casting polyurethane, polyester and epoxy resins is recommended to prevent mold degradation.

Thickening Smooth-Sil® Silicones - **THI-VEX®** is made especially for thickening Smooth-On's silicones for vertical surface application (making brush-on molds). Different viscosities can be attained by varying the amount of THI-VEX®. See the **THI-VEX® technical bulletin** (available from Smooth-On or your Smooth-On distributor) for full details.

Thinning Smooth-Sil® Silicones - Smooth-On's **Silicone Thinner®** will lower the viscosity of Smooth-Sil® for easier pouring and vacuum degassing. **A disadvantage** is that ultimate tear and tensile are reduced in proportion to the amount of **Silicone Thinner®** added. ***It is not recommended to exceed 10% by weight of total system (A+B).*** See the **Silicone Thinner® technical bulletin** (available from Smooth-On or your Smooth-On distributor) for full details.

Mold Performance & Storage - The physical life of the mold depends on how you use it (materials cast, frequency, etc.). Casting abrasive materials such as concrete can quickly erode mold detail, while casting non-abrasive materials (wax) will not affect mold detail. Before storing, the mold should be cleaned with a soap solution and wiped fully dry. Two part (or more) molds should be assembled. Molds should be stored on a level surface in a cool, dry environment.

Call Us Anytime With Questions About Your Application.

Toll-free: **(800) 381-1733** Fax: **(610) 252-6200**

The new **www.smooth-on.com** is loaded with information about mold making, casting and more.

BÖHLER M200

Eigenschaften

Chrom-Mangan-Molybdän-legierter Kunststofformenstahl.
Durch Schwefelzusatz beste Zerspanbarkeit auch im vergüteten Zustand.
Hohe Durchvergütung, daher auch bei großen Abmessungen gleichmäßige Festigkeit über den gesamten Querschnitt.
Gute Polierbarkeit.
Bad- und Gasnitrieren sowie Einsatzhärten und Hartverchromen ist möglich.

Properties

Chromium - manganese - molybdenum steel with sulfur content.
Very good machinibility in hardened and tempered condition.
It is well hardened and tempered, which yields uniform hardness over the whole cross section, including large sizes.
Good polishability.
Bath and gas nitriding as well as case hardening and hard chromium plating are possible.

Verwendung

Große und mittlere Formen für die Kunststoffverarbeitung, Formrahmen für Kunststoff- und Druckgießindustrie.
Teile für den allgemeinen Maschinenbau.
Lieferzustand normalerweise vergütet mit einer Festigkeit von ca.1000 N/mm² (ca. 300 HB).
Es ist daher im allgemeinen keine Wärmebehandlung mehr erforderlich.

Application

Large and medium-sized moulds for plastic processing, mould frames for the injection moulding and die casting industries, components for general mechanical engineering.
Supplied in the condition as hardened and tempered to a tensile strength of approx.1000 N/mm² (approx. 300 HB).
Therefore no further heat treatment is required in general.

Chemische Zusammensetzung

(Anhaltswerte in %)

Chemical composition

(average %)

C	Si	Mn	S	Cr	Mo
0,40	0,40	1,50	0,080	1,90	0,20

Normen

Standards

EN / DIN	AISI
< 1.2312 > 40CrMnMoS8-6	~ P20

BÖHLER M200

Physikalische Eigenschaften

Physical properties

Dichte bei / Density at .....20°C..... 7,85 .....kg/dm^3

Wärmeleitfähigkeit bei / Thermal conductivity at .....20°C..... 33 .....W/(m.K)

Spezifische Wärme bei / Specific heat at .....20°C..... 460 .....J/(kg.K)

Spez. elektr. Widerstand bei / Electrical resistivity at .....20°C..... 0,19 .....Ohm.mm^2/m

Elastizitätsmodul bei / Modulus of elasticity at .....20°C..... 210 x 10^3 N/mm^2

Wärmeausdehnung zwischen 20°C und ...°C, 10^{-6} m/(m.K) bei Thermal expansion between 20° C and ...°C, 10^{-6} m/(m.K) at	Temperatur / Temperature	10^{-6} m/(m.K)
	100°C	12,8
	200°C	13,0
	300°C	13,8
	400°C	14,0
	500°C	14,2

Für Anwendungen und Verarbeitungsschritte, die in der Produktbeschreibung nicht ausdrücklich erwähnt sind, ist in jedem Einzelfall Rücksprache zu halten.

As regards applications and processing steps that are not expressly mentioned in this product description/data sheet, the customer shall in each individual case be required to consult us.

Appendix B Tool Heating System Design

The Z and C section tools were equipped with a heating system, this section presents the design and specifications of the heating system. A heat transfer model was formulated to determine the heat flux required to maintain a suitable heat distribution on the tool-laminate contact surface. Figure B.1 shows a diagram of the model. The heating was supplied using cylindrical heating cartridges. The supplied heat is consumed in 3 ways; the actual heating of the tool (conduction), heat lost to the environment by convection and, radiation.

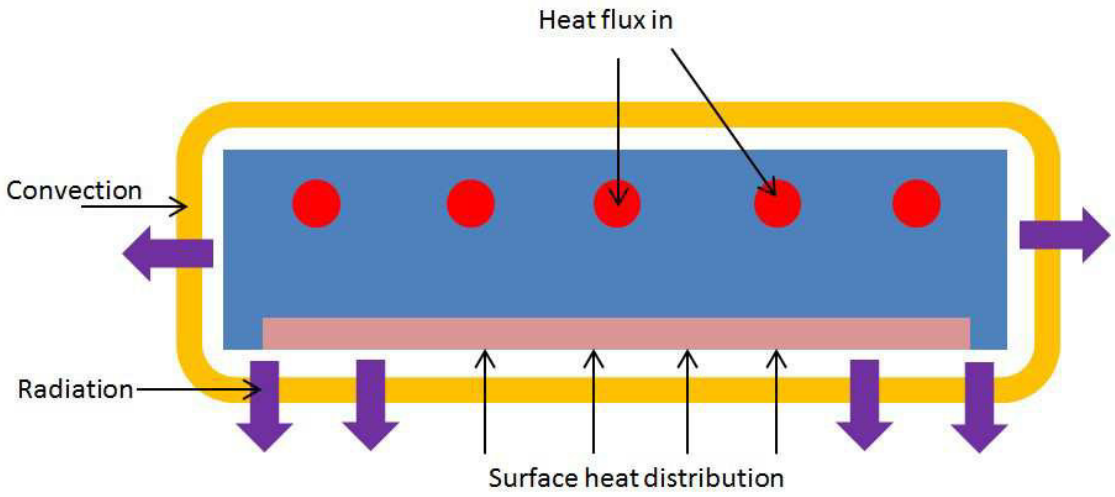


Figure B.1: A - Shear Angle, B - Fibre stress 1

B.0.0.1 Determination of Power Requirements

- **Conduction**

  The manufacturing instructions recommend the Carbon-PPS material to be consolidated with a tool at a temperature of 200°C ±20. The amount of energy required to raise the tool temperature from 25°C to the manufacturing temperature was 5978 KJ. A power rating of 2.21 kW was required to achieve this in a time duration of 45 min. The properties of material are shown in Table B.1 and the related equations thereafter.

Table B.1: Properties of the metal tool.

Property	**Symbol**	**Value**	**Units**
Density	ρ	7850	kg/m^3
Volume	V	8.64×10^3	m^3
Mass	m	68.7	kg
Heat Capacity	c	452	J/kg.K
Thermal Conductivity	k	40	W/m.K

Energy required to heat the tool, [11]

$$Q_{tool} = mc\Delta T = 5978 \times 10^3 \ J \qquad [11] \tag{B.1}$$

The power rating required to heat the tool in a time duration (t) of 45 minutes,

$$\dot{Q}_{tool} = \frac{Q_{tool}}{t} = \ 2.21kW \qquad [11] \tag{B.2}$$

- **Convection**

  Convection is heat energy transferred between a surface and a moving fluid at different temperatures [11]. Convection is described by Equation B.3 where h_c represents the convection co-efficient and A the wetted area. The behaviour of the convection co-efficient for airflow up to 20 m/s is described by Equation B.4. In this equation, v represents the velocity of the moving air, a velocity of 20 m/s was used to simulate a worst case scenario incident. The tool was used in a closed environment so that it is shielded from wind drafts. This gave a convection co-efficient of 35.2 W/m^{2}K and heat rate of 1.32 W was required to service the heat lost to convection.

$$\dot{Q}_{conv} = h_c A\Delta T = 1316.7 \ W[11] \tag{B.3}$$

$$h_c = 10.45 - v - 10\sqrt{v} = 35.2 \ W/m^2K[11] \tag{B.4}$$

- **Radiation**

  Radiation is heat transferred by electromagnetic waves or photons. This heat form presents as a heat loss to the system and the heat rate is described by Equation B.5. The heat rate attributed to radiation was found to be 0.11 kW.

$$\dot{Q}_{rad} = e\sigma A(T^4 - {T_a}^4) \qquad [11] \tag{B.5}$$

Material Properties

- Emissivity Factor: effectiveness of emitting energy as thermal radiation, $e = 0.2$ [6].
- Absorptivity Factor: absorption of incident radiation, $a = 0.2$ [6].

- **Total Power Requirements**

  The total power required in the system was,

$$\dot{Q}_{sys} = \dot{Q}_{tool} + \dot{Q}_{conv} + \dot{Q}_{rad} = 3.64\ kW \tag{B.6}$$

  With the consumption components consuming the following portions;

  - $\dot{Q}_{tool} = 60.8\%$.
  - $\dot{Q}_{conv} = 36.1\%$.
  - $\dot{Q}_{rad} = 3.1\%$.

- **Heat Flux Required to Maintain Sufficient Heat Distribution**

  The geometry of the tool affects the temperature distribution on the surface of the tool. The temperature of the faces of the tool that will be in contact with the laminate must fall in the required temperature range of 200°C±20. A model was formulated using Patran-Nastran to solve for the required heat flux for the tool geometry to achieve the required heat distribution. The Z-section tool required heat flux of 22 mW/mm^2. The resulting temperature distribution is presented in Figure B.2 (top). The temperature range on the forming surfaces is 183 - 217°C. The heat flux required for the C-section tool was 28 mW/mm^2. The resulting temperature distribution is presented in Figure B.2 (bottom). The temperature range on the forming surface is 194 - 216°C.

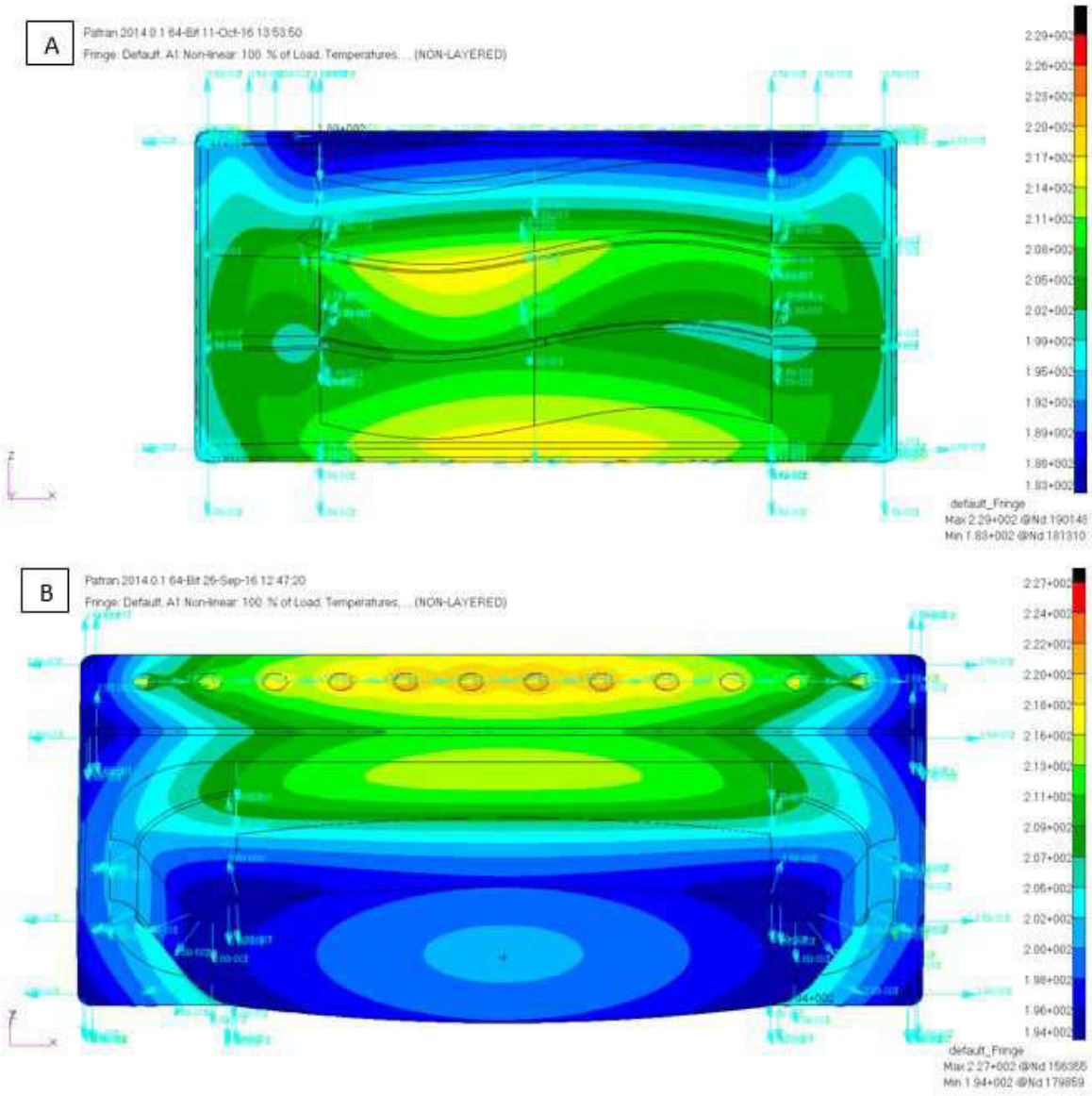


Figure B.2: Tool temperature distribution (A) Z-section, (B) C-section.

- **Power and Heat Flux Available**

  The heating cartridges acquired had the following properties.

  Table B.2: Heating Cartridge Properties

Property	**Value**	**Units**
Power output	750	W
Number of cartridges	12	
Length	180	mm
Diameter	12	mm

  Total power available

$$P_{availble} = 12 \times 750 = 9\ kW \tag{B.7}$$

  Heat flux available

$$HF_{availble} = \frac{P_{availble}}{SurfaceArea} = 110.5\ mW/mm^2 \tag{B.8}$$

  1. The power and heat flux supplied by the heating cartridges superseded the required values.

Parameter	**Required**	**Available**	**Safety Factor**
Power (kW)	3.64	9	2.47
Heat Flux (mW/mm^2)	28	110.5	3.95

  2. The predicted heat distribution of the tools was within the required range of 200±20°C.

Tool	**Temperature**
Z-Section	183 - 217° C
C-Section	194 - 216° C

The heating cartridges will be able to supply adequate power and heat flux to maintain the tool at the required temperature of 200°C ±20°.

Appendix C Spring Data

Page intentionally left blank

Product Details



Stainless Steel Extension Springs

Material to DIN 17224 No. 1 4310 or BS2056 EN58A with a right hand helix
All dimensions conform to DIN 2097 (Grade 2)

Springs: Tension

Add product to Compare

Specification

Not what you're looking for? Select the attributes you require, then click the button below.

Material	Stainless Steel
Free Length	47.6mm
Maximum Extended Length	147.30mm
Outside Diameter	7mm
Wire Diameter	0.63mm
Initial Tension	10.2N
Spring Rate	0.09N/mm

Product Details

Music Wire Extension Springs

Manufactured from high tensile strength piano/music wire, with a right-hand (clockwise) helix and loope
Materials to DIN17223 Class C or BS1408 CR3. Dimensions conform to DIN2097 Grade 2. Oiled finish.

Springs: Tension

Add product to Compare

Specification

Not what you're looking for? Select the attributes you require, then click the button below.

Material	Steel
Free Length	50mm
Maximum Extended Length	142.20mm
Outside Diameter	10mm
Wire Diameter	0.9mm
Initial Tension	24N
Spring Rate	0.23N/mm

Appendix D Simulation Results

The results from AniForm are presented in the following fashion: (with exception of the LCU results)

Title page

Page 1 Shear angle ply 1 & Shear angle ply 2

Page 2 Shear angle ply 3 & Shear angle ply 4

Page 3 Fibre stress 1 ply 1 & Fibre stress 1 ply 2

Page 4 Fibre stress 1 ply 3 & Fibre stress 1 ply 4

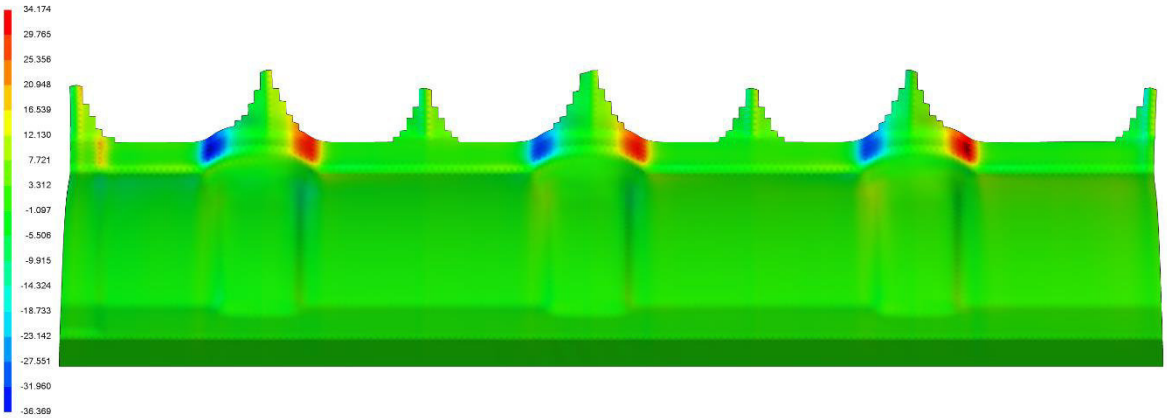
Page 5 Fibre stress 2 ply 1 & Fibre stress 2 ply 2

Page 6 Fibre stress 2 ply 3 & Fibre stress 2 ply 4

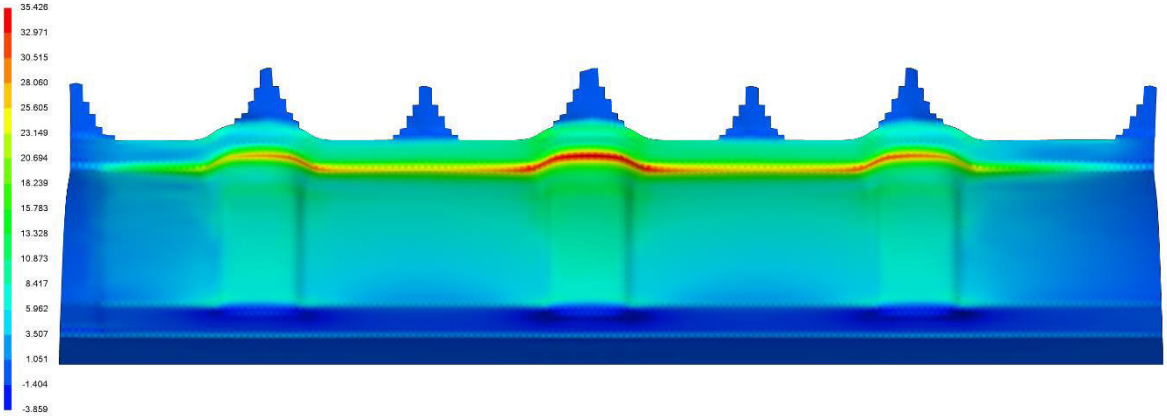
D.1 LCU Results

Page intentionally left blank

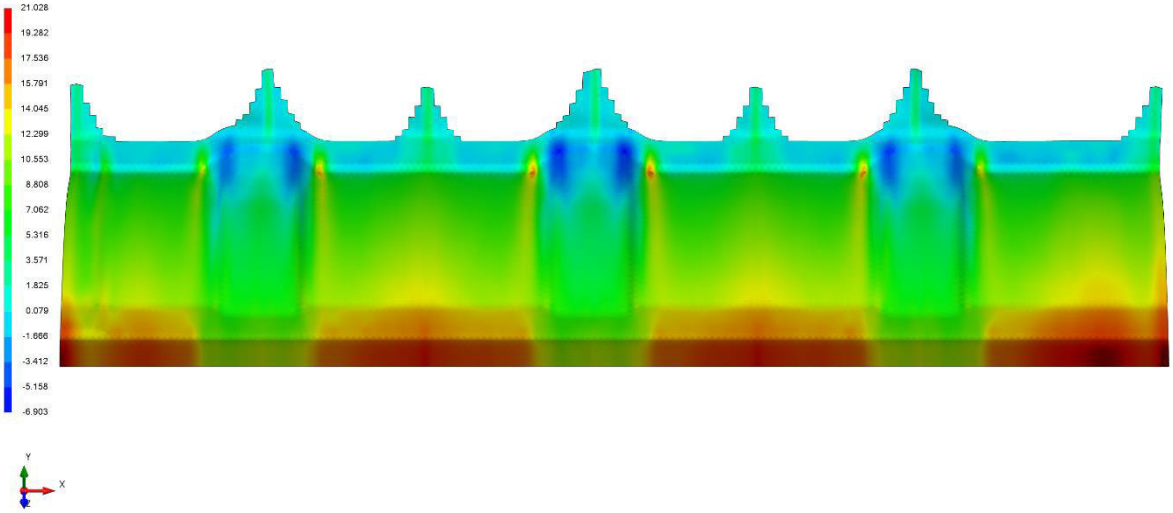
Shear angle f1_f2
s



Fiber stress 1
s

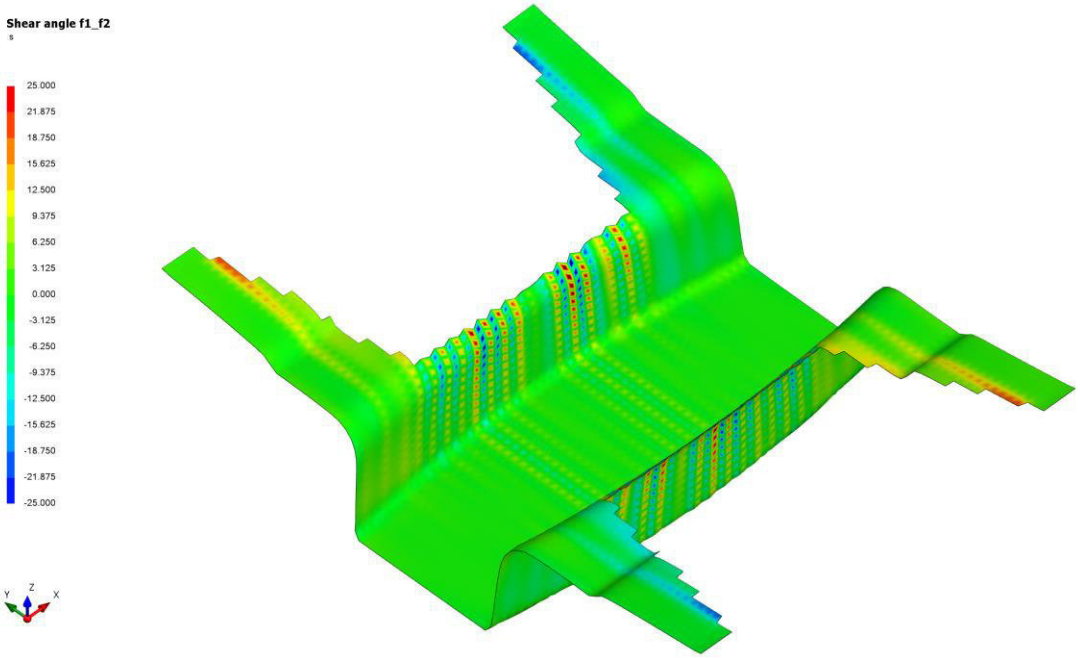


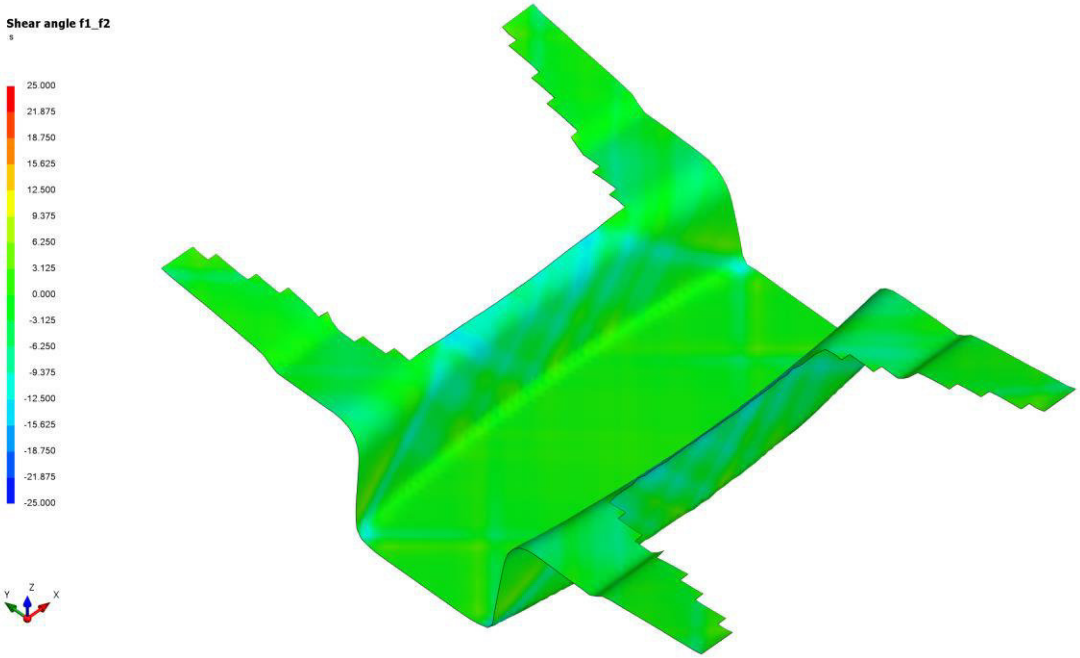
Fiber stress 2
s

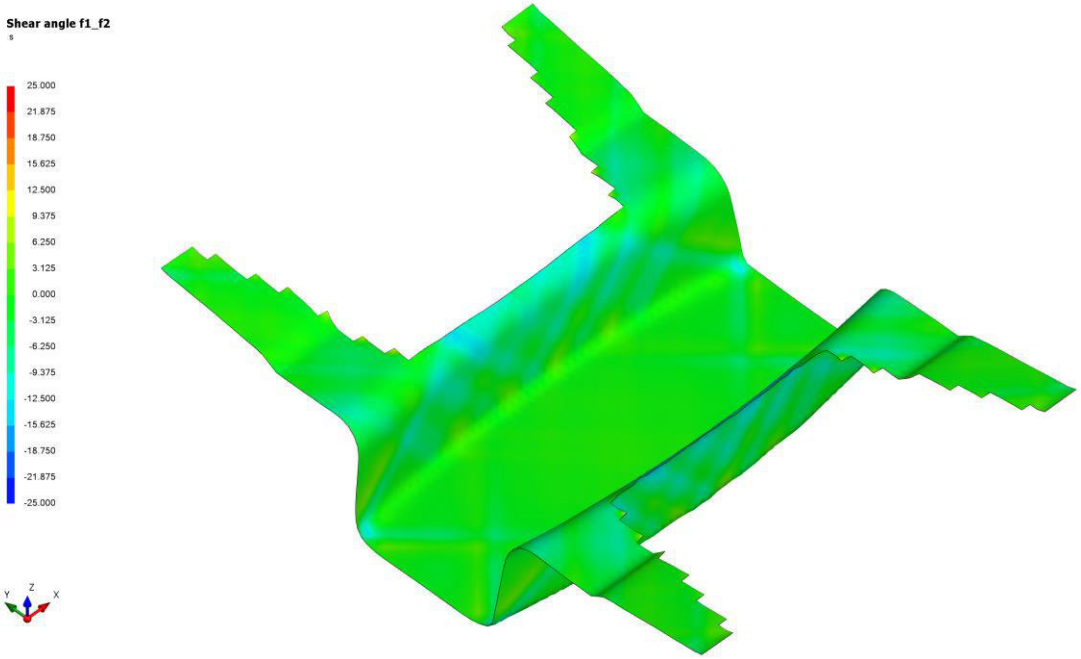


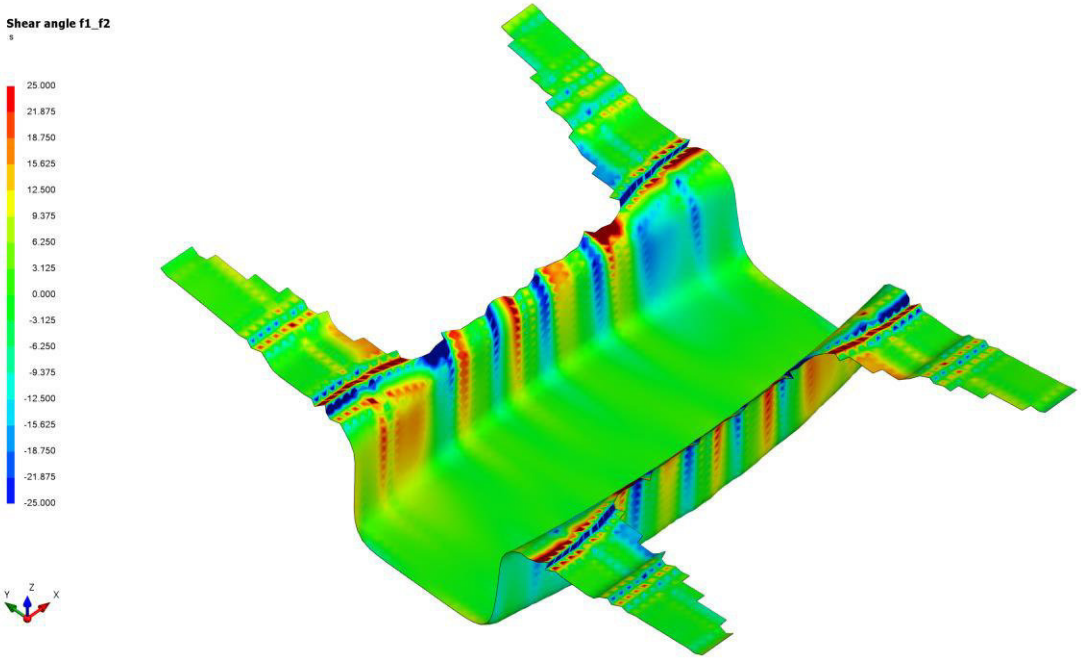
D.2 C-Section Results

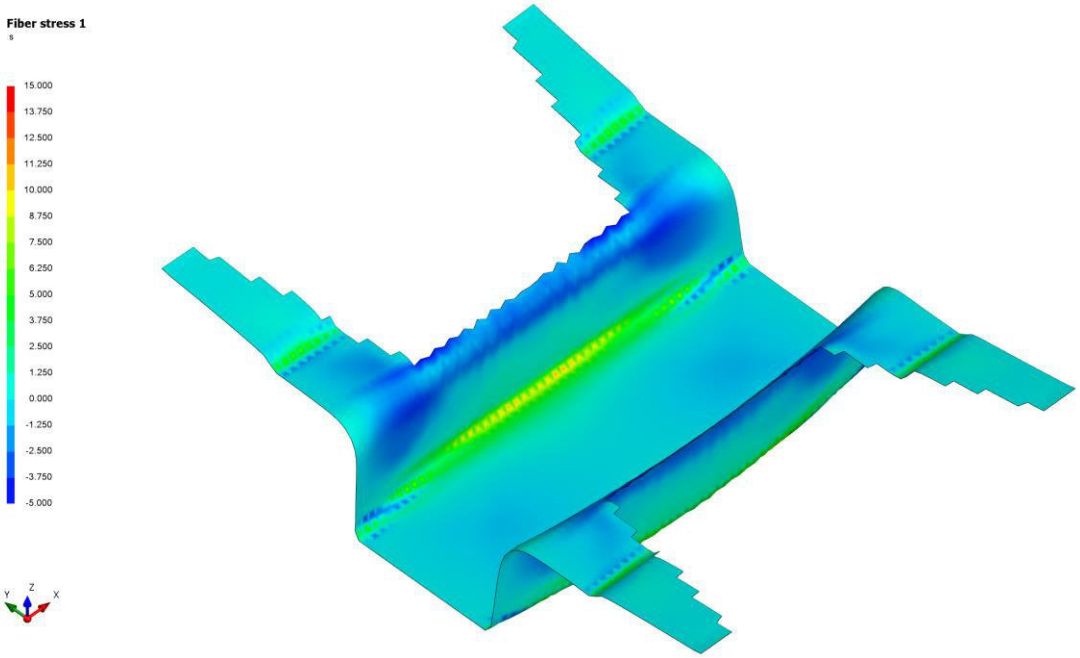
C-Section Blank 1

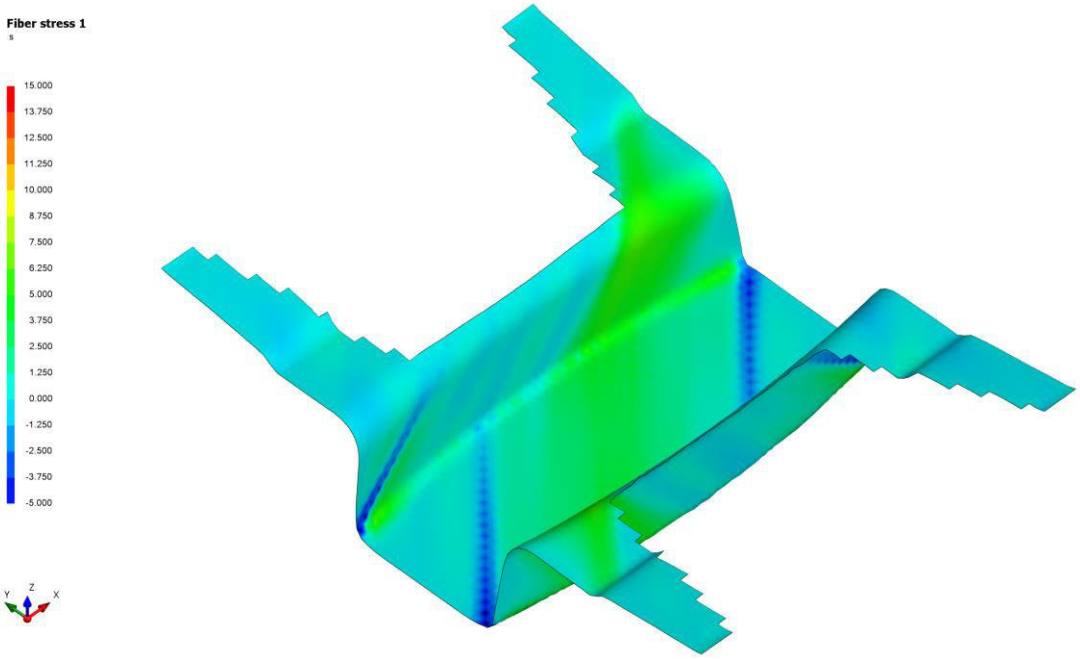

Shear angle f1_f2
s
25.000
21.875
18.750
15.625
12.500
9.375
6.250
3.125
0.000
-3.125
-6.250
-9.375
-12.500
-15.625
-18.750
-21.875
-25.000
Y
Z
X

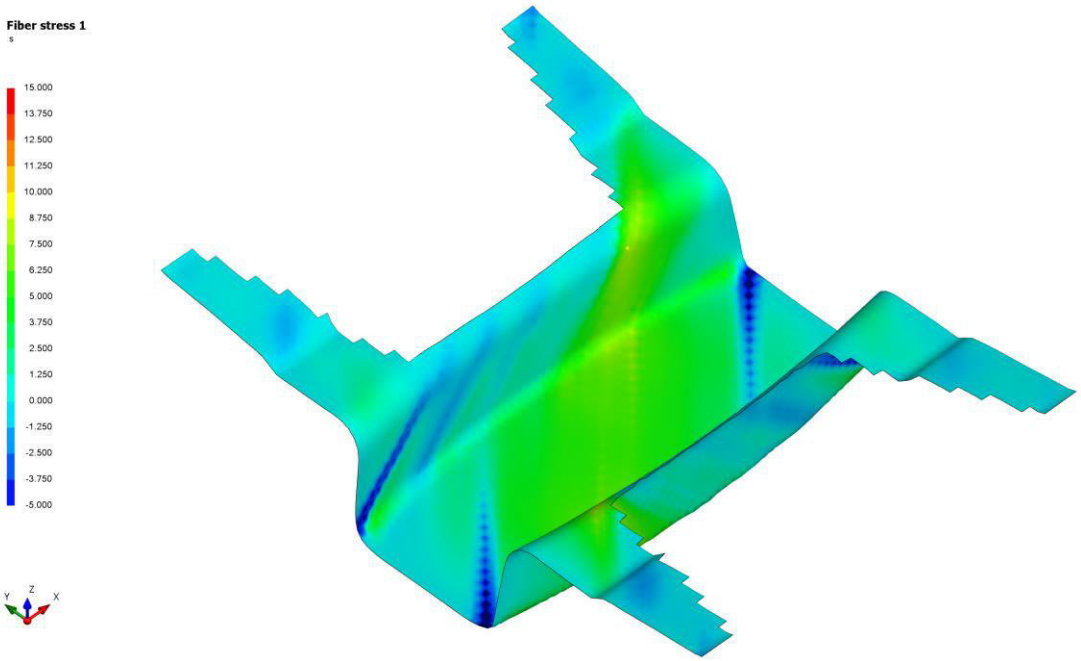

Shear angle f1_f2
s
25.000
21.875
18.750
15.625
12.500
9.375
6.250
3.125
0.000
-3.125
-6.250
-9.375
-12.500
-15.625
-18.750
-21.875
-25.000
Y
Z
X

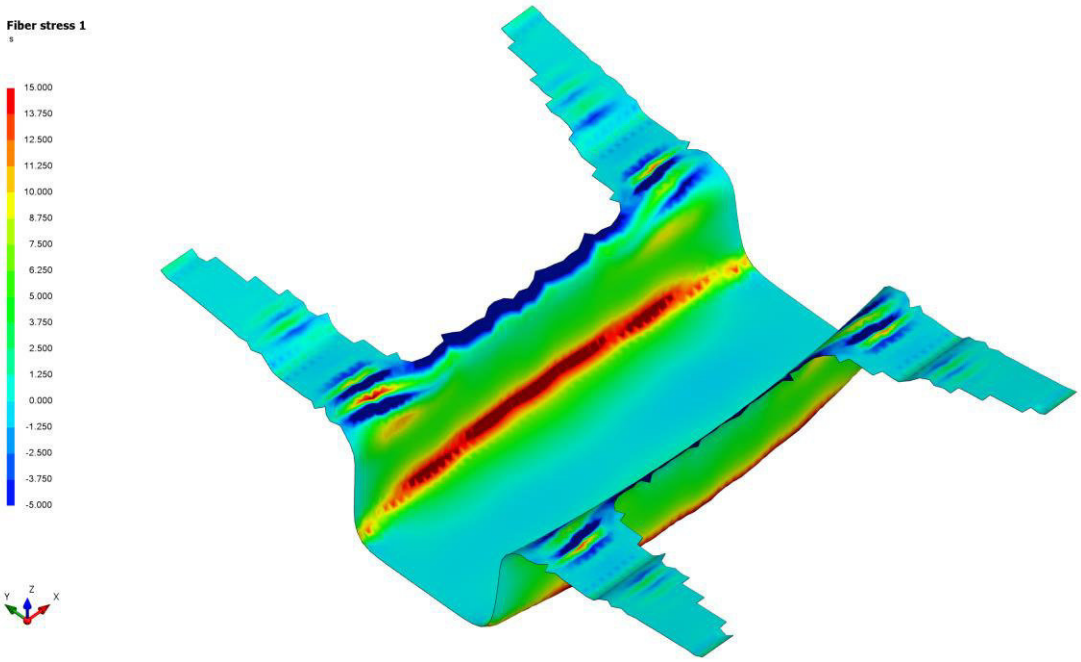

Shear angle f1_f2
s
25.000
21.875
18.750
15.625
12.500
9.375
6.250
3.125
0.000
-3.125
-6.250
-9.375
-12.500
-15.625
-18.750
-21.875
-25.000
Y
Z
X

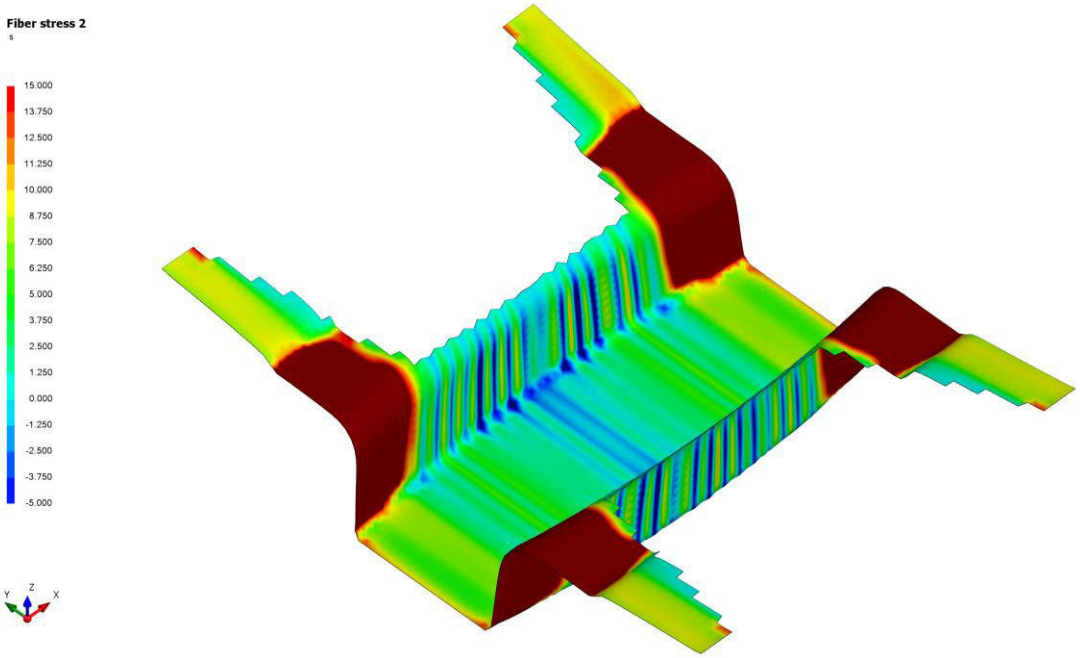

Shear angle f1_f2
s
25.000
21.875
18.750
15.625
12.500
9.375
6.250
3.125
0.000
-3.125
-6.250
-9.375
-12.500
-15.625
-18.750
-21.875
-25.000
Y
Z
X

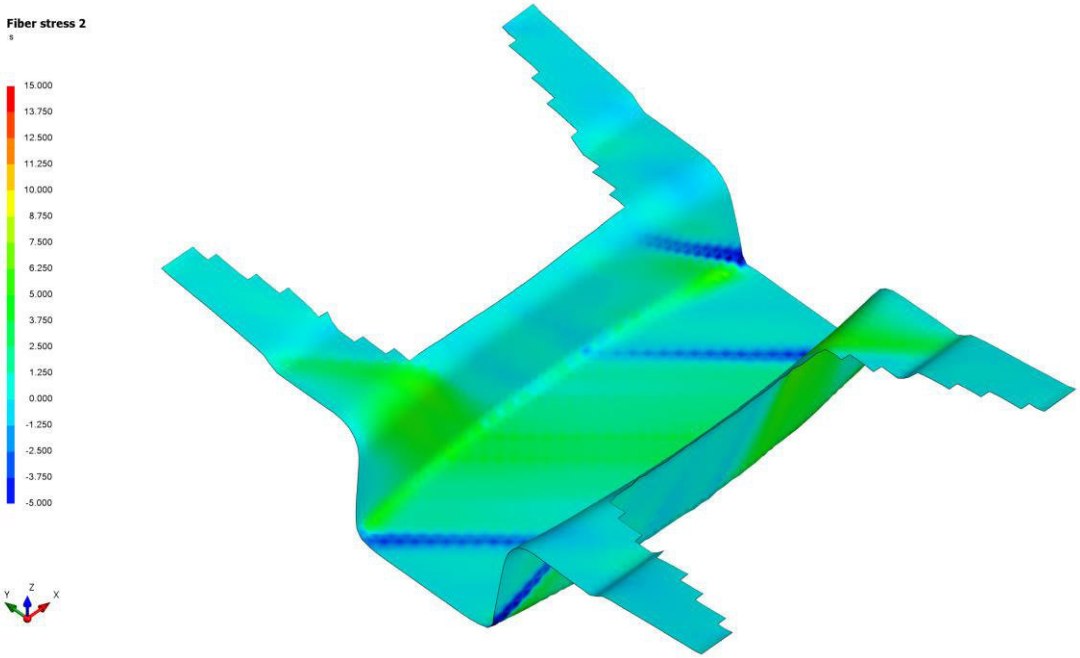

Fiber stress 1
s
15.000
13.750
12.500
11.250
10.000
8.750
7.500
6.250
5.000
3.750
2.500
1.250
0.000
-1.250
-2.500
-3.750
-5.000
Y
Z
X

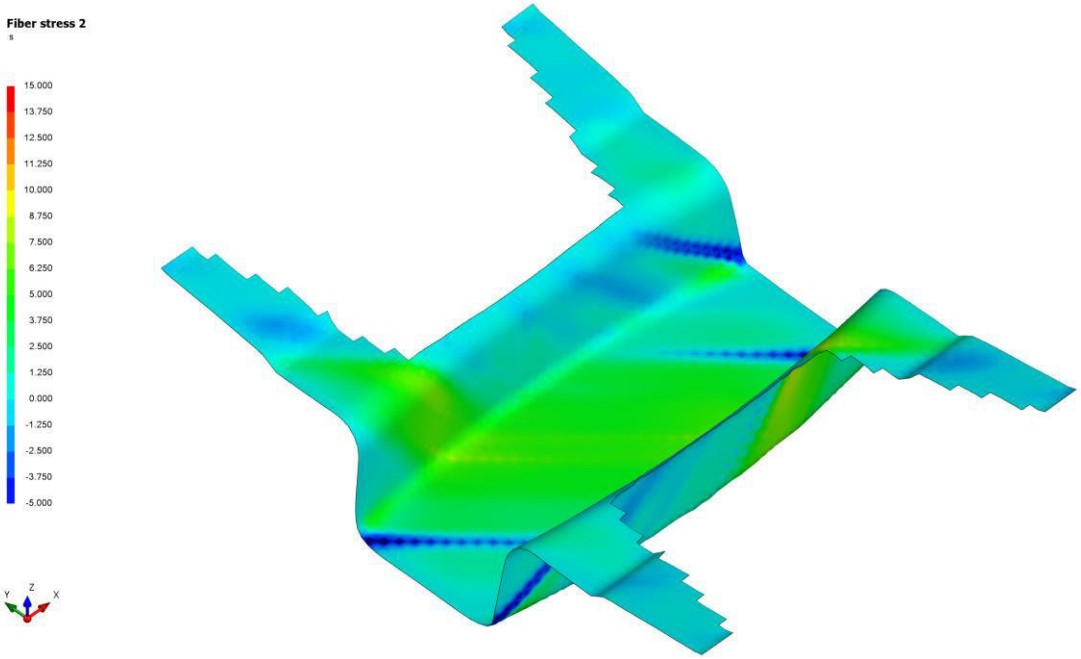

Fiber stress 1
s
15.000
13.750
12.500
11.250
10.000
8.750
7.500
6.250
5.000
3.750
2.500
1.250
0.000
-1.250
-2.500
-3.750
-5.000
Y
Z
X

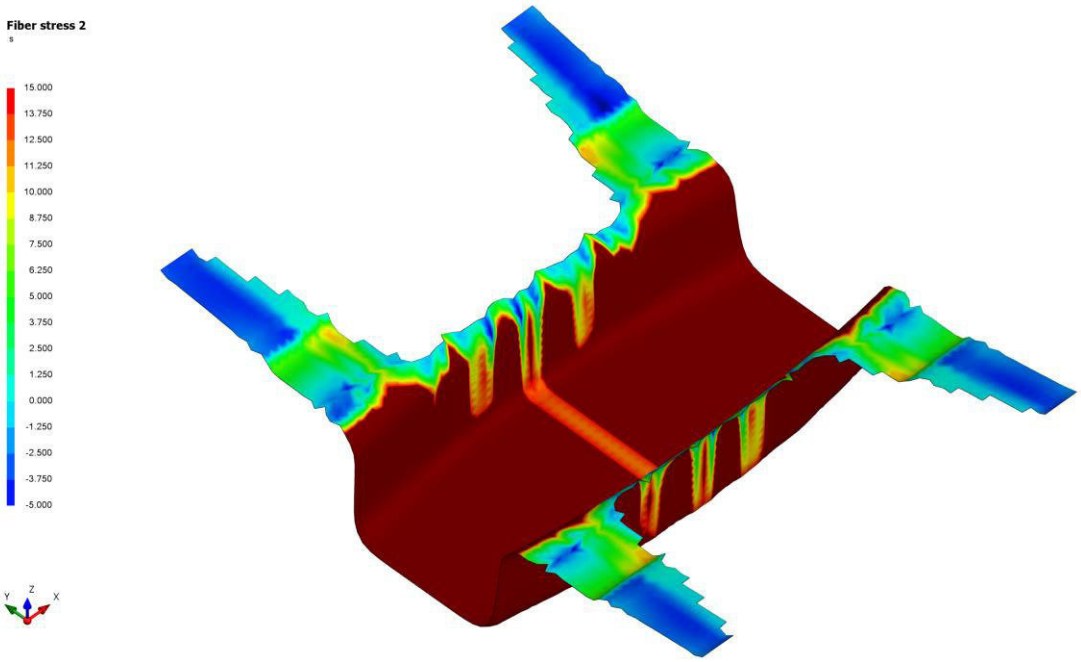

Fiber stress 1
s
15.000
13.750
12.500
11.250
10.000
8.750
7.500
6.250
5.000
3.750
2.500
1.250
0.000
-1.250
-2.500
-3.750
-5.000
Y
Z
X


Fiber stress 1
s
15.000
13.750
12.500
11.250
10.000
8.750
7.500
6.250
5.000
3.750
2.500
1.250
0.000
-1.250
-2.500
-3.750
-5.000
Y
Z
X

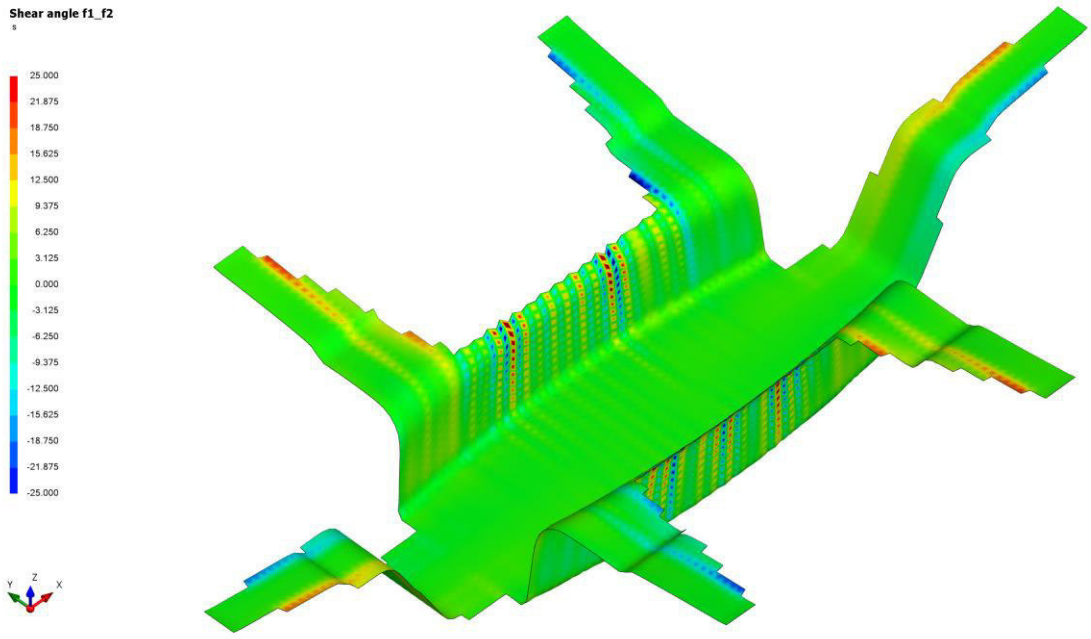

Fiber stress 2
s
15.000
13.750
12.500
11.250
10.000
8.750
7.500
6.250
5.000
3.750
2.500
1.250
0.000
-1.250
-2.500
-3.750
-5.000
Y
Z
X

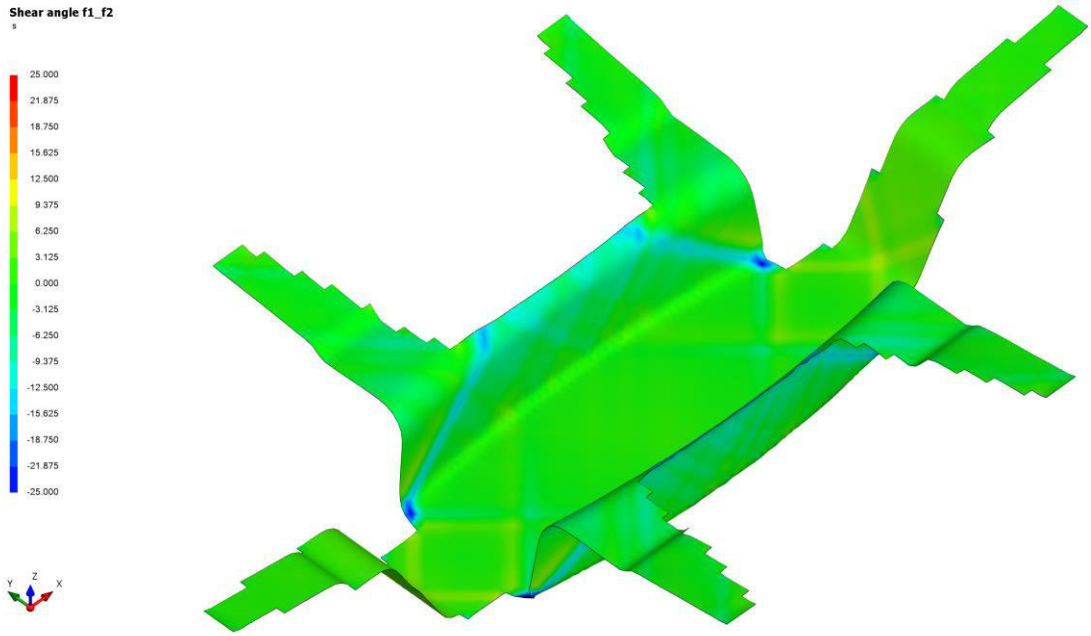

Fiber stress 2
s
15.000
13.750
12.500
11.250
10.000
8.750
7.500
6.250
5.000
3.750
2.500
1.250
0.000
-1.250
-2.500
-3.750
-5.000
Y
Z
X

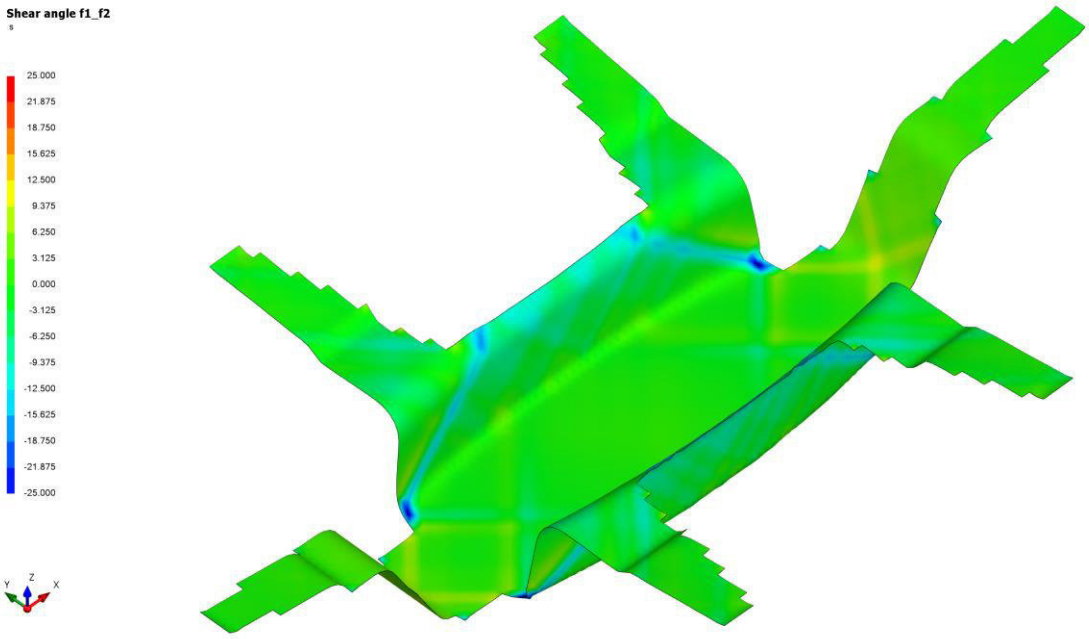

Fiber stress 2
s
15.000
13.750
12.500
11.250
10.000
8.750
7.500
6.250
5.000
3.750
2.500
1.250
0.000
-1.250
-2.500
-3.750
-5.000
Y
Z
X

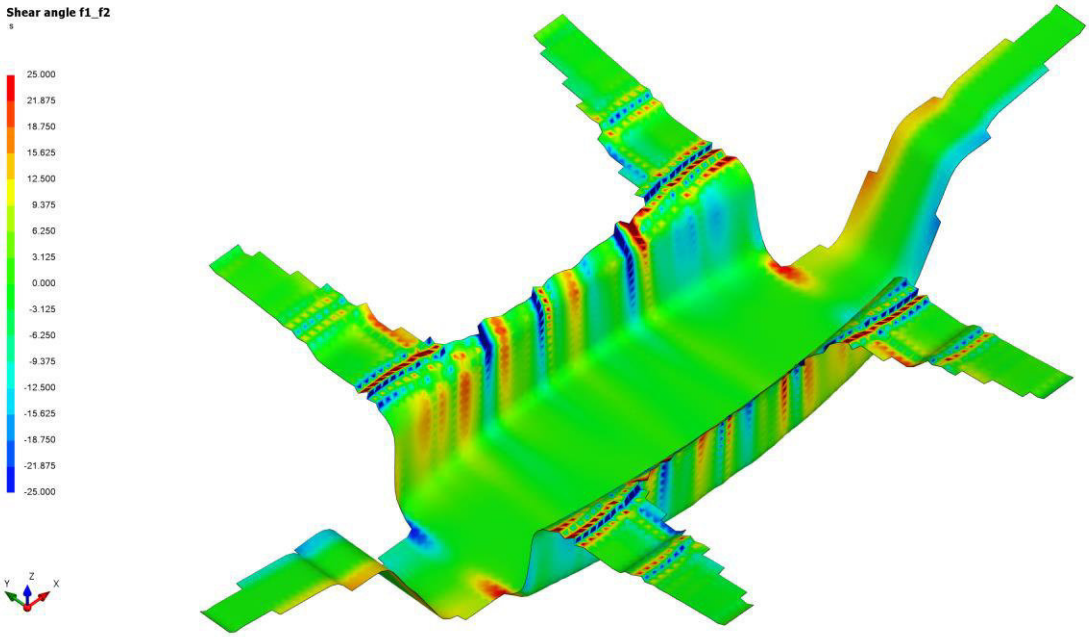

Fiber stress 2
s
15.000
13.750
12.500
11.250
10.000
8.750
7.500
6.250
5.000
3.750
2.500
1.250
0.000
-1.250
-2.500
-3.750
-5.000
Y
Z
X

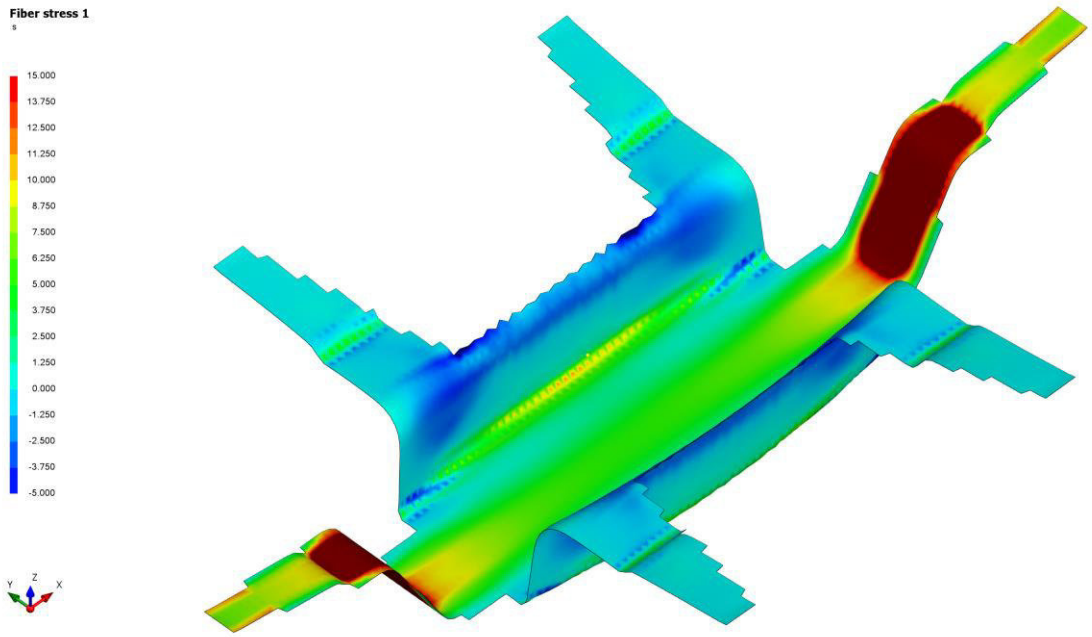
C-Section Blank 2

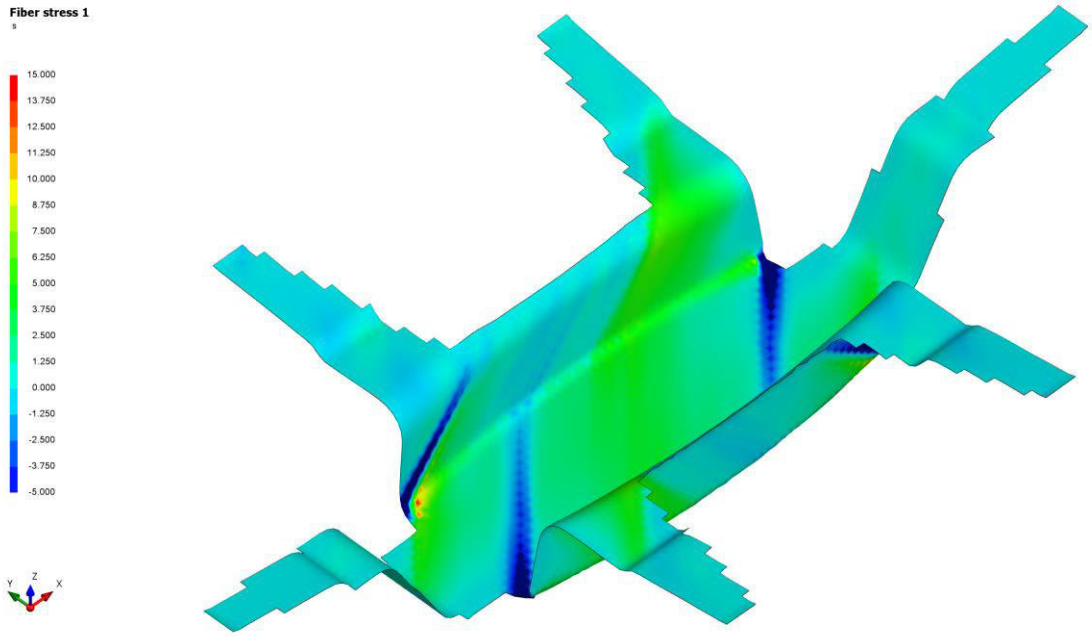

Shear angle f1_f2
s
25.000
21.875
18.750
15.625
12.500
9.375
6.250
3.125
0.000
-3.125
-6.250
-9.375
-12.500
-15.625
-18.750
-21.875
-25.000
Y
Z
X

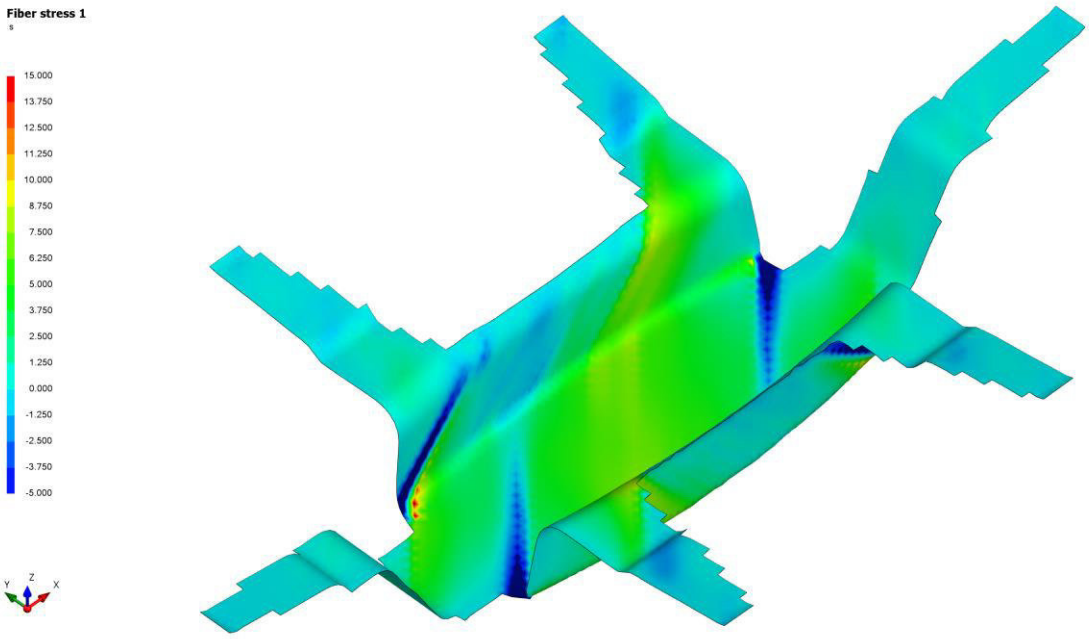

Shear angle f1_f2
s
25.000
21.875
18.750
15.625
12.500
9.375
6.250
3.125
0.000
-3.125
-6.250
-9.375
-12.500
-15.625
-18.750
-21.875
-25.000
Y
Z
X

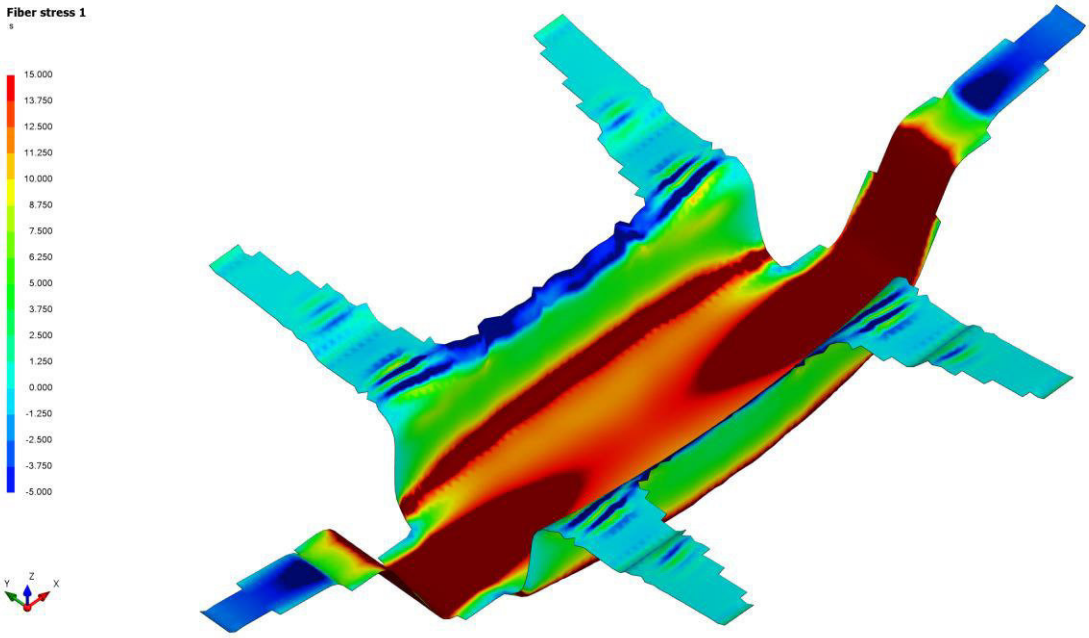

Shear angle f1_f2
s
25.000
21.875
18.750
15.625
12.500
9.375
6.250
3.125
0.000
-3.125
-6.250
-9.375
-12.500
-15.625
-18.750
-21.875
-25.000
Y
Z
X

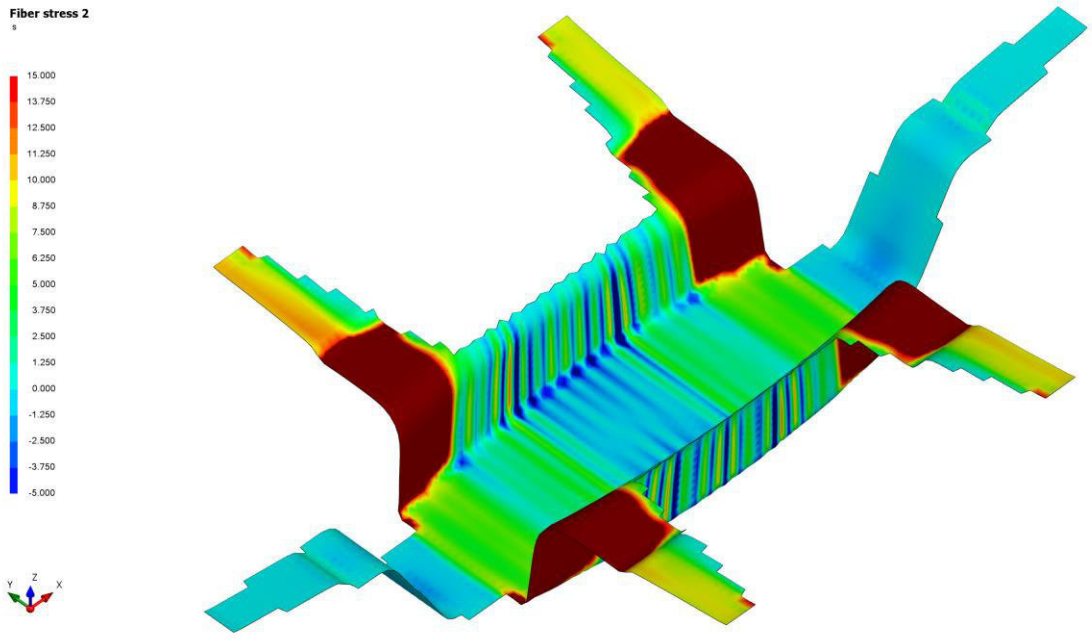

Shear angle f1_f2
s
25.000
21.875
18.750
15.625
12.500
9.375
6.250
3.125
0.000
-3.125
-6.250
-9.375
-12.500
-15.625
-18.750
-21.875
-25.000
Y
Z
X

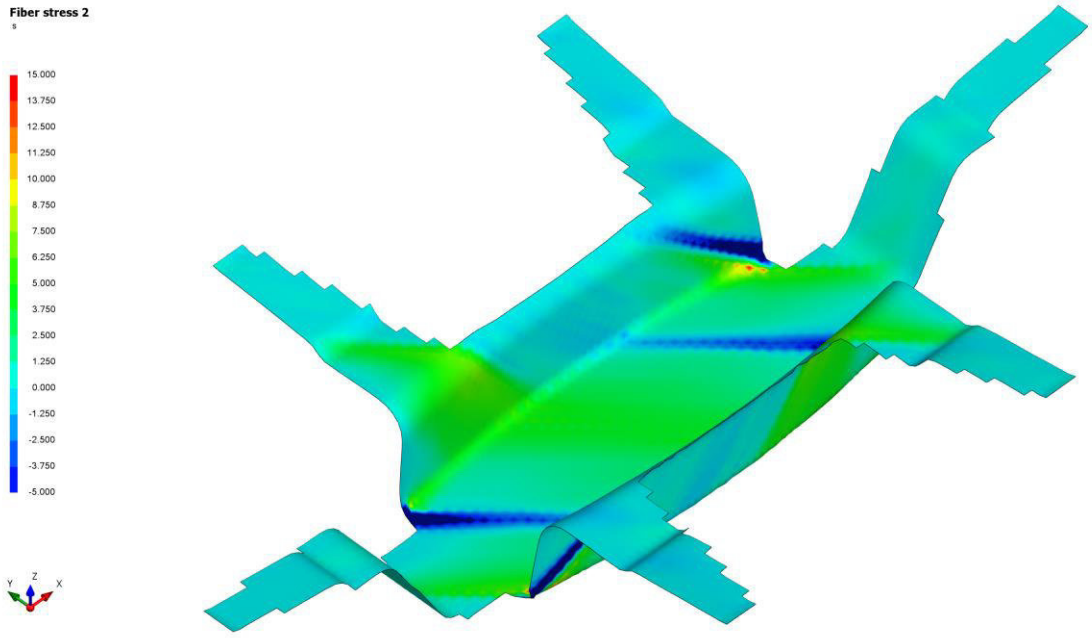

Fiber stress 1
s
15.000
13.750
12.500
11.250
10.000
8.750
7.500
6.250
5.000
3.750
2.500
1.250
0.000
-1.250
-2.500
-3.750
-5.000
Y
Z
X

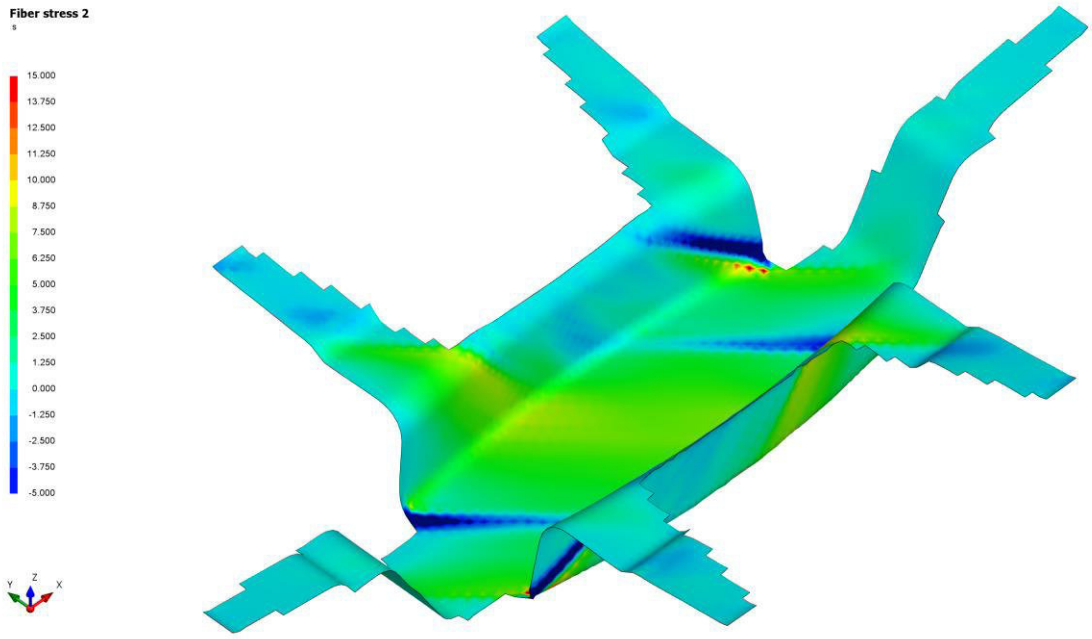

Fiber stress 1
s
15.000
13.750
12.500
11.250
10.000
8.750
7.500
6.250
5.000
3.750
2.500
1.250
0.000
-1.250
-2.500
-3.750
-5.000
Y
Z
X

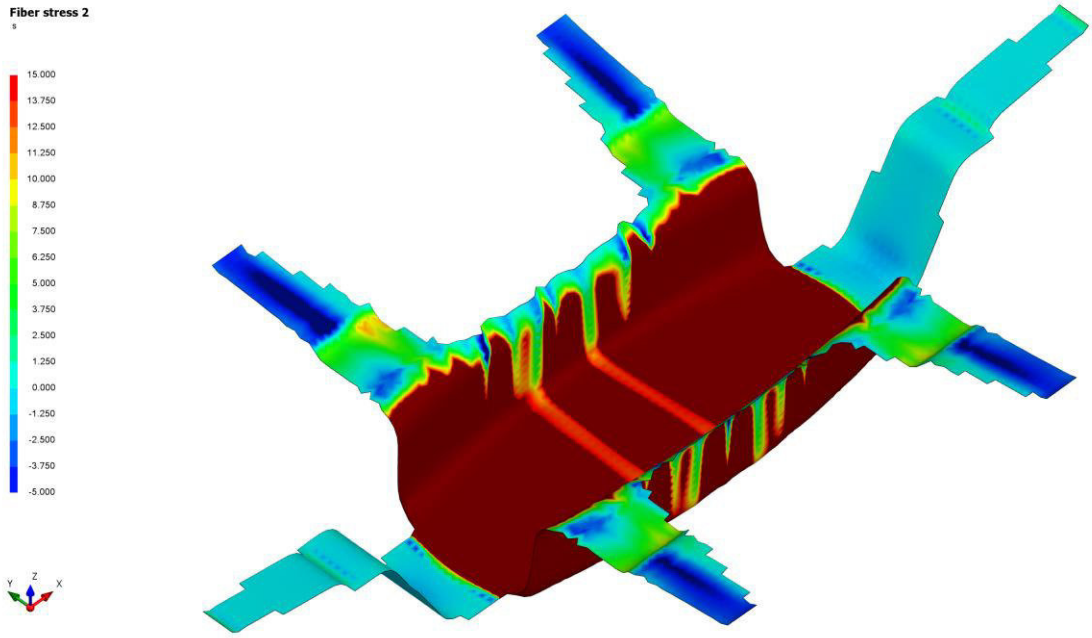

Fiber stress 1
s
15.000
13.750
12.500
11.250
10.000
8.750
7.500
6.250
5.000
3.750
2.500
1.250
0.000
-1.250
-2.500
-3.750
-5.000
Y
Z
X


Fiber stress 1
s
15.000
13.750
12.500
11.250
10.000
8.750
7.500
6.250
5.000
3.750
2.500
1.250
0.000
-1.250
-2.500
-3.750
-5.000
Y
Z
X

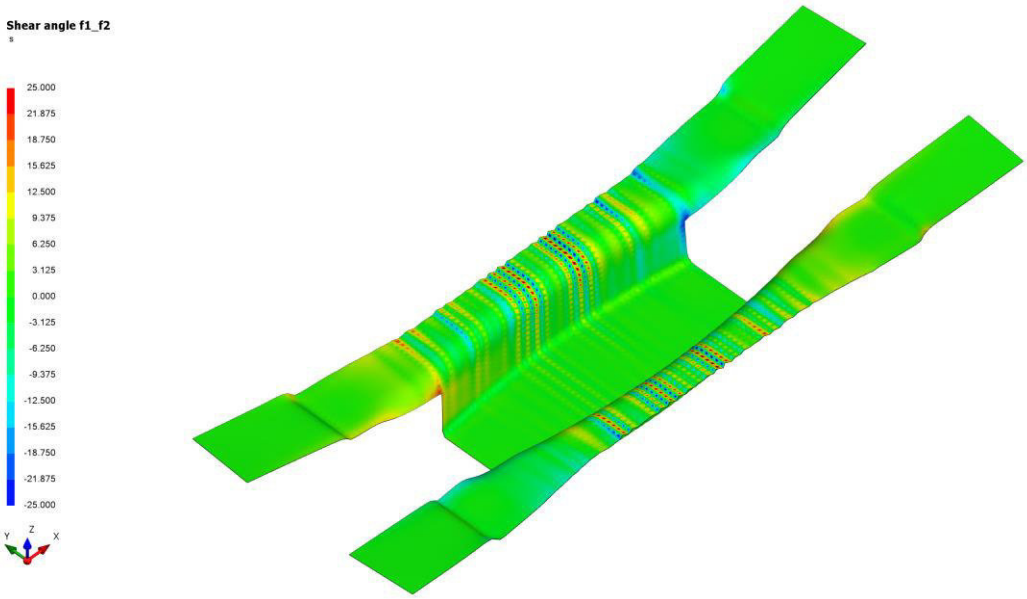

Fiber stress 2
S
15.000
13.750
12.500
11.250
10.000
8.750
7.500
6.250
5.000
3.750
2.500
1.250
0.000
-1.250
-2.500
-3.750
-5.000
Y
Z
X

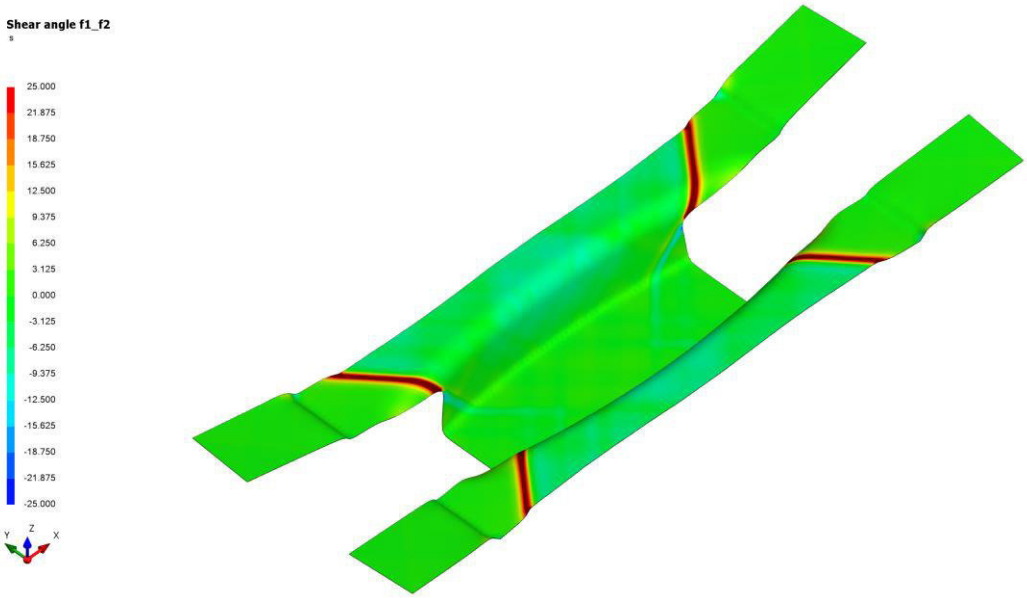

Fiber stress 2
S
15.000
13.750
12.500
11.250
10.000
8.750
7.500
6.250
5.000
3.750
2.500
1.250
0.000
-1.250
-2.500
-3.750
-5.000
Y
Z
X

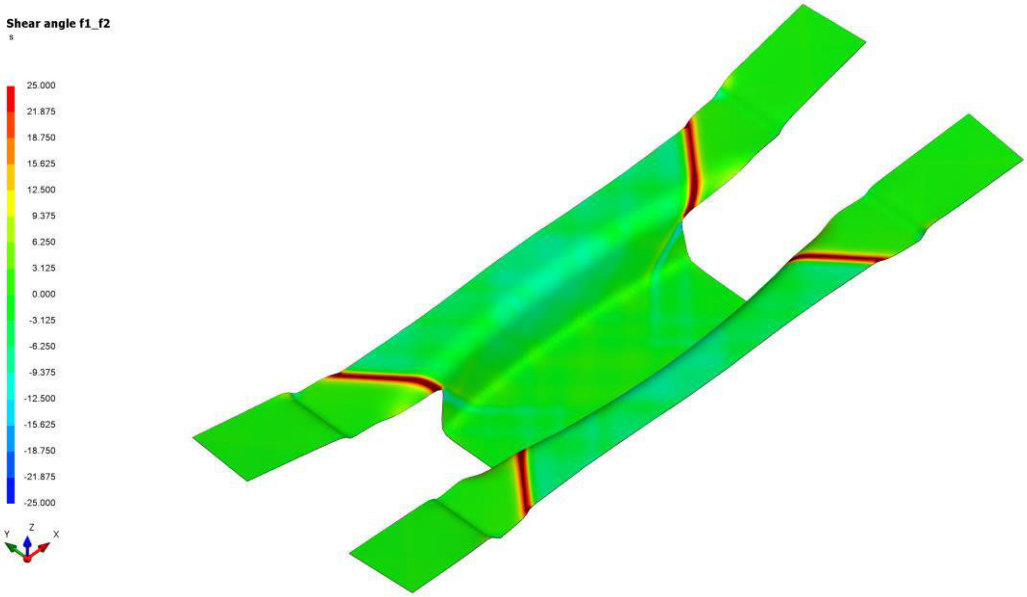

Fiber stress 2
s
15.000
13.750
12.500
11.250
10.000
8.750
7.500
6.250
5.000
3.750
2.500
1.250
0.000
-1.250
-2.500
-3.750
-5.000
Y
Z
X

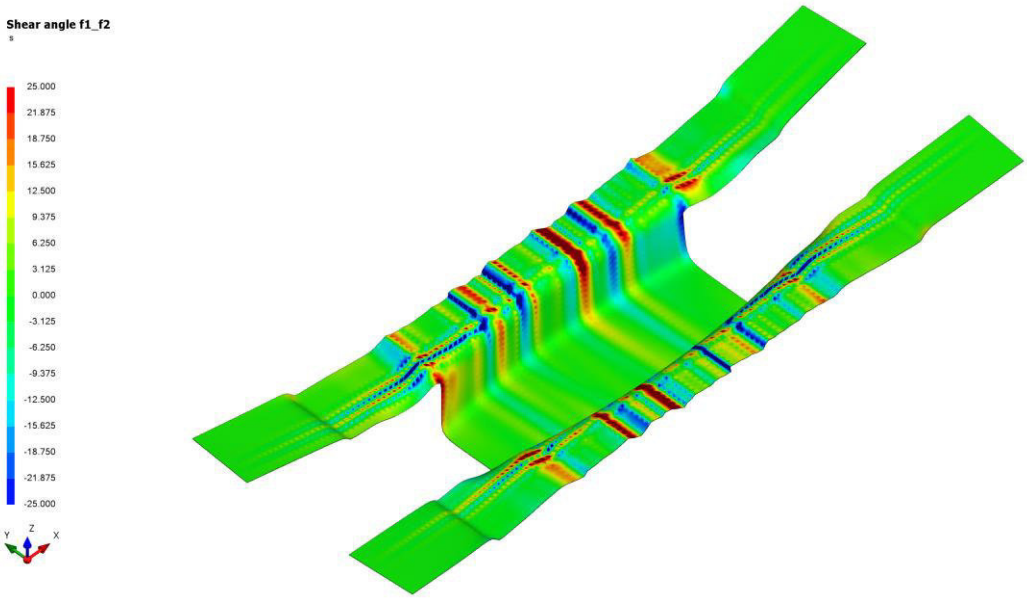

Fiber stress 2
s
15.000
13.750
12.500
11.250
10.000
8.750
7.500
6.250
5.000
3.750
2.500
1.250
0.000
-1.250
-2.500
-3.750
-5.000
Y
Z
X

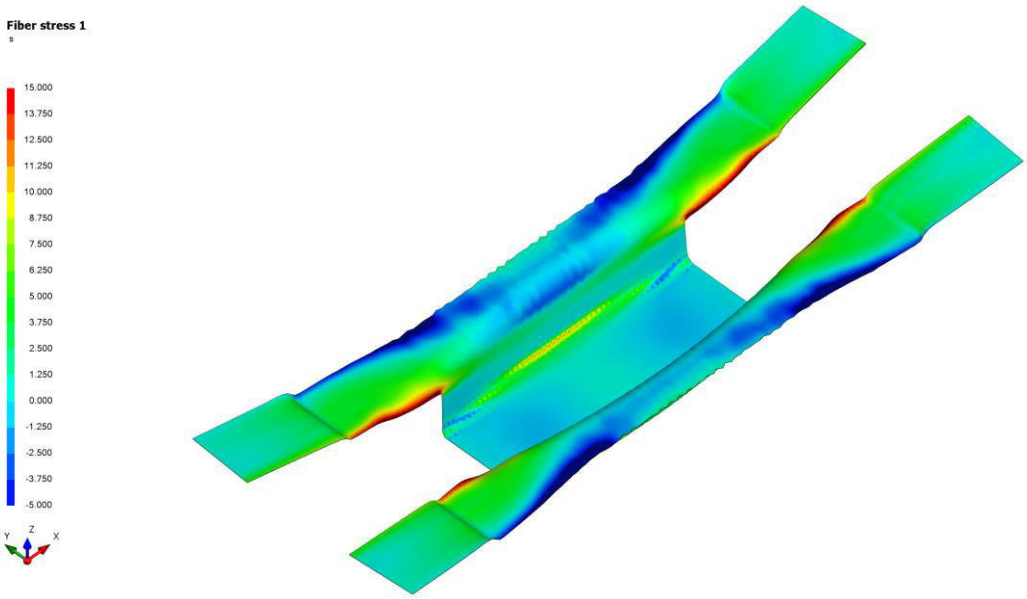
C-Section Blank 3 0.09 N/mm

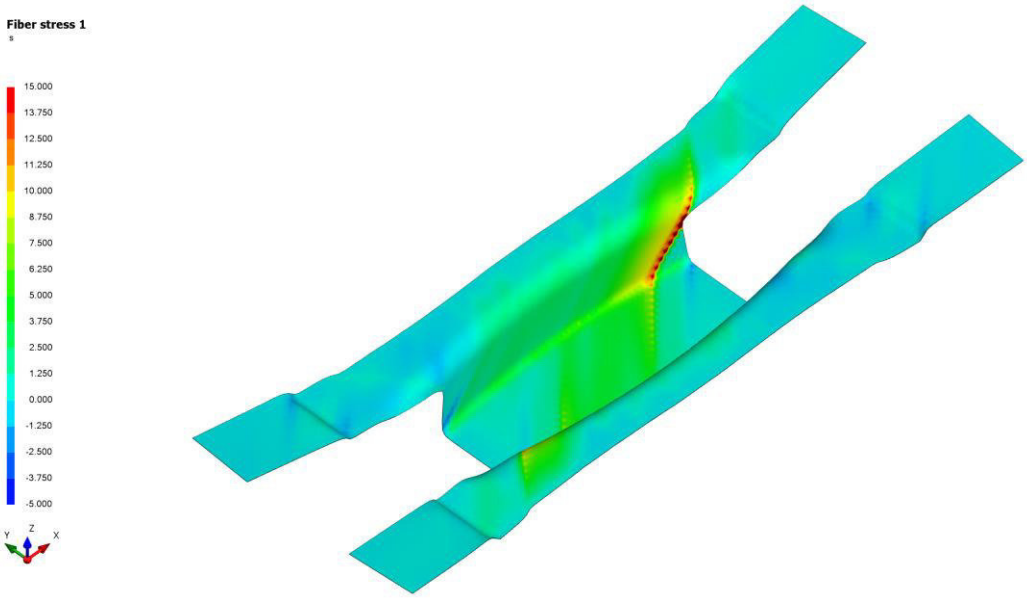

Shear angle f1_f2
s
25.000
21.875
18.750
15.625
12.500
9.375
6.250
3.125
0.000
-3.125
-6.250
-9.375
-12.500
-15.625
-18.750
-21.875
-25.000
Z
Y
X

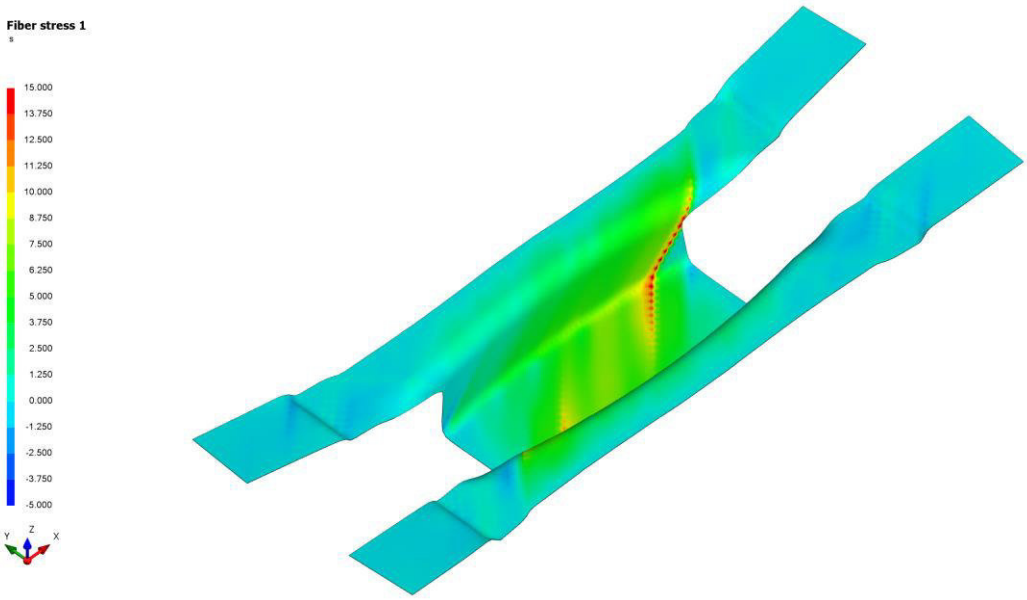

Shear angle f1_f2
s
25.000
21.875
18.750
15.625
12.500
9.375
6.250
3.125
0.000
-3.125
-6.250
-9.375
-12.500
-15.625
-18.750
-21.875
-25.000
Z
Y
X

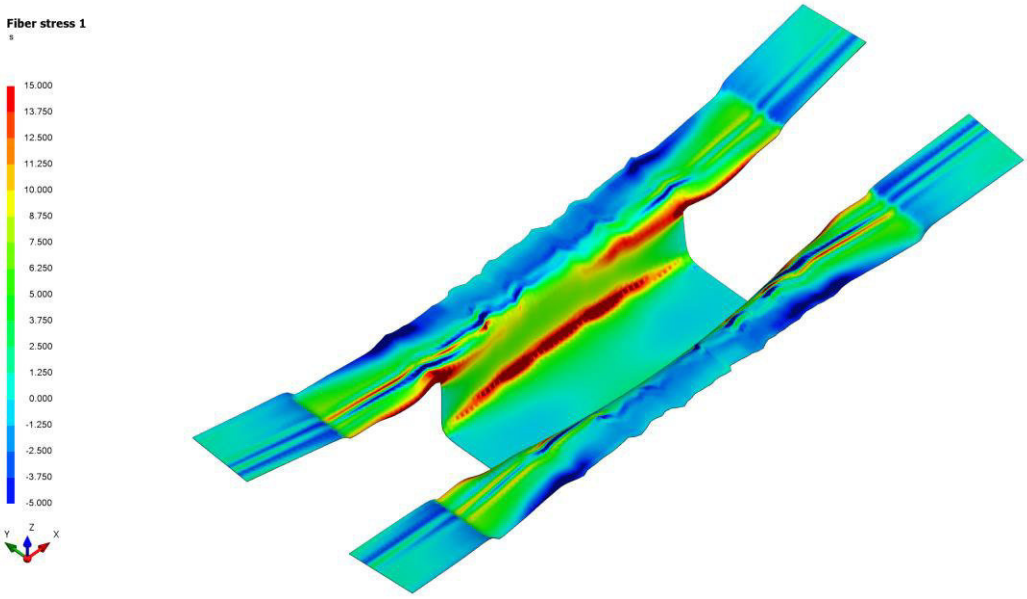

Shear angle f1_f2
s
25.000
21.875
18.750
15.625
12.500
9.375
6.250
3.125
0.000
-3.125
-6.250
-9.375
-12.500
-15.625
-18.750
-21.875
-25.000
Z
Y
X

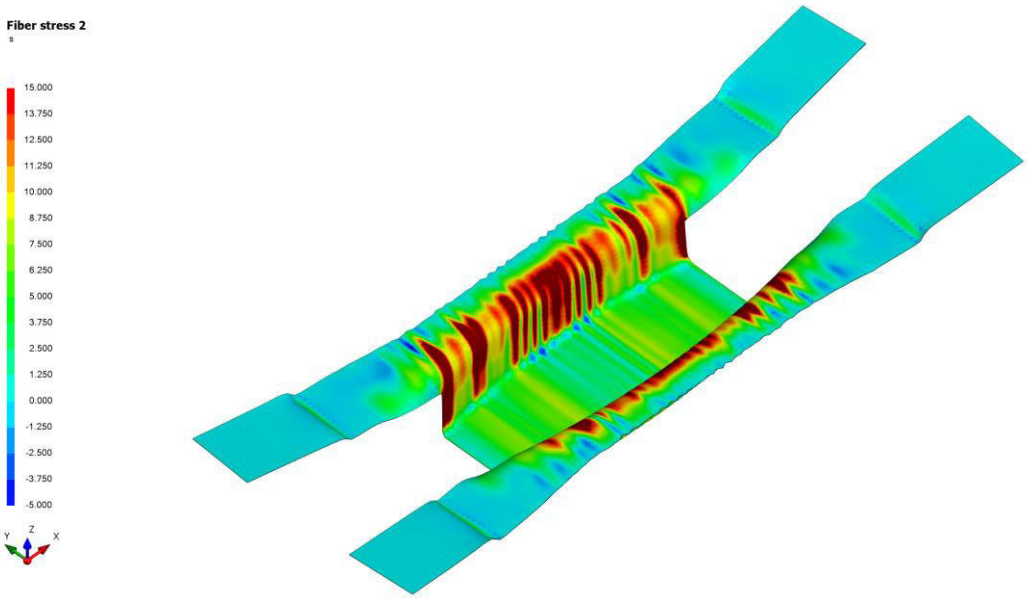

Shear angle f1_f2
s
25.000
21.875
18.750
15.625
12.500
9.375
6.250
3.125
0.000
-3.125
-6.250
-9.375
-12.500
-15.625
-18.750
-21.875
-25.000
Z
Y
X

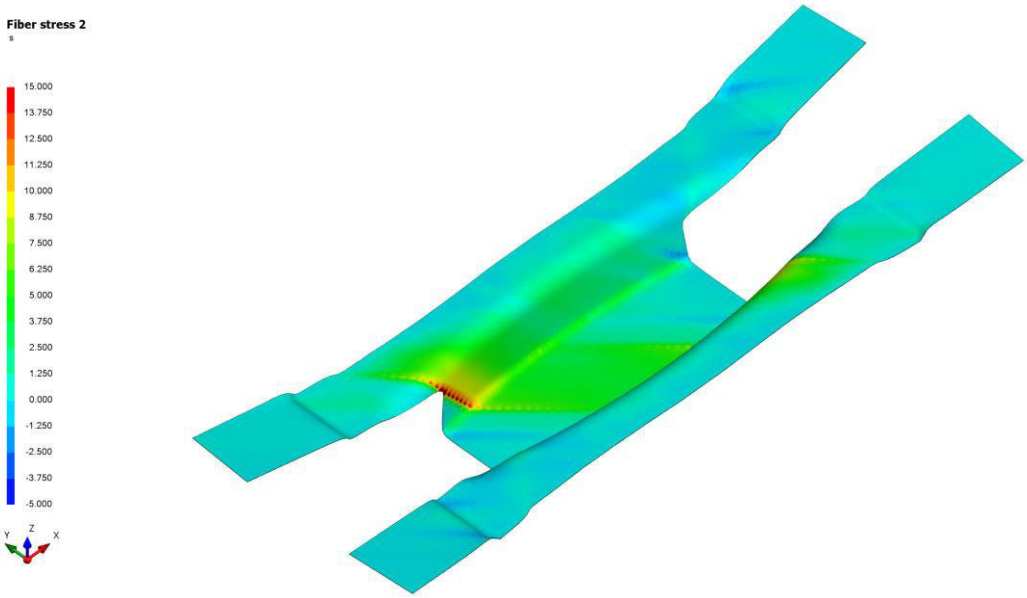

Fiber stress 1
s
15.000
13.750
12.500
11.250
10.000
8.750
7.500
6.250
5.000
3.750
2.500
1.250
0.000
-1.250
-2.500
-3.750
-5.000
Z
Y
X

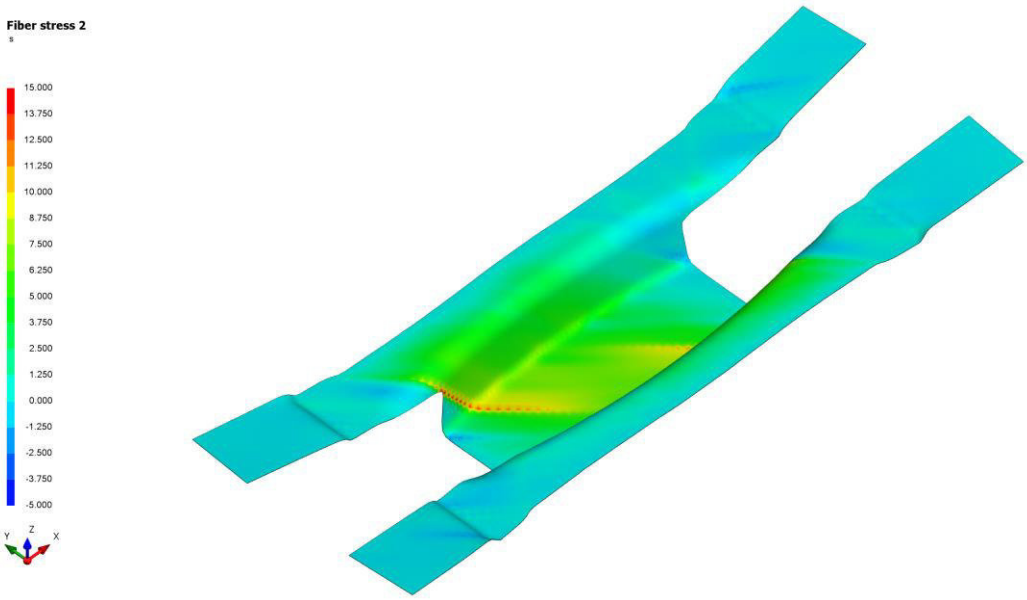

Fiber stress 1
s
15.000
13.750
12.500
11.250
10.000
8.750
7.500
6.250
5.000
3.750
2.500
1.250
0.000
-1.250
-2.500
-3.750
-5.000
Z
Y
X

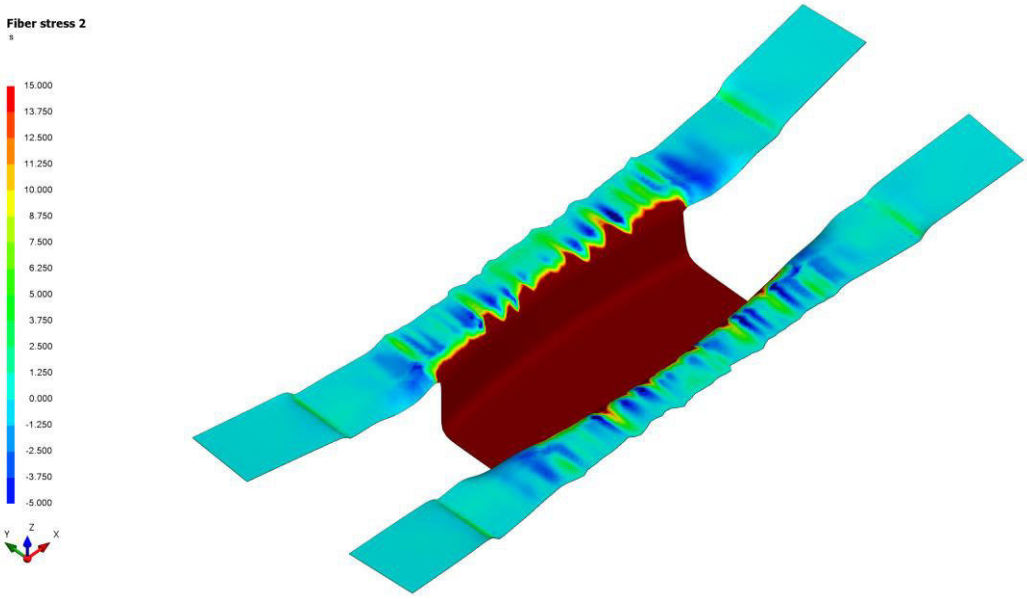

Fiber stress 1
s
15.000
13.750
12.500
11.250
10.000
8.750
7.500
6.250
5.000
3.750
2.500
1.250
0.000
-1.250
-2.500
-3.750
-5.000
Z
Y
X


Fiber stress 1
s
15.000
13.750
12.500
11.250
10.000
8.750
7.500
6.250
5.000
3.750
2.500
1.250
0.000
-1.250
-2.500
-3.750
-5.000
Z
Y
X

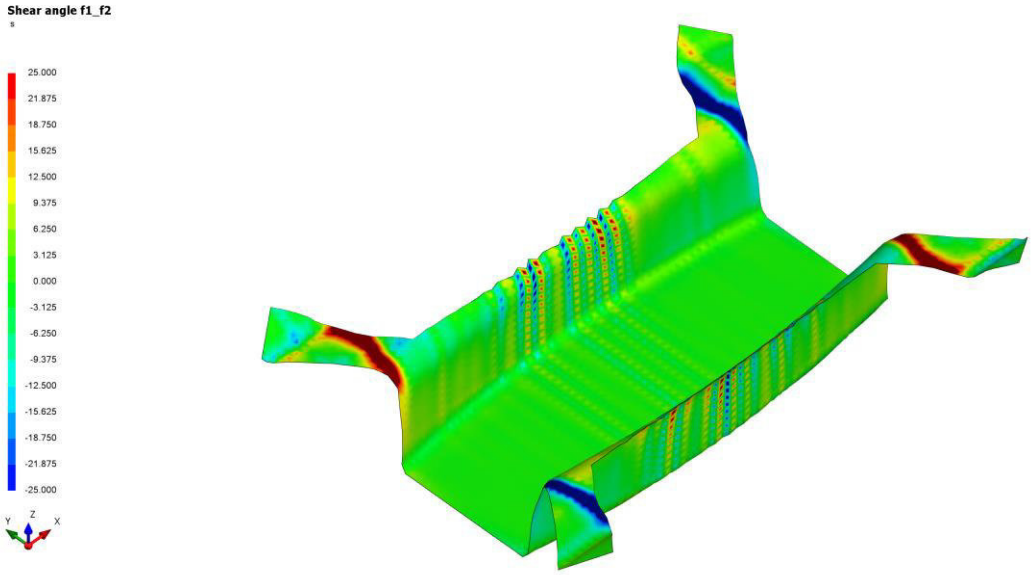

Fiber stress 2
s
15.000
13.750
12.500
11.250
10.000
8.750
7.500
6.250
5.000
3.750
2.500
1.250
0.000
-1.250
-2.500
-3.750
-5.000
Y
Z
X

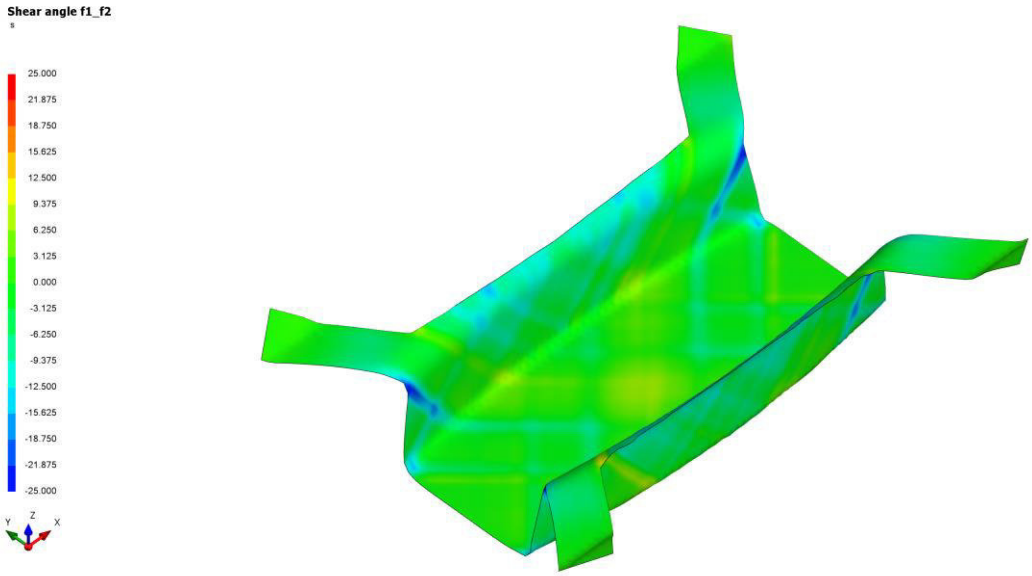

Fiber stress 2
s
15.000
13.750
12.500
11.250
10.000
8.750
7.500
6.250
5.000
3.750
2.500
1.250
0.000
-1.250
-2.500
-3.750
-5.000
Y
Z
X

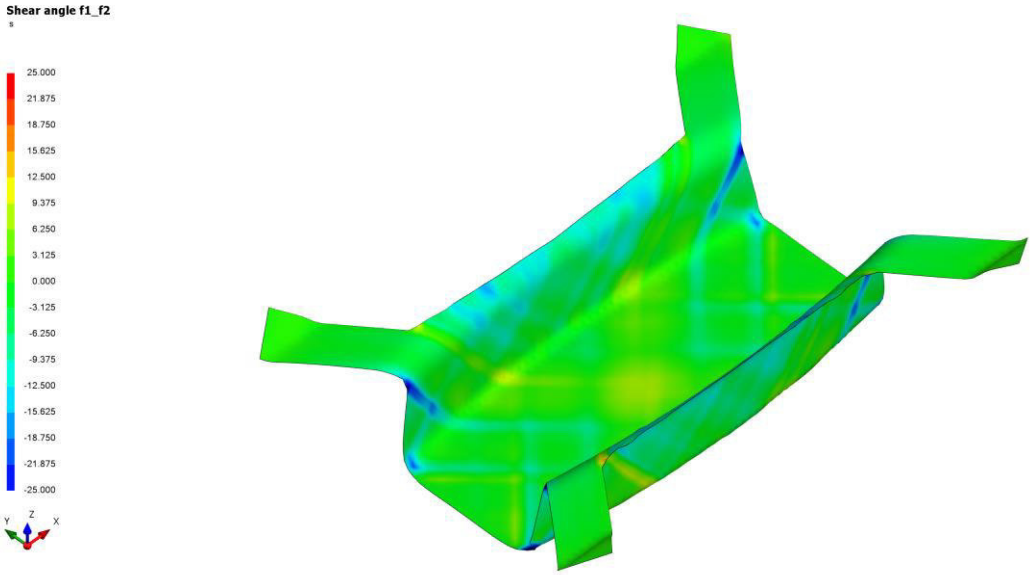

Fiber stress 2
s
15.000
13.750
12.500
11.250
10.000
8.750
7.500
6.250
5.000
3.750
2.500
1.250
0.000
-1.250
-2.500
-3.750
-5.000
Y
Z
X

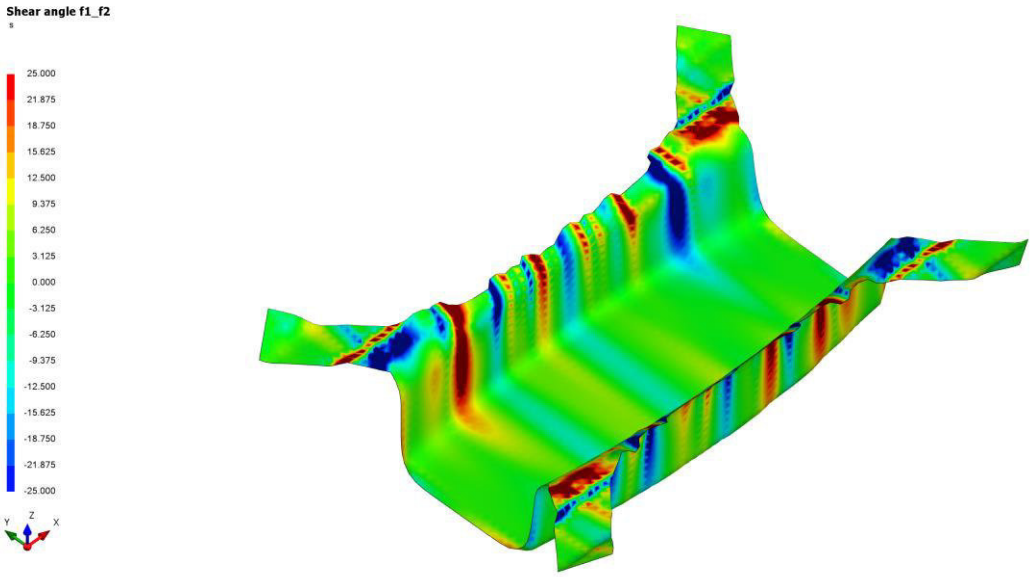

Fiber stress 2
s
15.000
13.750
12.500
11.250
10.000
8.750
7.500
6.250
5.000
3.750
2.500
1.250
0.000
-1.250
-2.500
-3.750
-5.000
Y
Z
X

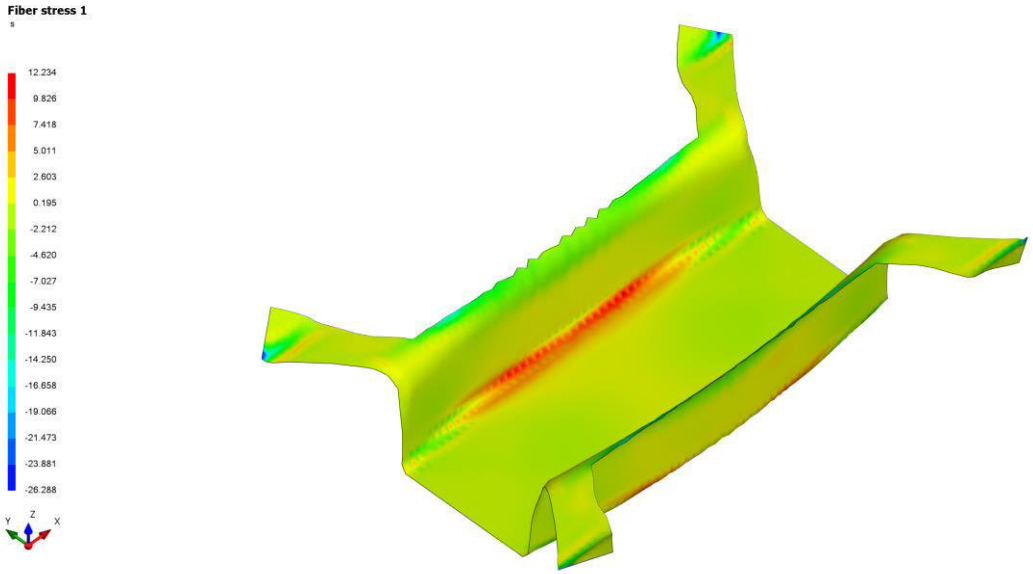
C-Section Blank 4

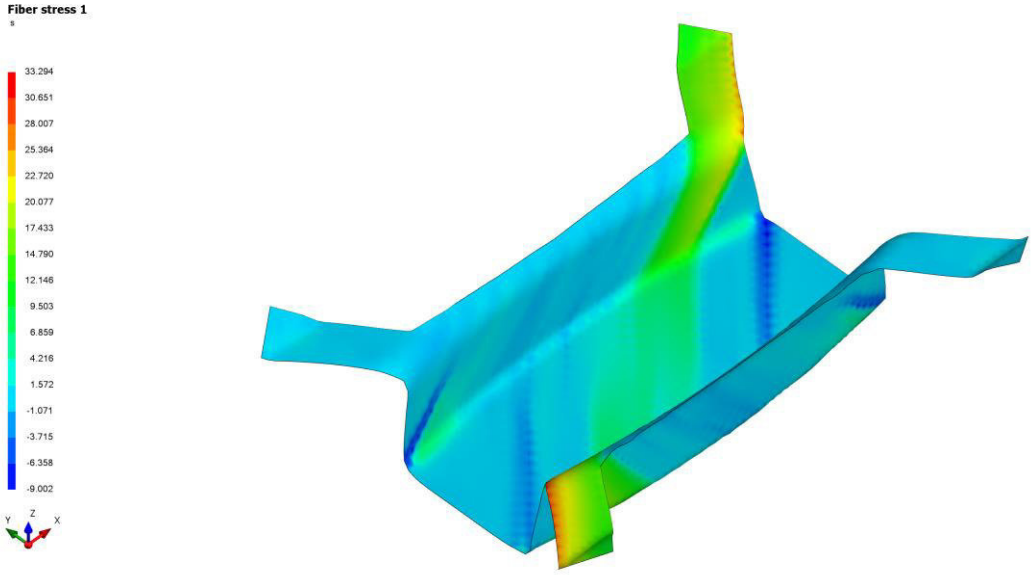

Shear angle f1_f2
S
25.000
21.875
18.750
15.625
12.500
9.375
6.250
3.125
0.000
-3.125
-6.250
-9.375
-12.500
-15.625
-18.750
-21.875
-25.000
Z
Y
X

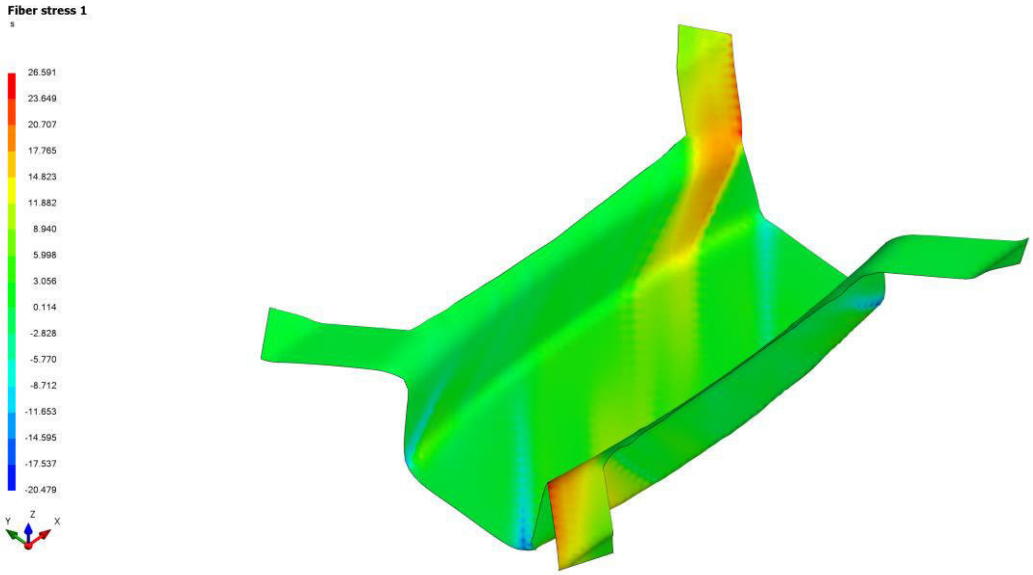

Shear angle f1_f2
S
25.000
21.875
18.750
15.625
12.500
9.375
6.250
3.125
0.000
-3.125
-6.250
-9.375
-12.500
-15.625
-18.750
-21.875
-25.000
Z
Y
X

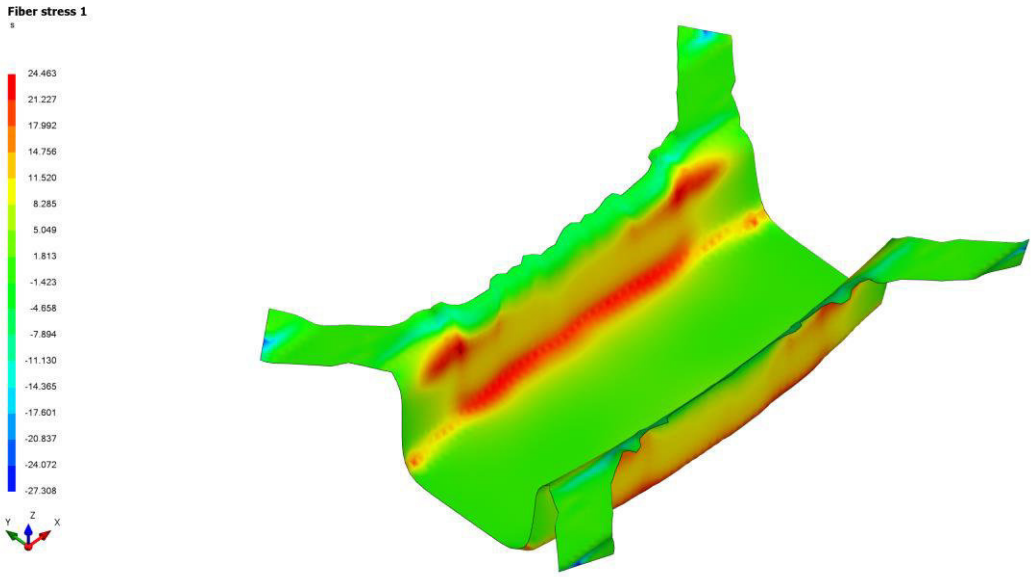

Shear angle f1_f2
s
25.000
21.875
18.750
15.625
12.500
9.375
6.250
3.125
0.000
-3.125
-6.250
-9.375
-12.500
-15.625
-18.750
-21.875
-25.000
Y
Z
X

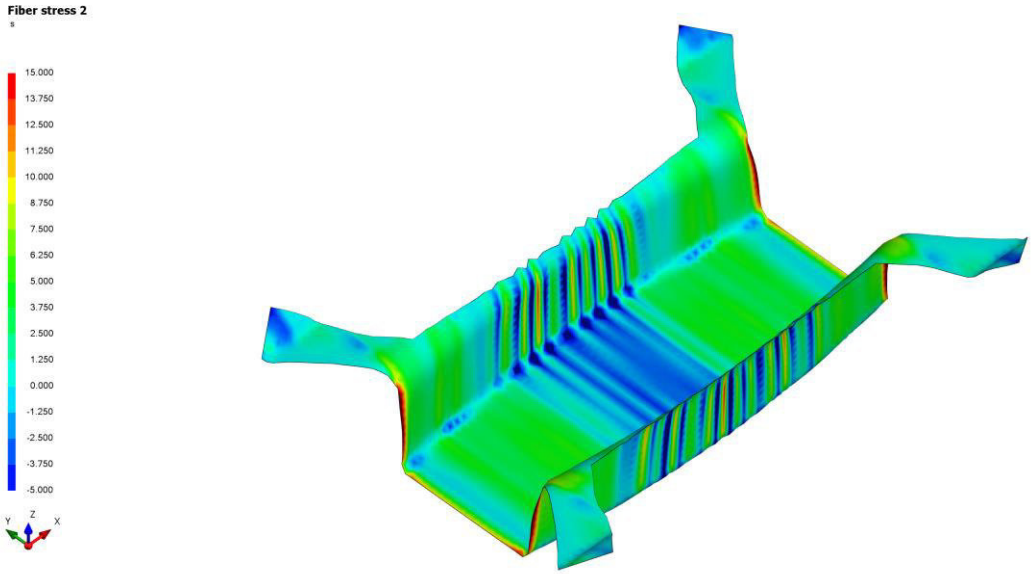

Shear angle f1_f2
s
25.000
21.875
18.750
15.625
12.500
9.375
6.250
3.125
0.000
-3.125
-6.250
-9.375
-12.500
-15.625
-18.750
-21.875
-25.000
Y
Z
X

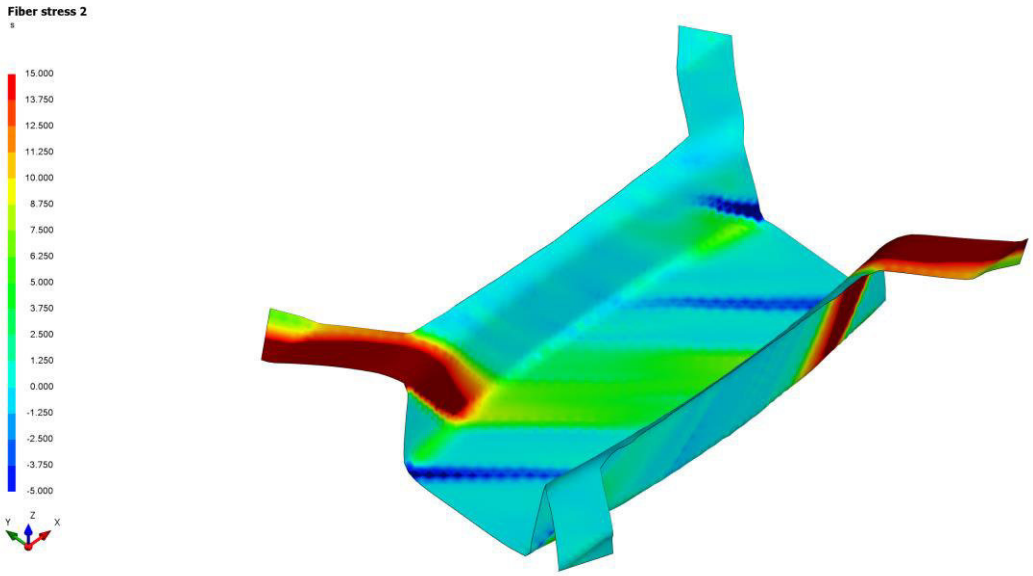

Fiber stress 1
s
12.234
9.826
7.418
5.011
2.603
0.195
-2.212
-4.620
-7.027
-9.435
-11.843
-14.250
-16.658
-19.066
-21.473
-23.881
-26.288
Y
Z
X

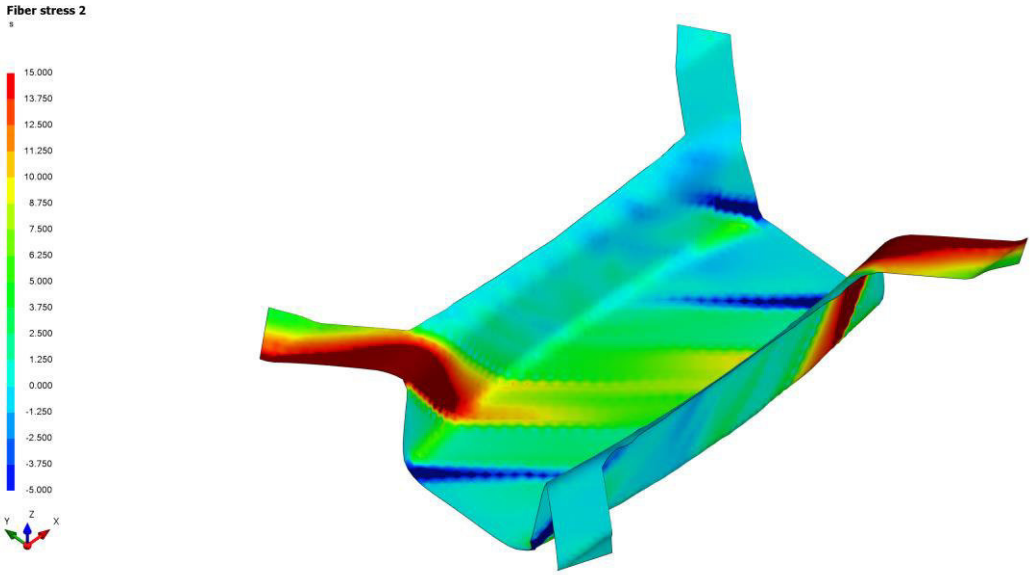

Fiber stress 1
s
33.294
30.651
28.007
25.364
22.720
20.077
17.433
14.790
12.146
9.503
6.859
4.216
1.572
-1.071
-3.715
-6.358
-9.002
Y
Z
X

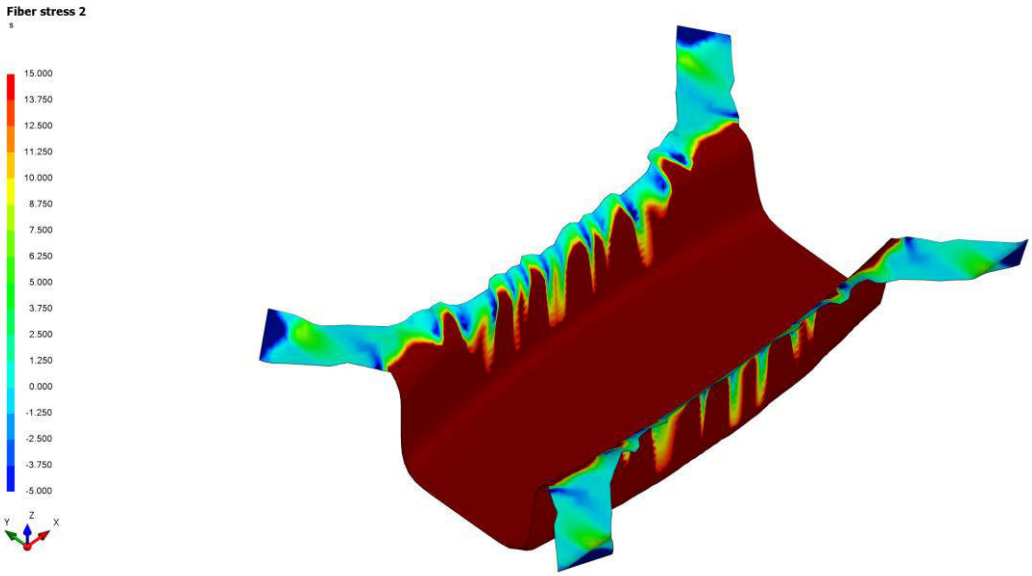

Fiber stress 1
s
26.591
23.649
20.707
17.765
14.823
11.882
8.940
5.998
3.056
0.114
-2.828
-5.770
-8.712
-11.653
-14.595
-17.537
-20.479
Y
Z
X


Fiber stress 1
s
24.463
21.227
17.992
14.756
11.520
8.285
5.049
1.813
-1.423
-4.658
-7.894
-11.130
-14.365
-17.601
-20.837
-24.072
-27.308
Y
Z
X

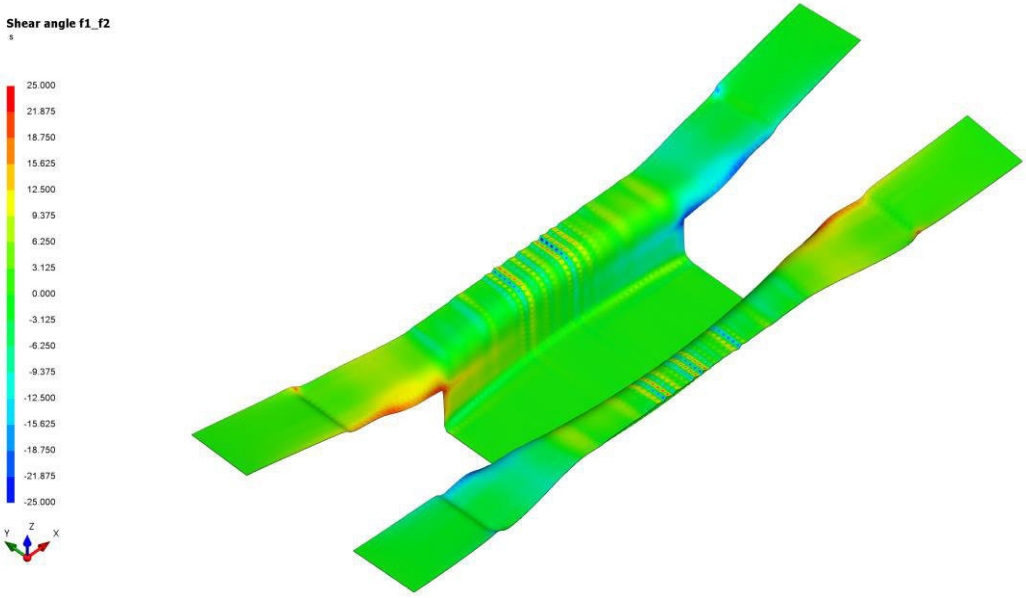

Fiber stress 2
s
15.000
13.750
12.500
11.250
10.000
8.750
7.500
6.250
5.000
3.750
2.500
1.250
0.000
-1.250
-2.500
-3.750
-5.000
Y
Z
X

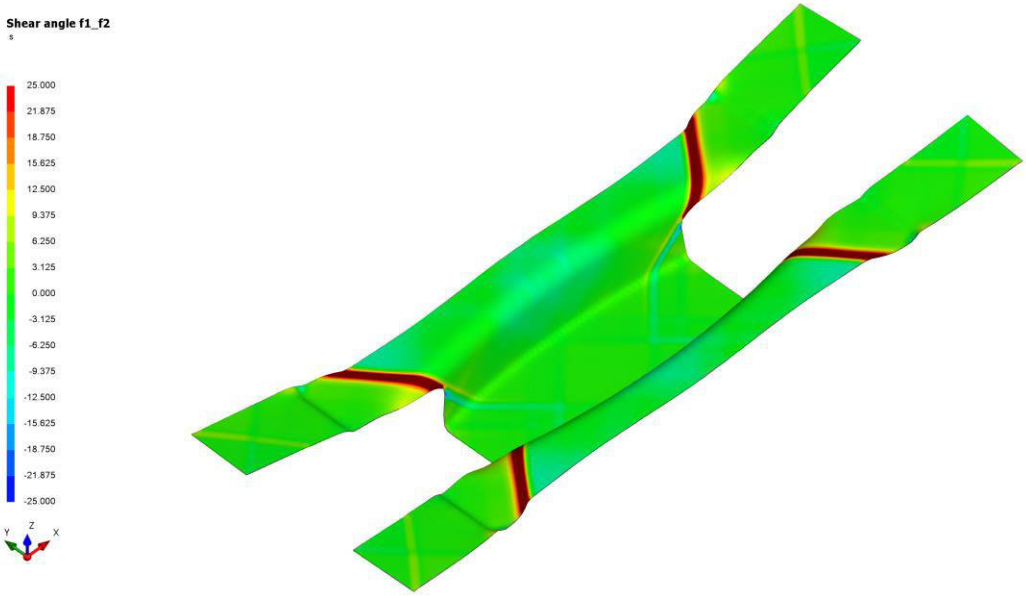

Fiber stress 2
s
15.000
13.750
12.500
11.250
10.000
8.750
7.500
6.250
5.000
3.750
2.500
1.250
0.000
-1.250
-2.500
-3.750
-5.000
Y
Z
X

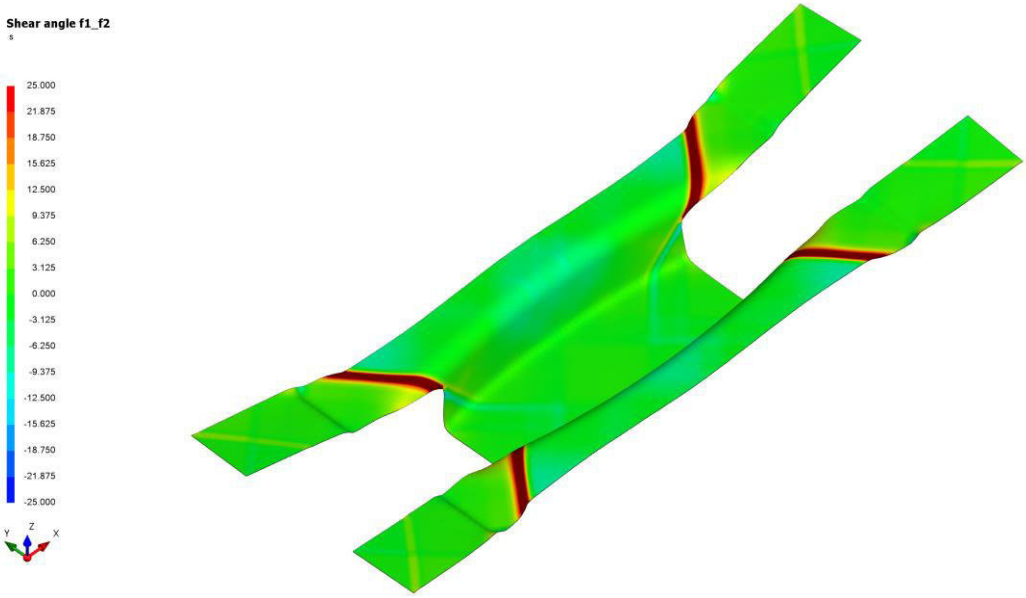

Fiber stress 2
s
15.000
13.750
12.500
11.250
10.000
8.750
7.500
6.250
5.000
3.750
2.500
1.250
0.000
-1.250
-2.500
-3.750
-5.000
Z
Y
X

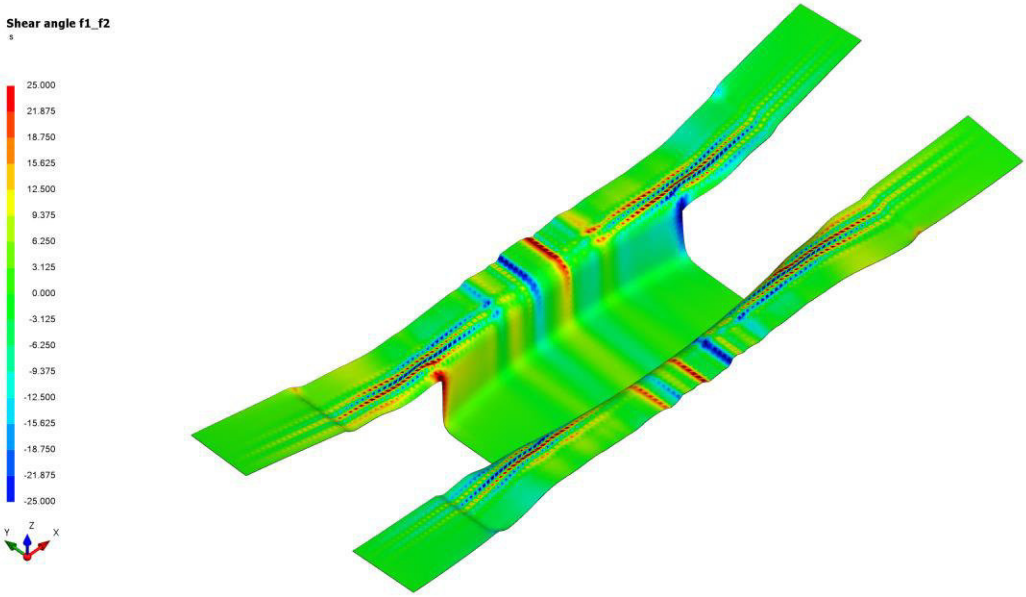

Fiber stress 2
s
15.000
13.750
12.500
11.250
10.000
8.750
7.500
6.250
5.000
3.750
2.500
1.250
0.000
-1.250
-2.500
-3.750
-5.000
Z
Y
X

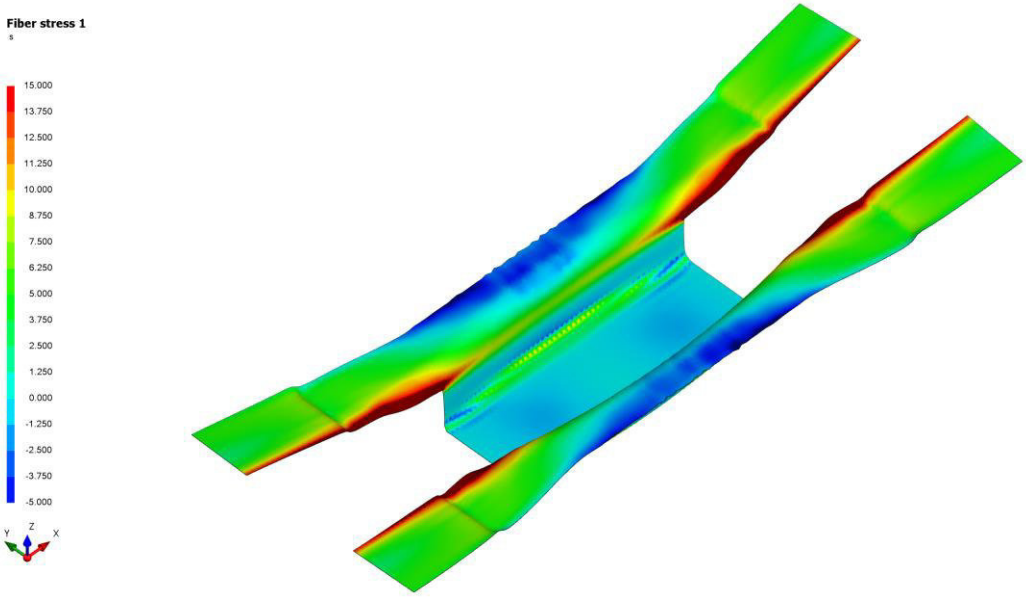
C-Section Blank 3 Stiffness 0.23 N/mm

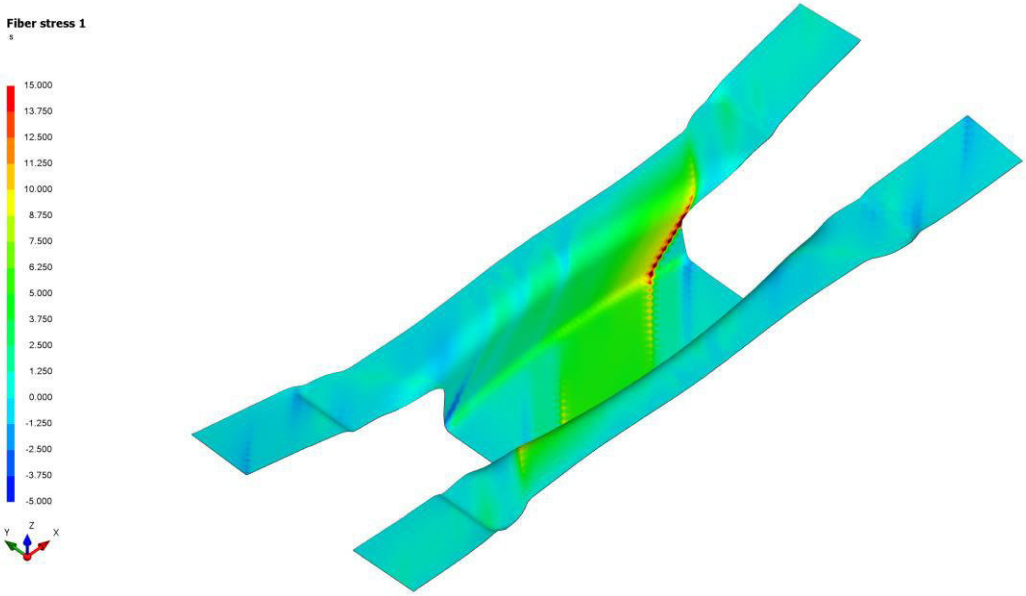

Shear angle f1_f2
s
25.000
21.875
18.750
15.625
12.500
9.375
6.250
3.125
0.000
-3.125
-6.250
-9.375
-12.500
-15.625
-18.750
-21.875
-25.000
Y
Z
X

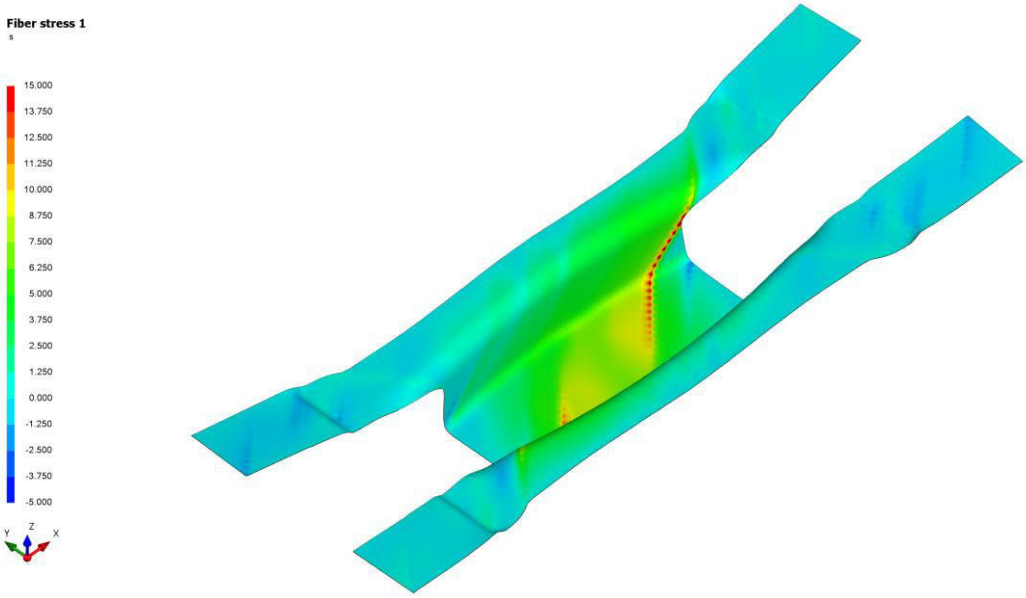

Shear angle f1_f2
s
25.000
21.875
18.750
15.625
12.500
9.375
6.250
3.125
0.000
-3.125
-6.250
-9.375
-12.500
-15.625
-18.750
-21.875
-25.000
Y
Z
X

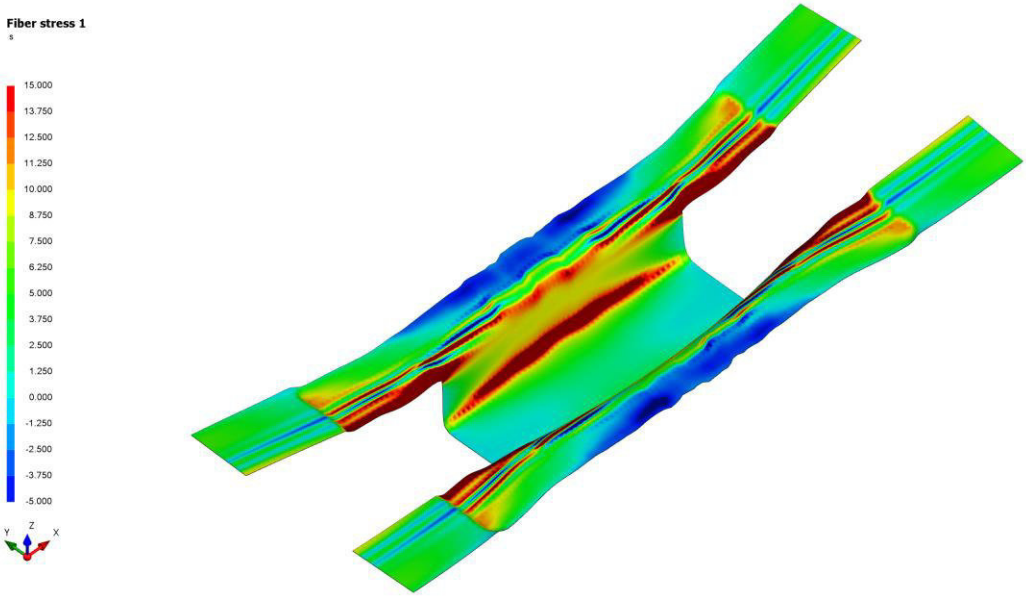

Shear angle f1_f2
s
25.000
21.875
18.750
15.625
12.500
9.375
6.250
3.125
0.000
-3.125
-6.250
-9.375
-12.500
-15.625
-18.750
-21.875
-25.000
Y
Z
X

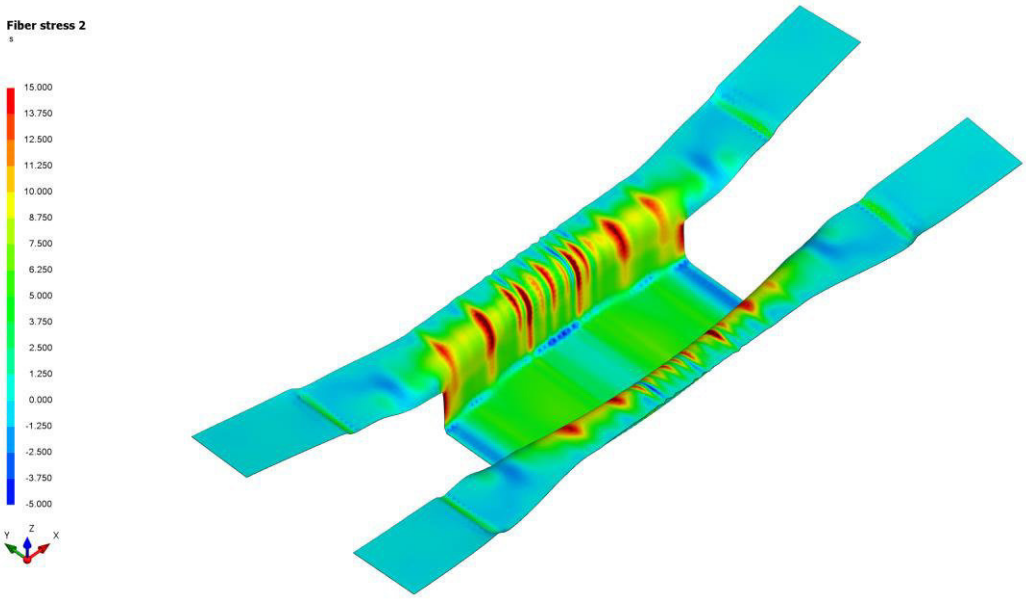

Shear angle f1_f2
s
25.000
21.875
18.750
15.625
12.500
9.375
6.250
3.125
0.000
-3.125
-6.250
-9.375
-12.500
-15.625
-18.750
-21.875
-25.000
Y
Z
X

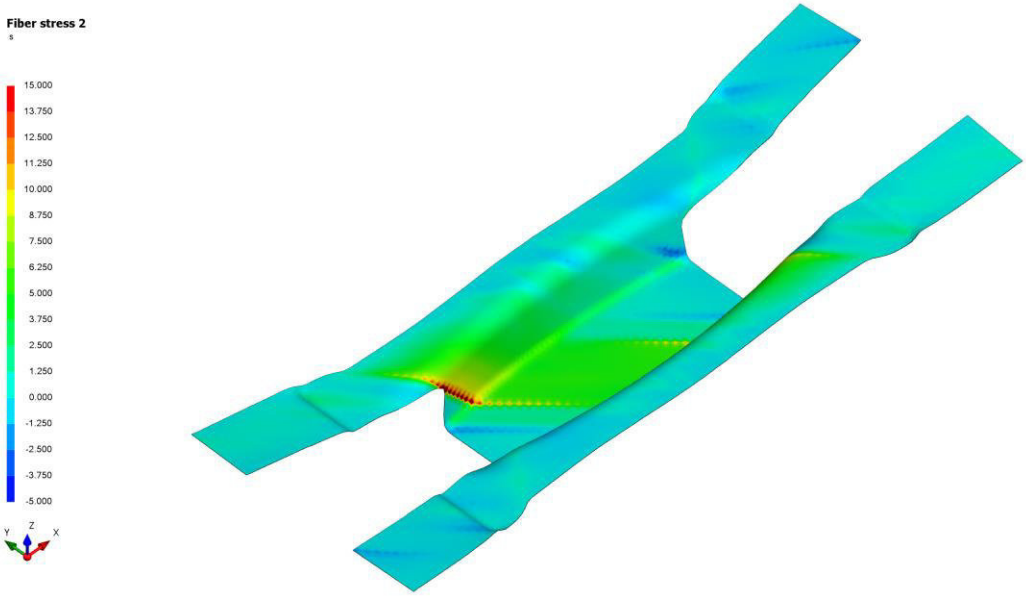

Fiber stress 1
s
15.000
13.750
12.500
11.250
10.000
8.750
7.500
6.250
5.000
3.750
2.500
1.250
0.000
-1.250
-2.500
-3.750
-5.000
Y
Z
X

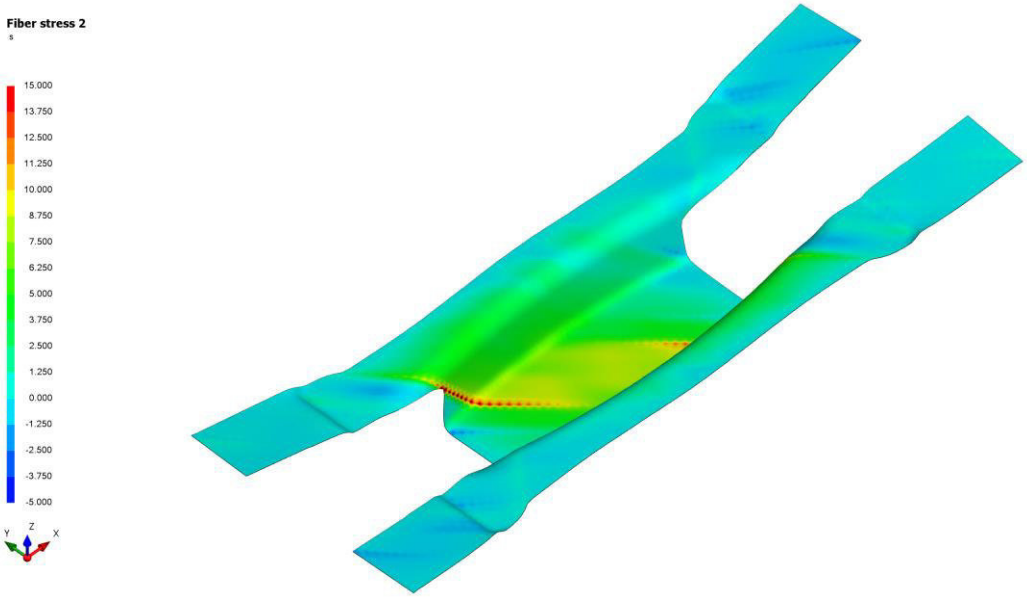

Fiber stress 1
s
15.000
13.750
12.500
11.250
10.000
8.750
7.500
6.250
5.000
3.750
2.500
1.250
0.000
-1.250
-2.500
-3.750
-5.000
Y
Z
X

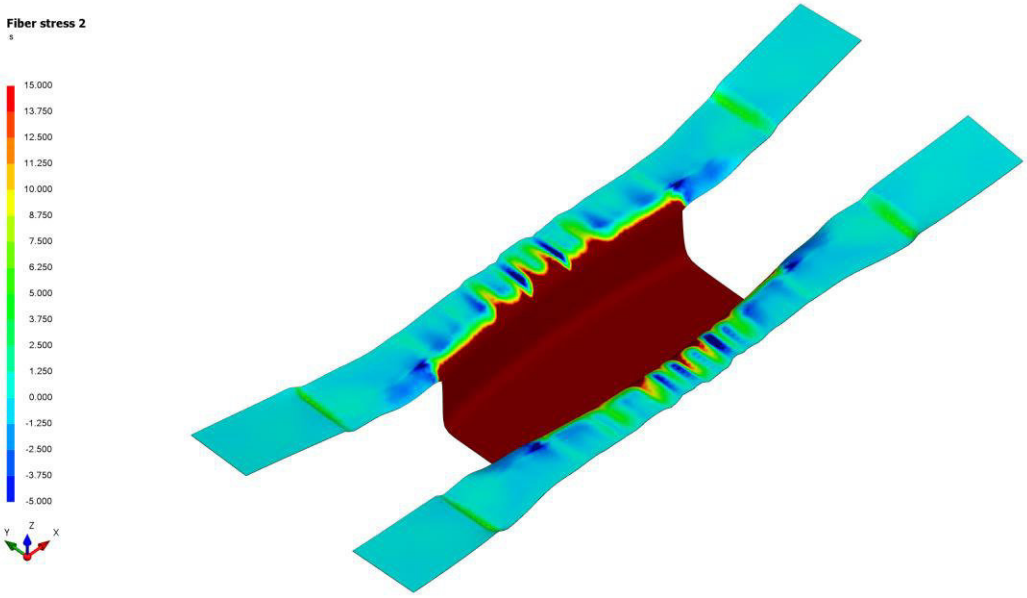

Fiber stress 1
s
15.000
13.750
12.500
11.250
10.000
8.750
7.500
6.250
5.000
3.750
2.500
1.250
0.000
-1.250
-2.500
-3.750
-5.000
Y
Z
X


Fiber stress 1
s
15.000
13.750
12.500
11.250
10.000
8.750
7.500
6.250
5.000
3.750
2.500
1.250
0.000
-1.250
-2.500
-3.750
-5.000
Y
Z
X


Fiber stress 2
s
15.000
13.750
12.500
11.250
10.000
8.750
7.500
6.250
5.000
3.750
2.500
1.250
0.000
-1.250
-2.500
-3.750
-5.000
Y
Z
X


Fiber stress 2
s
15.000
13.750
12.500
11.250
10.000
8.750
7.500
6.250
5.000
3.750
2.500
1.250
0.000
-1.250
-2.500
-3.750
-5.000
Y
Z
X

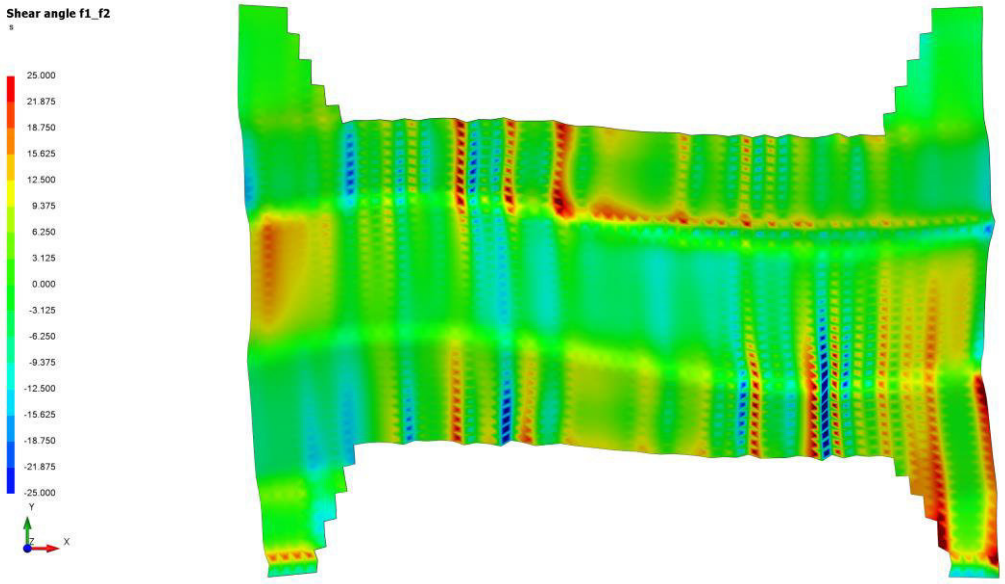

Fiber stress 2
s
15.000
13.750
12.500
11.250
10.000
8.750
7.500
6.250
5.000
3.750
2.500
1.250
0.000
-1.250
-2.500
-3.750
-5.000
Y
Z
X

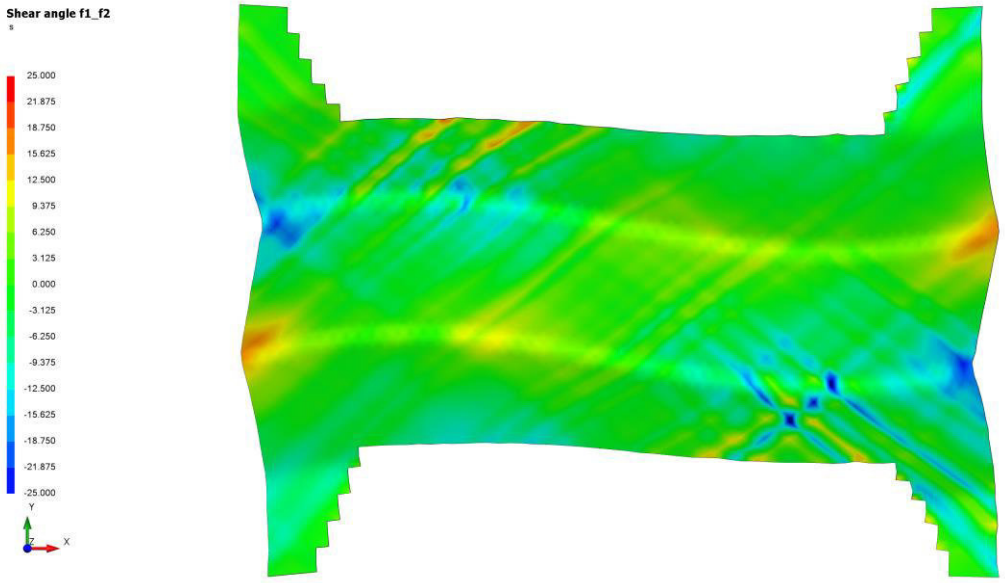

Fiber stress 2
s
15.000
13.750
12.500
11.250
10.000
8.750
7.500
6.250
5.000
3.750
2.500
1.250
0.000
-1.250
-2.500
-3.750
-5.000
Y
Z
X

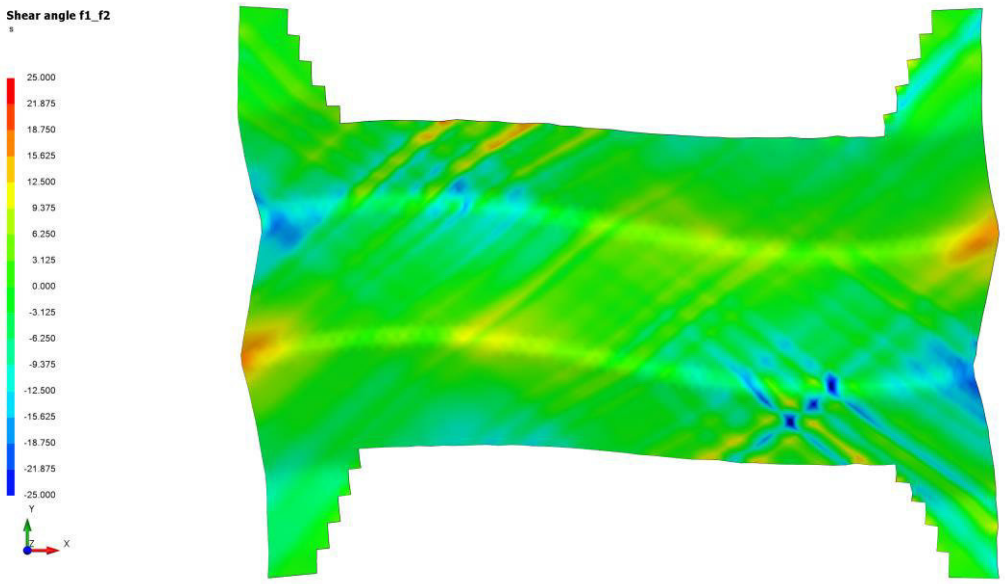
6C

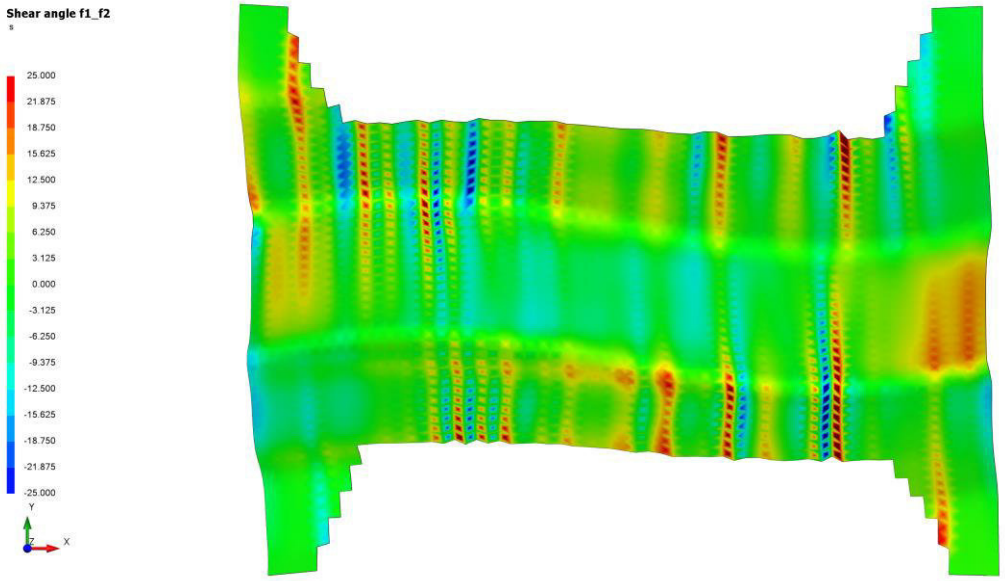
D.3 Z-Section Results

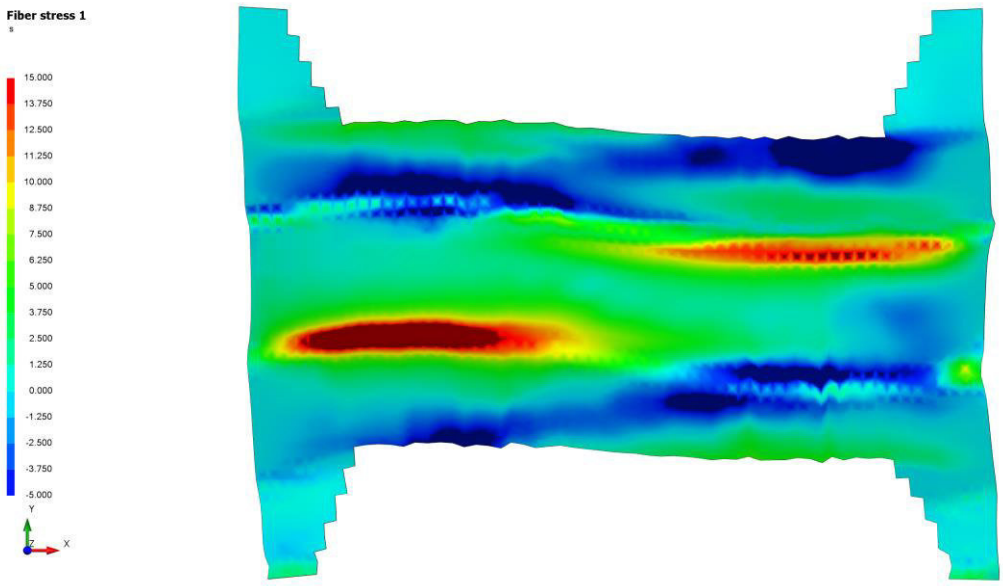
Z-Section Blank 1

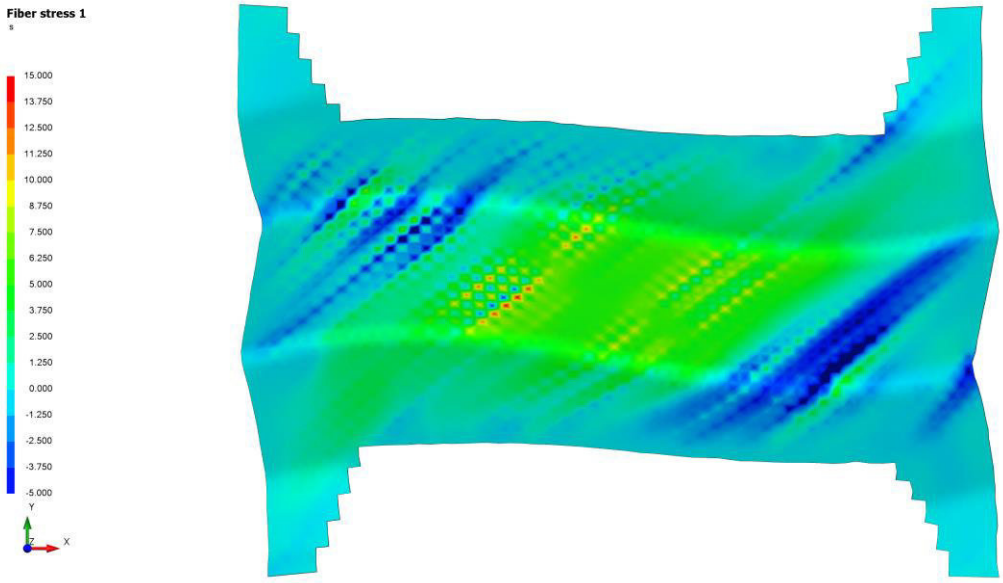

Shear angle f1_f2
s
25.000
21.875
18.750
15.625
12.500
9.375
6.250
3.125
0.000
-3.125
-6.250
-9.375
-12.500
-15.625
-18.750
-21.875
-25.000
Y
Z
X

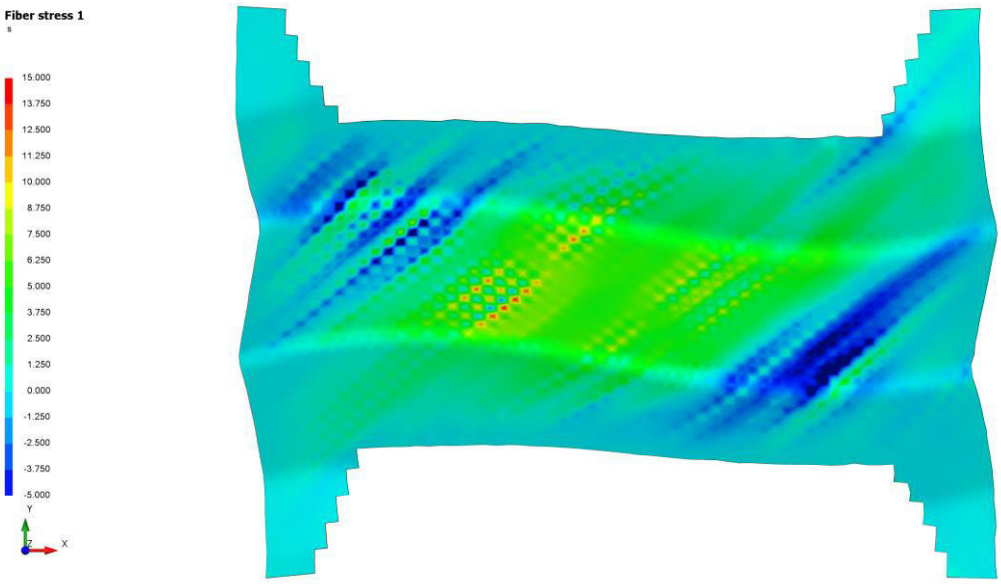

Shear angle f1_f2
s
25.000
21.875
18.750
15.625
12.500
9.375
6.250
3.125
0.000
-3.125
-6.250
-9.375
-12.500
-15.625
-18.750
-21.875
-25.000
Y
Z
X

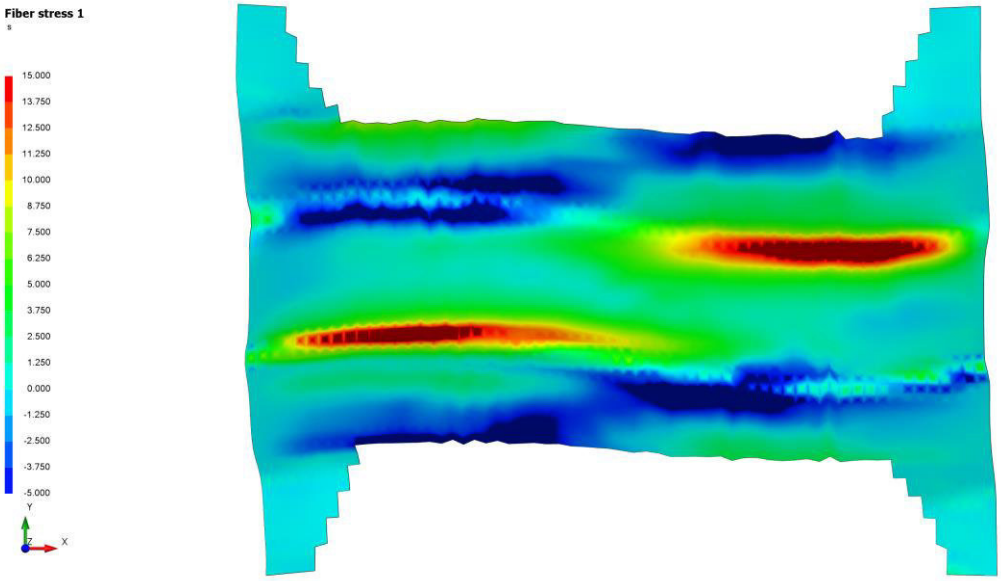

Shear angle f1_f2
s
25.000
21.875
18.750
15.625
12.500
9.375
6.250
3.125
0.000
-3.125
-6.250
-9.375
-12.500
-15.625
-18.750
-21.875
-25.000
Y
Z
X

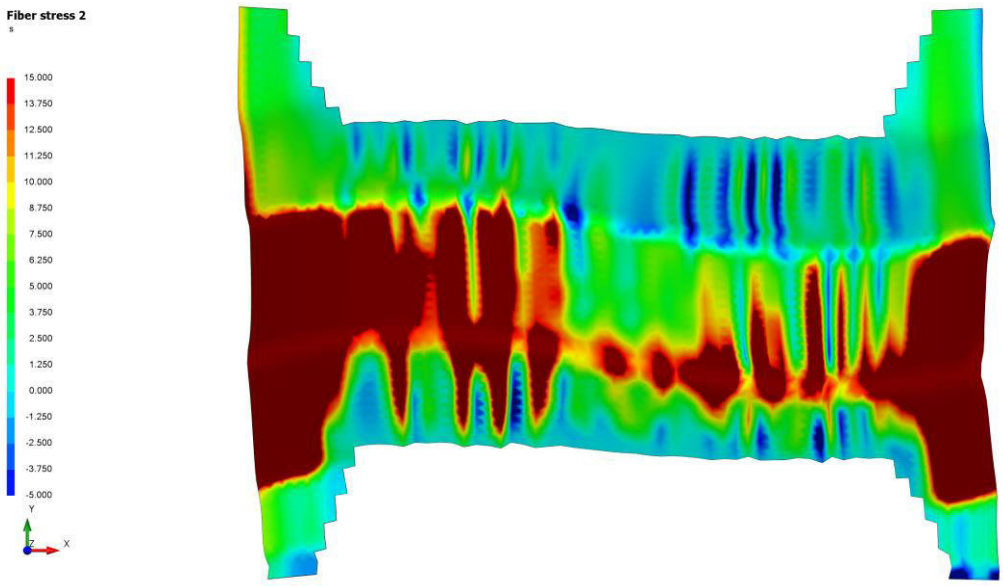

Shear angle f1_f2
s
25.000
21.875
18.750
15.625
12.500
9.375
6.250
3.125
0.000
-3.125
-6.250
-9.375
-12.500
-15.625
-18.750
-21.875
-25.000
Y
Z
X

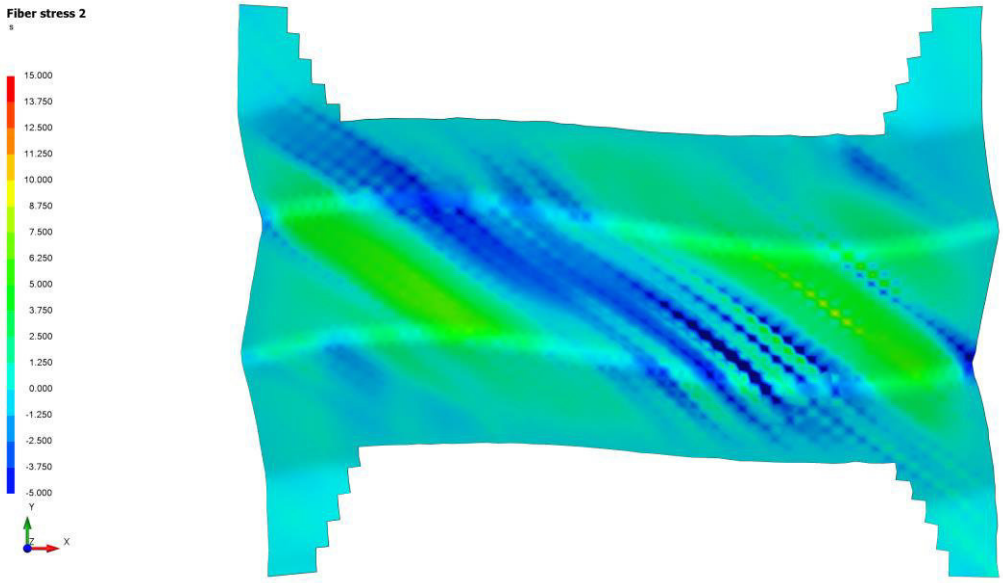

Fiber stress 1
s
15.000
13.750
12.500
11.250
10.000
8.750
7.500
6.250
5.000
3.750
2.500
1.250
0.000
-1.250
-2.500
-3.750
-5.000
Y
Z
X

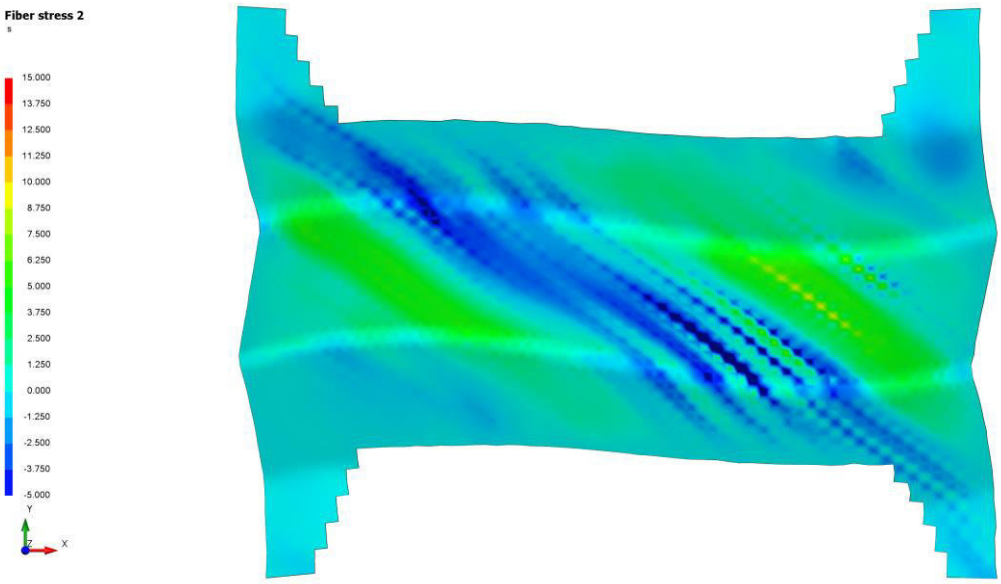

Fiber stress 1
s
15.000
13.750
12.500
11.250
10.000
8.750
7.500
6.250
5.000
3.750
2.500
1.250
0.000
-1.250
-2.500
-3.750
-5.000
Y
Z
X

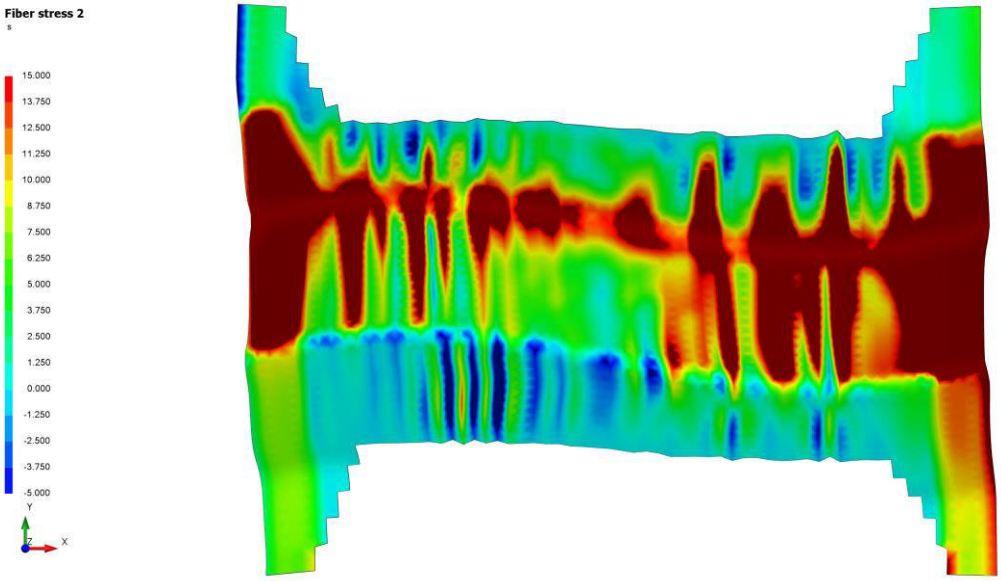

Fiber stress 1
s
15.000
13.750
12.500
11.250
10.000
8.750
7.500
6.250
5.000
3.750
2.500
1.250
0.000
-1.250
-2.500
-3.750
-5.000
Y
Z
X


Fiber stress 1
s
15.000
13.750
12.500
11.250
10.000
8.750
7.500
6.250
5.000
3.750
2.500
1.250
0.000
-1.250
-2.500
-3.750
-5.000
Y
Z
X


Fiber stress 2
s
15.000
13.750
12.500
11.250
10.000
8.750
7.500
6.250
5.000
3.750
2.500
1.250
0.000
-1.250
-2.500
-3.750
-5.000
Y
Z
X


Fiber stress 2
s
15.000
13.750
12.500
11.250
10.000
8.750
7.500
6.250
5.000
3.750
2.500
1.250
0.000
-1.250
-2.500
-3.750
-5.000
Y
Z
X

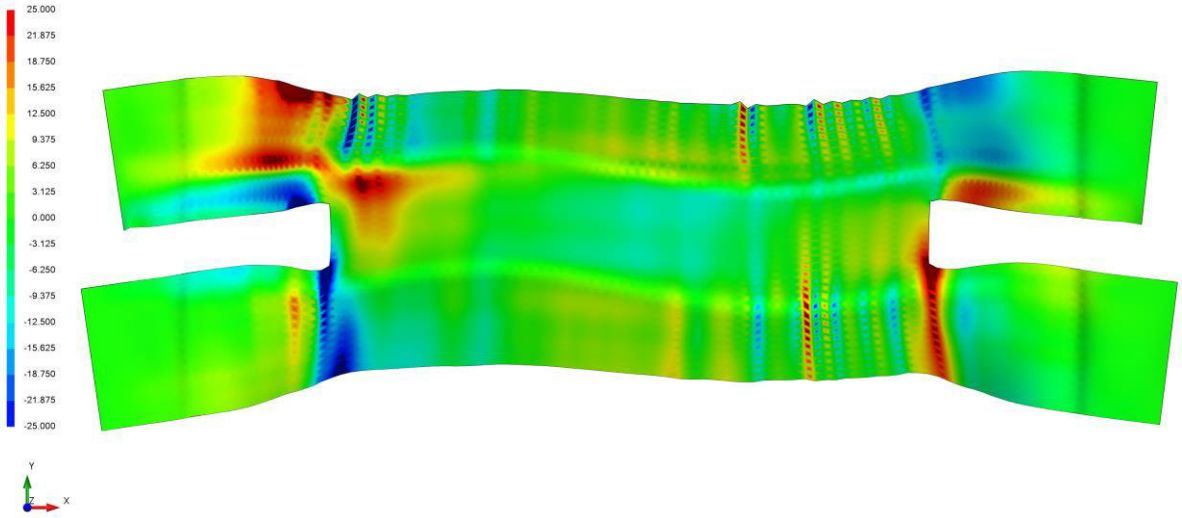

Fiber stress 2
s
15.000
13.750
12.500
11.250
10.000
8.750
7.500
6.250
5.000
3.750
2.500
1.250
0.000
-1.250
-2.500
-3.750
-5.000
Y
Z
X


Fiber stress 2
s
15.000
13.750
12.500
11.250
10.000
8.750
7.500
6.250
5.000
3.750
2.500
1.250
0.000
-1.250
-2.500
-3.750
-5.000
Y
Z
X

Z-Section Blank 2 Stiffness 0.09 N/mm

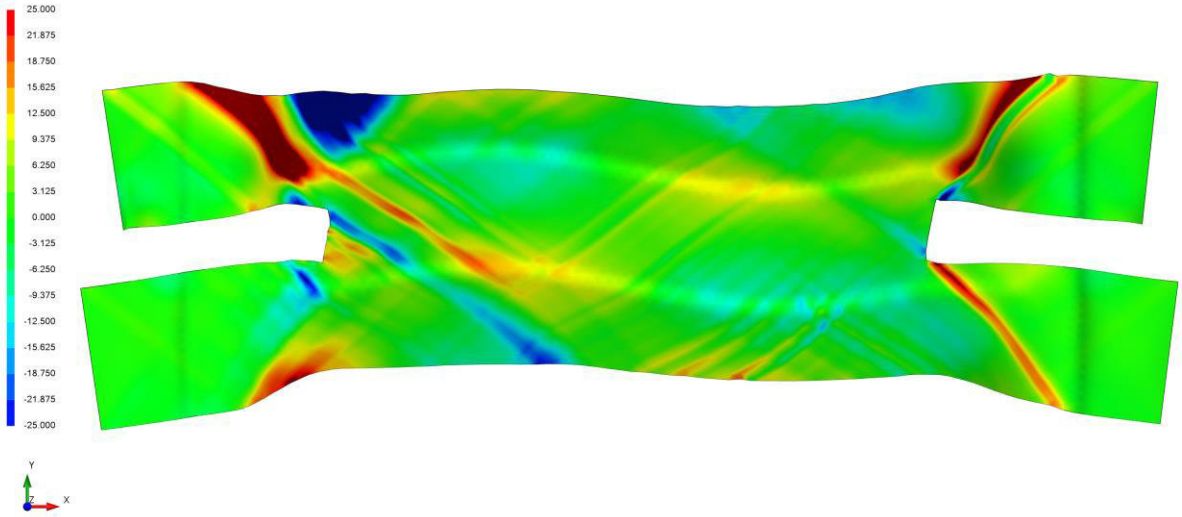
Shear angle f1_f2

s

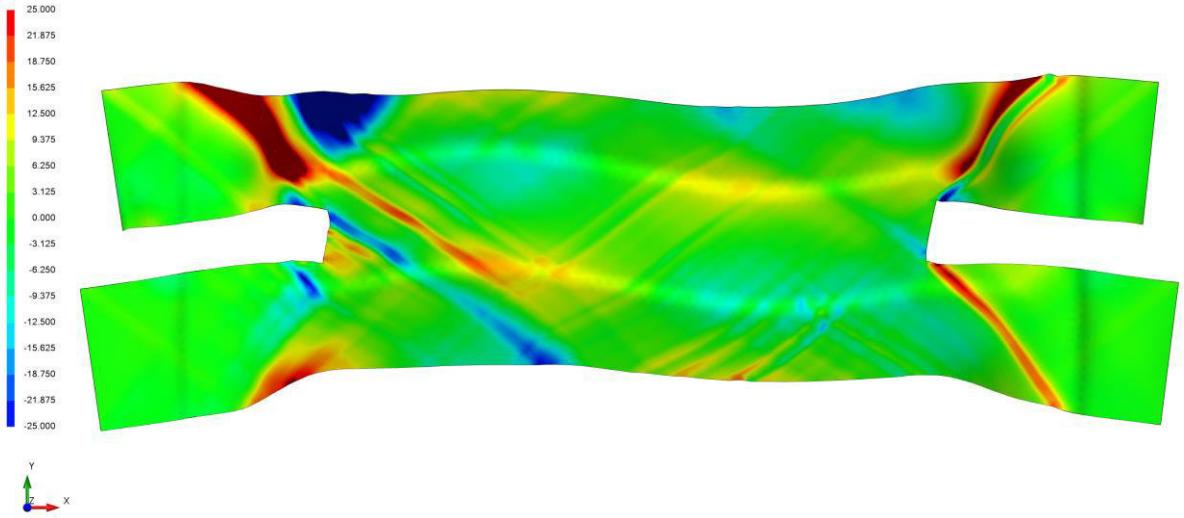


Shear angle f1_f2

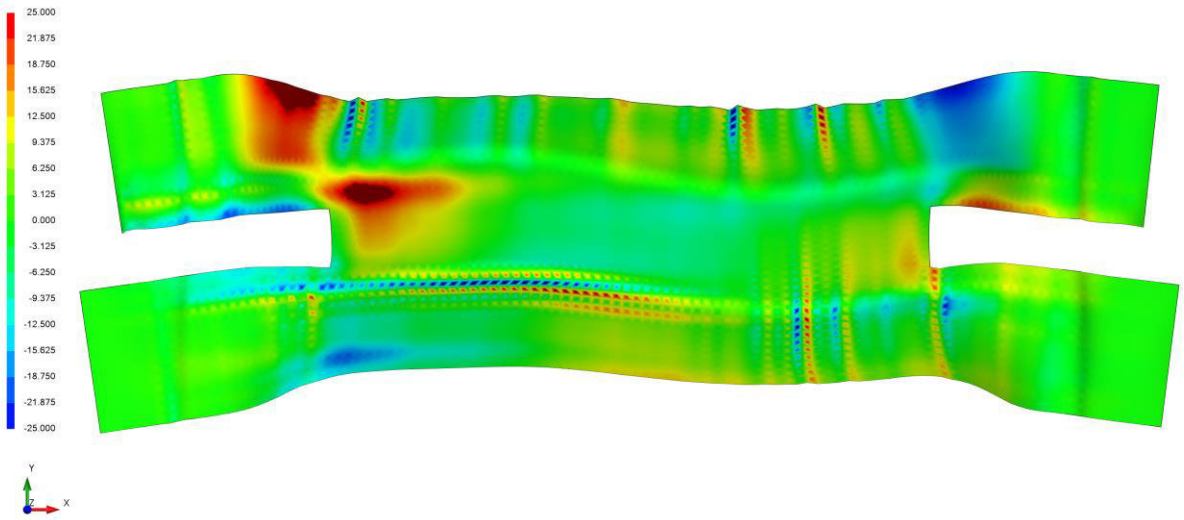
s



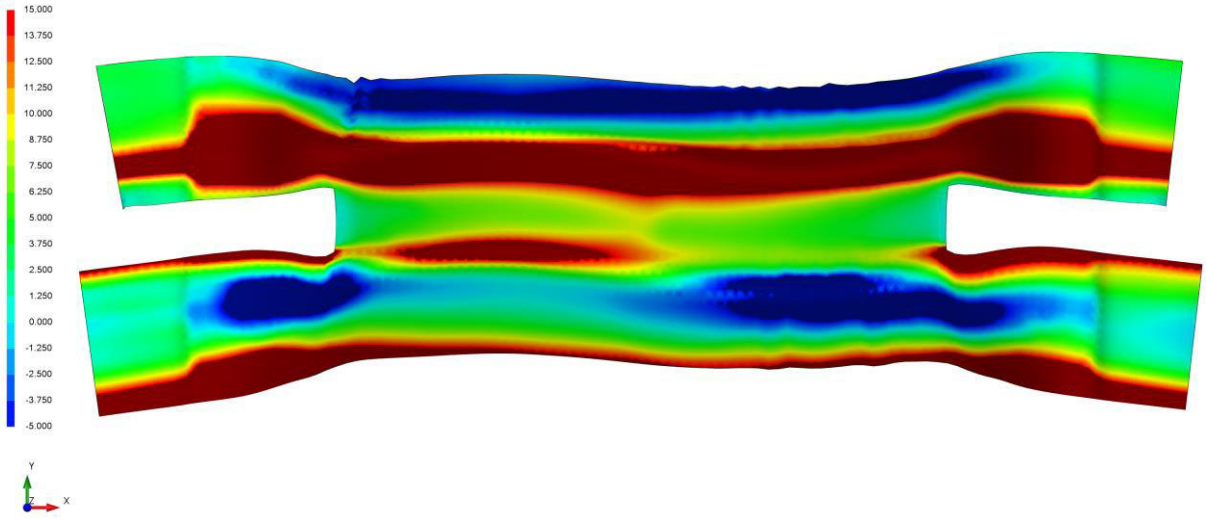
Shear angle f1_f2
s



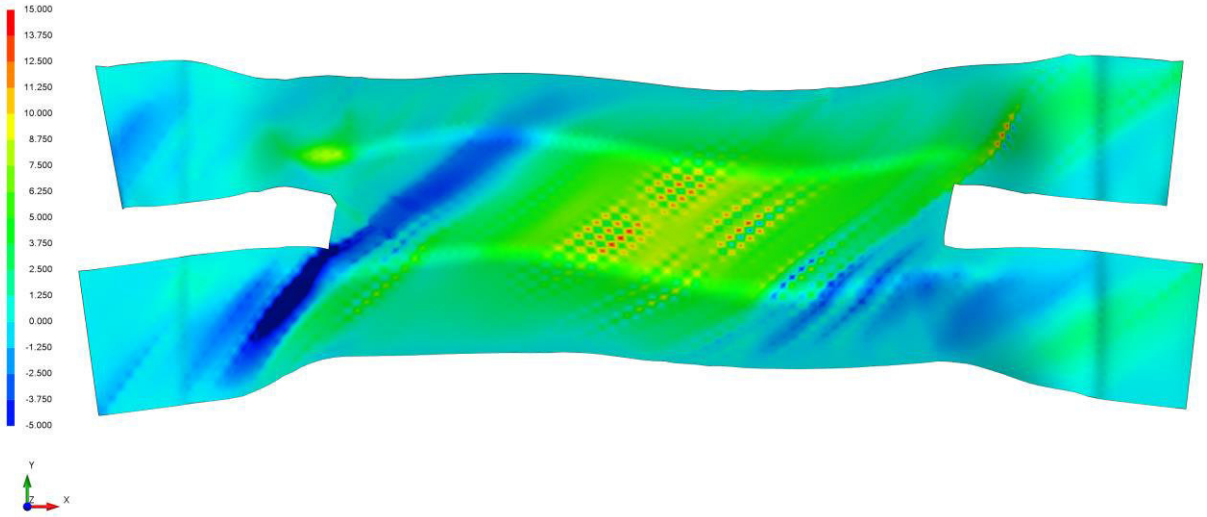
Shear angle f1_f2
s



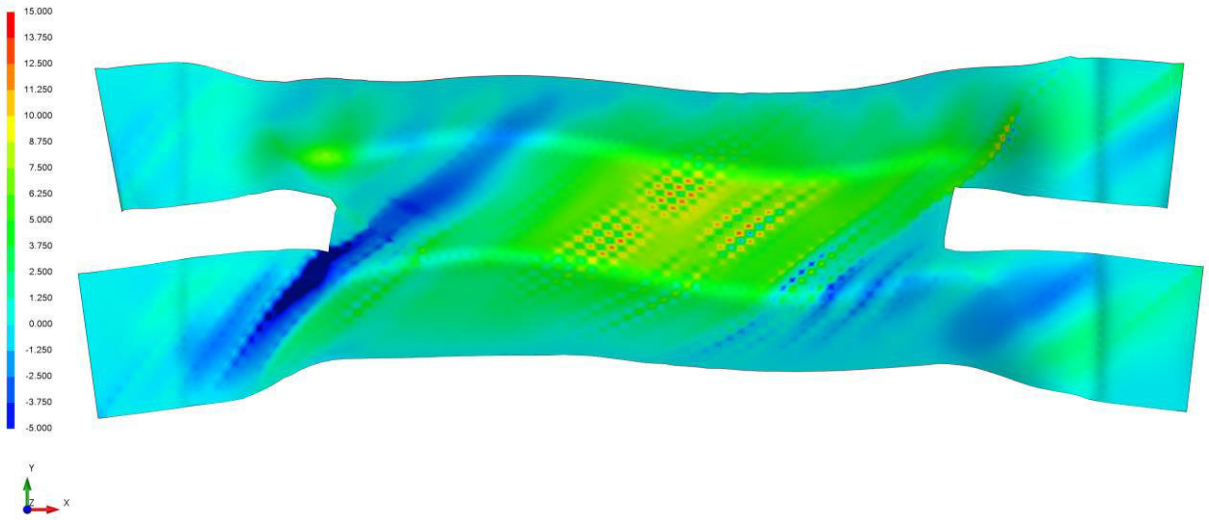
Fiber stress 1
s



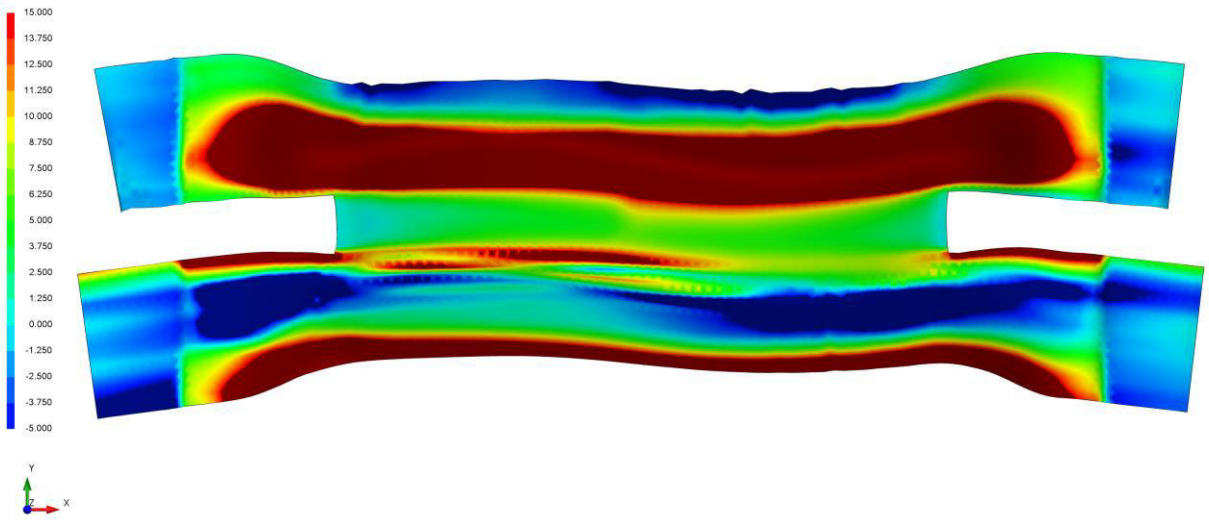
Fiber stress 1
s



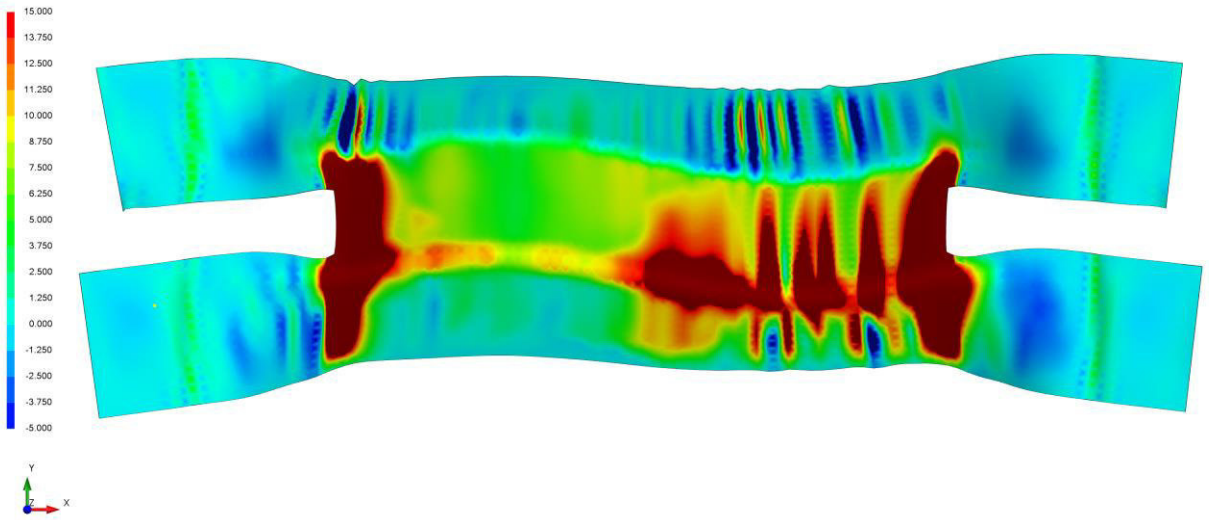
Fiber stress 1
s



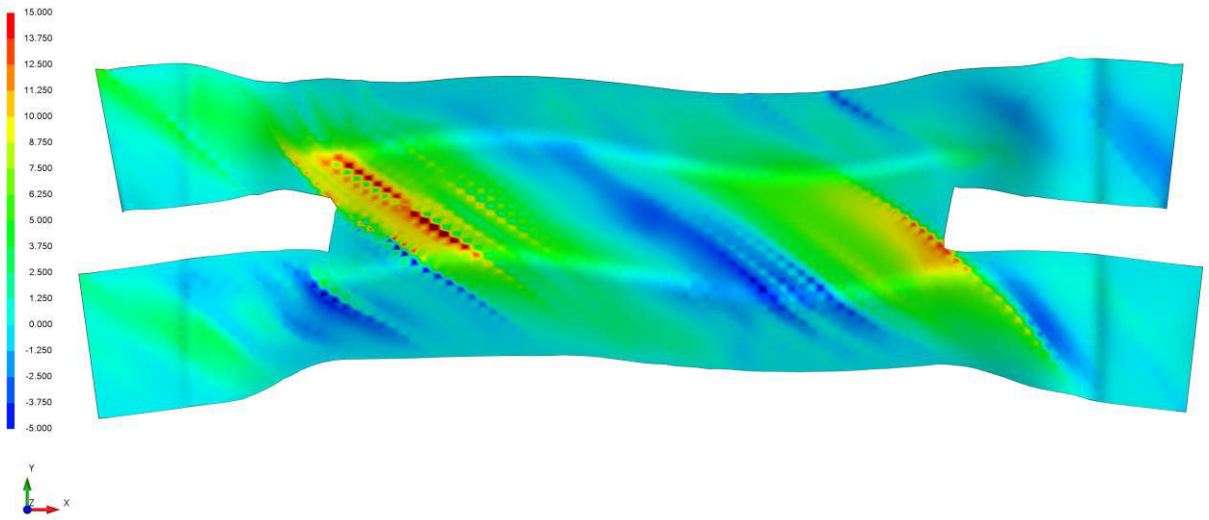
Fiber stress 1
s

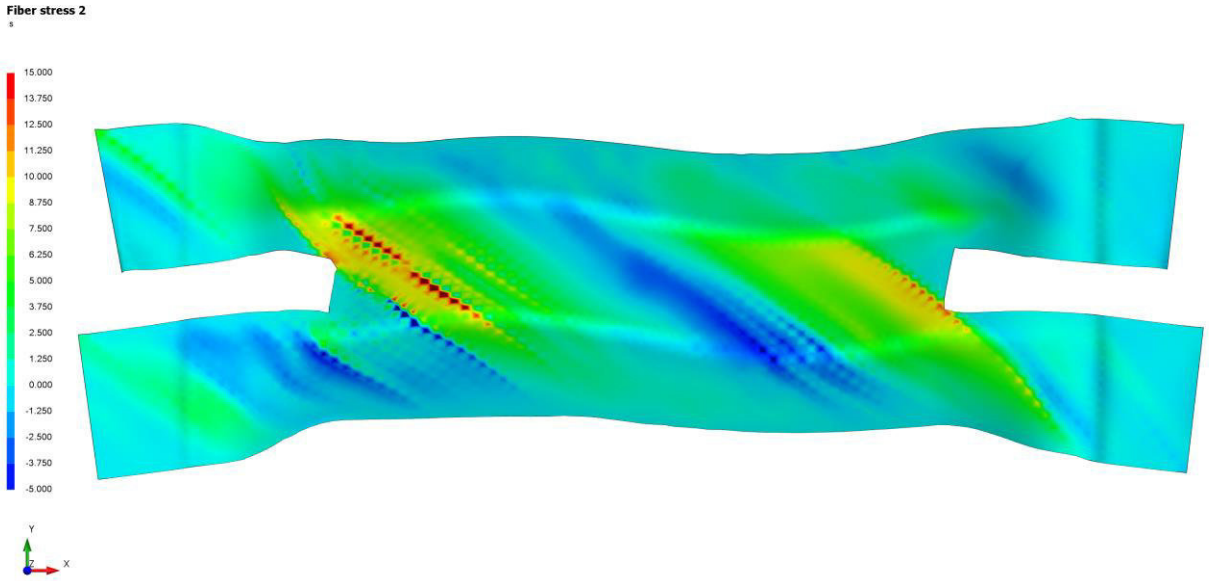


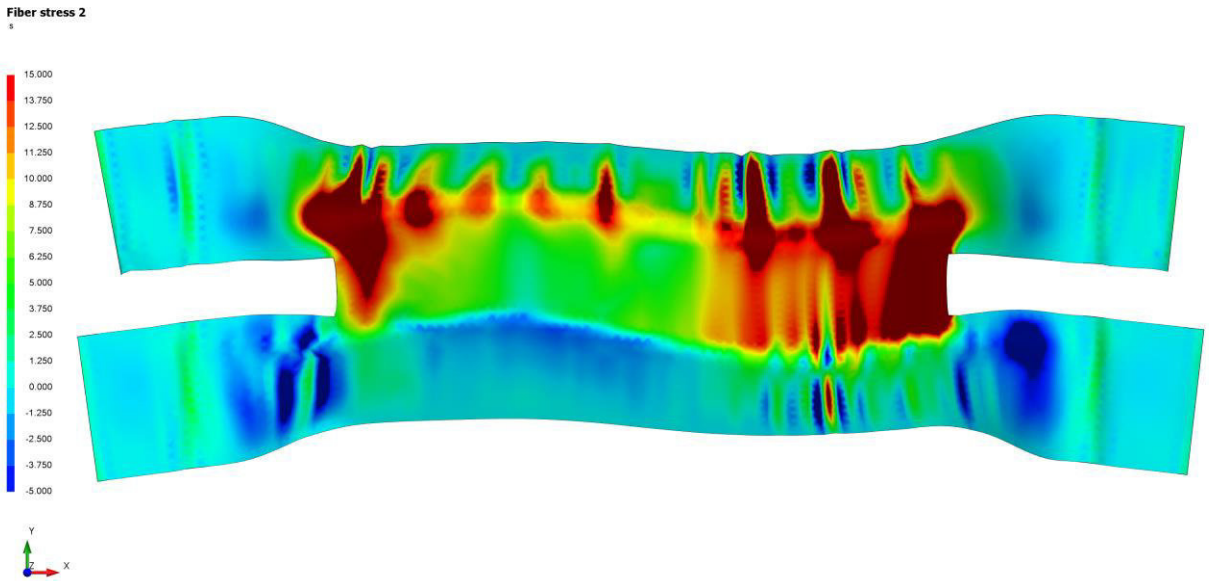
Fiber stress 2
s



Fiber stress 2
s



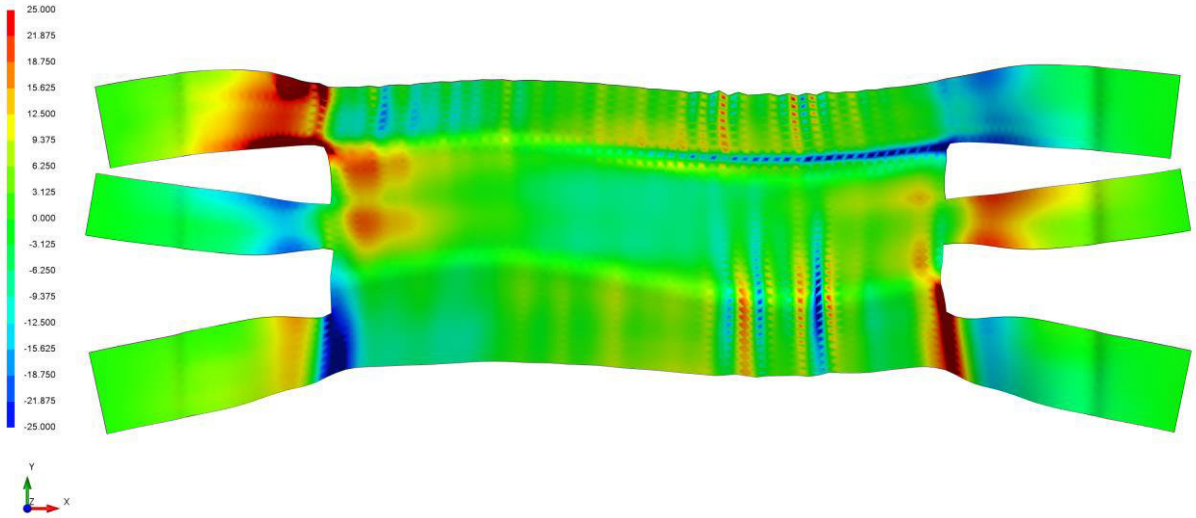

Fiber stress 2
s
15.000
13.750
12.500
11.250
10.000
8.750
7.500
6.250
5.000
3.750
2.500
1.250
0.000
-1.250
-2.500
-3.750
-5.000
Y
Z
X


Fiber stress 2
s
15.000
13.750
12.500
11.250
10.000
8.750
7.500
6.250
5.000
3.750
2.500
1.250
0.000
-1.250
-2.500
-3.750
-5.000
Y
Z
X

Z-Section Blank 3

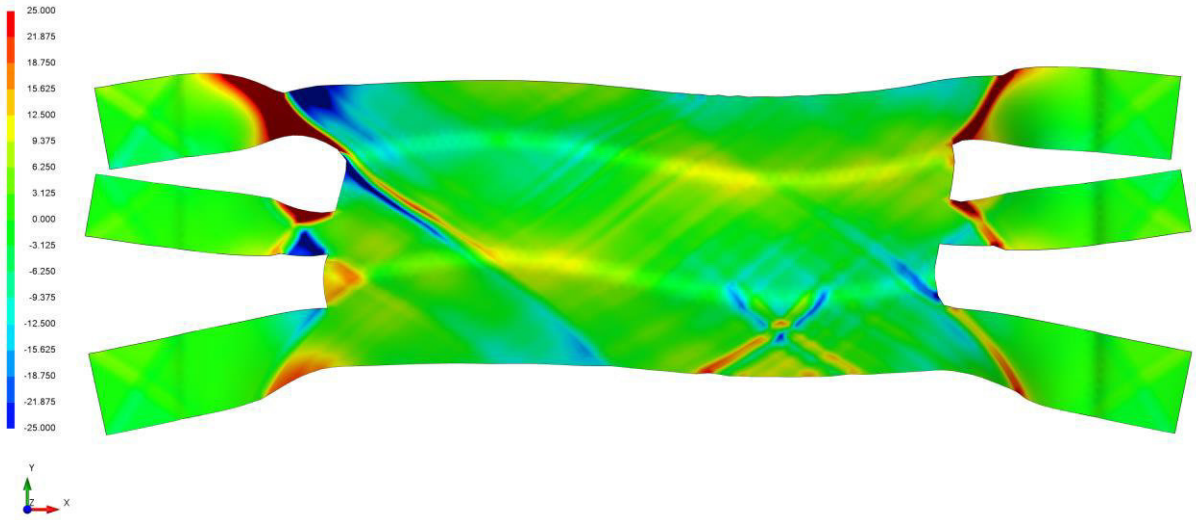
Shear angle f1_f2

s



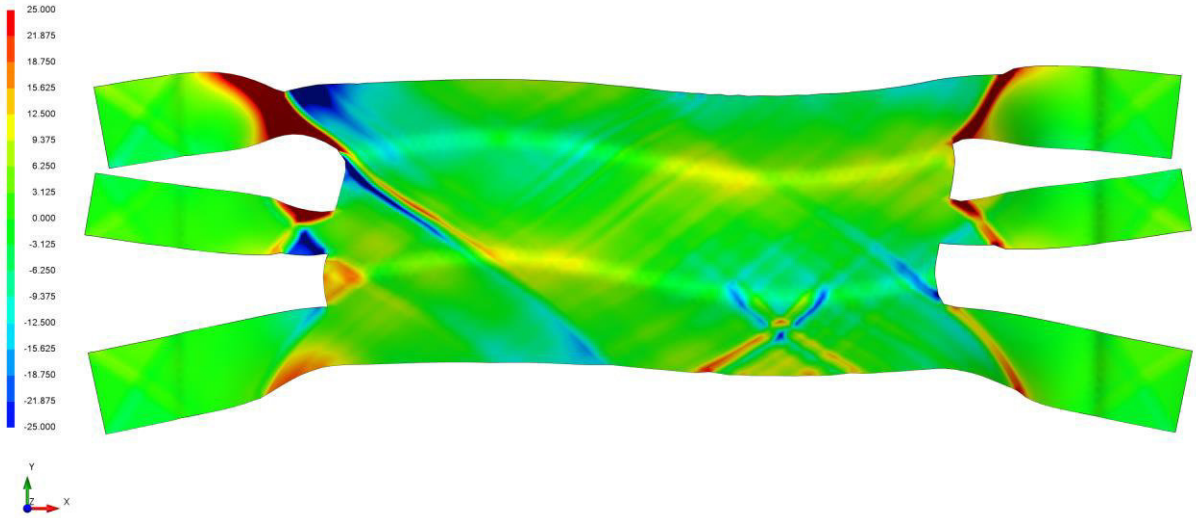
Shear angle f1_f2

s



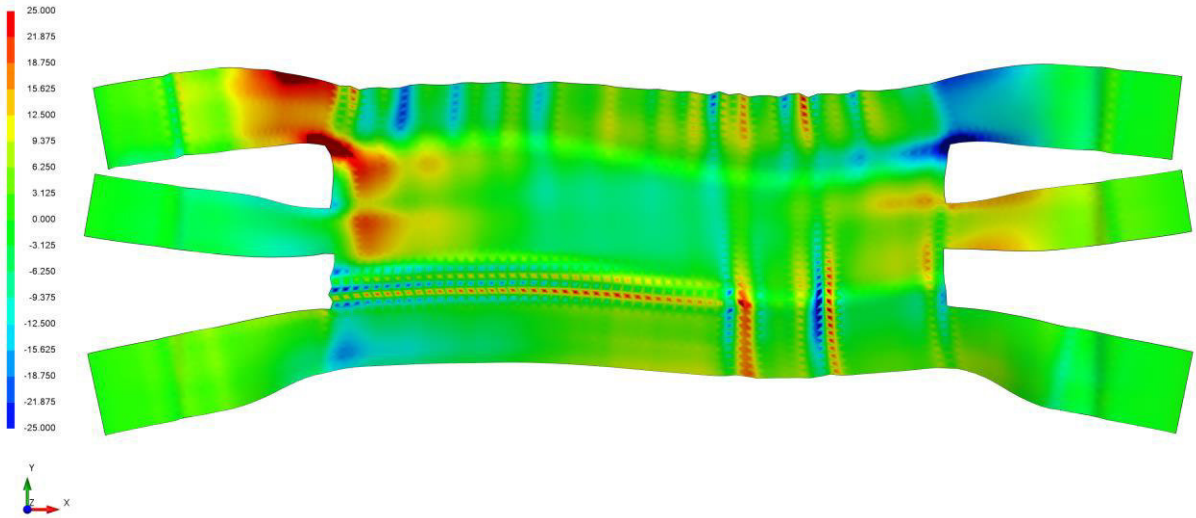
Shear angle f1_f2

s

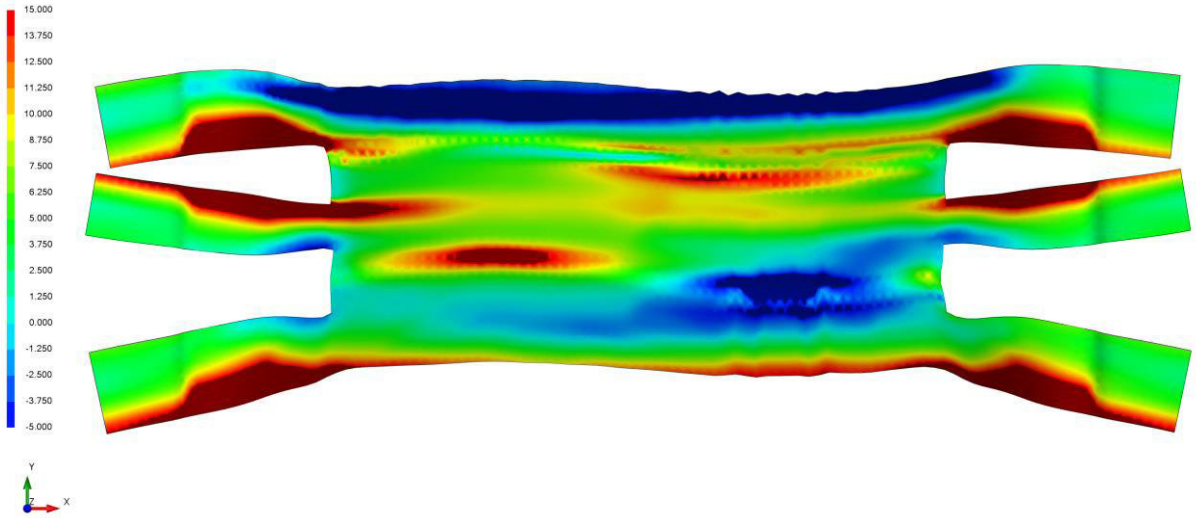


Shear angle f1_f2

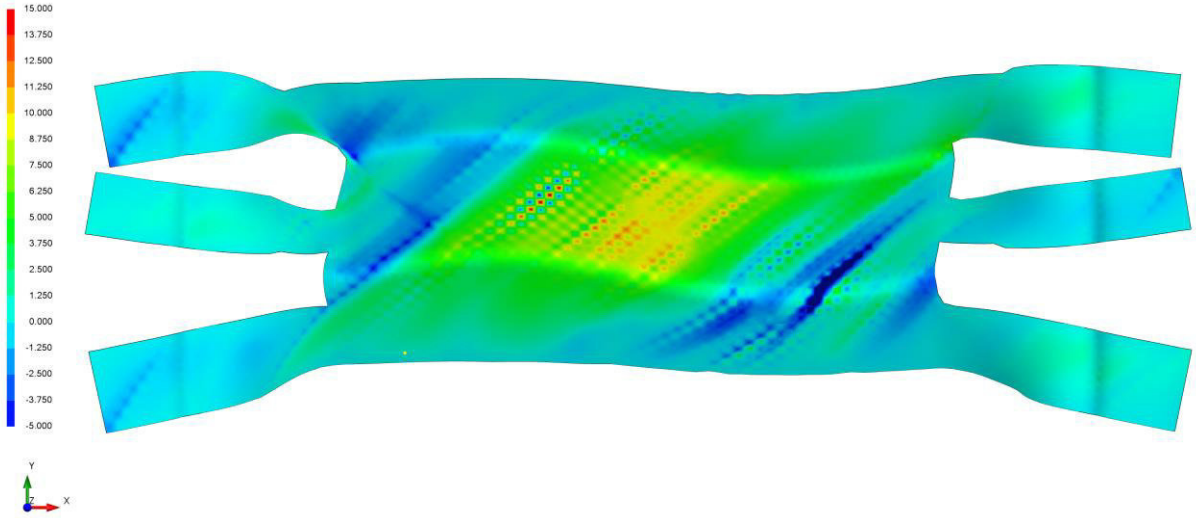
s



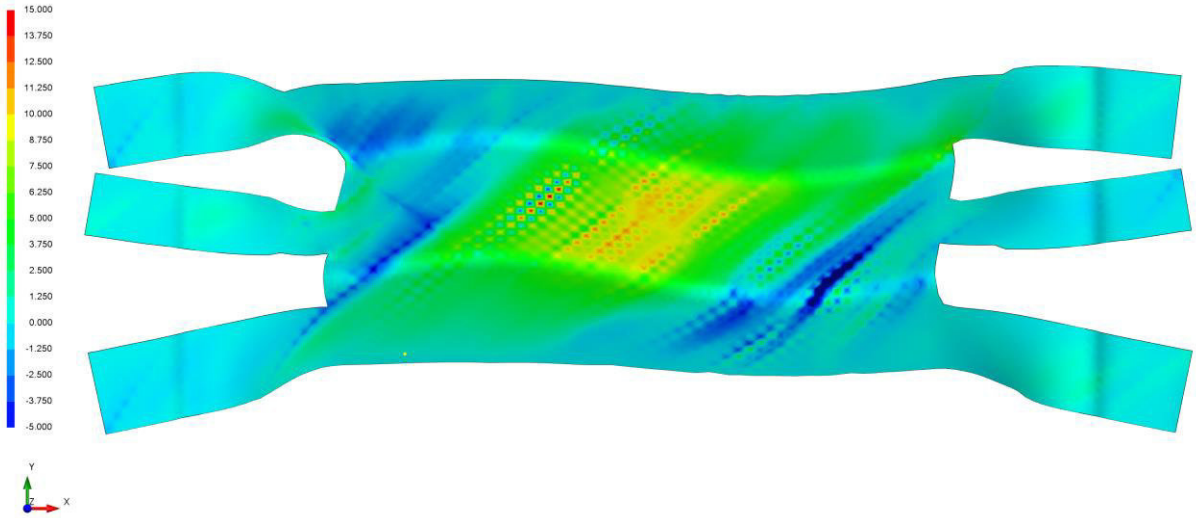
Fiber stress 1
s



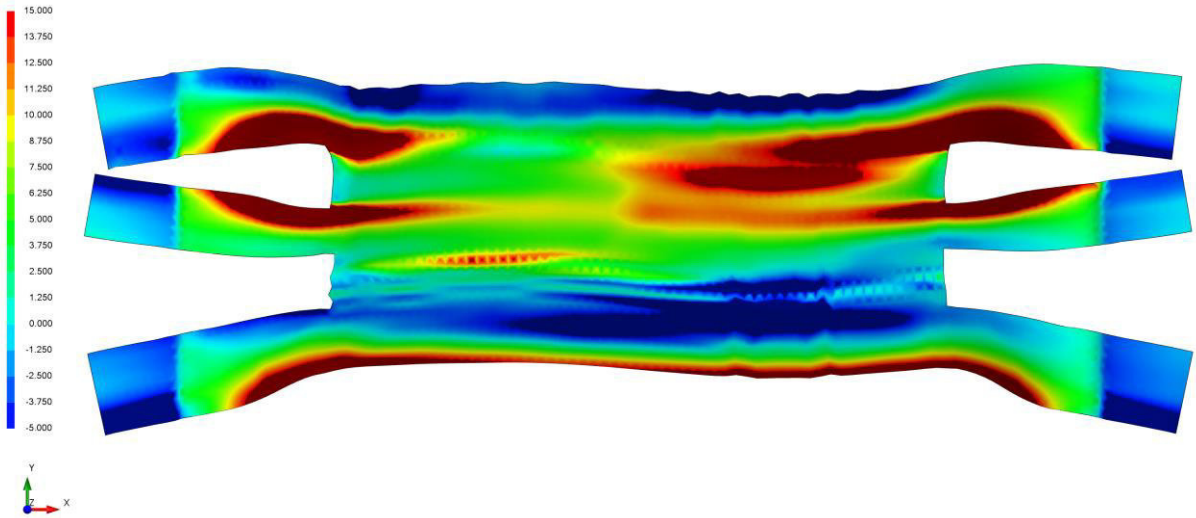
Fiber stress 1
s



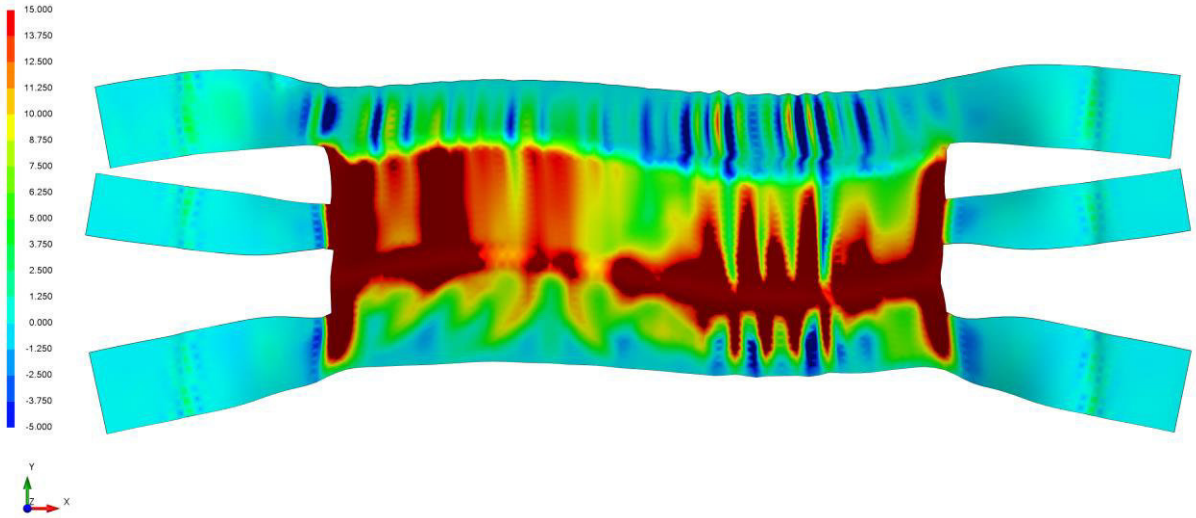
Fiber stress 1
s



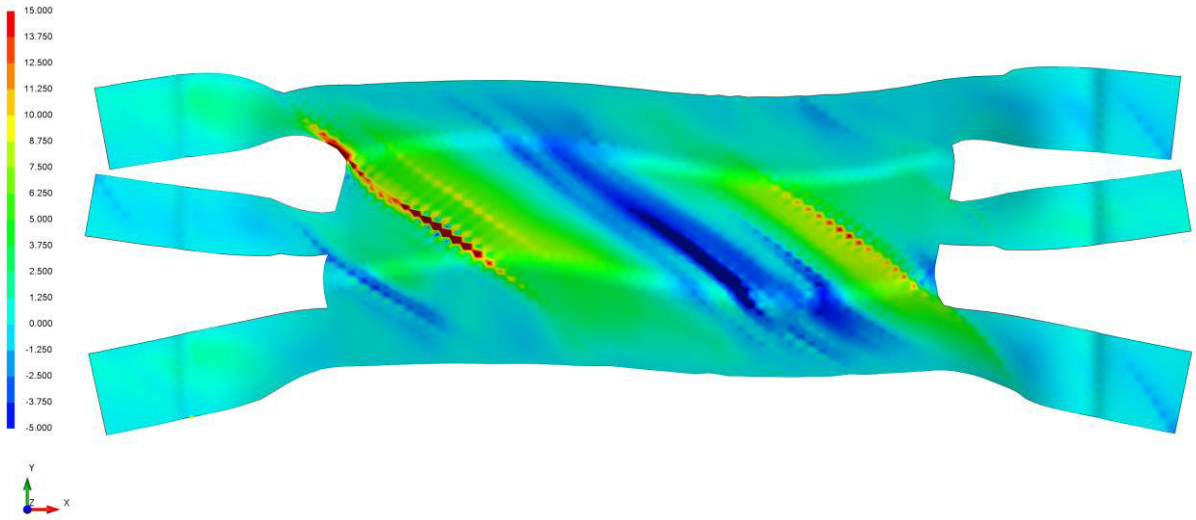
Fiber stress 1
s



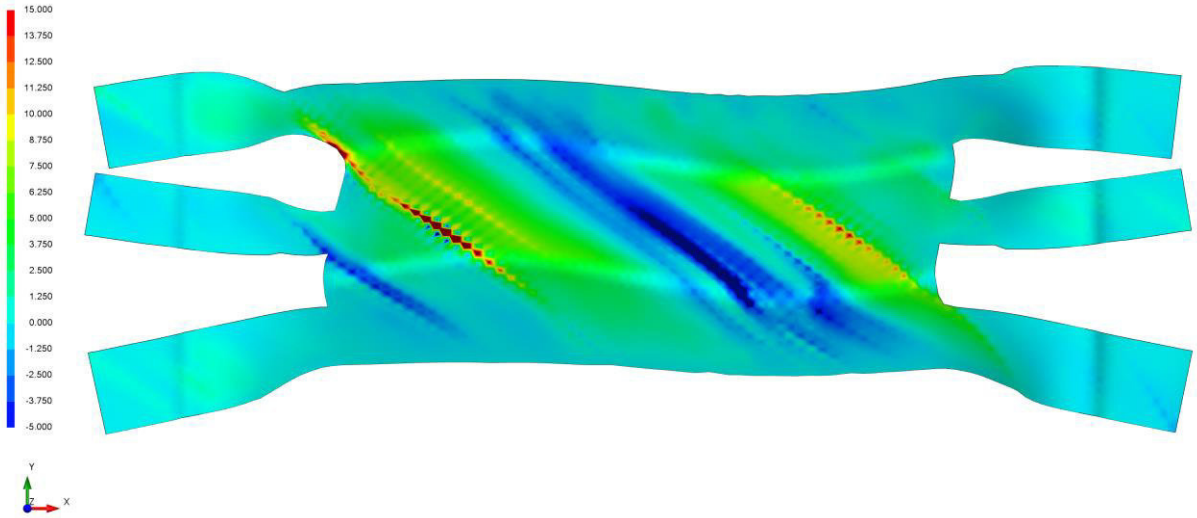
Fiber stress 2
s



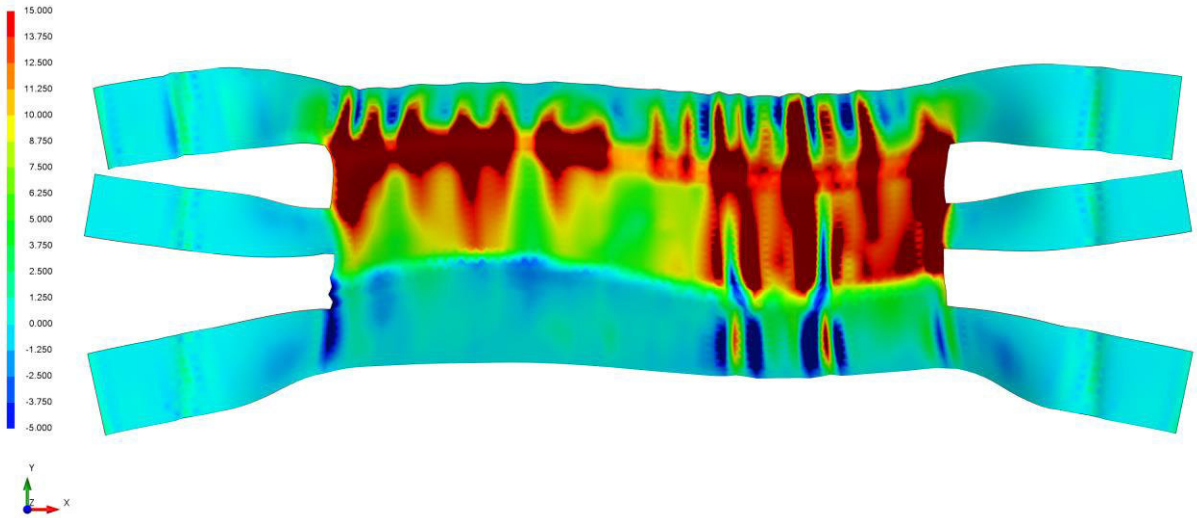
Fiber stress 2
s



Fiber stress 2
s

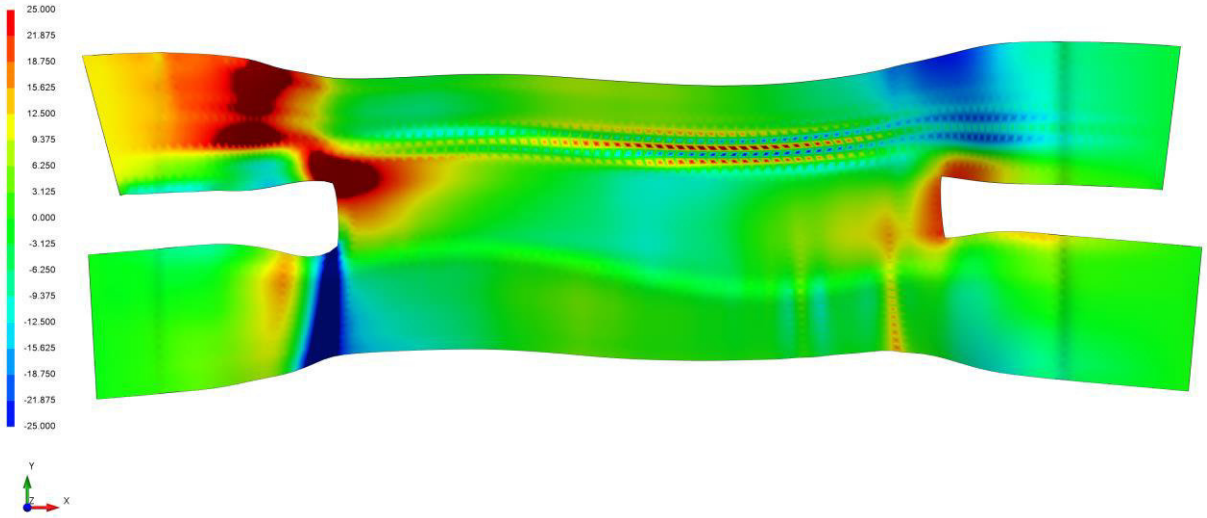


Fiber stress 2
s

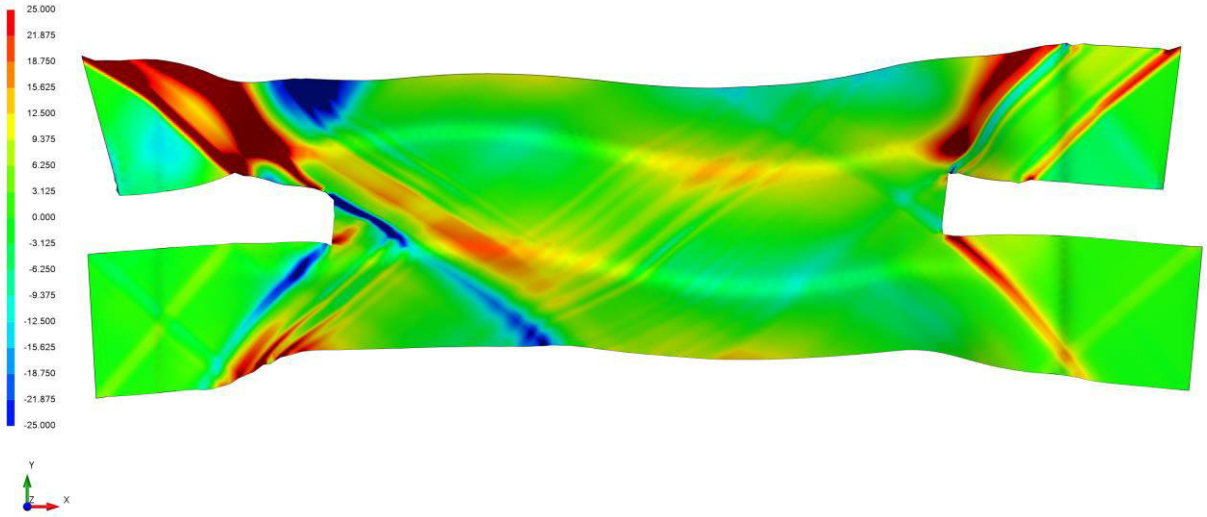


Z-Section Blank 2 Stiffness 0.23 N/mm

Shear angle f1_f2
s

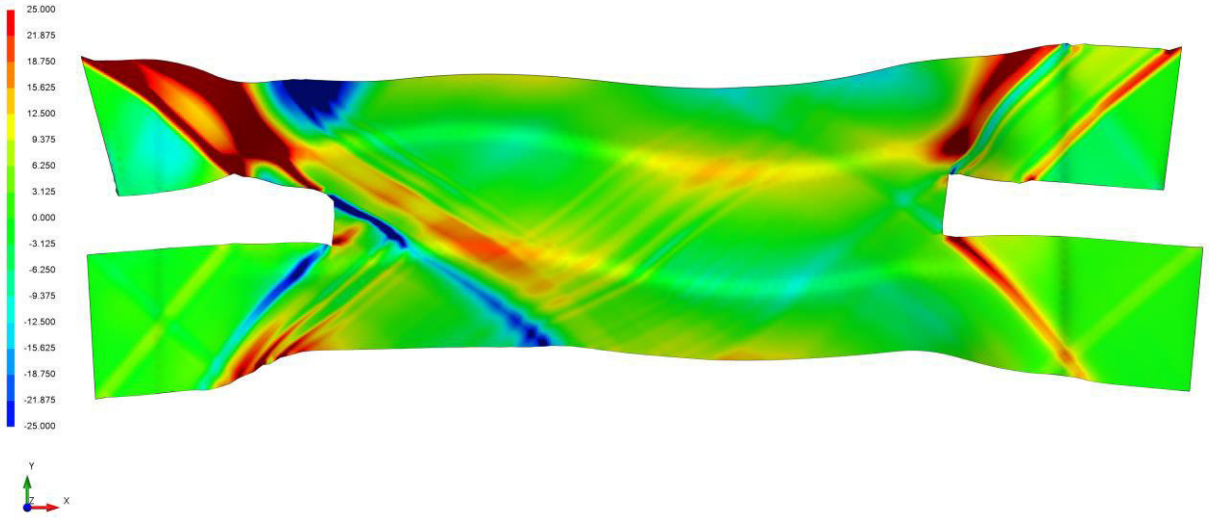


Shear angle f1_f2
s



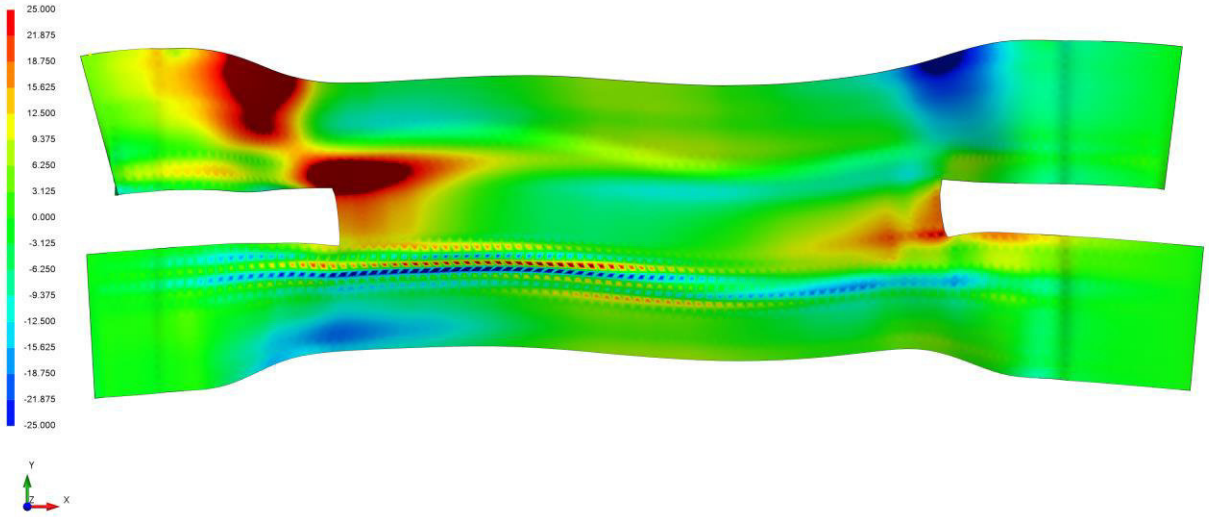
Shear angle f1_f2

s

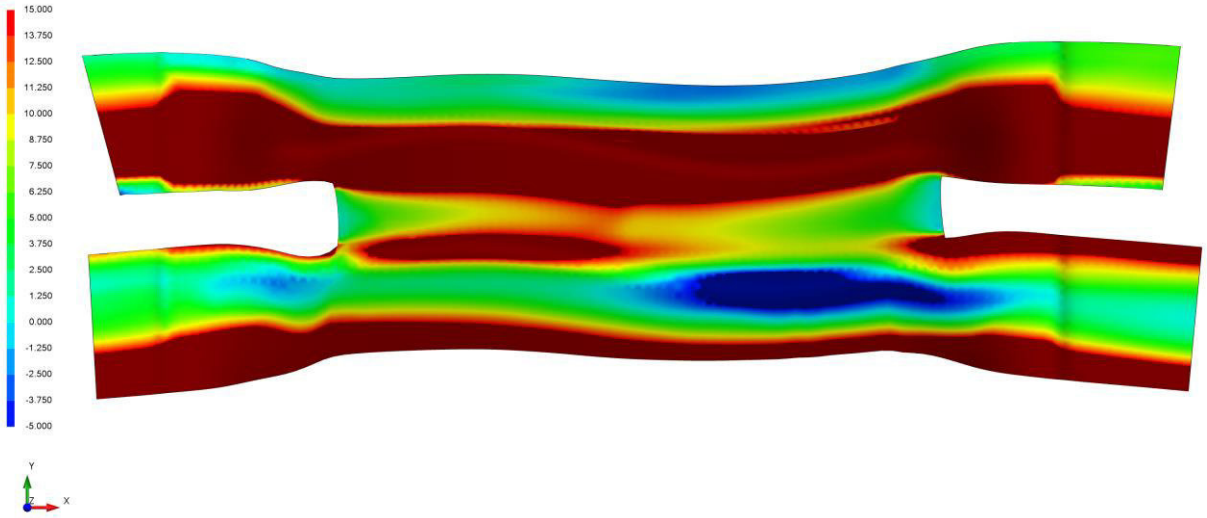


Shear angle f1_f2

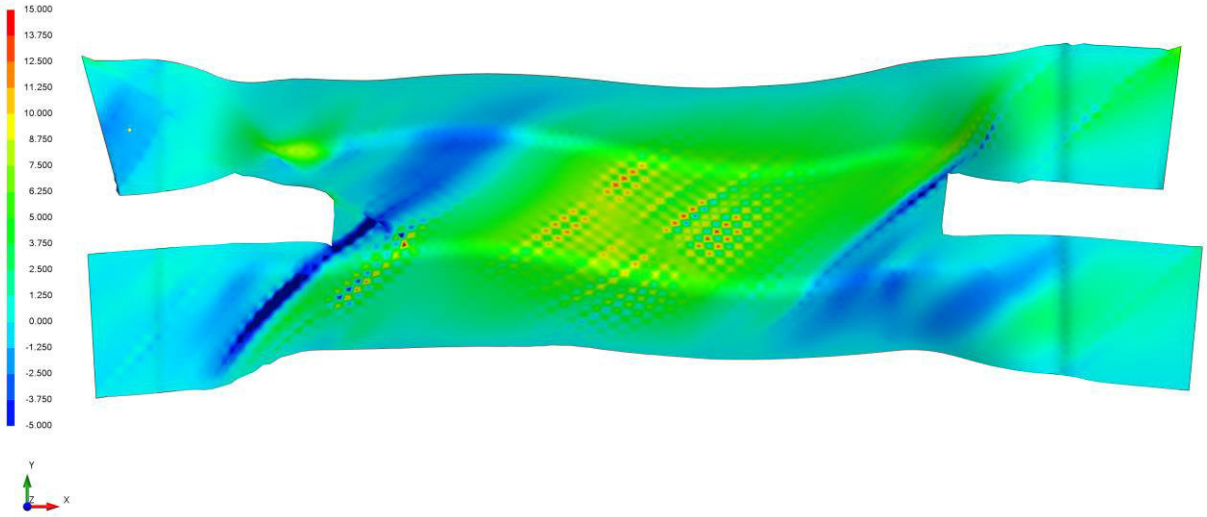
s



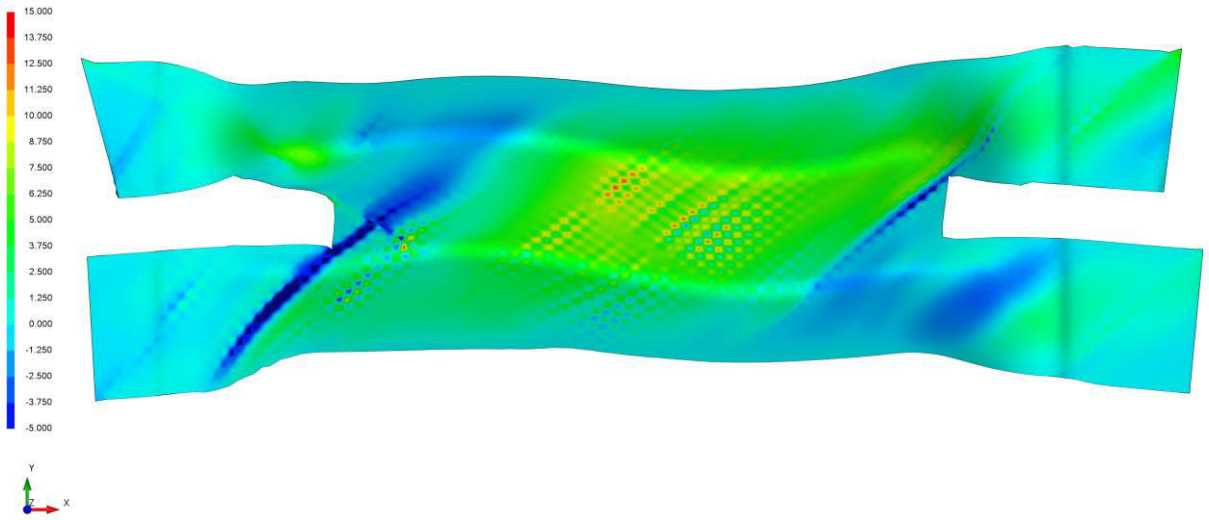
Fiber stress 1
s



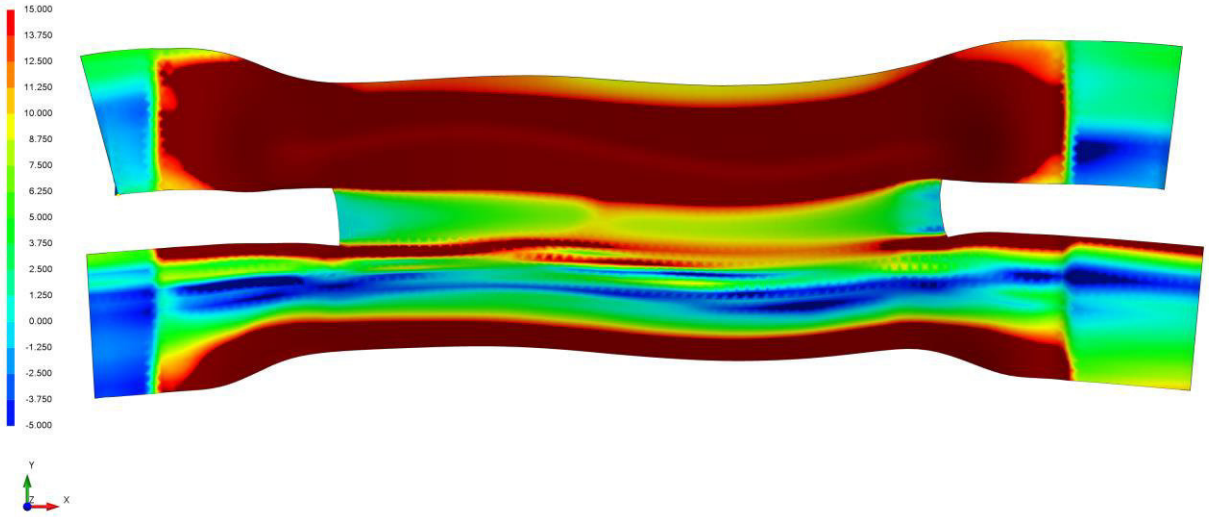
Fiber stress 1
s



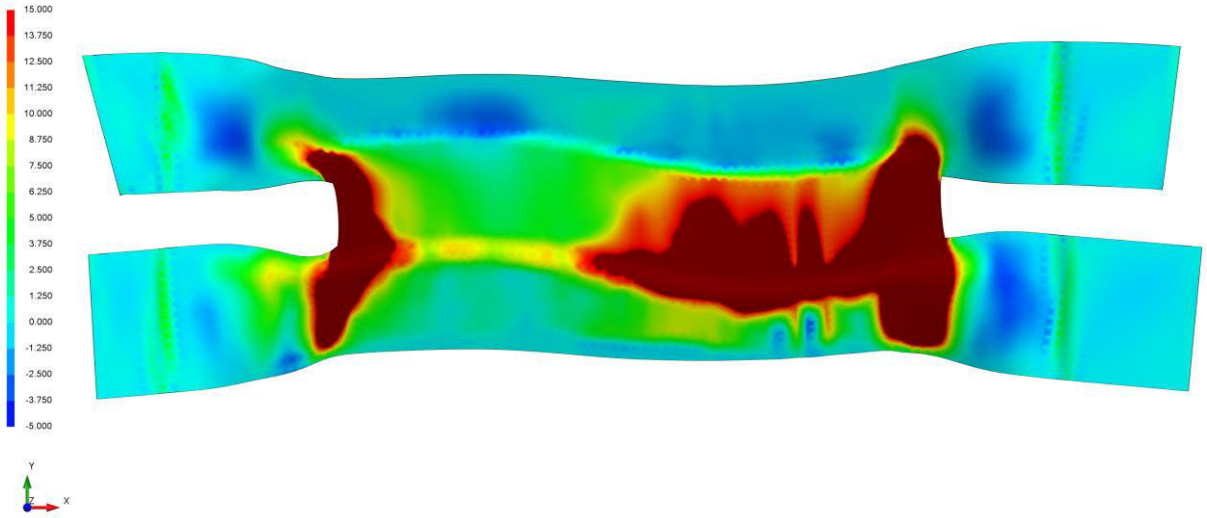
Fiber stress 1
s



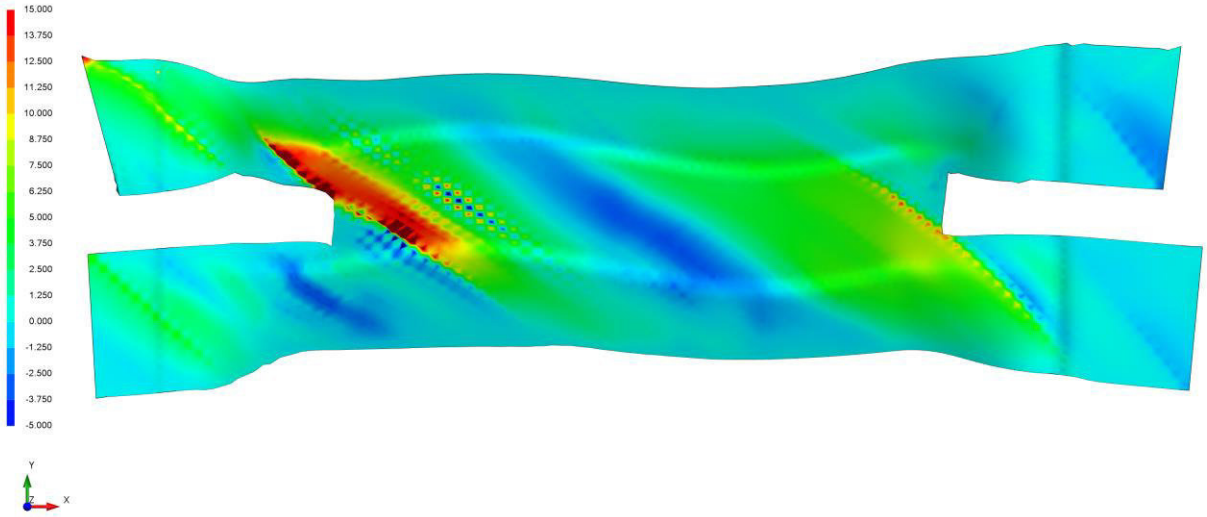
Fiber stress 1
s



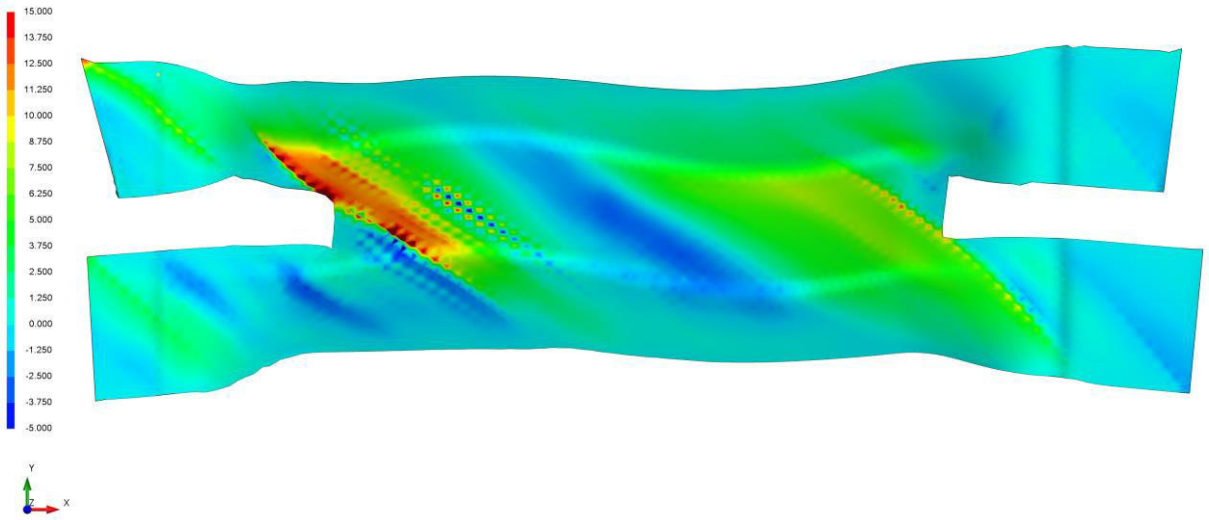
Fiber stress 2
s



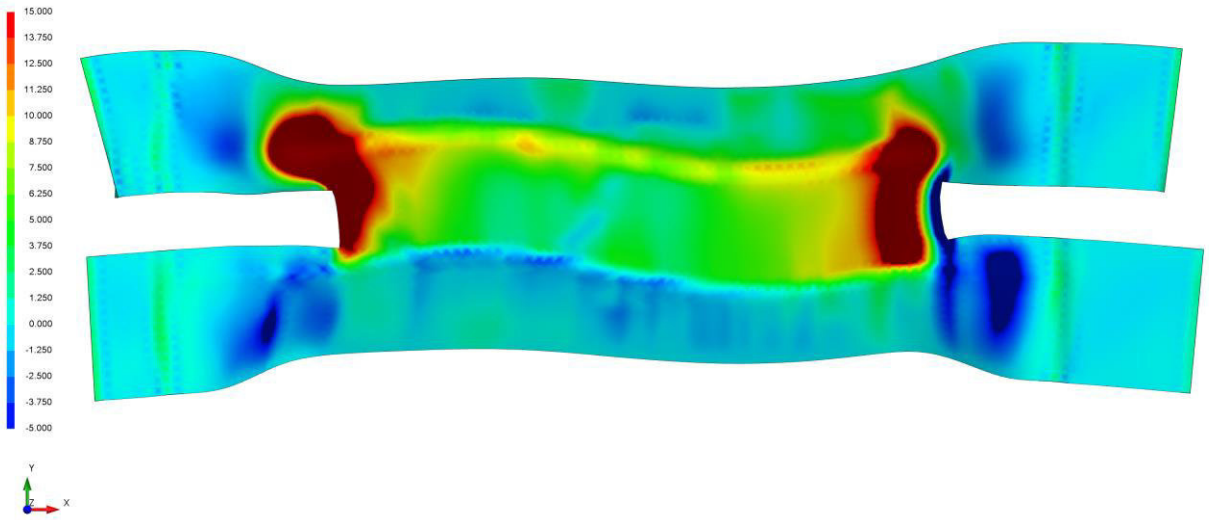
Fiber stress 2
s



Fiber stress 2
s

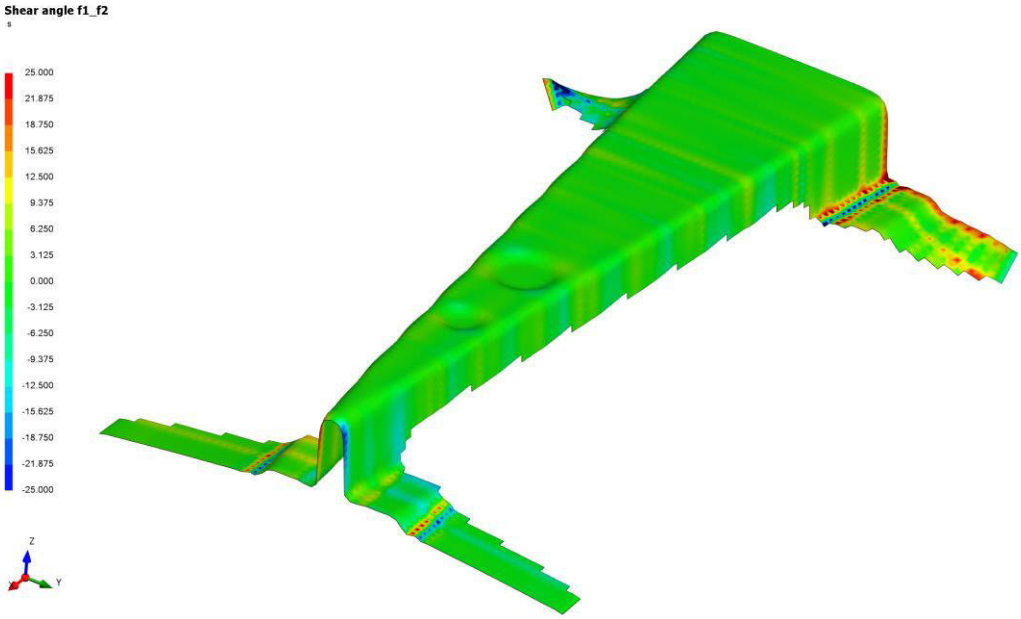


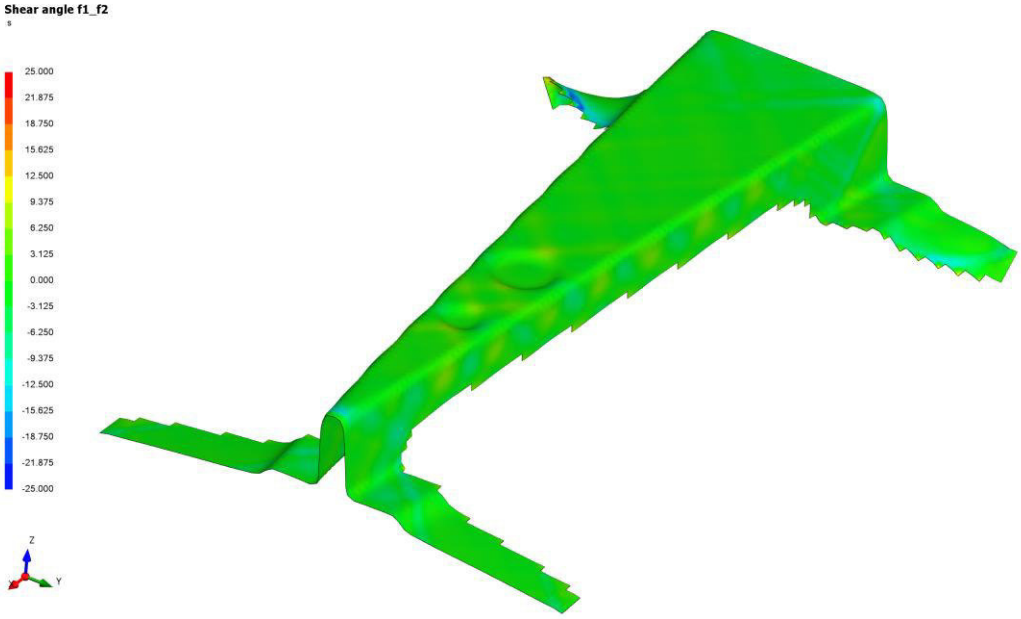
Fiber stress 2
s

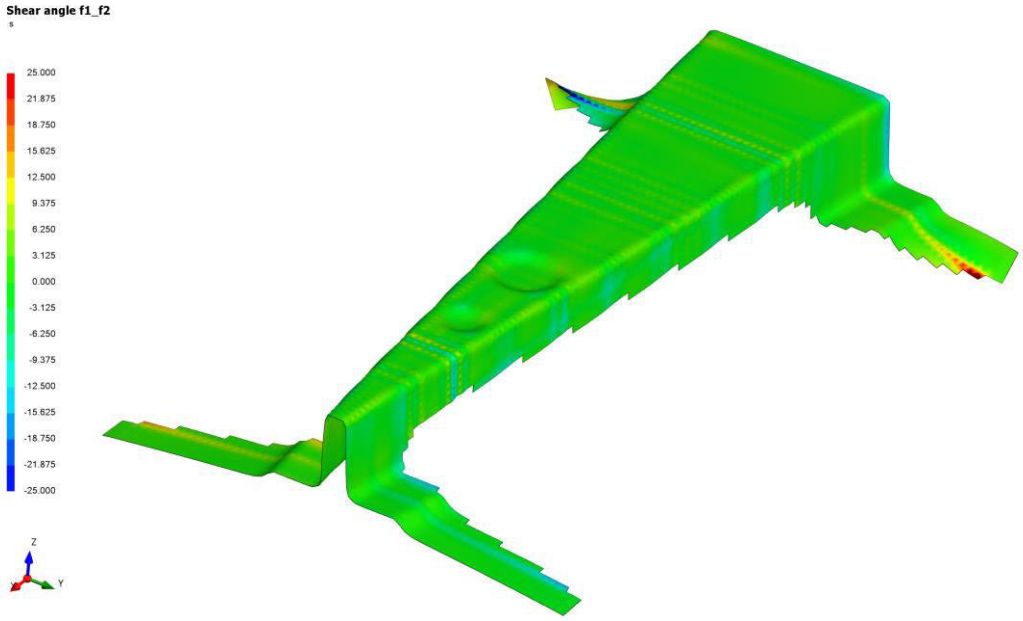


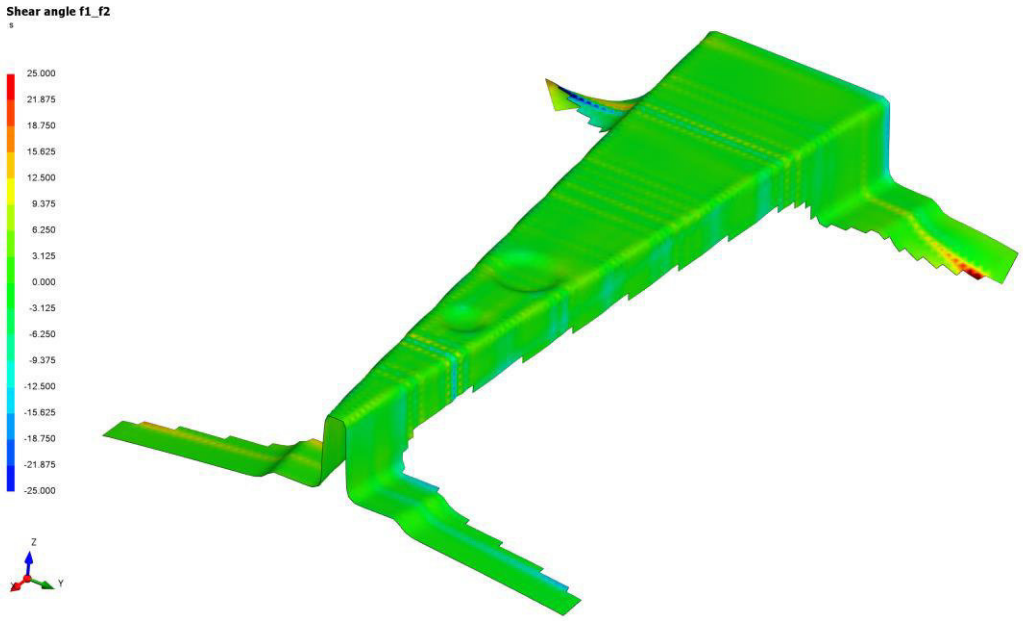
D.4 Rib Results

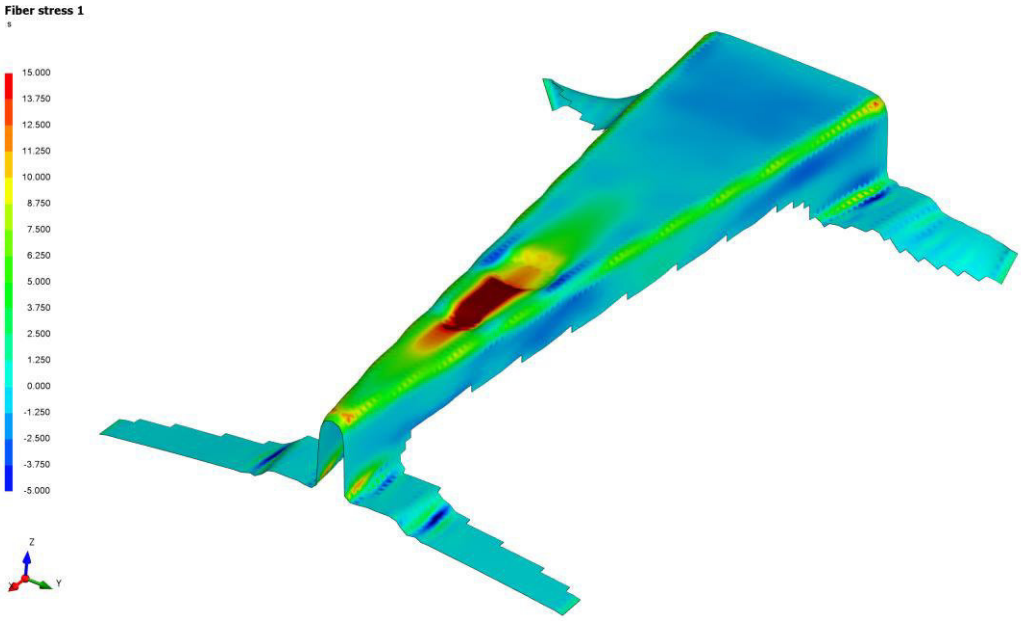
Page intentionally left blank

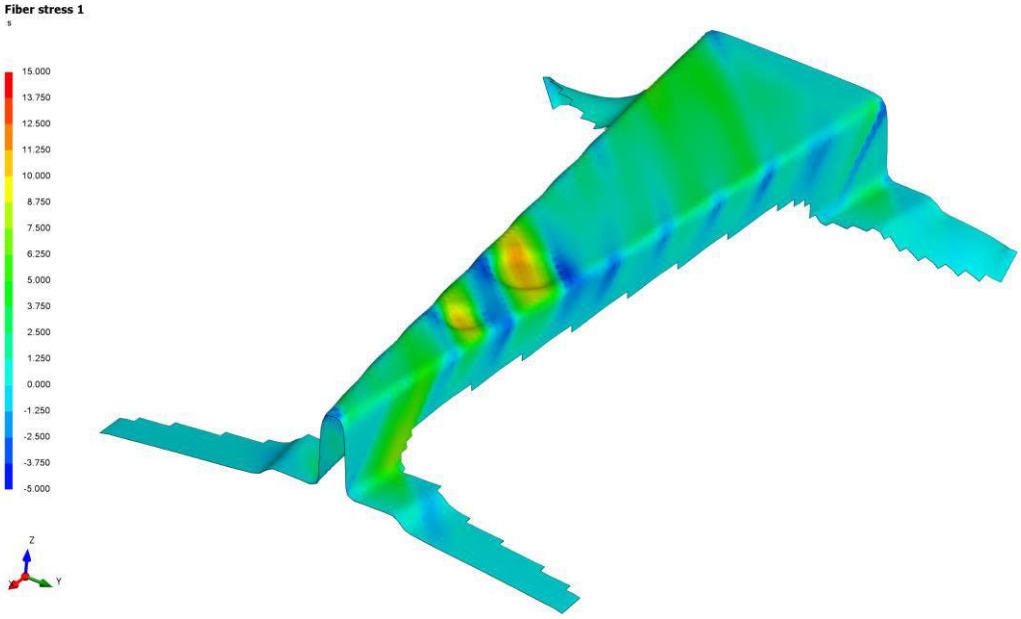

Shear angle f1_f2
s
25.000
21.875
18.750
15.625
12.500
9.375
6.250
3.125
0.000
-3.125
-6.250
-9.375
-12.500
-15.625
-18.750
-21.875
-25.000
Z
Y

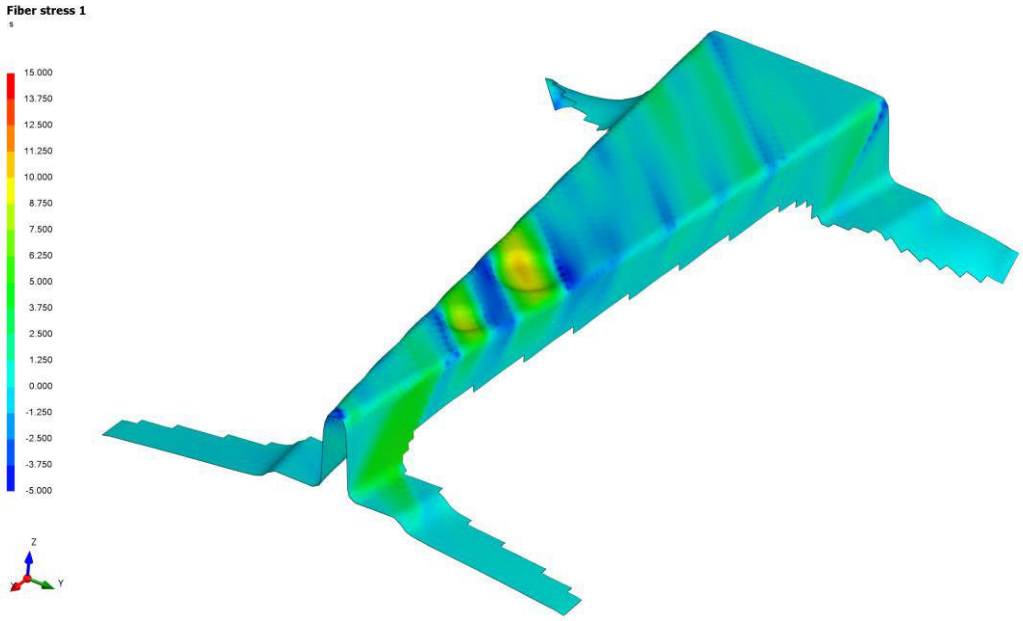

Shear angle f1_f2
s
25.000
21.875
18.750
15.625
12.500
9.375
6.250
3.125
0.000
-3.125
-6.250
-9.375
-12.500
-15.625
-18.750
-21.875
-25.000
Z
Y

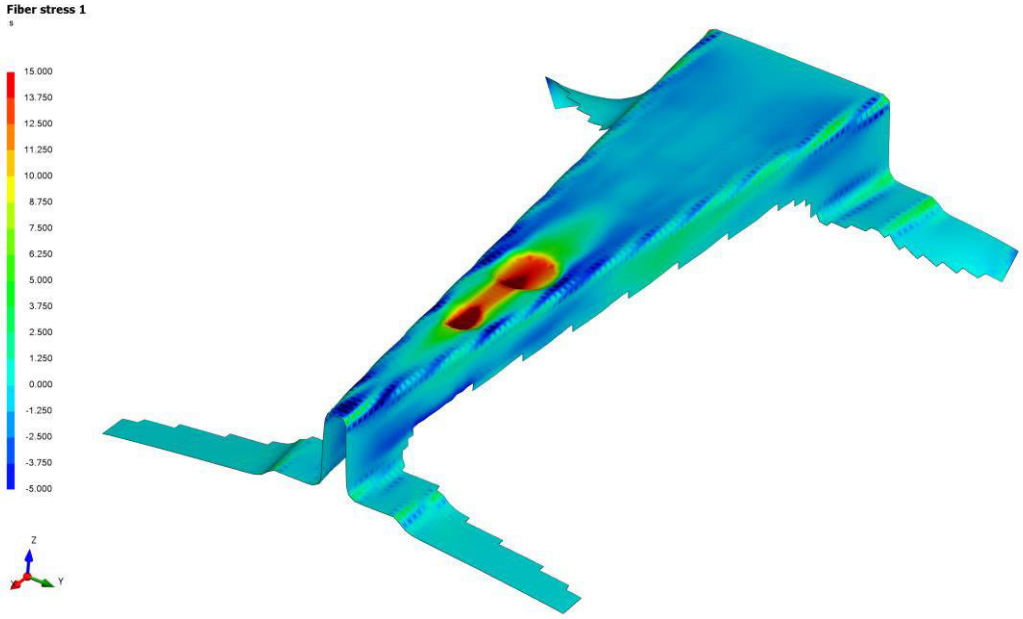

Shear angle f1_f2
s
25.000
21.875
18.750
15.625
12.500
9.375
6.250
3.125
0.000
-3.125
-6.250
-9.375
-12.500
-15.625
-18.750
-21.875
-25.000
Z
Y

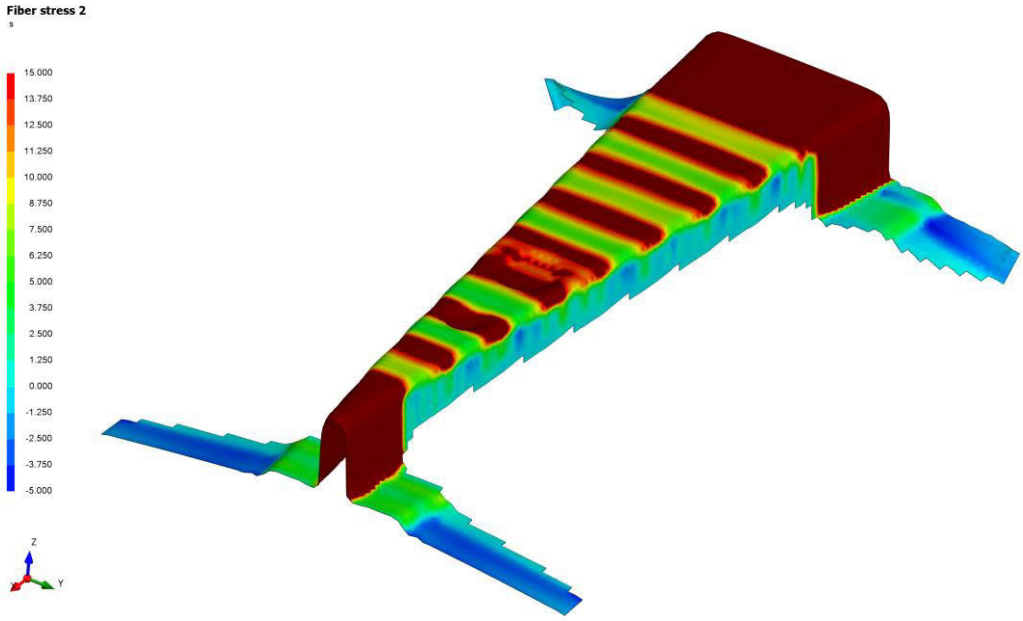

Shear angle f1_f2
s
25.000
21.875
18.750
15.625
12.500
9.375
6.250
3.125
0.000
-3.125
-6.250
-9.375
-12.500
-15.625
-18.750
-21.875
-25.000
Z
Y

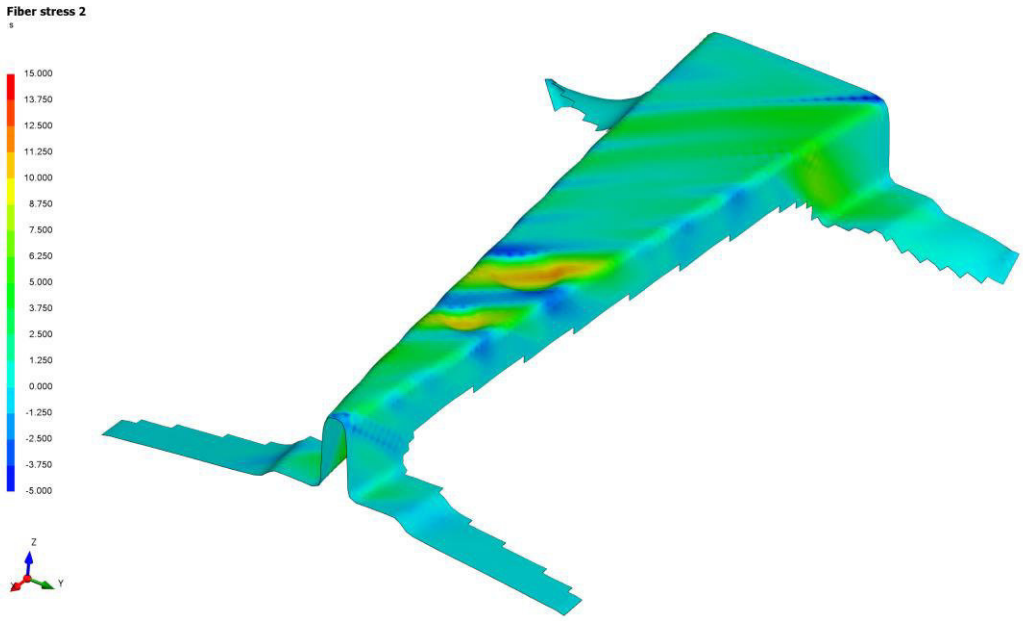

Fiber stress 1
s
15.000
13.750
12.500
11.250
10.000
8.750
7.500
6.250
5.000
3.750
2.500
1.250
0.000
-1.250
-2.500
-3.750
-5.000
Z
Y

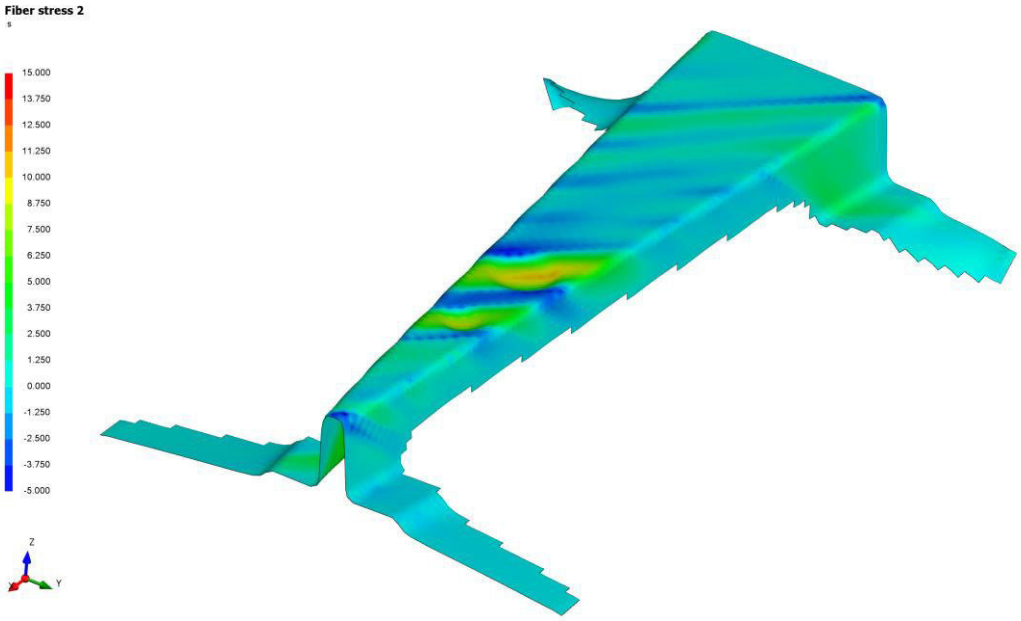

Fiber stress 1
s
15.000
13.750
12.500
11.250
10.000
8.750
7.500
6.250
5.000
3.750
2.500
1.250
0.000
-1.250
-2.500
-3.750
-5.000
Z
Y

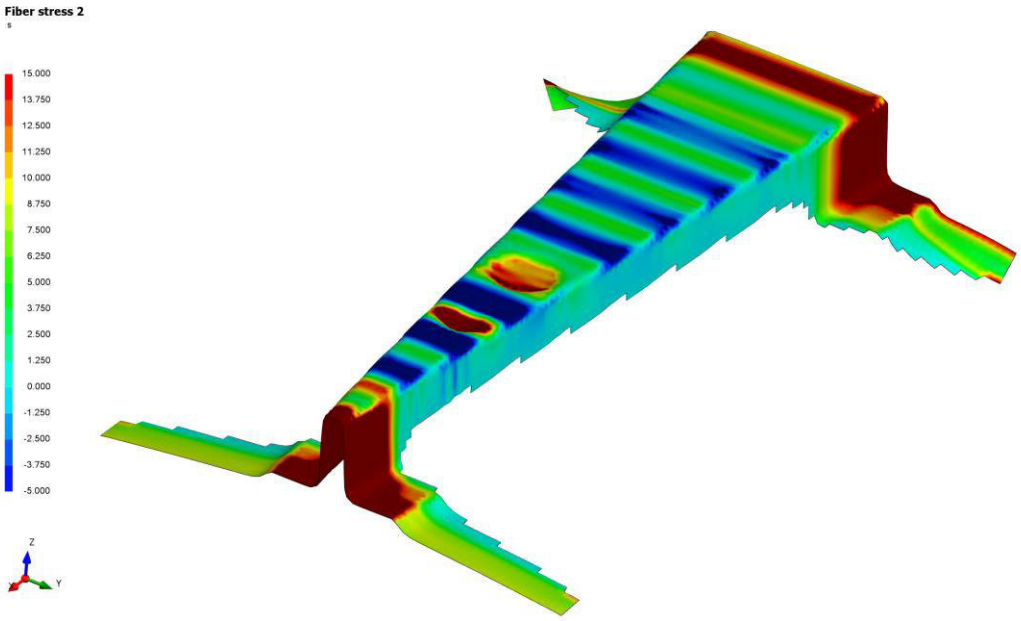

Fiber stress 1
s
15.000
13.750
12.500
11.250
10.000
8.750
7.500
6.250
5.000
3.750
2.500
1.250
0.000
-1.250
-2.500
-3.750
-5.000
Z
Y


Fiber stress 1
s
15.000
13.750
12.500
11.250
10.000
8.750
7.500
6.250
5.000
3.750
2.500
1.250
0.000
-1.250
-2.500
-3.750
-5.000
Z
Y


Fiber stress 2
s
15.000
13.750
12.500
11.250
10.000
8.750
7.500
6.250
5.000
3.750
2.500
1.250
0.000
-1.250
-2.500
-3.750
-5.000
Z
Y


Fiber stress 2
s
15.000
13.750
12.500
11.250
10.000
8.750
7.500
6.250
5.000
3.750
2.500
1.250
0.000
-1.250
-2.500
-3.750
-5.000
Z
Y


Fiber stress 2
s
15.000
13.750
12.500
11.250
10.000
8.750
7.500
6.250
5.000
3.750
2.500
1.250
0.000
-1.250
-2.500
-3.750
-5.000
Z
Y


Fiber stress 2
s
15.000
13.750
12.500
11.250
10.000
8.750
7.500
6.250
5.000
3.750
2.500
1.250
0.000
-1.250
-2.500
-3.750
-5.000
Z
Y

Appendix E Theoretical Investigation Results

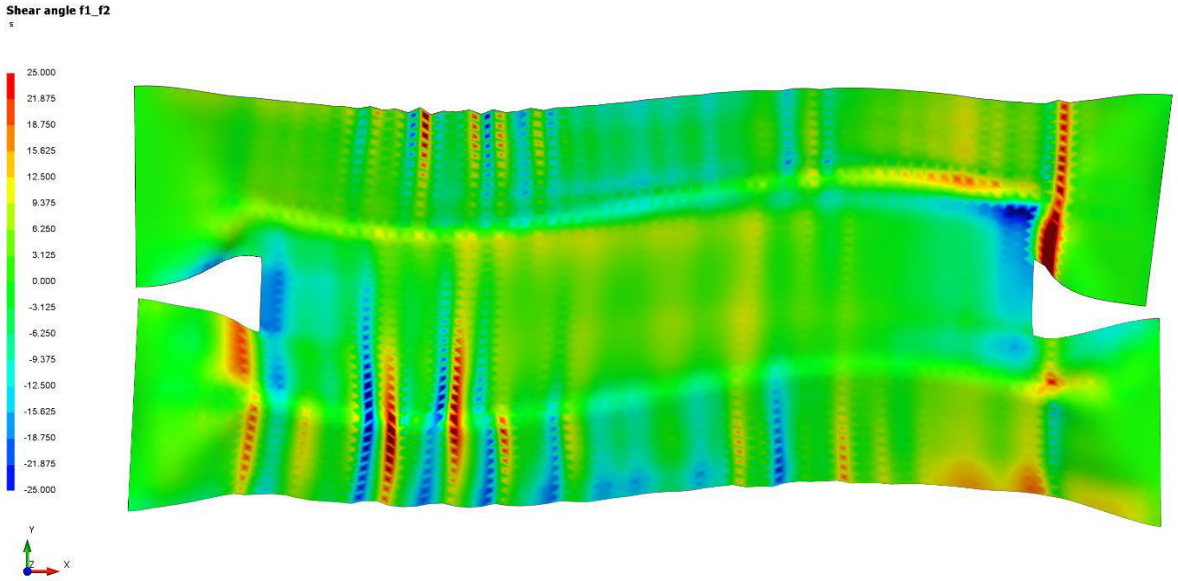
Page left intentionally blank

E.1 Tool Inclination

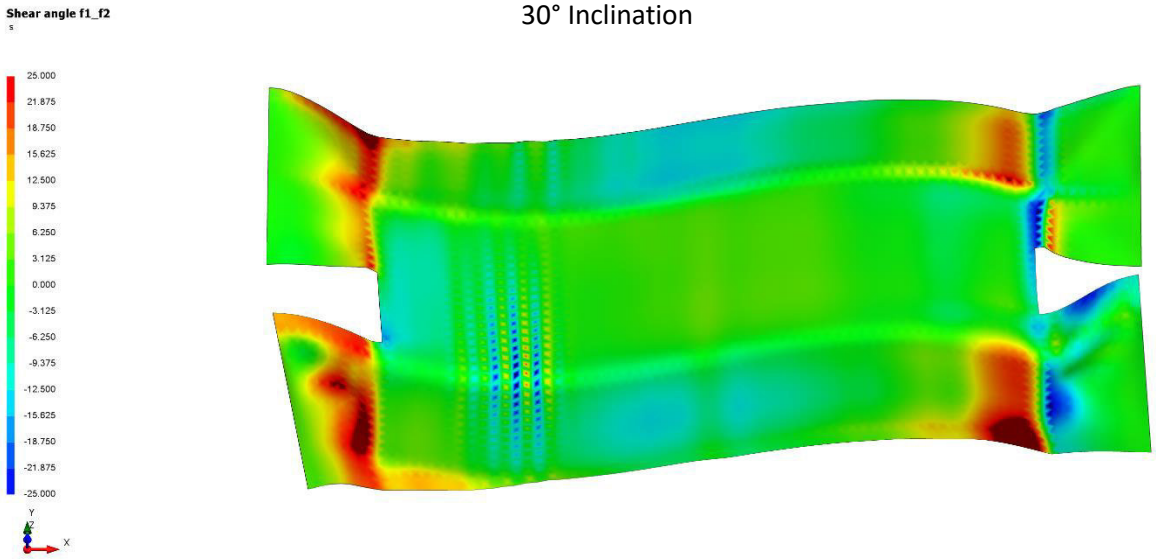
Page left intentionally blank

Shear Angle Ply 1

0° Inclination

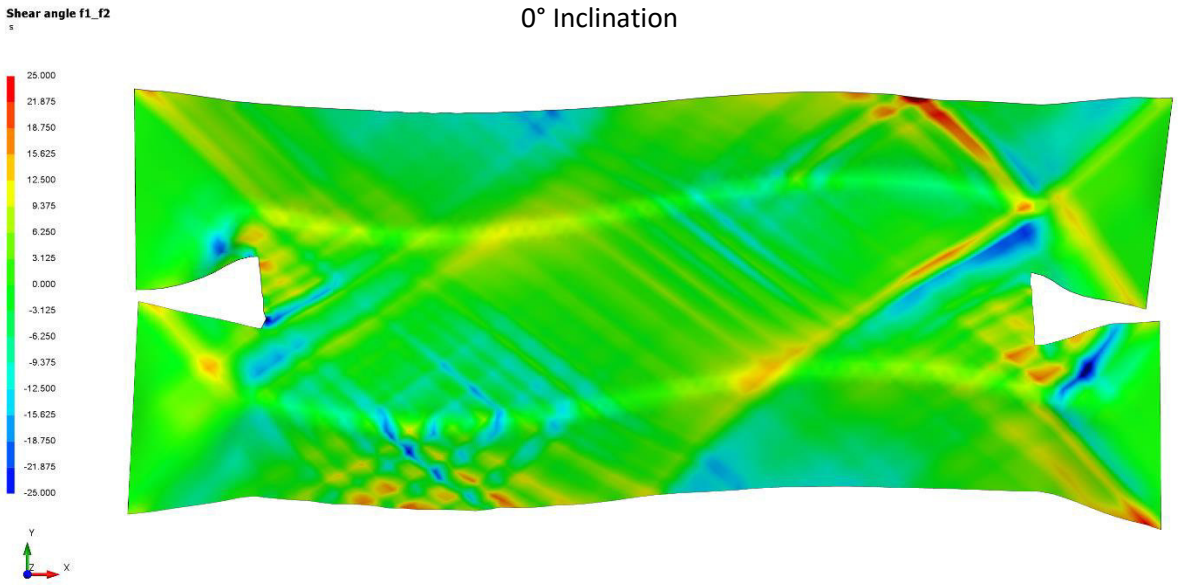


30° Inclination

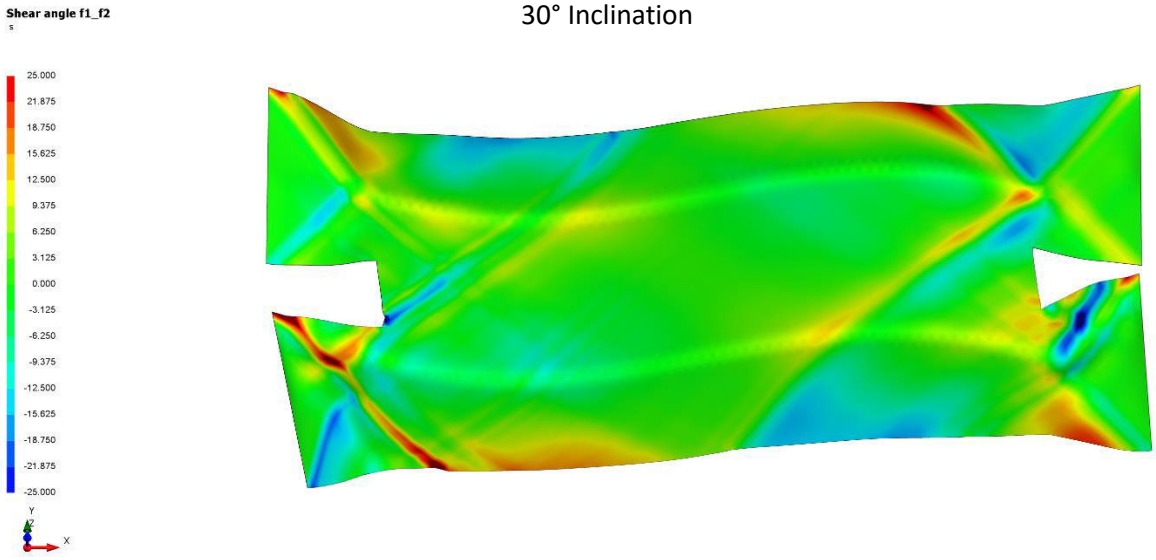


Shear Angle Ply 2 Ply 1

0° Inclination

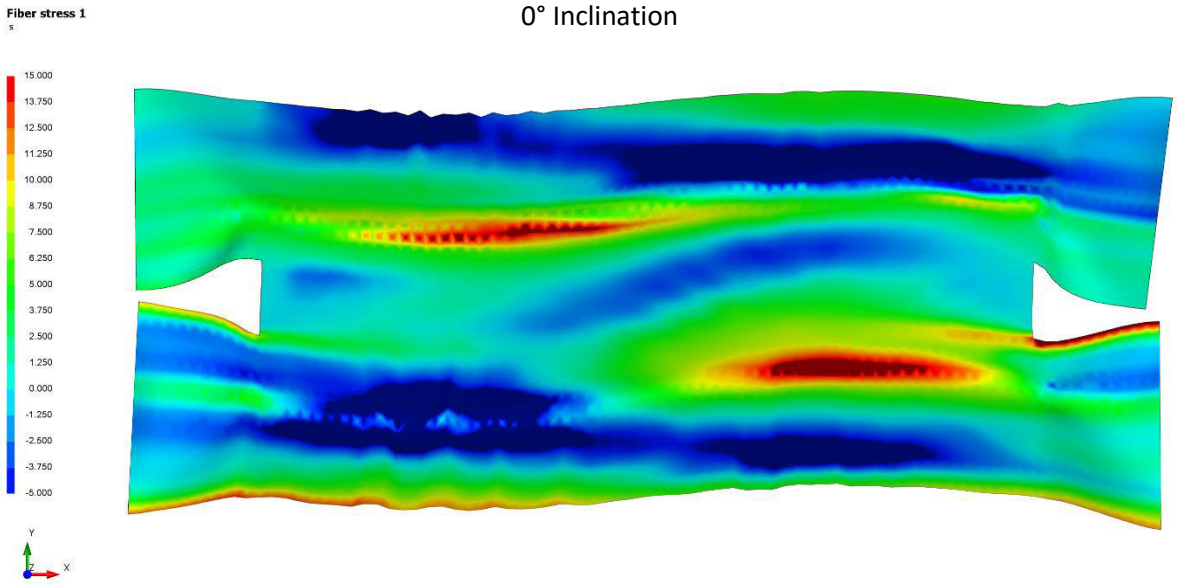


30° Inclination

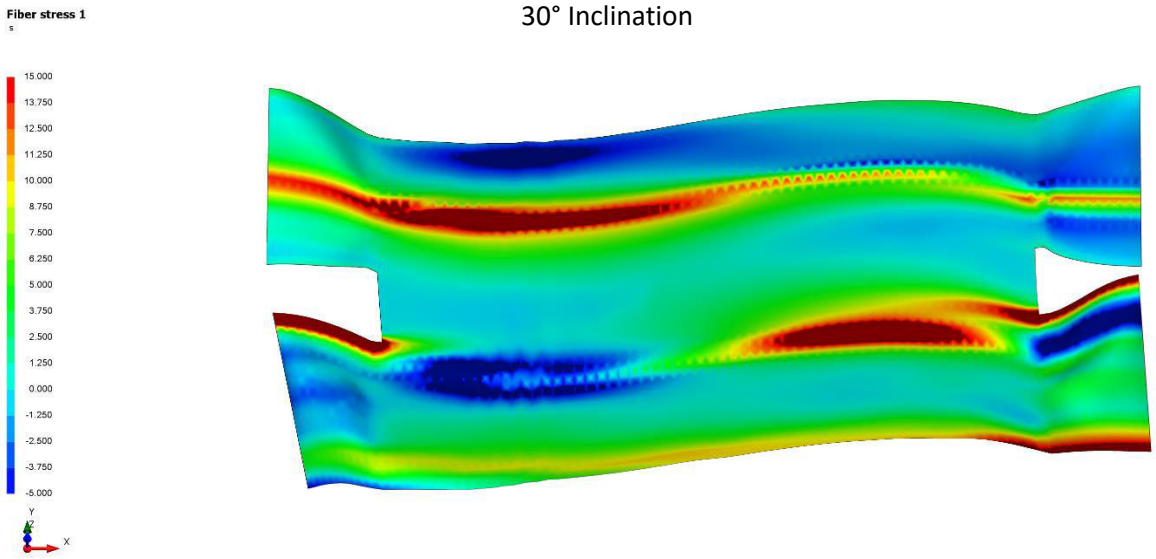


Fibre Stress 1

0° Inclination

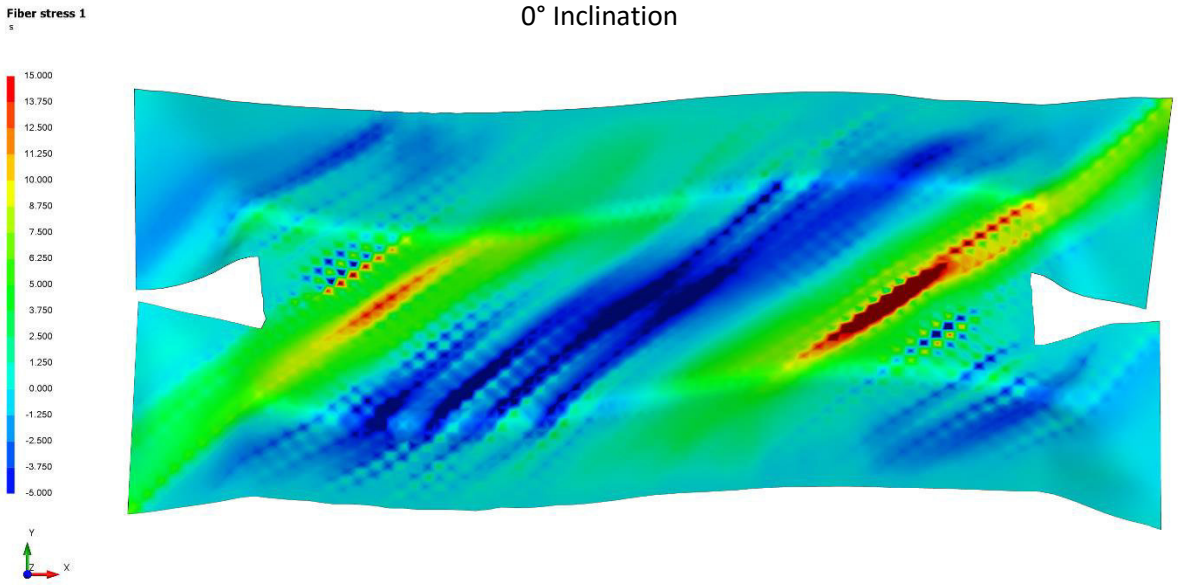


30° Inclination

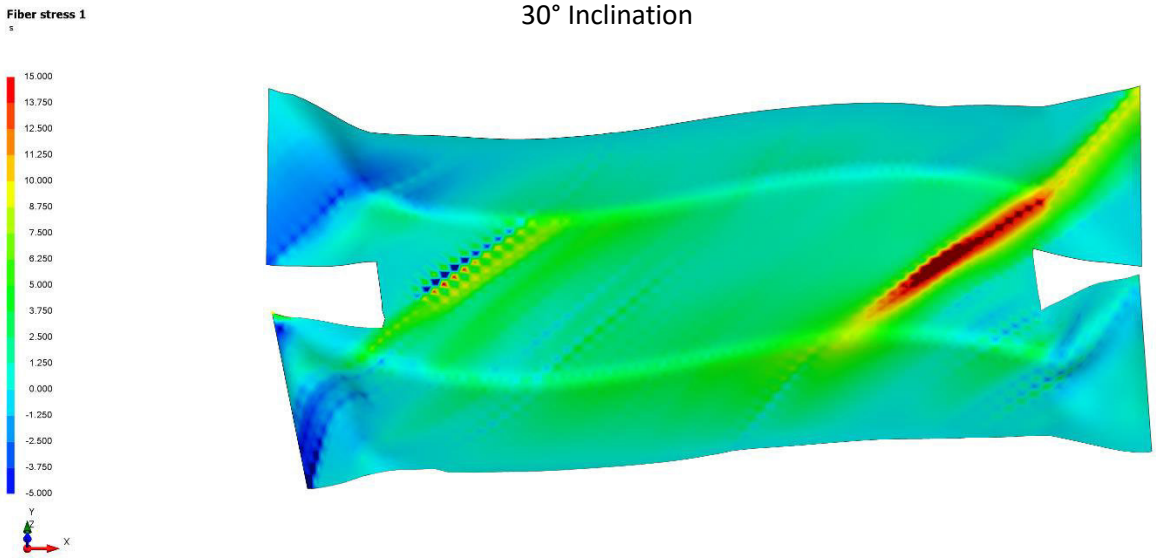


Fibre Stress 1 Ply 2

0° Inclination

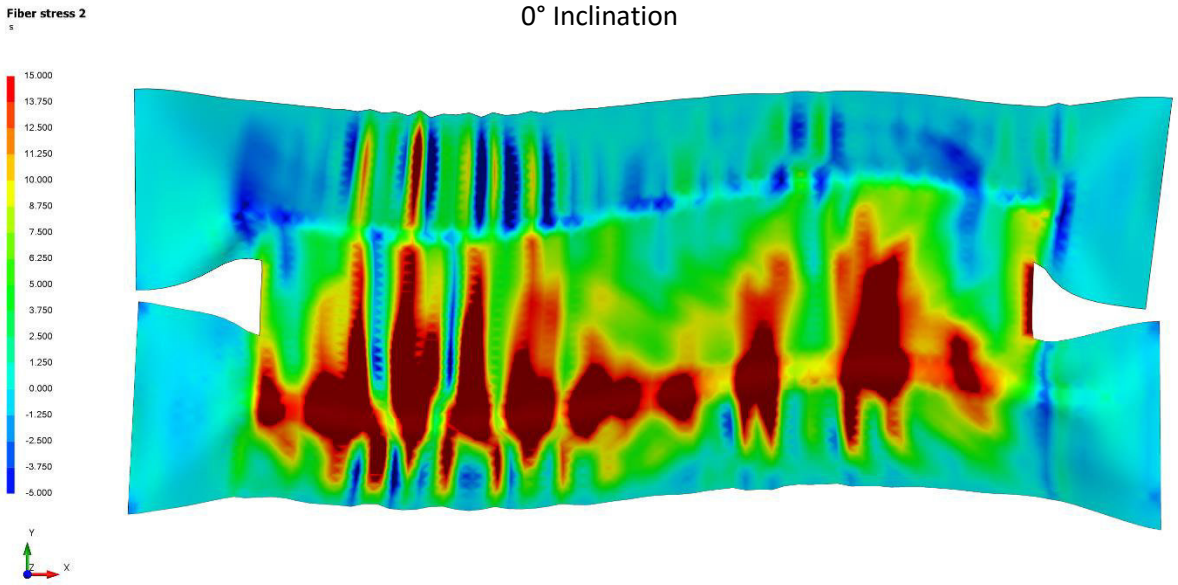


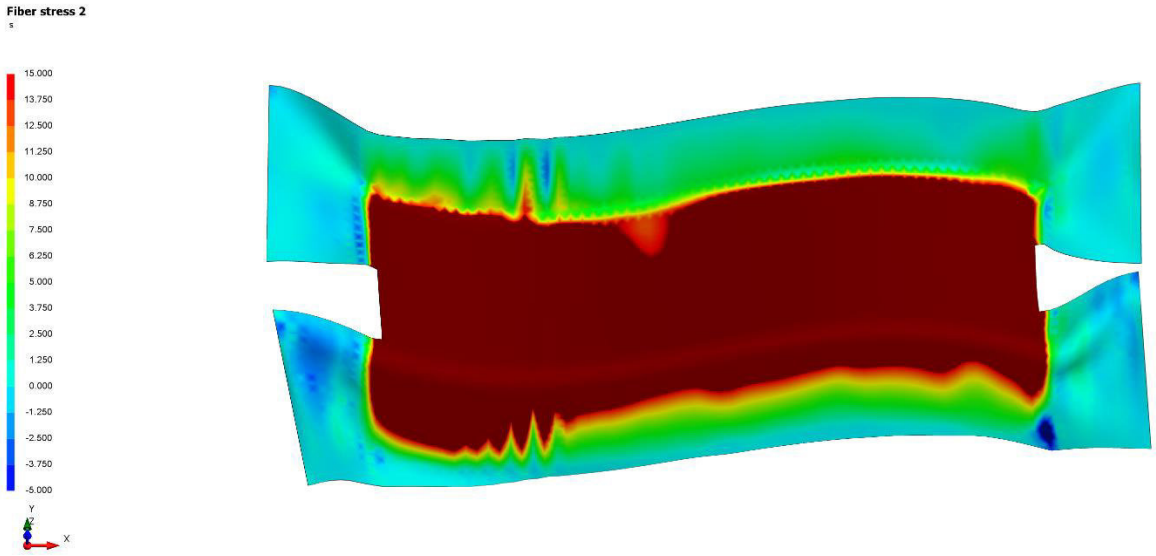
30° Inclination



Fibre Stress 2 Ply 1

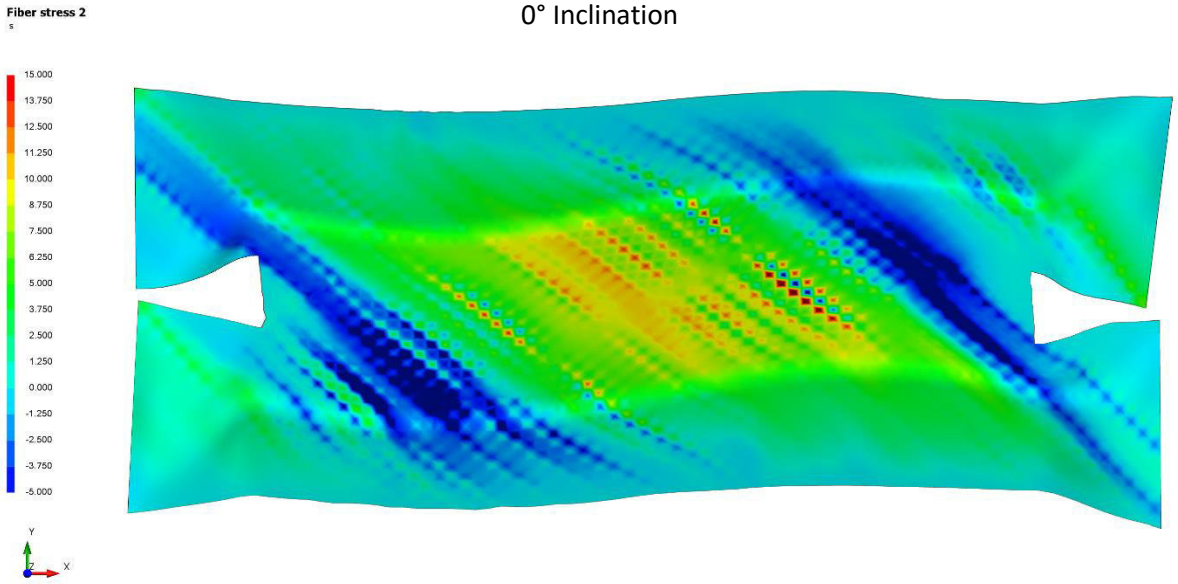
0° Inclination

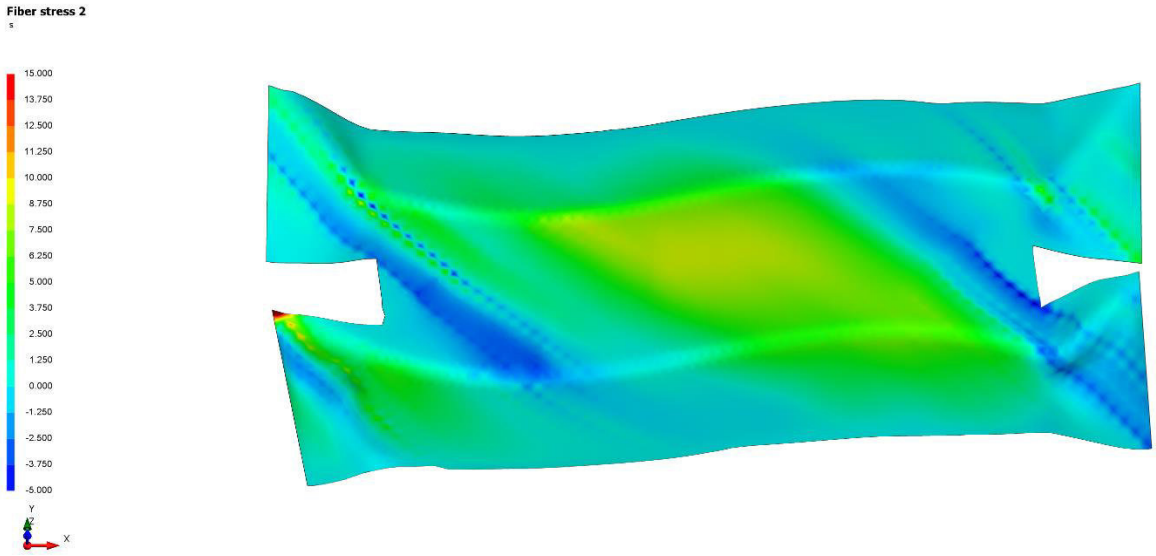




Fibre Stress 2 Ply 2

0° Inclination



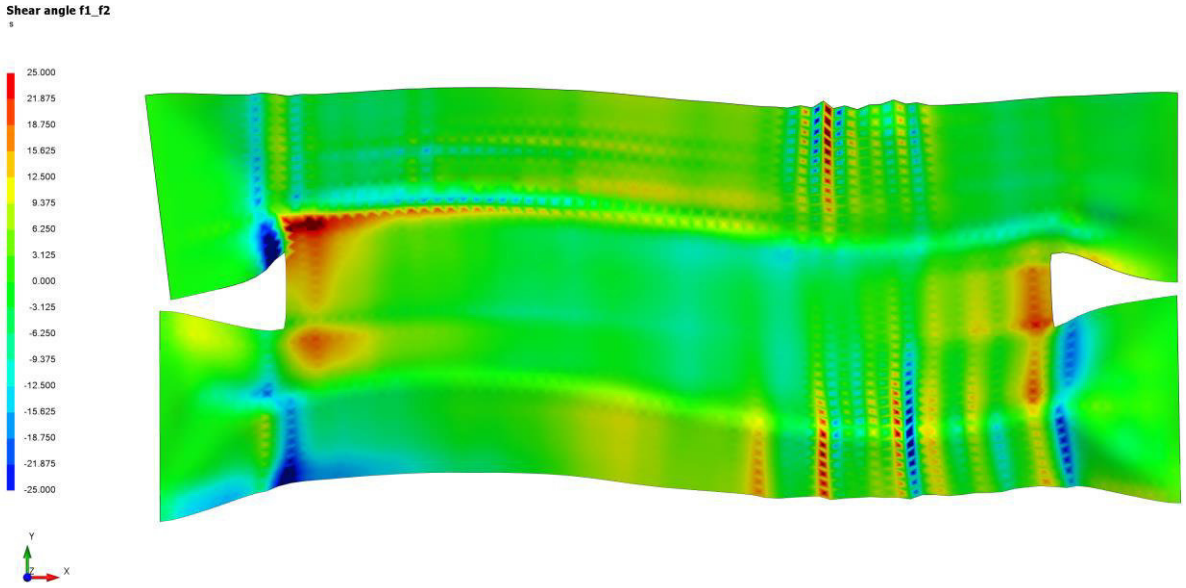


E.2 Tool Direction

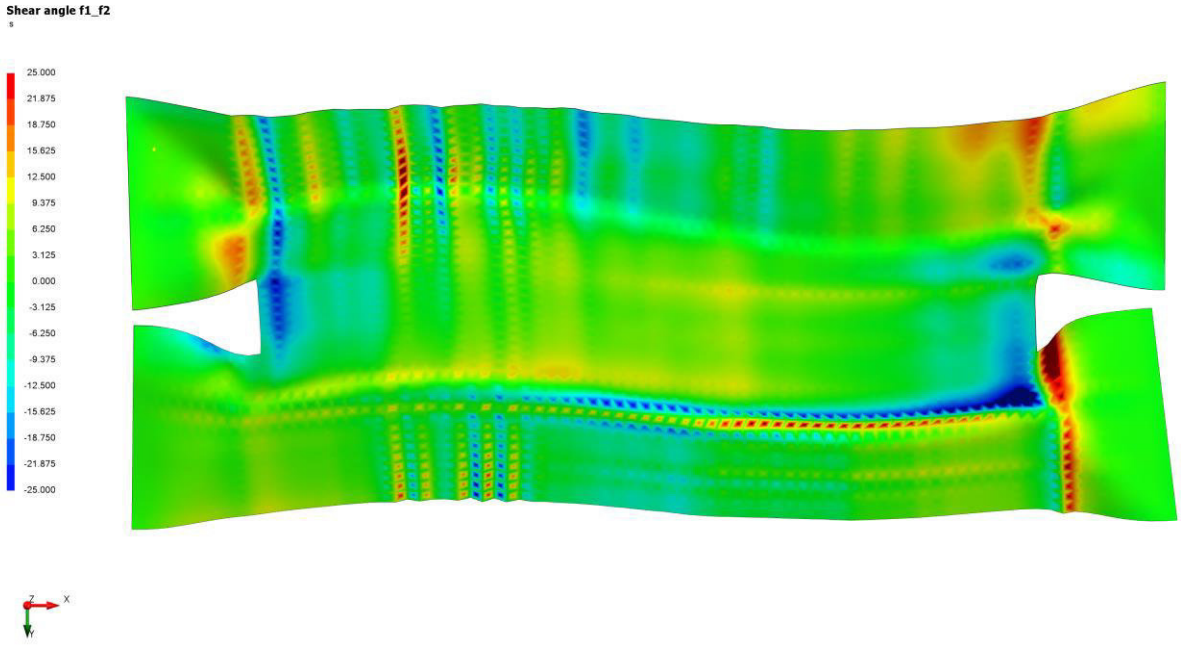
Page left intentionally blank

Shear Angle Ply 1

Direction 1

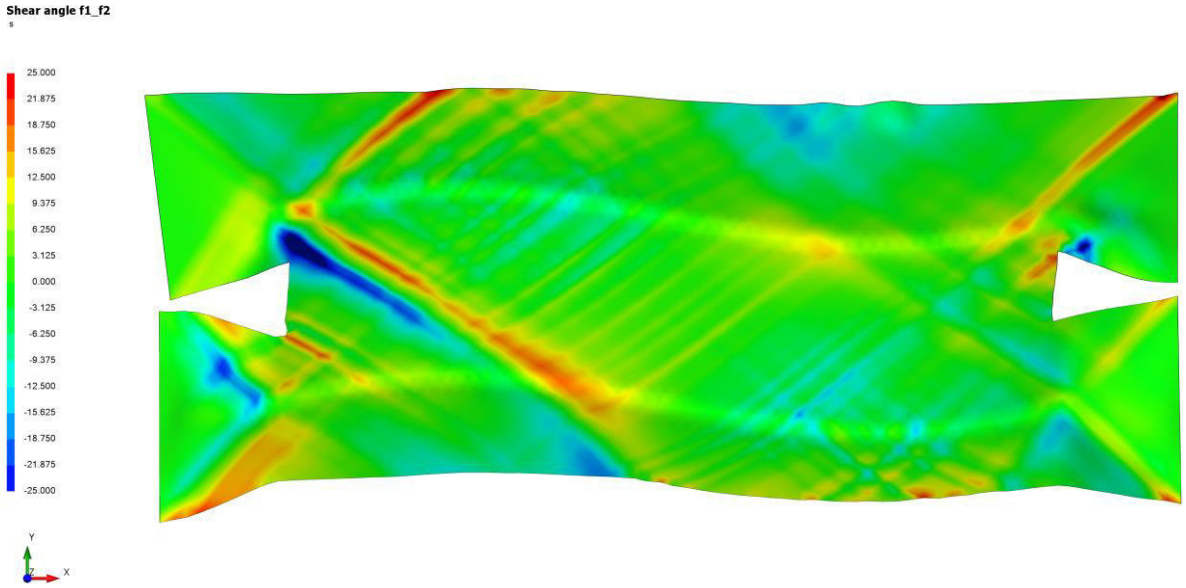


Direction 2

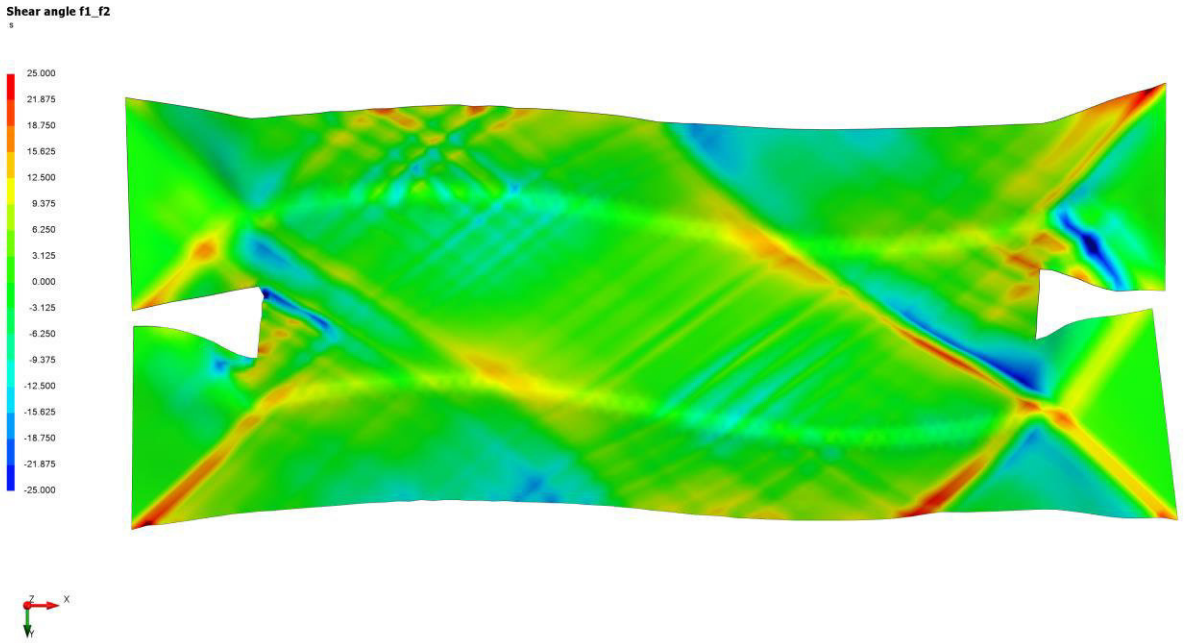


Shear Angle Ply 2

Direction 1

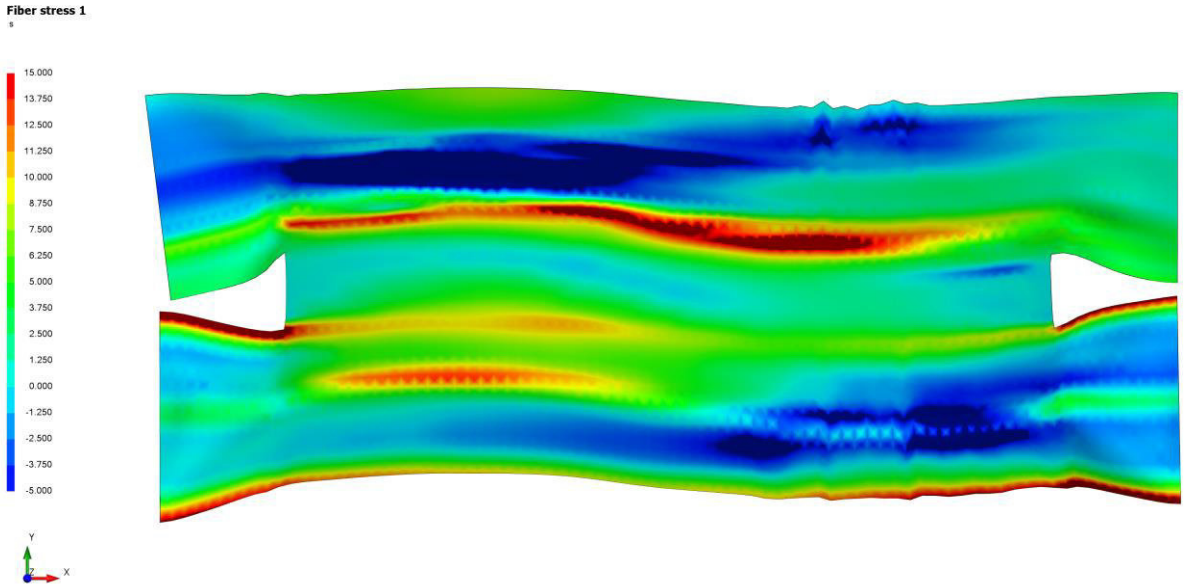


Direction 2

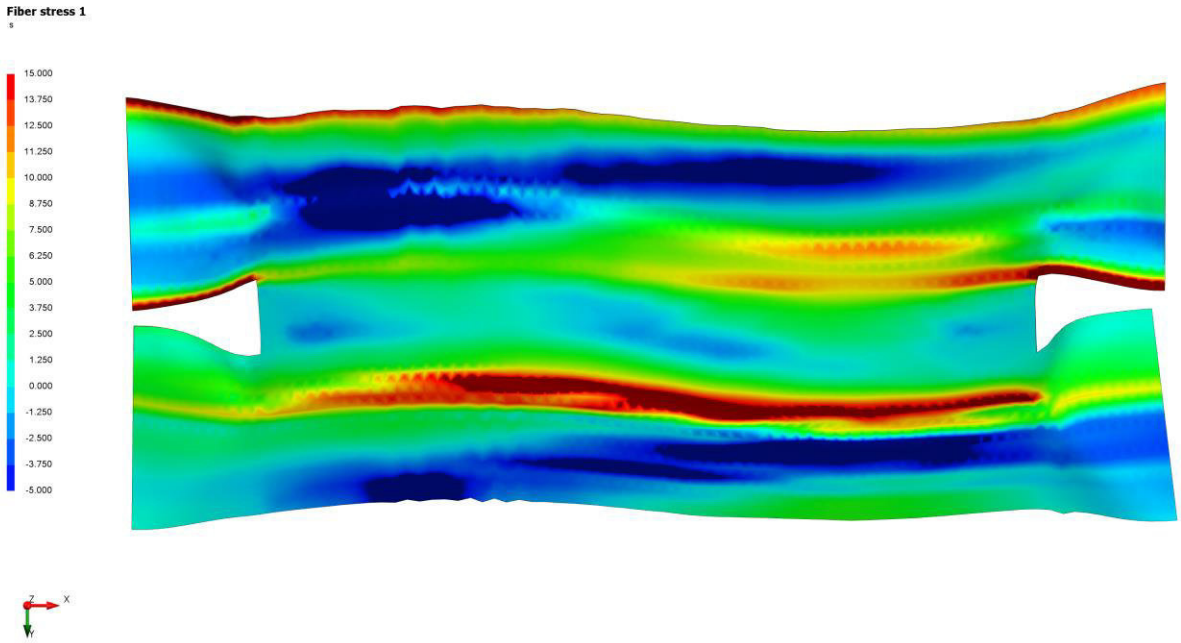


Fibre Stress 1 Ply 1

Direction 1

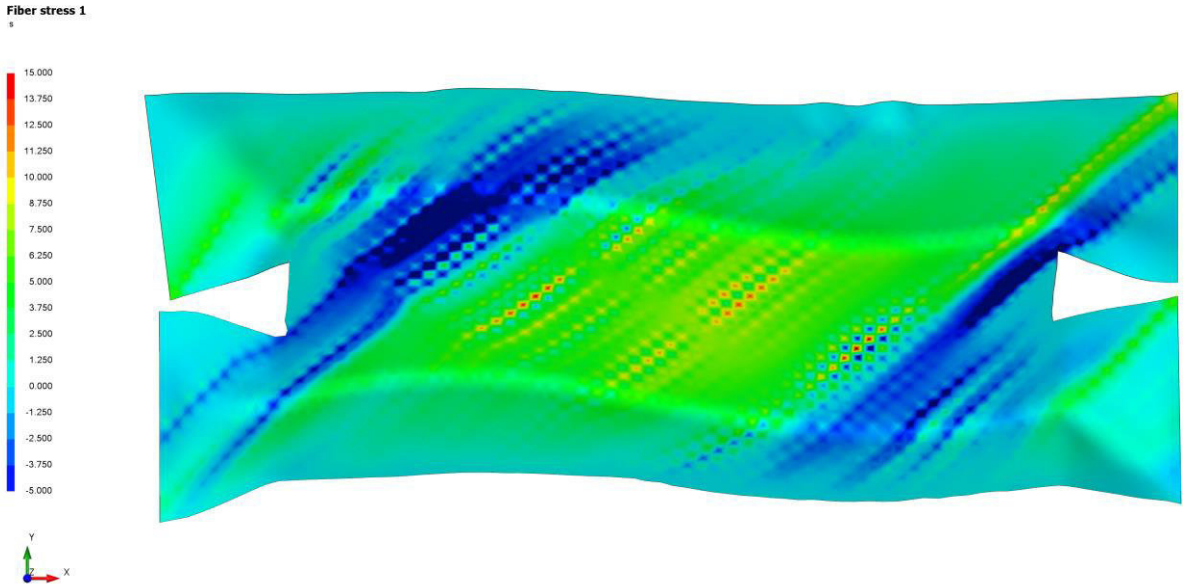


Direction 2

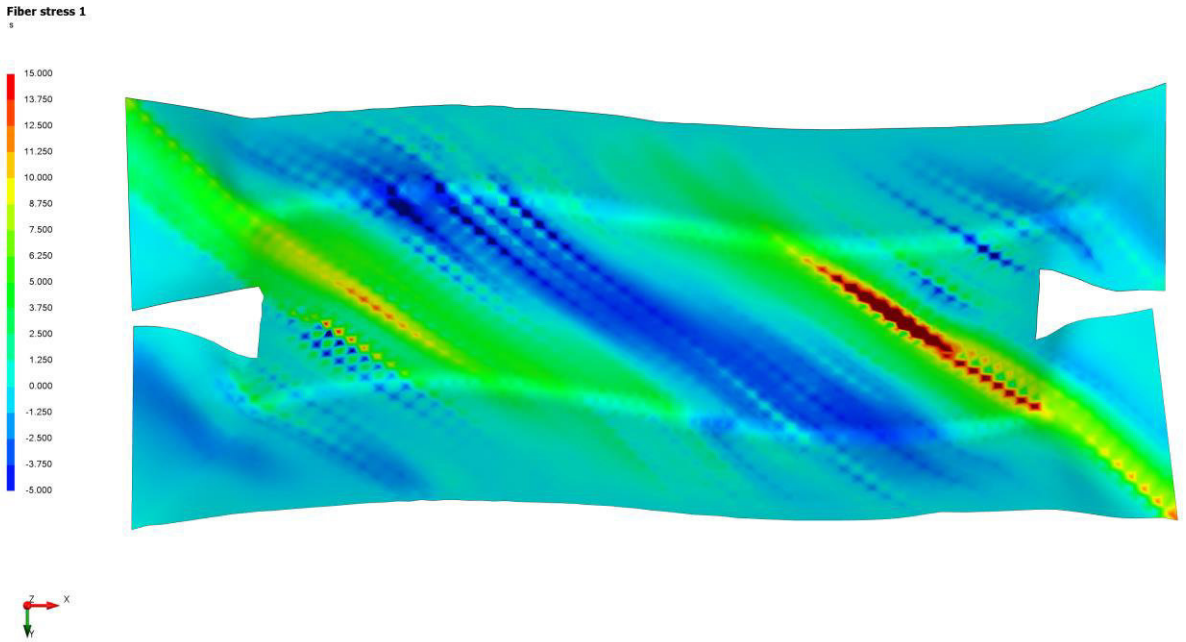


Fibre Stress 1 Ply 2

Direction 1

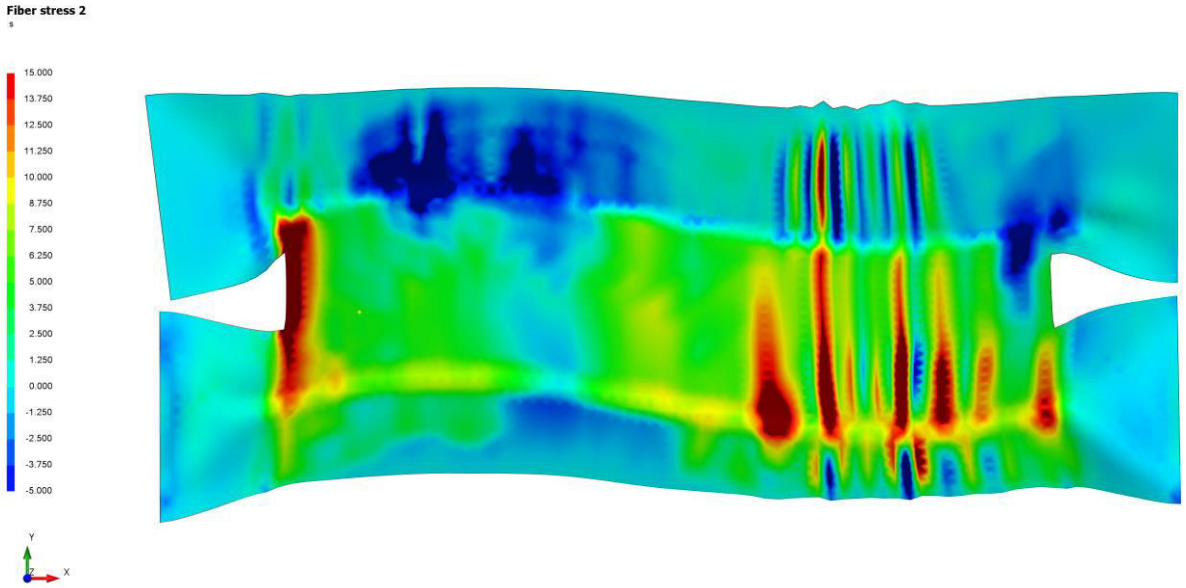


Direction 2

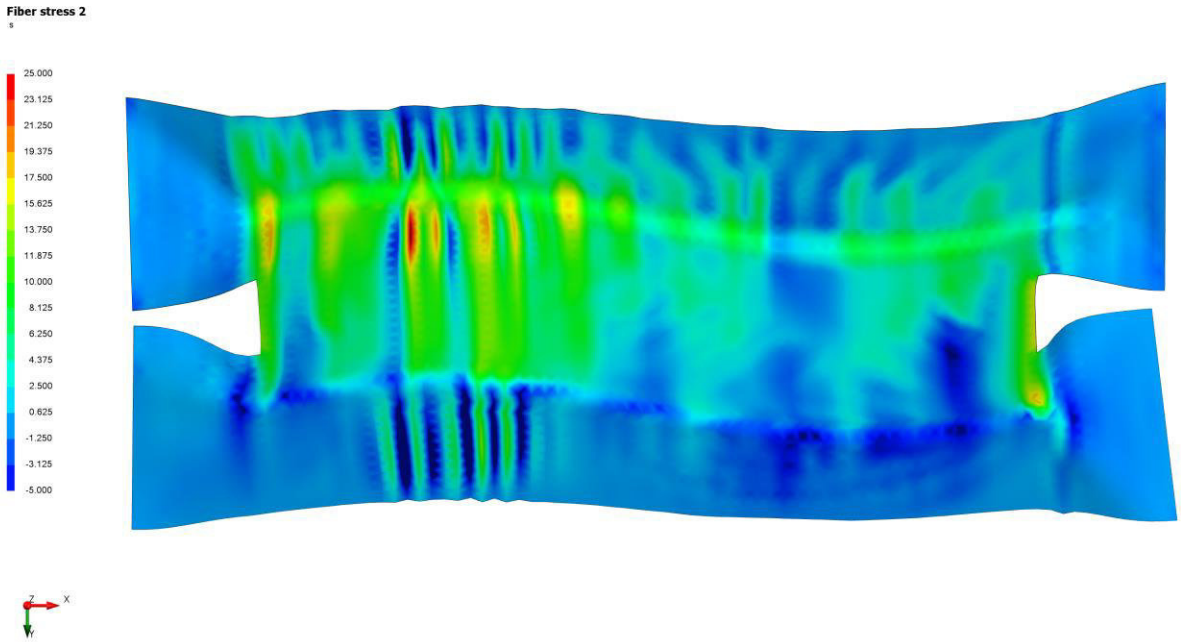


Fibre Stress 2 Ply 1

Direction 1

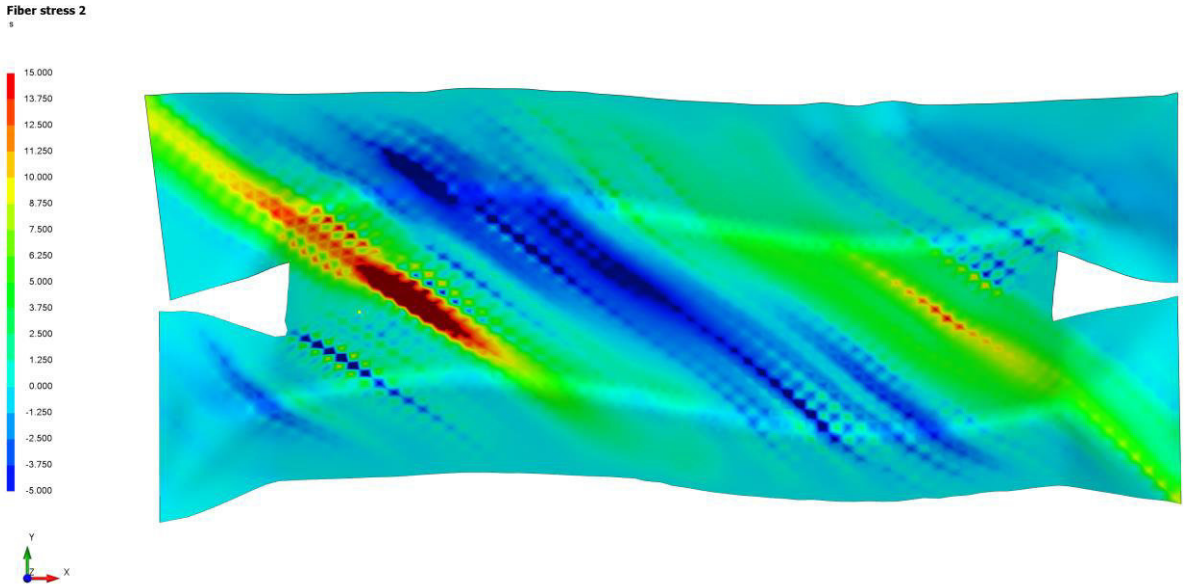


Direction 2

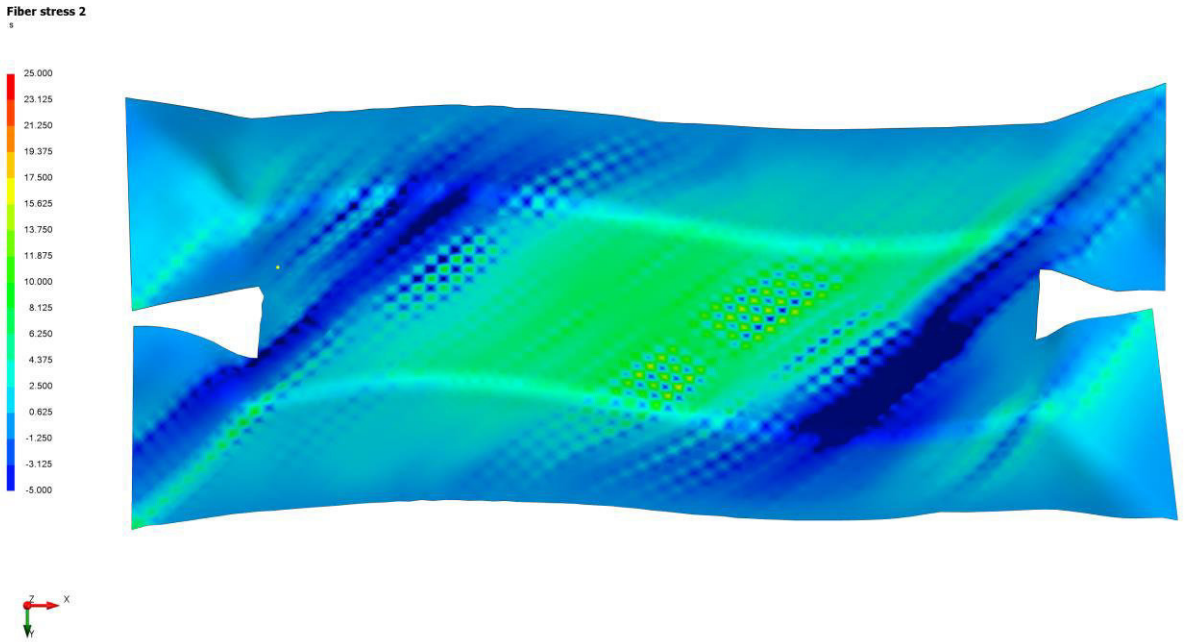


Fibre Stress 2 Ply 1

Direction 1



Direction 2

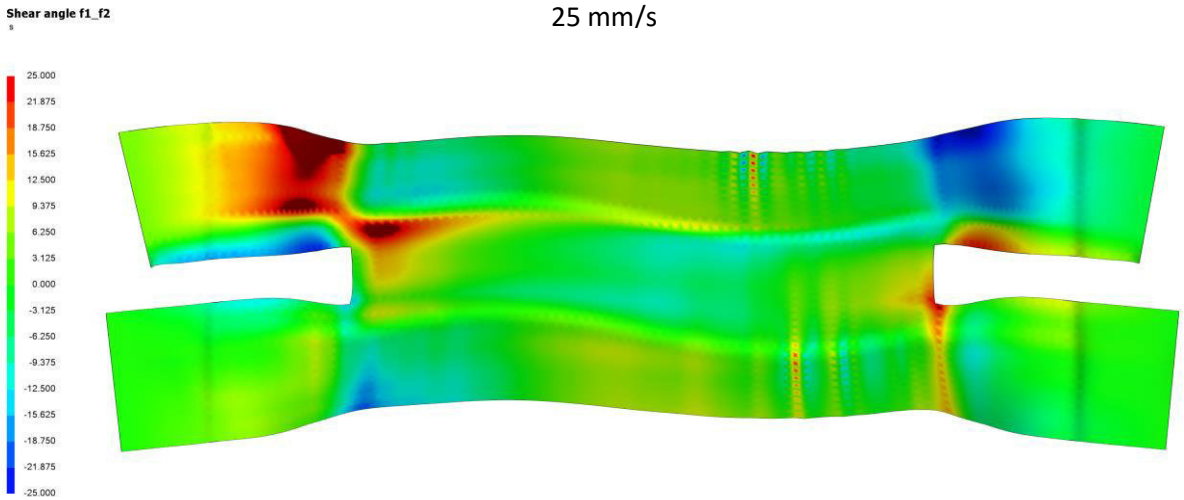


E.3 Forming Speed

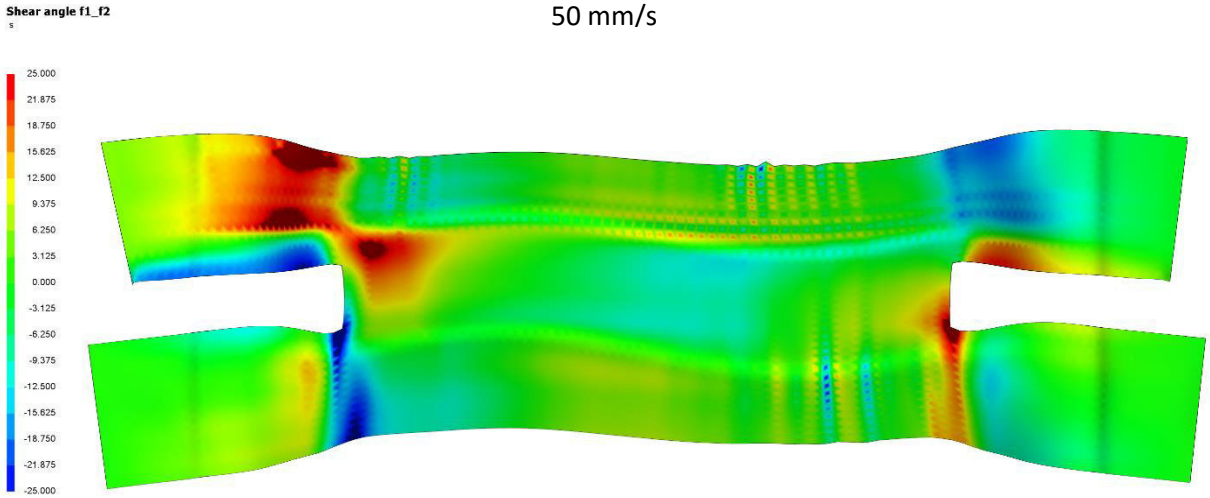
Page left intentionally blank

Shear Angle Ply 1

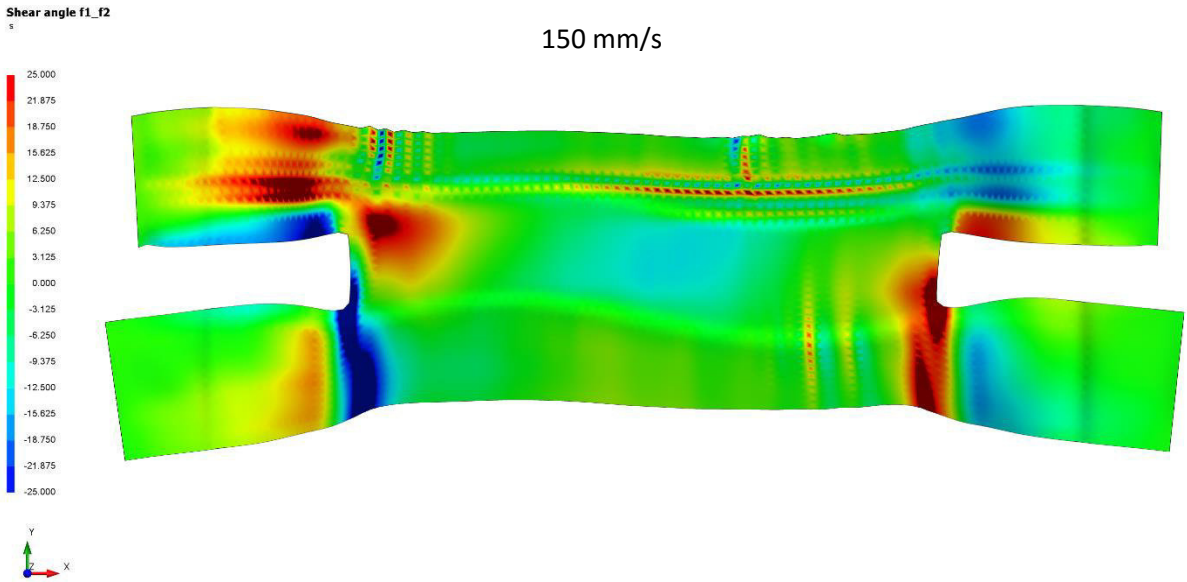
25 mm/s



50 mm/s

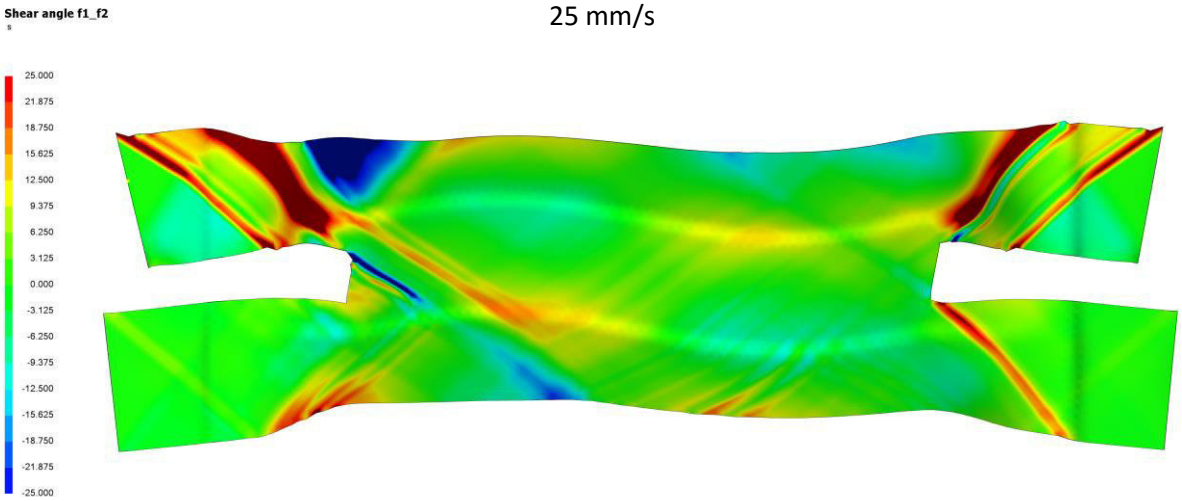


150 mm/s

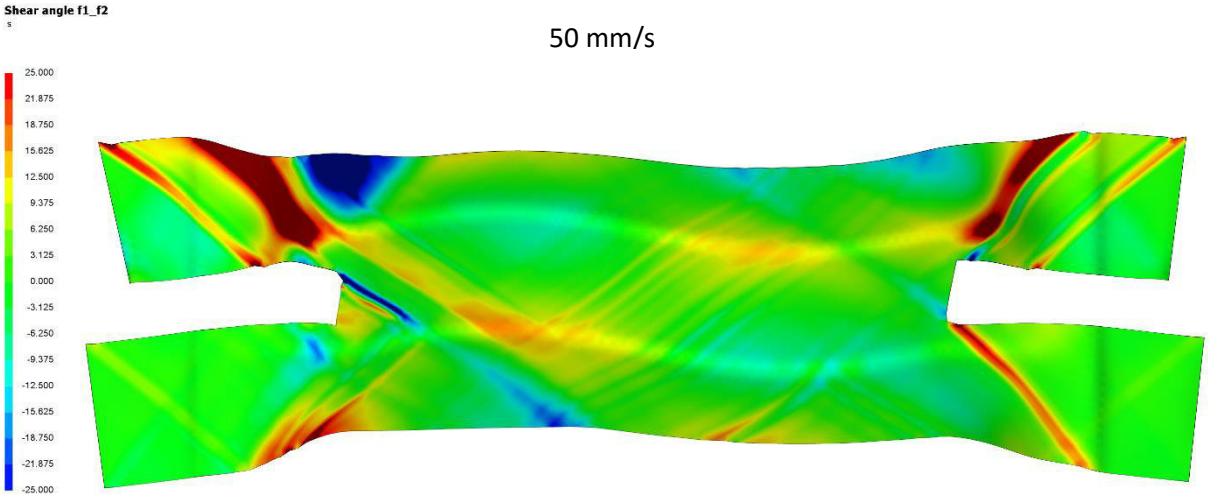


Shear Angle Ply 2

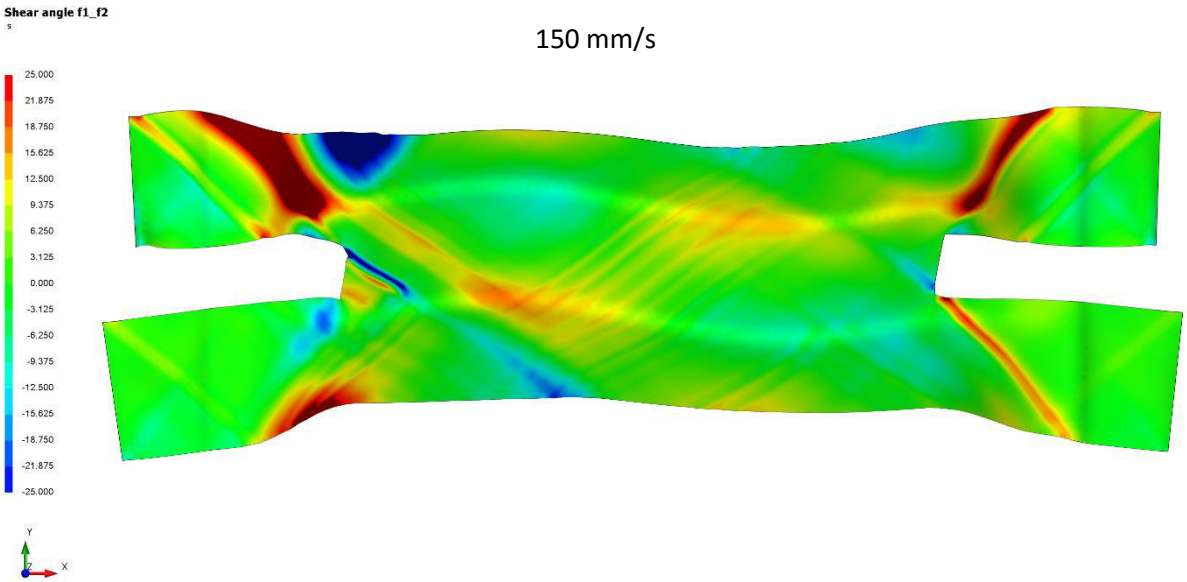
25 mm/s



50 mm/s

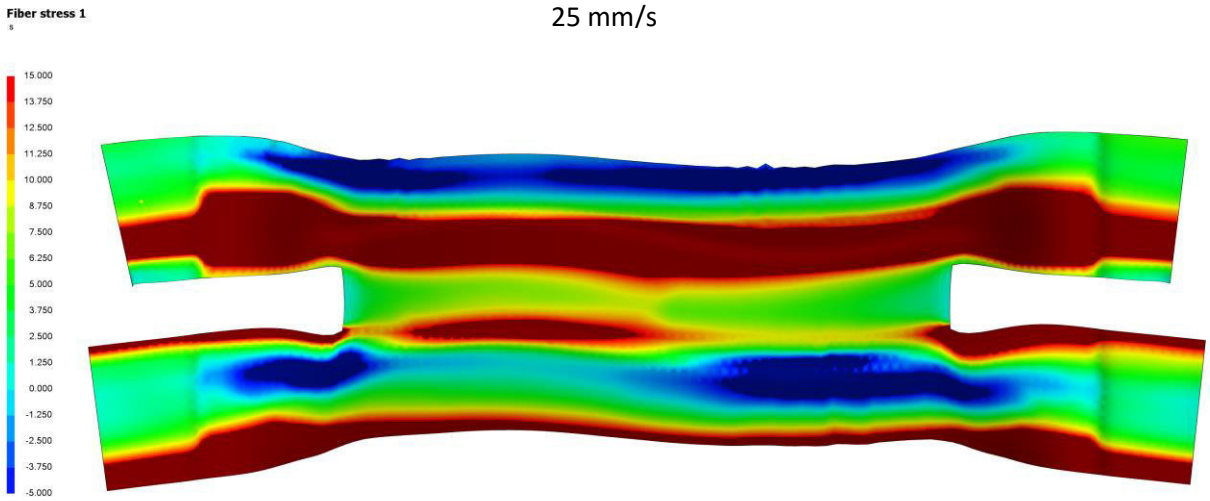


150 mm/s

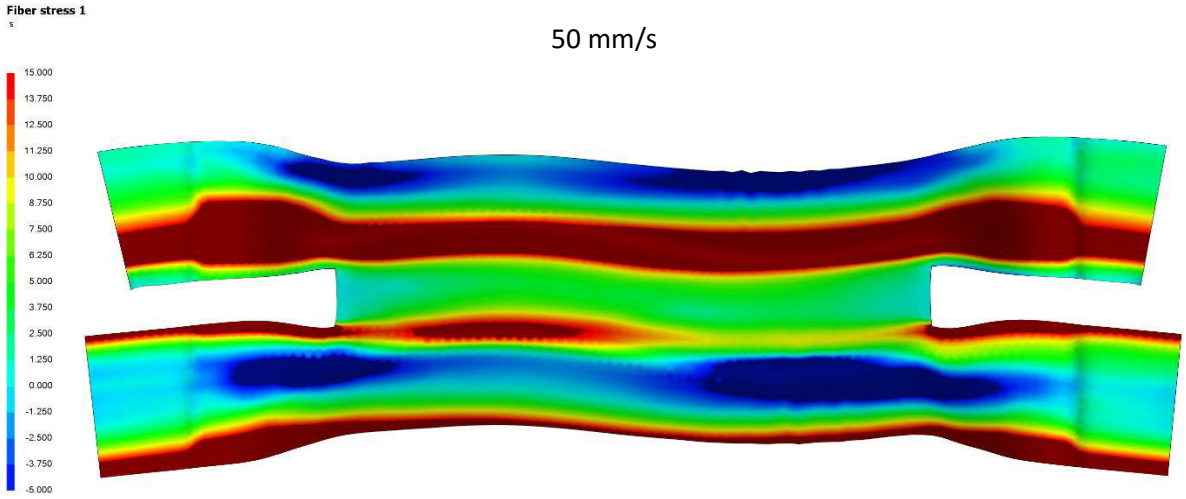


Fibre Stress 1 Ply 1

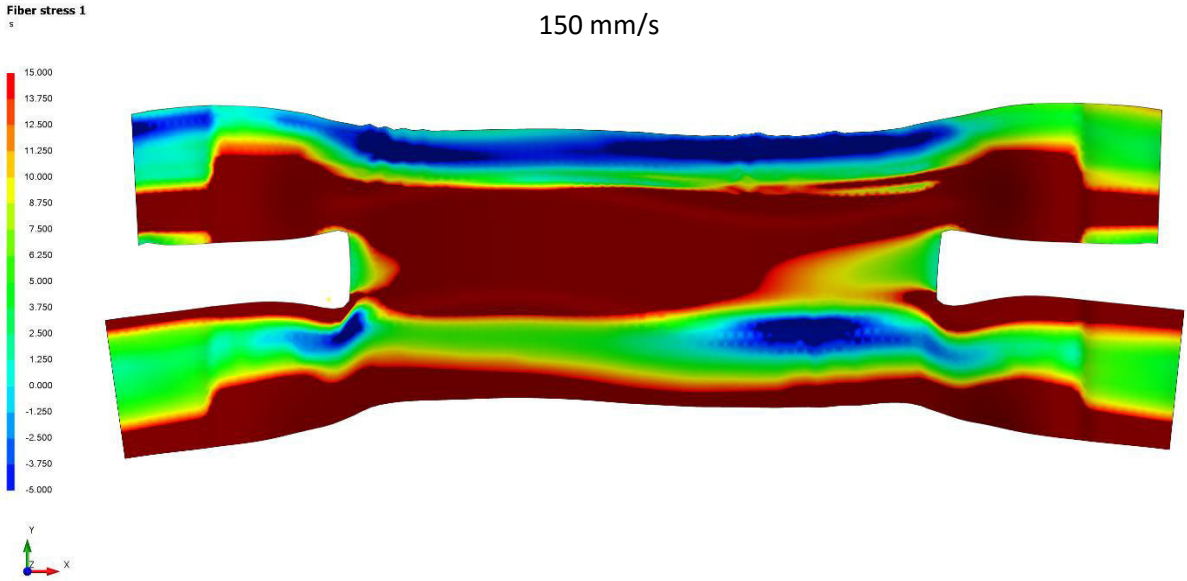
25 mm/s



50 mm/s

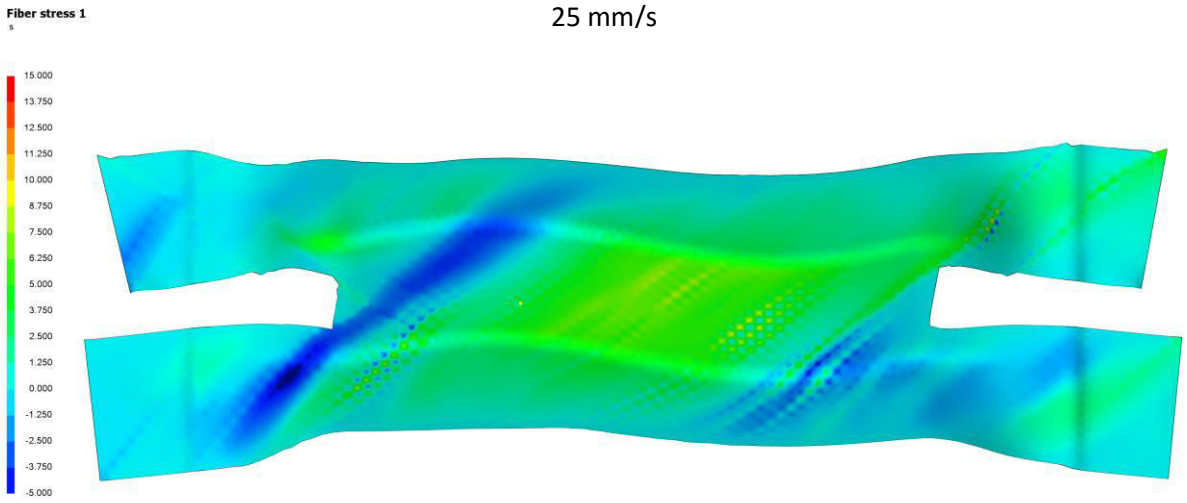


150 mm/s

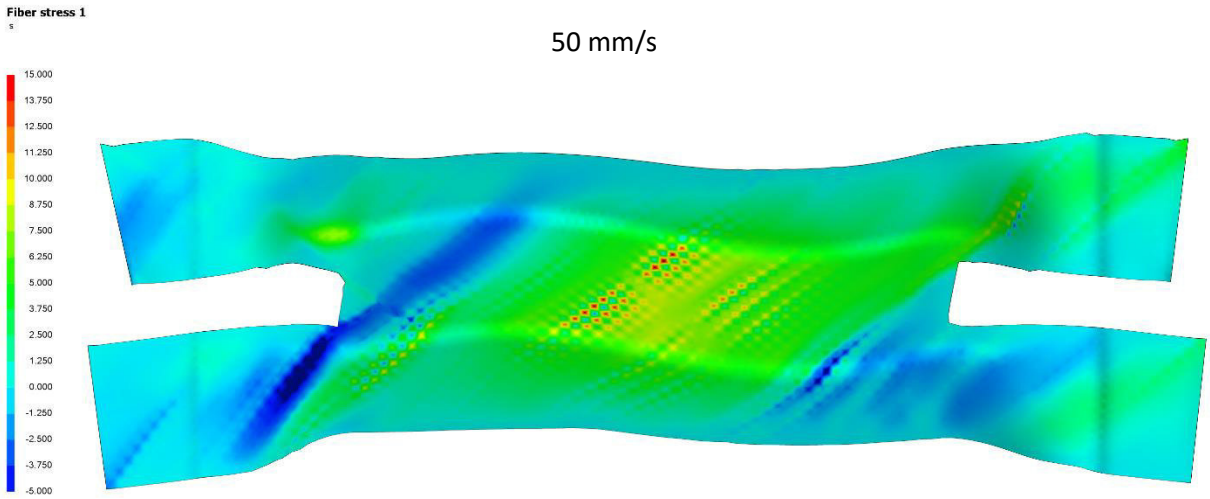


Fibre Stress 1 Ply 2

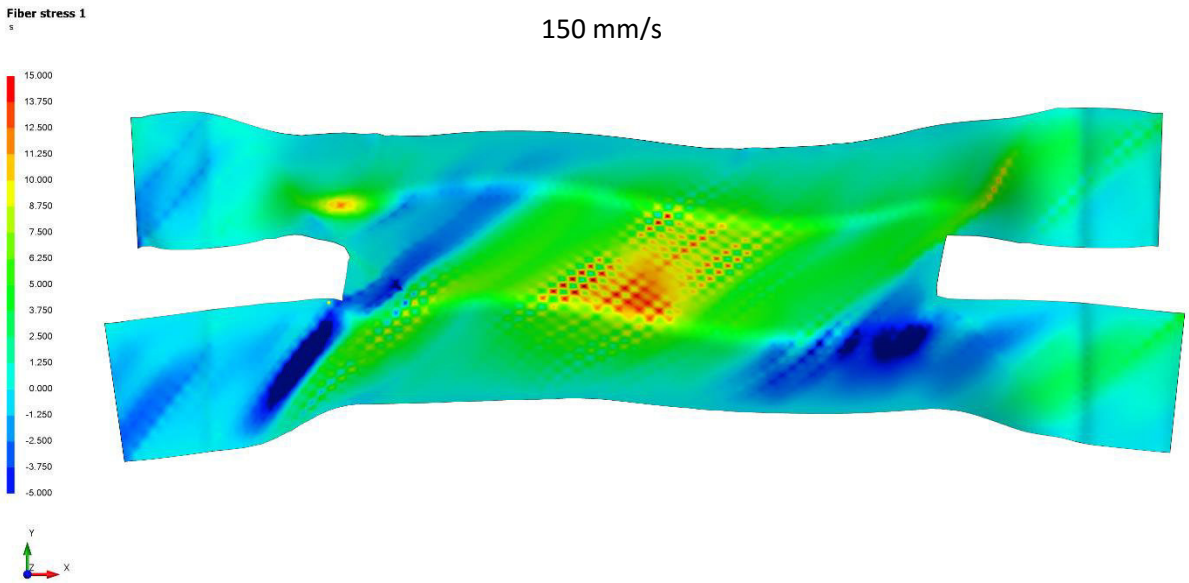
25 mm/s



50 mm/s

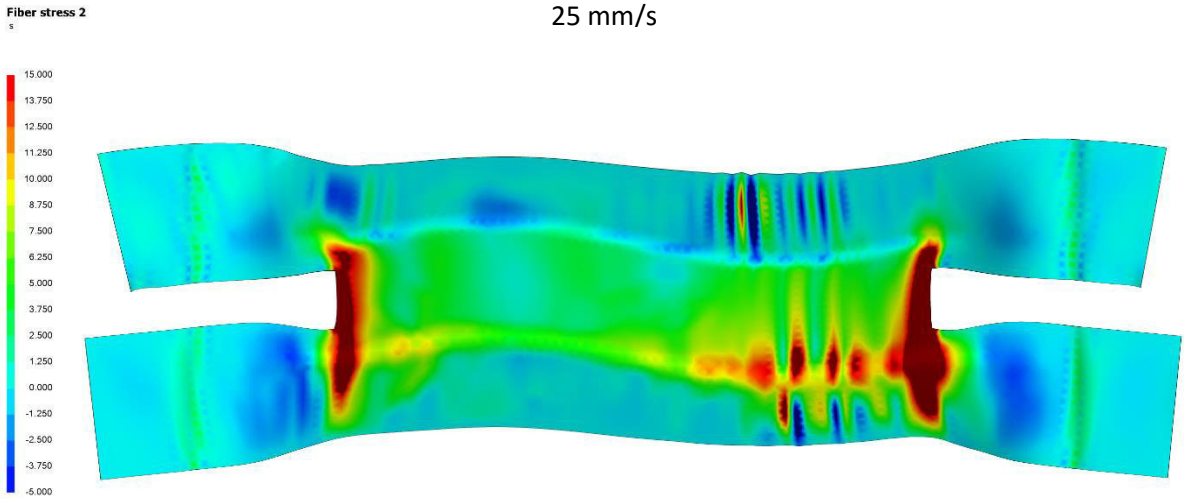


150 mm/s

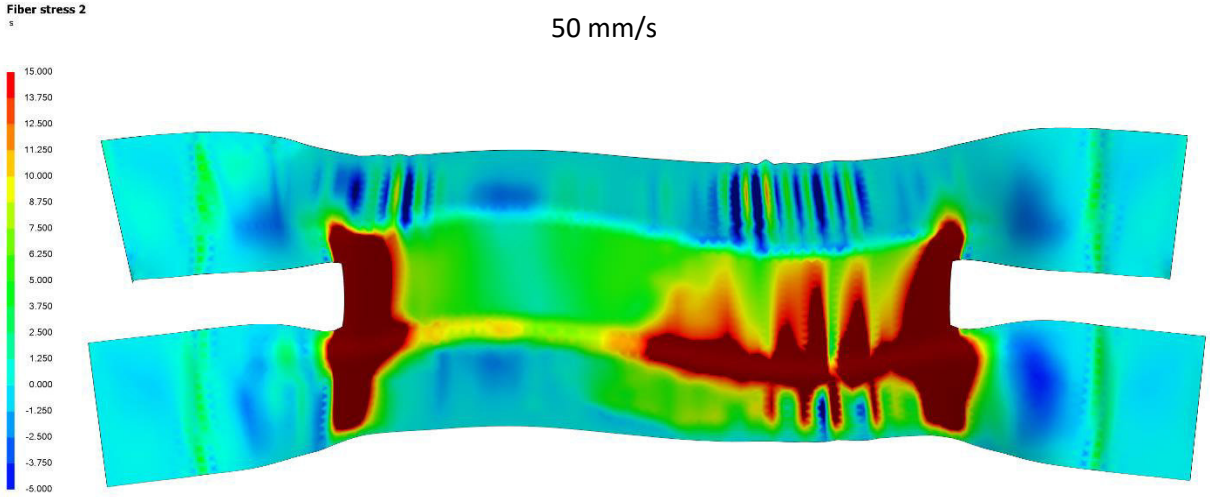


Fibre Stress 2 Ply 1

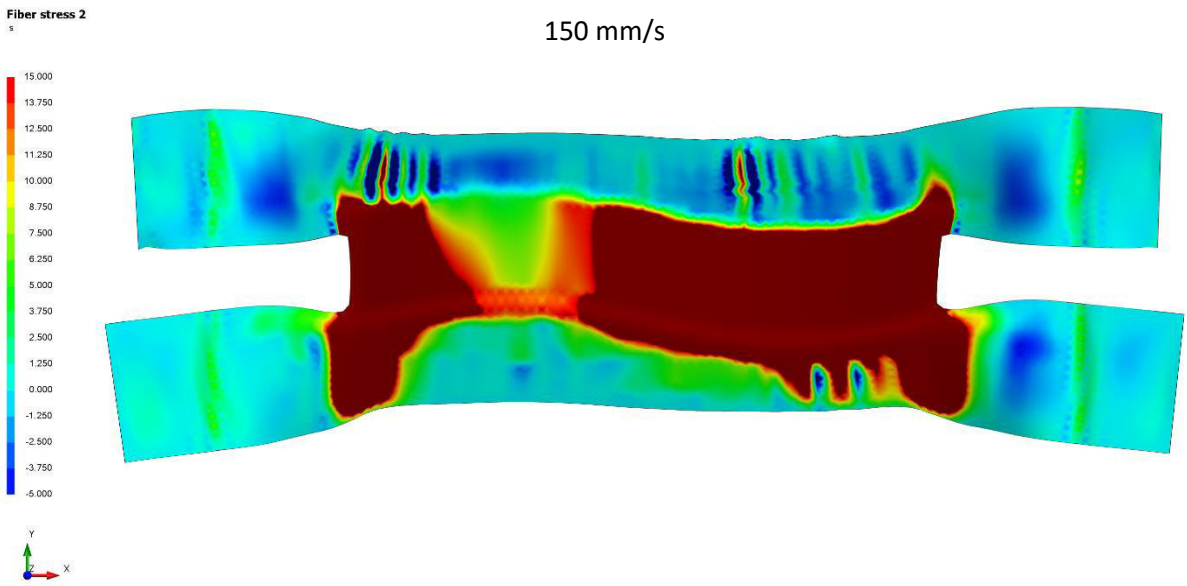
25 mm/s



50 mm/s

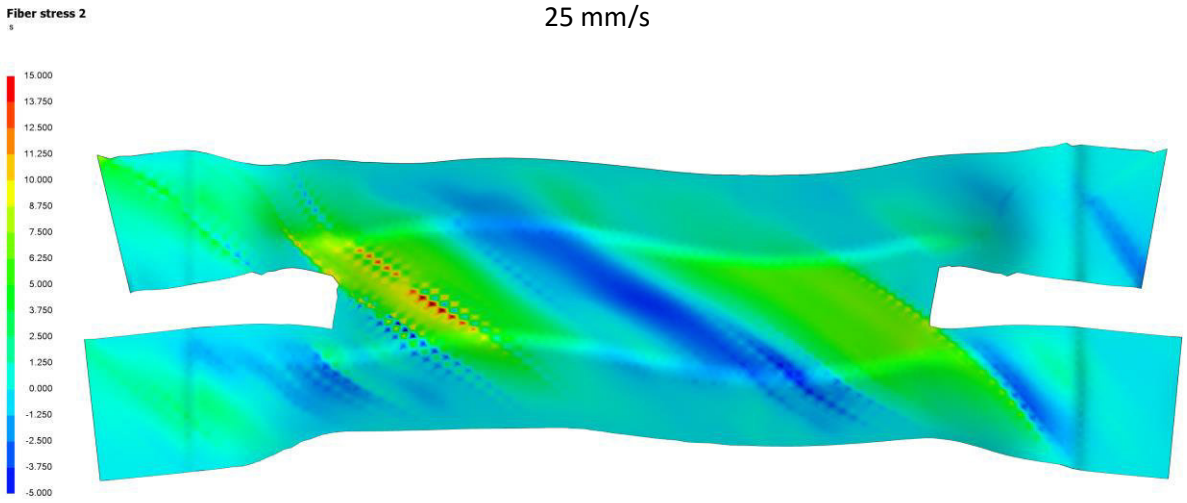


150 mm/s

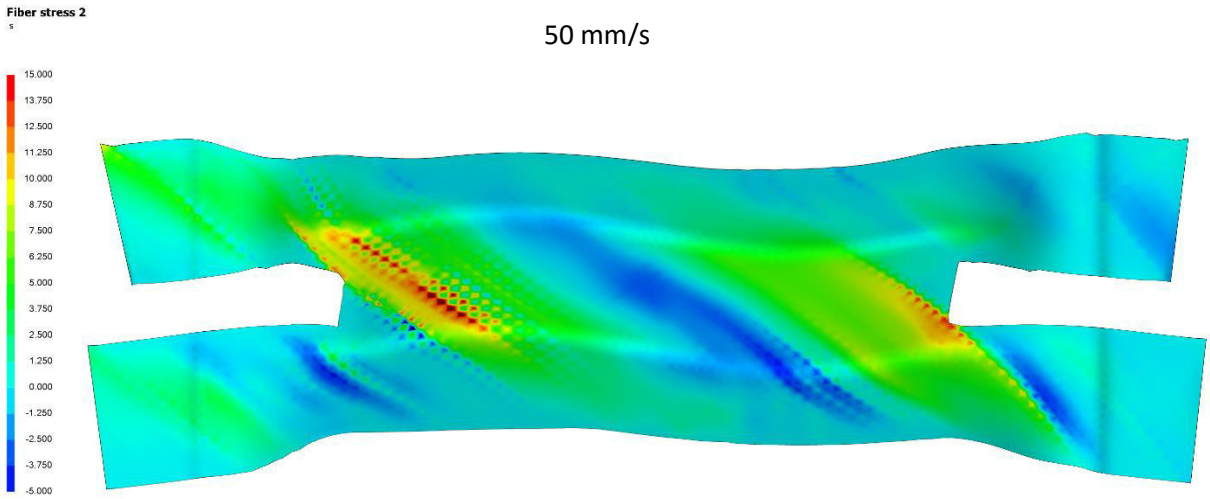


Fibre Stress 2 Ply 2

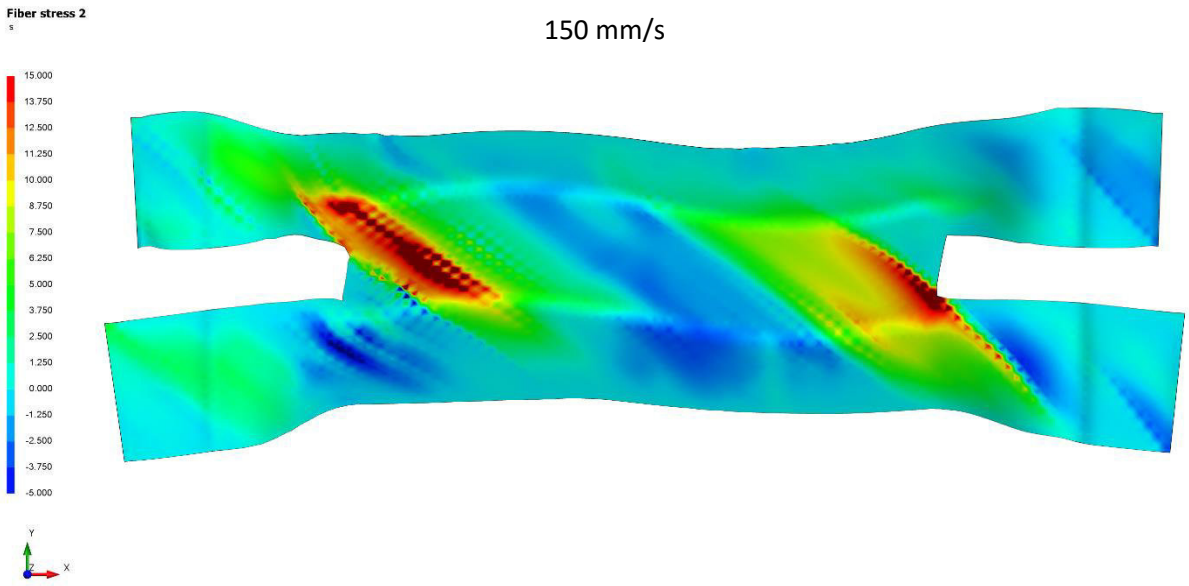
25 mm/s



50 mm/s



150 mm/s



Appendix F Non Destructive Inspection Report

Page intentionally left blank

AFRICAN NDT CENTRE

AD-HOC INSPECTION REPORT
Ultrasonic Testing

Report No: OUT-17-001
Date: 2017-01-18

Client Information

Client:	Aerosud	**Part Description:**	Blank Z8-4 and C 4-3
Division:	Aviation	**Order No:**	AVN- 110017

Item/Part Information

Parts No:	BLANK Z8-4 & BLANKC4-3	**Manufacturing process:**	Press forming
Material Details:	See PS 001090/ 001094	**Extent of Inspection:**	All flat surfaces

TECHNIQUE INFORMATION
Semi-Automated (C-scan)

Calibration Block/Reference Standard:	NA	**UT Equipment:**	NA
Probe Type:	NA	**Coupling Agent:**	NA
Probe Size:	NA	**Surface Temperature:**	NA
Probe Frequency:	NA	**Surface Condition:**	NA

TECHNIQUE INFORMATION
Hand scanning (A-scan)

Calibration Block/Reference Standard:	RS-II-AS-FL-011-1 4PLY PPS	**UT Equipment:**	Epoch 600
Probe Type:	0^0	**Coupling Agent:**	Water
Probe Size:	10mmØ	**Surface Temperature:**	Room Temperature
Probe Frequency:	5MHz	**Surface Condition:**	Smooth

TECHNICAL INFORMATION
Documentation

ANDTc Procedure:	**MP-UT-1234**	**Customers Procedure:**	**N/A**
ANDTc Work instruction:	**N/A**	**Customers Work instruction:**	**N/A**

TECHNICAL INFORMATION
Documentation

Acceptance criteria:	**Report all indications, above -6dB**

TECHNICAL INFORMATION
Inspector

Inspector Name	Report Date	Stamp	Signature:
Andre Klaassens Certification Level: SNT LEVEL II	2017-01-18	ANDTC 2L 05	
Report Information Checked (Name)	**Date Checked:**	**Stamp**	**Signature:**
Andre Klaassens	2017-01-18	ANDTC 2L 05	

INSPECTION RESULTS

Part Number/Description/Item	Quantity	Notes/Drawings	Finding/s
Blank Z8-4	**2**		**All flat surfaces showed no attenuation of more than -6dB.** **NOTE: The radii of the parts are too small to scan.**
Blank C4-3	**4**		**All flat surfaces showed no attenuation of more than -6dB.** **NOTE: The radii of the parts are too small to scan.**

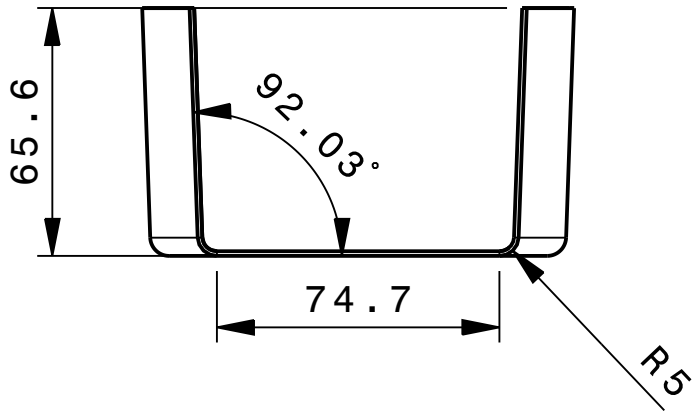
Appendix G Drawings

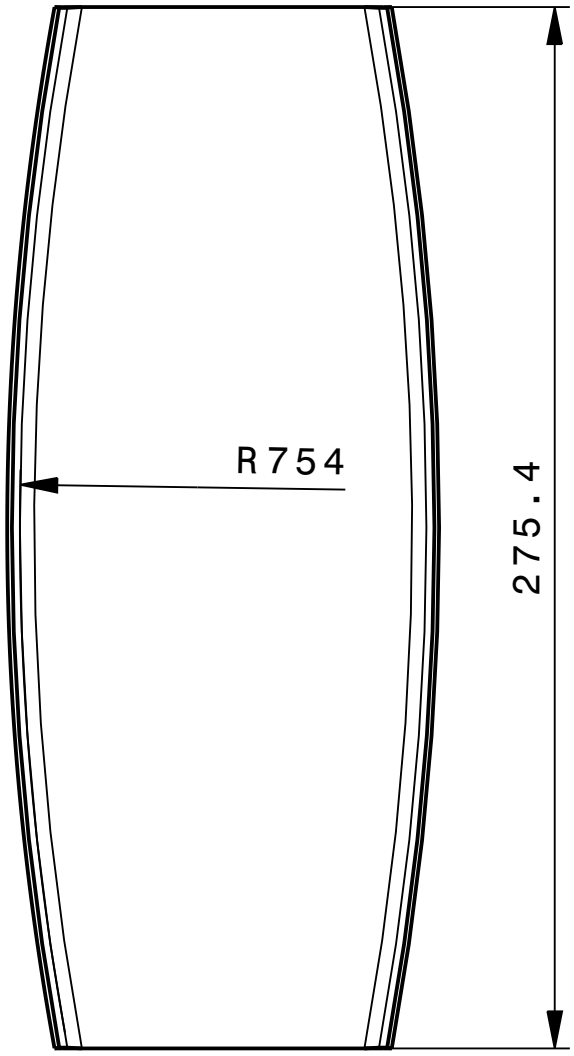
Page 1 C-section

Page 2 Z-section

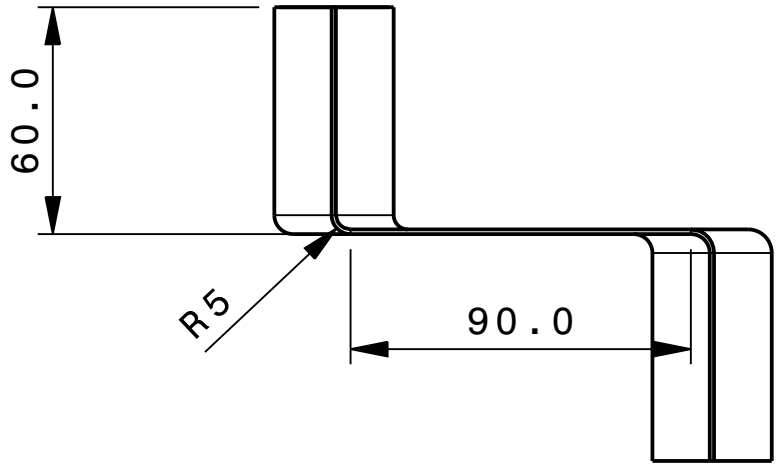
Page 3 Tool assembly for Z and C section tool

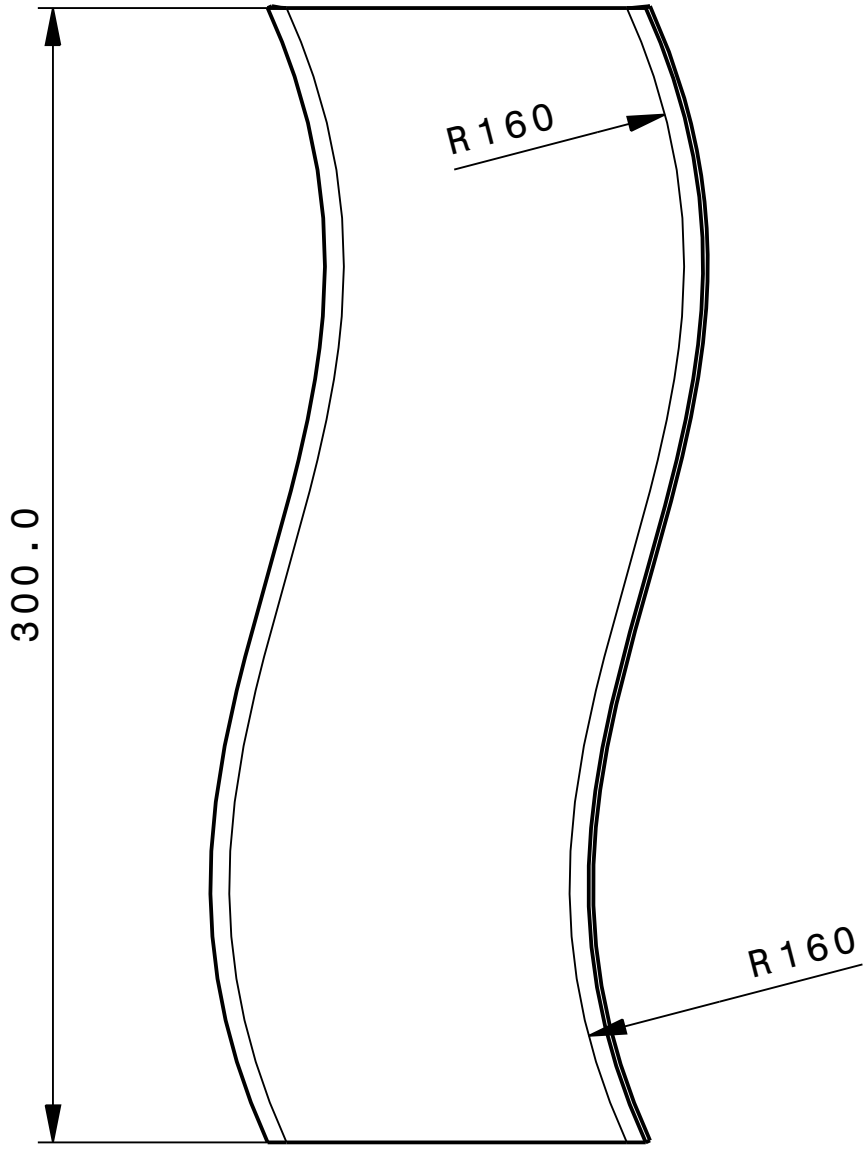
C-Section Drawing





Z-Section Drawing

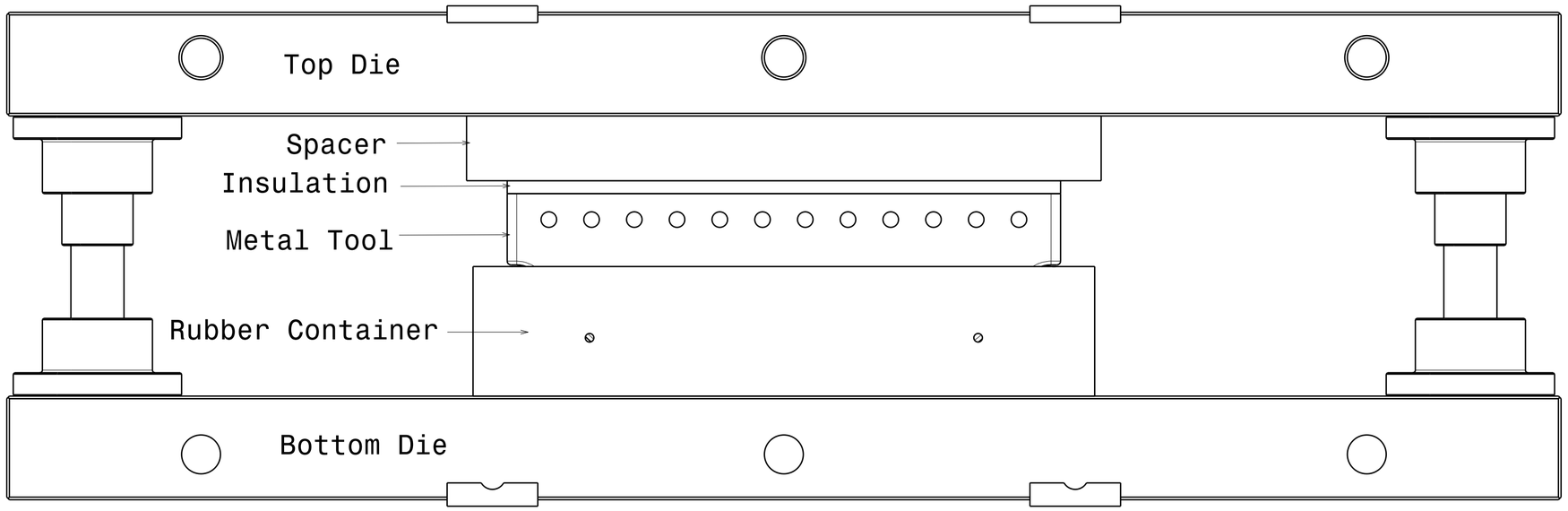




DO NOT SCALE

WHEN IN DOUBT ASK

ALL DIMENSIONS IN MILLIMETERS UNLESS OTHERWISE STATED



Front view
Scale: 1:3

AEROSUD Aviation	LIMITS (UNLESS OTHERWISE STATED) ONE DECIMAL 0.0 = ±0.2 ANGULAR ±1 DEG	1 TO 250 mm = ±0.7 250 TO 1000 mm = ±1.0 1000 TO 2000 mm = ±1.5 2000 TO 4000 mm = ±2.0 4000 ABOVE = ±3.0	IDENTIFICATION MARKINGS APS.01.01	PROJECTION	
TITLE R&D Coupon Tool			DRAWING NUMBER Assembly	Sheet 1 of 1	
DRAWN shivasim DATE 29/09/2016	STRESS DATE	MANUF ENG DATE	OVERALL APPR DATE	SCALE 1:1 U.O.S	ISSUE No A A2
CHECKED DATE	ENG DATE	DESIGN APPR DATE			